DIFFERENTIATION OF ISOMERIC NUCLEIC ACID COMPONENTS BY TIME-OF-FLIGHT SECONDARY ION MASS SPECTROMETRY

A Thesis submitted to
the Faculty of Graduate Studies
in partial fulfillment of the requirements
for the Degree of
Doctor of Philosophy

by

FRANÇOIS LAFORTUNE

Department of Chemistry
University of Manitoba
CANADA

July 1992

ISBN 0-315-77755-9

DIFFERENTIATION OF ISOMERIC NUCLEIC ACID COMPONENTS BY TIME-OF-FLIGHT SECONDARY ION MASS SPECTROMETRY

BY

FRANCOIS LAFORTUNE

A Thesis submitted to the Faculty of Graduate Studies of the University of Manitoba in partial fulfillment of the requirements for the degree of

DOCTOR OF PHILOSOPHY

À Simon, mon fils.

Puisses-tu ne jamais

étancher ta soif

d'apprendre

et de t'émerveiller.

ACKNOWLEDGEMENTS

First of all, I would like to express my gratitude to my thesis supervisor, Dr. John Westmore, for his expert guidance and his patience throughout the course of this work.

My deepest thanks also go to my physics supervisor, Dr. Ken Standing, for his insight and his help, scientific, financial and personal.

Dr. Standing's dynamic lab team has always been a great help to me, providing both a stimulating environment in which knowledge could prosper as well as great advice pertaining to the physics and instrumental problems encountered. For this, I am particularly indebted to Dr. Werner Ens, Xuejun Tang and Ron Beavis .

I also wish to thank Dr. Frank Hruska for providing the alkylated nucleosides and nucleotides analyzed in chapter 3, 4 and 6, and for the very fruitful discussions that always emphasized the importance of logic. Many thanks also to Dr. K.K. Ogilvie and Dr. M.J. Damha, for providing the nucleotides analyzed in chapter 5. Technical assistance by Mr. Wayne Buchannon is also acknowledged.

The study leave and flexible work schedule which Le Collège Universitaire de Saint-Boniface consented to have been of invaluable help to me in facilitating the completion of this work. Special thanks to Dr. F. Girard, Dr. A. Fréchette and Dr. Paul Ruest who were instrumental in making them possible.

Finally, I wish to thank Jocelyne for her unconditional support, love and affection, that gave me the courage to complete the last stretch of this marathonian endeavour.

ABSTRACT

The differentiation of sequence, positional and stereomeric isomers of small nucleic acid components by secondary ion time-of-flight mass spectrometry is described. Compounds studied include O-alkylated thymidines, O-alkylated di- and trinucleotides, and protected di- and trinucleotides.

This thesis first of all reviews mass spectrometric (MS) approaches used to differentiate isomeric bases, nucleosides, nucleotides, small oligonucleotides and closely related analogs. This review appears to be the first one to focus specifically on isomeric differentiation of nucleic acid components presented on a class of compound basis, instead of gravitating towards a particular MS technique.

First-order rate constants and half-lives have been measured for the decomposition of several metastable ions in the secondary ion time-of-flight mass spectra of 4- and 2-O-alkylthymidines. These spectra were obtained with the Manitoba TOF I mass spectrometer. Some of the factors which influence the accuracy of the measurements have been analyzed. Relative values of kinetic parameters appear to be a more reliable indicator of isomeric form than the "normal" mass spectra.

The same compounds have also been investigated with the Manitoba TOF II mass spectrometer. The effect on fragmentation of the presence, size and location of the alkyl group has been studied. Emphasis has been placed on the interpretation of direct spectra, with reference to their metastable ion decompositions, whenever they provided clues to mechanisms of ion formation.

Negative ion mass spectra generated by the Manitoba TOF II instrument were obtained for a series of protected oligoribodi- and trinucleotides. Most compounds contain unusual 2'-5' phosphodiester linkage. $[M-H]^-$ and sequence ions have been detected, and the location and nature of protecting goups have been confirmed, along with numerous isomeric indicators.

O4-alkylated di- and trinucleotides have also been analyzed by fast atom bombardment (FAB) as well as time-of-flight secondary ion mass spectrometry (TOF-SIMS) in the negative ion mode. For dimers, a greater 5'-phosphate/3'-phosphate (pN_2^-/N_1p^-) relative abundance ratio was found in TOF-SIMS spectra while a greater loss of a nucleobase from those sequence ions was observed in FAB spectra. Other examples of the complementary nature of these two mass spectrometric approaches are discussed, as well as the effects of the presence and site of alkylation on fragmentation patterns.

CONTENTS

LIST OF FIGURES

LIST OF TABLES

CHAPTER 1

INTRODUCTION

Nucleic acids are polymers consisting of nucleosides joined by 3'-5' phosphodiester linkages. The nucleosides are composed of a sugar and a heterocyclic base. The sugar is D-ribose in RNA and D-2'-deoxyribose in DNA. Each sugar is attached to one of four heterocyclic bases via a β-glycosyl C1'-N linkage. The heterocycles are the purine bases adenine (A) and guanine (G) and the pyrimidine bases cytosine (C) and thymine (T). The latter is found mostly in DNA; although thymine is also found in RNA, it is usually replaced by uracil (U), as shown in Figure 1.1.

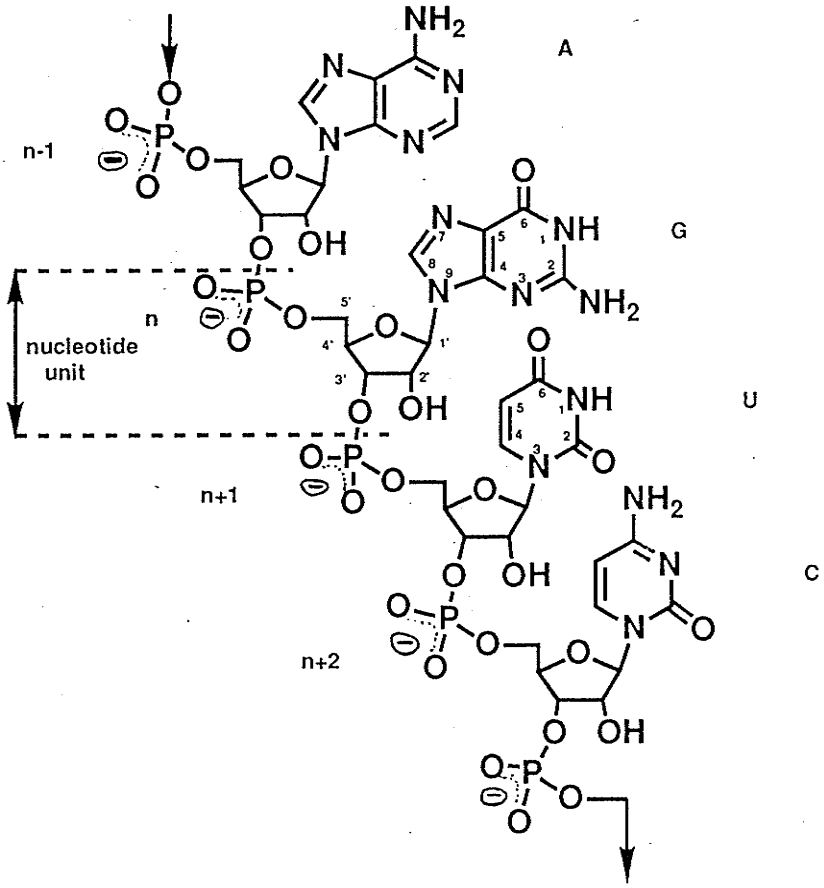

Figure 1.1 Schematic structure of an arbitrary RNA fragment containing the four common bases. The numbering of the bases and ribose ring is shown. In DNA, the hydroxyl group attached to the C2' is replaced by hydrogen and uracil is replaced by thymine.

Nucleic acids play a quintessential role in the most important processes in the living cell. DNA contains the hereditary material of the cell, the genes themselves, which store all the information required to specify the structure of the RNAs and proteins of a given organism.

The development of recombinant DNA technology, initiated in the mid-1970s, has revolutionized the field of biological reseach. One of the rapidly advancing areas of study today is molecular genetic engineering, the modification of the DNA of an organism in a controlled fashion, to produce new genes with new characteristics[1]. The production of genetically engineered proteins, such as human insulin or human growth hormone, is a striking example of the increasing impact of genetic engineering on our lives. Better understanding of the 4000 inherited disorders afflicting mankind is a likely consequence of the massive efforts currently being deployed under an international megaproject called the Human Genome Project[2], which aims at sequencing the estimated 100,000 human genes. The success of this enormous undertaking will undoubtedly depend upon rapid developments in mapping, cloning and DNA sequencing techniques. The following section will provide a short survey of some main analytical approaches used to characterize the structure and properties of nucleic acids.

1.1 ANALYSIS OF NUCLEIC ACID COMPONENTS: METHODS OTHER THAN MASS SPECTROMETRY

As for other biopolymers such as proteins, nucleic acids can be considered to comprise a primary, secondary and tertiary structure. The primary structure of nucleic acids comprises the covalent backbone and the sequence of nucleotide residues. The secondary structure relates to the residue by residue conformation of the backbone of polynucleotide chains (e.g. the double helix of DNA). The tertiary structure is the

three-dimensional conformation of the polynucleotide chain (e.g. the folding of DNA in chromosomes).

The determination of the primary structure of nucleic acids, i.e. sequencing, usually involves cloning techniques and electrophoresis[3]. Mass spectrometry has also been used for that purpose, but only with extremely short polynucleotide chains. A more thorough discussion regarding the role of mass spectrometry in the analysis of nucleic acid components will be the subject of the next section. Secondary and tertiary structure information has been obtained with X-ray crystallography, and complemented by many spectroscopic methods, such as NMR, Raman, IR, UV and circular dichroism spectroscopies. A brief discussion of each approach is presented next.

1.1.1 Primary Structure of Nucleic Acid Constituents: Sequencing

Even though the following discussion will focus on sequencing techniques, it should be mentioned that sequencing represents only one step in the integrated strategies used for gene structure analysis, which also involve isolation, cloning and purification techniques.

Nucleic acids are polyelectrolytes which, when placed on a gel submitted to an electric field, move at rates corresponding to their size. We refer to this technique as gel electrophoresis[4]. DNA fragments containing up to 8 million bases have been separated by electrophoresis on agarose gels. However, sequencing of DNA fragments containing around 600 bases is currently an upper practical limit for electrophoretic resolution at the level of single base differences in length[5]. It means that larger fragments must be reduced to that size with restriction enzymes, which cleave DNA at particular sites. Cloning techniques are then used to generate smaller segments in a pure form and in sufficient quantities.

Two of the most well known techniques that have been developed for DNA sequencing are the Maxam-Gilbert procedure[6] and the Sanger procedure[7]. The first is called the chemical method, while the second is referred to as the enzymatic,

chain-termination or plus-minus method. Both utilize electrophoresis and radioactive (or fluorescent) markers. A brief account of the Sanger method will be presented here.

1.1.1.1 Sanger Enzymatic DNA Sequencing

This technique consists of generating a DNA strand complementary to the single-stranded DNA sequence to be determined. As shown in Figure 1.2, synthesis starts with incorporation of a radioactive (or fluorescent) polynucleotide of known sequence (called primer). By addition of an enzyme (DNA polymerase) and deoxynucleotides (dNTPs), the complementary chain extension occurs from the 3'-end of the primer. The key to this method is that syntheses are carried out in four separate vessels, each containing a small amount of a specific dideoxynucleotide (ddNTP) whose lack of a 3'-hydroxyl group causes chain termination[8]. Random low level incorporation of ddNTPs results in a mixture of different length chains, all starting at the 5'-end of the primer, and ending at every possible position, corresponding to the incorporation of the specific ddNTP.

Polyacrylamide gel electrophoresis of each mixture produces a ladder sequence, similar to that shown in Figure 1.2, which yields one by one each nucleotide of the complementary sequence. With automation and robotic innovations, it is now possible to analyze up to 20 sequences (12,000 bases) simultaneously[9].

One of the main goals of the Human Genome Project is to determine the nucleotide sequence contained in all 24 human chromosomes. Considering that the smallest chromosomes include more than 50 million bases, it is not expected that this goal will be reached before the next ten years, unless there are innovations and improvements in reading capacity of DNA sequences[8].

Figure 1.2

Sanger enzymatic sequencing

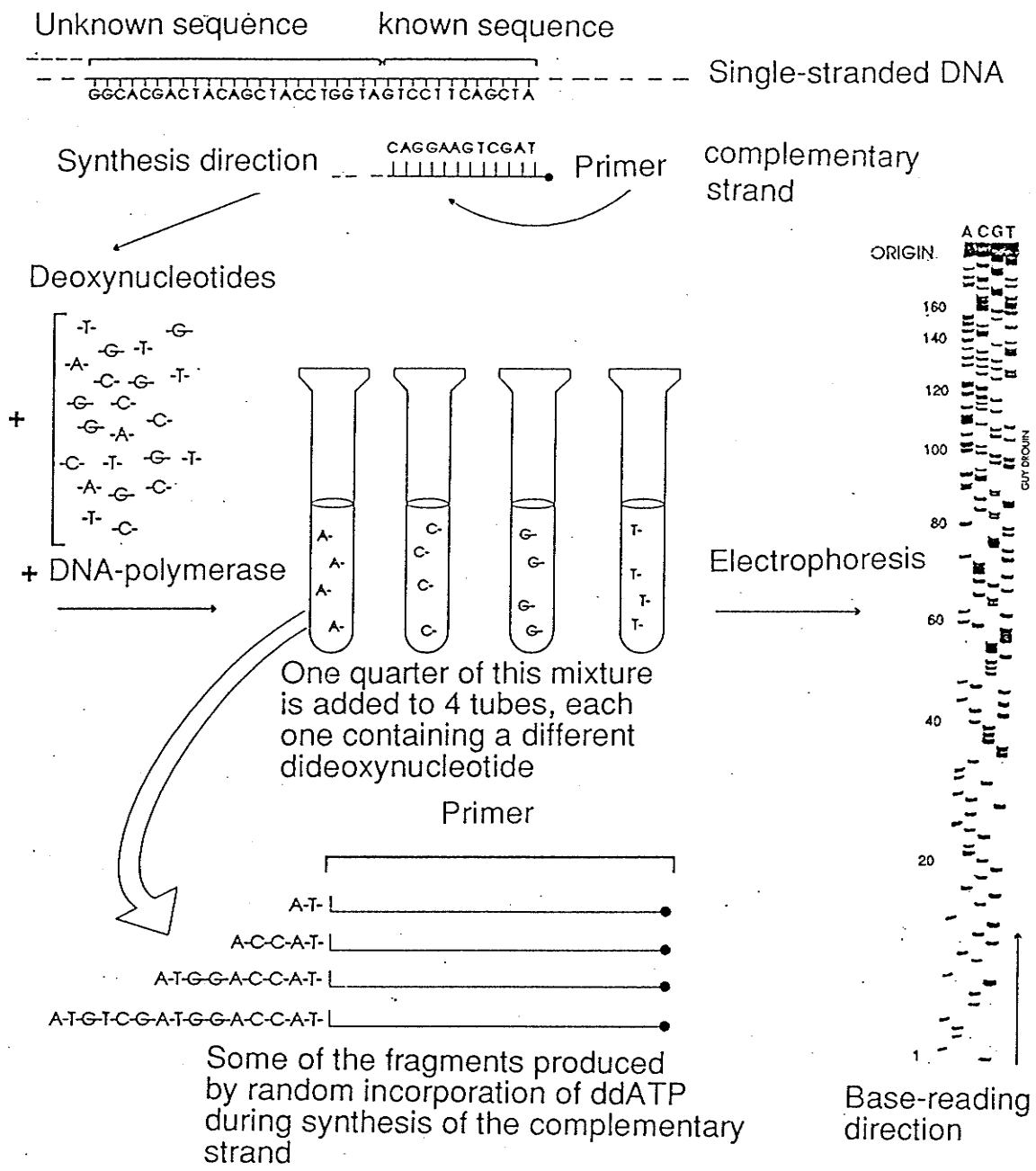

1.1.2 Secondary and Tertiary Structure of Nucleic Acids

1.1.2.1 X-ray crystallography

Structural studies of nucleosides, nucleotides and nucleic acids in the solid state have mostly been performed by X-ray crystallographic techniques[10]. The amount of detailed structural information is dependent on the size of the molecule and on the availability of the material in crystalline, or in quasi-crystalline form. Short oligonucleotides, for instance, obtainable as crystals, have been analyzed by X-ray crystallography at near atomic resolution. On the other hand, X-ray diffraction of quasi-crystalline polymers such as DNA gives only overall information, e.g. the double helical structure deduced in 1953 by Watson and Crick[11]. With molecules larger than ca. 2000 daltons, model building and other spectroscopic methods are usually utilized, in conjunction with X-ray diffraction, to derive atomic coordinates and spatial relationship information between nucleotidic units.

1.1.2.2 NMR spectroscopy

Of all spectroscopic methods, nuclear magnetic resonance (NMR) has been the most widely applied to conformational studies of nucleic acid components in solution[12,13], and to intermolecular interaction studies, such as hydrogen bonding and base stacking.

Possible conformations of polynucleotides in solution include unstructured single strands, hairpins, and regular duplexes formed by complementary strands. Most studies have focussed on ^{1}H NMR, although ^{13}C, ^{15}N and ^{31}P techniques are also used. While NMR parameters, such as spin-spin coupling constants (J), are sensitive to differences in conformation due to sugar puckering modes and to base orientations relative to the sugar moiety, tautomerism, hydrogen bonding and base stacking can be deduced from other parameters such as chemical shifts[14-16] (δ). The development of spectrometers with higher magnetic fields and multi-dimensional analysis capability[17] has established NMR as one of the most powerful tools in detailing features of secondary and tertiary structures

of nucleic acid components.

1.1.2.3 Other spectroscopic methods: Raman, IR, UV and circular dichroism

The kind of information provided by Raman scattering spectra is essentially the same as that provided by infrared (IR) absorption spectra. The greatest utility of Raman and IR spectra in nucleic acid research appears to be in the identification of specific atoms or groups of atoms that are involved in the stabilizing interactions of nucleic acid secondary and tertiary structures. Conclusions are primarily drawn from analogies with spectral data from model compounds of known composition and structure[18]. An important advantage of Raman spectra over infrared lies in the fact that water does not cause interference. Additionally, vibrations in the nucleic acid backbone can be better detected in Raman spectra than in absorption spectra, which usually mostly reveal transitions taking place in the base residues. IR spectra, hence, may be better suited to study keto-enol tautomerism and base-base association through hydrogen bonding[19].

On the other hand, ultraviolet (UV) and circular dichroism (CD) spectroscopy have been particularly used to study the formation and breakdown of double helices, i.e. helix-coil transitions[20,21], which are sensitive to base stacking effects with polynucleotides. For optically active compounds, CD often provides spectral details that are absent in the UV spectra, such as handedness of nucleic acid helical structures.

1.2 ANALYSIS OF NUCLEIC ACID COMPONENTS BY MASS SPECTROMETRY

Table 1.1 describes some of the main areas of application of mass spectrometry (MS), as well as leading references pertaining to the analysis of nucleic acid constituents. As revealed in table 1, MS has been applied to a wide variety of problems and compounds from biological and synthetic sources, ranging in size from a single base[70] (~100 daltons)

up to more than 75 nucleotidic units (~25,000 daltons)[96].

There are, for instance, more than 80 different bases or nucleosides known in RNA and DNA, most of them having been discovered from transfer RNA (tRNA), one of the smallest nucleic acids[31]. With less abundant sources of material, which can often be isolated only in submicrogram level quantities, the high sensitivity and structure specificity of MS has led to its ever increasing use in nucleic acid chemistry over the past twenty years[22-34].

Apart from molecular weight and structural information obtained for naturally occurring bases, nucleosides, nucleotides and oligonucleotides, MS has been particularly useful in the qualitative and quantitative analysis of hosts of modified compounds, which are often obtained in quantities too small for characterization by chemically-based methods. These include modifications induced in DNA by a physical agent such as UV light or gamma radiation [37,38,80], by chemical carcinogens, mutagens or drugs[39,40,80-87], metal complexes[81-84], nucleoside antibiotics[35,36], and other analogs of medicinal importance such as anti-cancer agents[88-93]. MS has also been used as a tool to follow the fate of various modified nucleosides in biological media, in biosynthesis studies[94,95] for example, or for quantification of metabolites at physiological concentrations[41].

The growing interest in synthetic oligonucleotides in molecular biology has forced continuous improvements in instrumental methods for sequencing synthetic gene fragments, for instance, which are at intermediate stages of synthesis and therefore could contain chemical protecting groups at reactive sites. MS has been used to characterize those intermediates, protected or not [42-61], replacing time-consuming methods that necessarily involve complete deprotection, enzymatic degradation, separation and analysis of degradation products[56].

TABLE 1.1

MASS SPECTROMETRY: APPLICATIONS TO NUCLEIC ACID COMPONENTS

	References
NATURAL SOURCES	
- general structure and molecular weight determination of bases, nucleosides, nucleotides and oligonucleotides.	22-28
- identification of modified nucleosides in tRNA hydrosylates.	29-34
- identification of nucleoside antibiotics.	35-36
- *in vitro* modifications by physical agents (e.g. UV, γ).	37-38
- identification of adducts of nucleic acid constituents with drugs or other chemicals.	39-40
- quantification of metabolites at physiological concentrations.	41
SYNTHETIC SOURCES	
- characterization of synthetic intermediates, including by-products, sequence determination of oligonucleotides.	42-61
- fundamental mechanistic studies, fragmentation pathways, proton affinity determination, gaseous ion chemistry.	62-68
- Isomer differentiation.	69-79
- modifications by physical agents (e.g. UV, γ).	80
- metal complexes and products of interactions with carcinogens and mutagens.	81-87
- analogs of medicinal importance, antagonists, anti-cancer agents.	88-93
- biosynthesis studies, including isotopic labelling.	94-95

Additionally, underlying most of the above mentioned applications in nucleic acid chemistry, but not to be overlooked even if perhaps less applied, are MS reports on fundamental mechanistic studies such as: determination of fragmentation pathways, correlation between chemical stability and stability of molecular ions, measurement of proton affinities, and other gaseous ion chemistry studies[62-68].

Finally, the need to study modifications to nucleic acid constituents induced at various base, sugar or phosphate positions by physical of chemical agents also led to numerous mass spectrometric investigations focussing on the differentiation of sequence, positional, or stereomeric isomers[69-79]. This is the central theme of this thesis, for which a more detailed outline will be provided at the end of this chapter.

It must be emphasized that this section has provided an overview of mass spectrometric applications in nucleic acid research; it is pertinent to indicate that the outlined classification was based on structural differences without reference to instrumental requirements for successful MS investigations. The next section will depict how closely the entry of MS into the nucleic acid domain has been linked to increased capabilities of mass spectrometers.

Since its discovery in 1912 by Thompson[97], mass spectrometry (MS) has developed into one of the most powerful and versatile analytical methods available for the study of biomolecules. Its basic principle, i.e. the production, separation and recording of the mass of ionized species, applies regardless of the MS instrumental approach used. The most common and widely used ionization sources and mass analysis techniques applied to nucleic acid components will now be described briefly.

1.2.1 Electron Impact Ionization

Sincethe publication of the first MS spectrum of a nucleoside 30 years ago by Biemann and McCloskey[98], electron impact mass spectrometry (EI-MS) has been, and remains, one of the most widely used ionization mode for analysis of nucleic acid constituents (NACs)[62]. In general, much more structural information results from electron impact-MS than by, for

instance, desorption or chemical ionization methods[31]. However, due to involatility and thermal lability of nucleotides and oligonucleotides, EI-MS is limited to examination of bases and less polar nucleosides. Even by increasing the analyte volatility by chemical derivatization, analysis of nucleic acid components is limited to ~1200 daltons by EI-MS[33]. Fortunately, nucleosides are generally the preferred level at which to work for characterization of new natural NACs. This is, first of all, due to the availability of effective enzymes that can release nucleosides quantitatively from nucleic acids, and also, to the fact that mass spectra of a nucleotide usually do not yield more information than the corresponding nucleoside,while producing phosphate-containing ions that complicate the mass spectra[31].

1.2.2 Chemical Ionization

Chemical ionization (CI) mostly plays a complementary role to EI-MS. Ionization of the analyte in CI results from a gas phase chemical reaction (with CH_5^+, for example), rather than by bombardment with energetic electrons. Since this ionization process imparts less energy to species of interest, CI is considered a "softer" ionizing method, compared to EI. As a result, less fragmentation, and therefore, enhanced molecular ion abundances are observed in CI spectra[67]. CI has the disadvantage of producing fewer structurally informative fragments, but has the advantage of decreasing analyte detection limits[63], which is of considerable importance in trace analysis. Establishing the molecular weight of a compound has been the major utility of CI in nucleic acid component structural analysis[28].

1.2.3 Desorption Chemical Ionization

Contrary to CI and EI, which require that the analyte be in the gas phase, desorption chemical ionization (DCI) allows analysis of solid and low vapor pressure compounds. DCI hence produces CI-like spectra, primarily $[M+H]^+$ ions from analytes that would

normally decompose before evaporation[99]. The sample is placed on an emitter wire through which a current is passed. The sample is desorbed and ionized by a CI reagent gas plasma . Compared to desorption from a liquid matrix, which is the case with fast atom bombardment (FAB), DCI has advantages in sensitivity and selectivity. The reagent gas can be changed, enabling some control over the degree of fragmentation. Direct analysis of nucleosides[100], including a series of pyridinium nucleoside salts[101] and subpicomole quantitation of an alkylated dinucleotide[86] are examples of DCI applications for NACs. However, particle-induced desorption methods of ionization have been applied to a much larger extent than DCI to analysis of NACs.

1.2.4 Field Desorption

Field desorption (FD) takes place when a non-volatile sample coated onto an emitting surface is placed in proximity of a large electric potential, which causes ionization. It has been successfully applied to the analysis of non-volatile and thermally labile compounds. However, because of a lack of emitter reproducibility, the absence of structurally informative fragments, and other instrumental difficulties[102], other desorption techniques of ionization have attracted much wider attention than FDMS in NAC analysis. Nevertheless, FDMS has been used successfully for analysis of underivatized nucleic acid components such as sequence specific fragment or isomeric dinucleotides[77] and in low-detection complex mixture analysis[102].

1.2.5 Particle-Induced Desorption

Some of the most successfully used methods of ionization for NAC analysis from condensed phases involve particle-induced desorption. Desorption and ionization of samples are induced by bombardment with atom, fission fragment, ion or photon beams. Each approach will now be individually described.

1.2.5.1 Fast Atom Bombardment

Since its introduction in 1981 by Barber *et al* [103], FAB has become the most widely used MS methods for NAC analysis. Its simplicity of use, the low cost of necessary equipment, and the extended time over which ions can be detected have all contributed to its popularity despite limitations, such as matrix interference and loss of structural information compared to EI spectra[104].

Energy for desorption in FAB is supplied by a beam of atoms from a suitable gas, such as xenon or argon, having energy in the range of a few keV. FAB is a popular alternative of secondary-ion mass spectrometry (SIMS), which will be described in section 1.2.5.3. In FAB investigations, the sample is usually dissolved in a polar, low-boiling solvent, such as glycerol, prior to bombardment. This provides a medium in which the surface is replenished with analyte by diffusion, to replace that removed by desorption[105].

In contrast to FD and DCI, FAB results have been shown to be more reproducible among laboratories, and the long-lived ion currents in FAB allow time-consuming procedures, such as metastable ion analysis, to be accomplished without repeating sample loading[104]. FAB has been used widely in combination with double focusing magnetic sector instruments. Probably the best approach to overcome matrix interference in FAB mass spectra is tandem mass spectrometry (MS-MS) with collisionally activated dissociation (CAD). Literature regarding the use of FAB for NAC analysis covers all aspects of the field, as attested by numerous reviews on the subject[31,42,93,104]. FAB provides unambiguous molecular weight determination, identification of the bases and sugars of most nucleosides, sequence information of short nucleotides and free deoxyoligonucleotides up to 10 residues in length, mostly in the negative ion mode, both from natural and synthetic sources. However, analysis of fully protected

oligodeoxynucleotides has not been as successful[48].

1.2.5.2 ^{252}Cf-Plasma Desorption

Plasma desorption mass spectrometry (PDMS), which uses ^{252}Cf fission fragments (100-130 MeV of energy) as desorbing and ionizing particles, was introduced by Macfarlane and Torgerson in 1974[106]. PDMS was the first method to open up the field of mass spectrometry to the analysis of complicated molecules of biological origin. The ion source is usually coupled to a time-of-flight (TOF) mass analyzer whose mass range, limited only by detector efficiency, is especially well suited to analysis of larger NACs. PDMS is also virtually nondestructive, as typically only about 10^{-10}% of a sample is consumed by the desorption process[107]. Essentially all of the sample can thus be recovered intact. Advantages of PD, relative to FAB, for NACs analysis, include the possibility of characterizing fully protected synthetic intermediates used in the synthesis of oligonucleotides, to verify base sequence and the integrity of the blocking groups[44], as well as reliability and speed[33]. Oligomers as long as 14 units have been characterized by PDMS[46].

1.2.5.3 keV Ion Desorption

Secondary ion mass spectrometry (SIMS) involves bombarding the sample with a beam of primary ions of a few keV of energy, and analyzing the secondary ions that emerge from the sample surface. Its use for analysis of organic molecules was pioneered by Benninghoven[24,108]. Spectra of NACs are usually quite similar to those obtained with PD [53,109]. Fully protected oligonucleotides can also be analyzed by SIMS, an advantage shared with PDMS over FABMS[54]. Apart from the Benninghoven group, most of SIMS analyses of NACs were performed by the Standing group[53,54,109-112] on their Manitoba TOF I and TOF II SIMS instruments, as detailed in chapters 3,4,5 and 6 of this thesis.

1.2.5.4 Laser Desorption

In a manner analogous to the use of an ion gun in SIMS or FAB, lasers can be seen as photon guns that can be used to bombard a sample. Short, nanosecond photon pulses in the far ultraviolet (UV) or far infrared (IR) have typically been used to desorb parent molecular ions or specific fragments[113], mostly in conjunction with TOF or ion cyclotron resonance Fourier transform (ICR-FT) mass spectrometers. Before 1988, only a few nucleosides had been analyzed by laser desorption mass spectrometry (LDMS)[114-115]. The introduction of matrix-assisted UV LDMS in 1988 by Karas and Hillenkamp[116] was a real breakthrough in the analysis of very large biomolecules; they detected the molecular ion of bovine albumen (m/z ~67,000), which included a signal at $3M^+$ (m/z ~200,000). Oligonucleotides 3-20 base units in length have since been analyzed with the same approach[117-118], a signal that mass spectrometric analysis of large, natural nucleic acid components has indeed become possible.

1.2.6 Electrospray and Ion Spray Ionization

Significant new capabilities for the mass spectrometric analysis of NACs have been obtained with the development of ion-spray (ISI)[27] and electrospray ionization (ESI)[96] mass spectrometry, which involve formation of highly charged liquid droplets in an ion source interfaced, typically, with a quadrupole mass spectrometer. For both techniques, the underlying mechanism of ion formation is described as being field-assisted desorption of solute ions, as originally described by Iribarne and Thomson[118]. An electrospray is generally produced by application of a high electric field to a small flow of liquid (~1-10μL/min) from a capillary tube, which disrupts the liquid surface and produces highly charged liquid droplets. Those droplets are dispersed and reduced in size, either by electric fields alone (ESI), or by electric fields plus pneumatic nebulization (ISI). Ion spray, therefore, is essentially electrospray with the assistance of pneumatic

nebulization[119].

Typical mass spectra consist of a distribution of molecular ion charge states with marginal contributions due to dissociation. High detection efficiency of the multiply charged molecular ions produced by ESI or ISI, combined with very high ionization efficiency, has enabled detection of natural deoxyribo- and ribonucleotide oligomers extending up to 76-mers for transfer RNAs, in concentrations as low as 10^{-10}M (corresponding to flow rates of ~10^{-18}mol / s) [96].

Finally, molecular weight accuracies are generally at least one order of magnitude greater than those obtainable with electrophoretic methods. However, resolution decreases significantly for NACs over M_r~30,000 , to reach ~1% for 60-mers[96], which is still better than that obtained by other methods.

1.3 ISOMERIC DIFFERENTIATION OF NUCLEIC ACID COMPONENTS BY TIME-OF-FLIGHT SECONDARY ION MASS SPECTROMETRY: THE MANITOBA CONNECTIONS

This thesis describes how structural isomers and stereomeric nucleosides and nucleotides can be differentiated by time-of-flight secondary ion mass spectrometry. Most frequently, distinctions between spectra stems from different relative abundances of isobaric secondary ions. To a lesser extent, the presence of particular peaks for one isomer that are absent in the spectrum of another has also been used for isomeric differentiation, as well as differences in lifetimes of parent ions, as estimated by unimolecular decay measurements. When deemed appropriate, mechanistic rationalizations were suggested to account for mass spectral differences between isomers.

Results have been obtained from two secondary ion mass spectrometers, Manitoba

TOF I and Manitoba TOF II. Some of their main features and principles of operation will now be described briefly.

1.3.1 Instrumental considerations

The operating principle of a time-of-flight (TOF) mass spectrometer involves generating ions from target material, accelerating them to constant kinetic energy, and measuring the time between ion production and their arrival at a detector located at the end of the flight tube. Because of their different masses, ions separate in the field free region according to their velocity. The m/z value of an ion is determined by its time of arrival at the detector; the relationship between time of flight, velocity and m/z for an ion travelling a distance L, is as follows:

$$TOF = L/v = L[m / (2zeV)]^{1/2}$$

Hence, an ion of mass 1000 and of charge +1, accelerated to 10 keV and travelling a distance of 1.5 m, would require ~34 μs to reach the detector.

As represented in the schematic diagram of Manitoba TOF I[120], in figure 1.3, secondary ions are produced by a pulsed (~2 ns) primary beam of Cs^+ ions striking the target at a ~ 20° angle from the normal[121]. The primary beam is swept across a narrow slit at a repetition rate of 4 kHz. The secondary ions ejected from the target are electrostatically accelerated between the target (HV) and the grid (ground potential) to ~5 keV, at the end of which they enter the drift region and strike the detector.

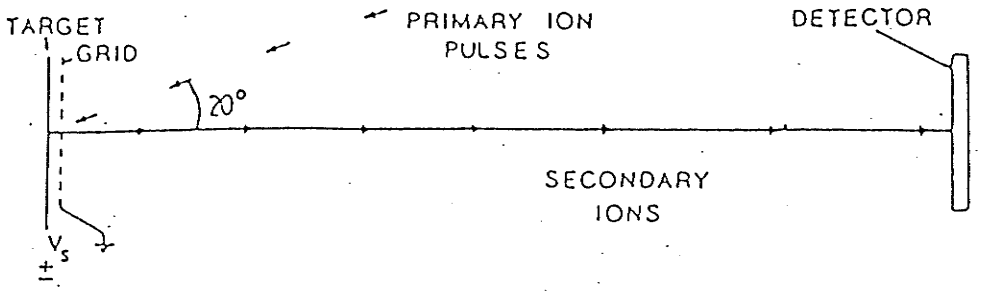

Figure 1.3. Schematic diagram of the linear TOF mass spectrometer

Compared to quadrupole or sector mass spectrometers, time-of-flight instruments offer many advantages[122]. One of them , high efficiency, *i.e.* the ratio of the number of ions recorded in the spectrum to the number of ions ejected from the target, is greater than in most other types of mass spectrometers, since no slits or mass scanning are needed. Additionally, a whole mass spectrum can be obtained from one primary ion pulse. Together, those factors mean that the sensitivity of a TOF mass spectrometer is very high; it has been estimated to be typically ~10^5 times greater than that of a quadrupole mass spectrometer[123].

A characteristic of linear time-of-flight instruments that affects both efficiency and resolution is the fact that TOF mass spectra portray distributions of secondary ions formed within a very short time (<100 ns) after emission from the target, even though their flight times are several tens of μs. Most other types of spectrometer require much longer (>10 μs) to permit detection at their original mass.

Daughter ions of decomposing metastable parent ions have about the same velocity as their parent ions and therefore appear at almost the same position as their parents in the TOF mass spectrum, although kinetic energy released during the decomposition causes peak broadening. It appears, therefore, that the increase in efficiency is achieved at the expense of resolution, which is further reduced by initial energy spread of the secondary ions.

Figure 1.4 illustrates a slightly more elaborate schematic diagram of the Manitoba TOF I mass spectrometer in the configuration used for the work reported in chapter 3 of this thesis. It incorporates an electrostatic mirror[124] that enables metastable ion studies such as determination of first-order rate constants, half-lives and correlations between neutral and charged daughter ions[125]. How this is achieved is described in chapter 3,

which includes analysis of some of the factors which influence the accuracy of the measurements.

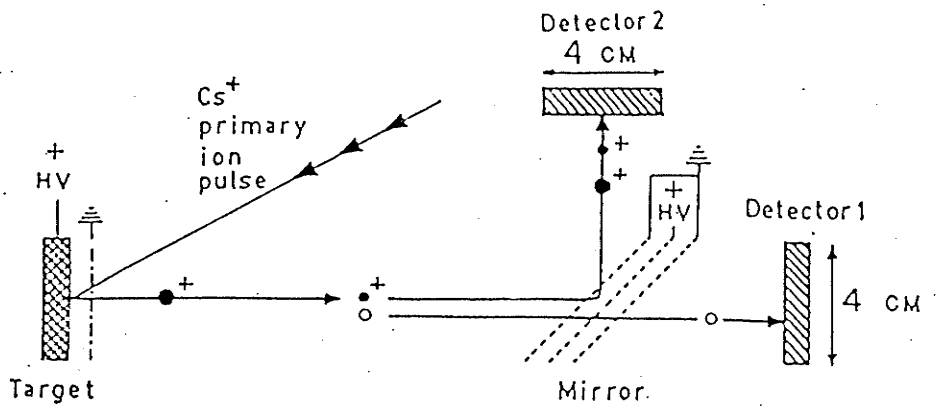

Figure 1.4. Instrumental arrangement for the analysis of positive ions

Although it is very convenient for measuring rate constants as well as daughter masses from metastable decay, the Manitoba TOF I instrument that contains a 45^{o} mirror does little to improve the resolution set by the initial velocity spread of the ejected secondary ions. Moreover, daughter mass measurement accuracy is limited, since masses are estimated from small flight time differences between the time of arrival of a daughter ion and that of its parent at the 90^{o} detector, after passage through the mirror.

To circumvent these difficulties, while keeping all other advantages of linear TOF instruments, the Manitoba TOF II mass spectrometer was constructed in 1985. Its schematic diagram is illustrated in figure 1.5.

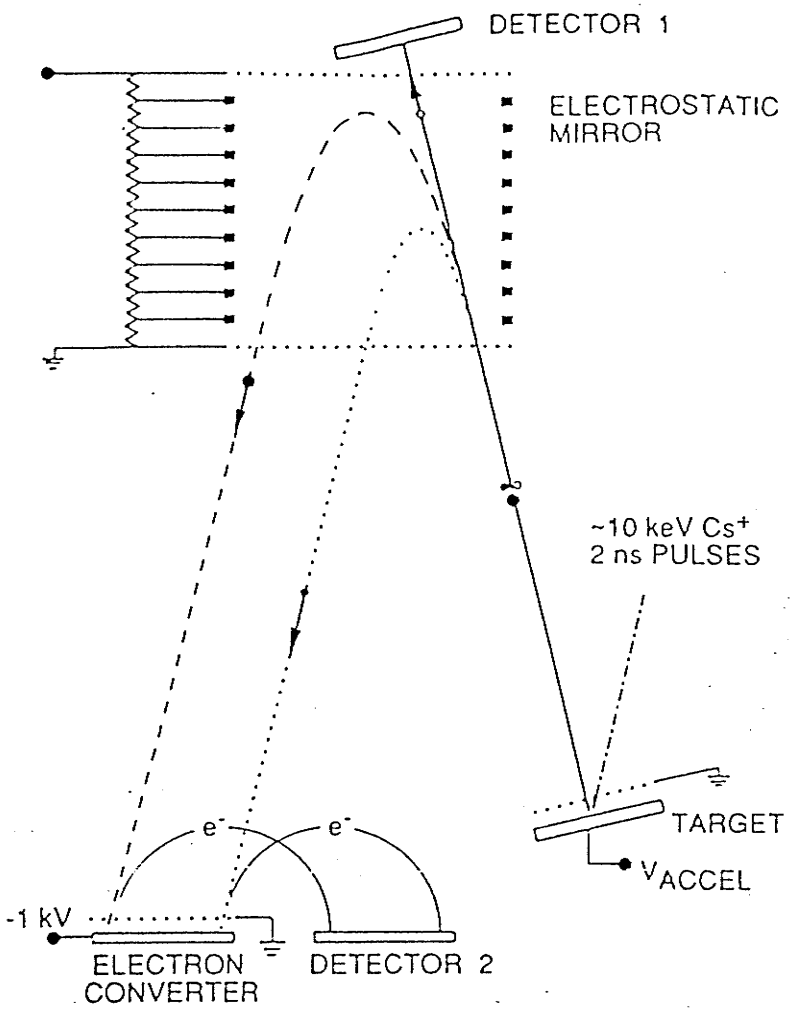

Figure 1.5. Schematic diagram of the Manitoba TOF II mass spectrometer

It is a reflecting time-of-flight mass spectrometer which incorporates an ion mirror to compensate for the initial velocity spread of the secondary ions, according to a principle developed by Mamyrin[128]. In such a configuration, ions of higher kinetic energy penetrate more deeply into the mirror than lower kinetic energy ions. The increased time spent in the mirror compensates for the shorter time spent in the total field free region of the instrument by the higher kinetic energy ions. Significant improvements in resolving power ($m/\Delta m_{FWHM}$ = 10000), an increase of ~3 over Manitoba TOF I [126],

as well as improved signal / background ratios, were achieved with Manitoba TOF II.

As shown in figure 1.5, this instrument uses two detectors. When an electric field is applied within the mirror, undissociated parent and daughter ions are reflected through ~177^{o} towards detector 2, while neutral fragments, unaffected by the mirror, pass through and strike detector 1. As described in chapter 4 of this thesis, correlations between charged and neutral daughter fragments yield information similar to that obtained by tandem (MS/MS) mass spectrometry[126,127].

Sample preparation and deposition of nucleic acid components analyzed in this work are described in the experimental sections of chapters 3-6. Detailed discussions pertaining to the data system[129-130], mass resolution and other parameters influencing Manitoba TOF I and TOF II specifications and performance have been discussed *in extensio* elsewhere[126,127,131].

1.3.2 Outline of this thesis

This thesis mostly describes how Manitoba TOF I and TOF II, in various configurations, can be used for differentiation of structural isomers and stereoisomers of small nucleic acid constituents.

While a number of reviews dealing with the implications of MS in general structural analysis of NACs have appeared over recent years, most of them have gravitated towards a particular MS technique. Chapter 2 reviews MS approaches used to differentiate isomeric NACs and closely related analogs. This review is presented, not on a MS technique basis, but on a class of compound basis: bases, nucleosides, nucleotides and small oligonucleotides.

Chapter 3 examines how O2- and O4-alkylthymidines can be distinguished by studying the rates of decomposition of metastable ions (+ve mode) with a small electrostatic mirror incorporated in the Manitoba TOF I mass spectrometer. Half-life

estimations are based on measurement of the proportion of parent ions that survive long enough to exit the ion mirror. The compounds studied were synthesized by Dr. K.L. Sadana, based on an idea of Dr. F.E. Hruska , both members of our chemistry department.

The same compounds have been investigated in the positive and the negative ion mode with the Manitoba TOF II mass spectrometer in chapter 4. The effect on fragmentation of the presence, size and location of the alkyl group is studied. Emphasis is placed on the interpretation of direct spectra with reference to their metastable ion decompositions, whenever they provide clues to mechanisms of ion formation.

Some protected oligonucleotides are analyzed in chapter 5. They include a pair of stereoisomeric trinucleotides and three pairs of positional isomers of an unusual kind: they contain either 3'-5' or 2'-5' phosphodiester bonds. This TOF-SIMS is performed on the Manitoba TOF II instrument in the direct, negative ion mode. To gain more insight on the structure-function relationships of these compounds, a series of analogous trinucleotides and a tetranucleotide that contain vicinal 2'-5' and 3'-5' phosphodiester linkages are also investigated. These branched RNA fragments, synthesized at McGill University by Dr. K. K. Ogilvie *et al*, are key constituents of lariats which are believed to play an essential role in the maturation process of RNA precursors.

Finally, in chapter 6, the level of complementarity between the FAB and TOF-SIMS approaches is evaluated for two pairs of isomeric dinuclotides, as well as three trinucleotides. Direct, negative TOF-SIMS results have been obtained on the Manitoba TOF II mass spectrometer, while the FAB spectra were recorded with the VG 7070E-HF double focussing instrument from our chemistry department. The presence and site of alkylation are discussed in terms of their effects on fragmentation patterns.

CHAPTER 2

ISOMERIC DIFFERENTIATION OF NUCLEOSIDES, NUCLEOTIDES AND OLIGONUCLEOTIDES BY MASS SPECTROMETRY

2.1 INTRODUCTION

Although many excellent reviews dealing with the application of mass spectrometry in the area of nucleic acid components have appeared over the last twenty years, most of them have focussed either on a particular mass spectrometric technique or on general structural determinations. This section focusses on the numerous approaches used by mass spectrometrists to single out differences between isomeric nucleosides, nucleotides and oligonucleotides. The compounds studied include structural isomers, stereoisomers and sequence isomers. In the first group are found structural isomers that differ in substituent or isotopic positions (base, sugar or phosphate), as well as in O-P bond positions. The second group includes enantiomers and diastereomers. The third group is composed of base sequence isomers, a special kind of structural isomers applicable to NACs larger than one nucleotidic unit. This review is comprehensive but not exhaustive. Only papers that discuss and show mass spectral analysis of two or more isomers have been used in this review. Excluded are cases where isomeric differentiation is discussed, but only one isomer has actually been analyzed, cases where mass spectrometry was not the main technique used to identify differences between isomeric compounds, cases where isomers were analyzed but reported data were either insufficient or devoid of clear isomeric indicators and also cases that really only show isomeric fragments stemming from molecular ions of nucleic acid components. In some instances isomers were produced by isotopic labelling either with deuterium or with 18-oxygen. These cases were excluded if they were mostly used to study fragmentation pathways of non-labelled

compounds. Whenever sufficient data were available for isomeric differentiation of labelled isomers, such examples were included in this review.

2.2 STRUCTURAL ISOMERS

2.2.1 Bases and nucleosides

Weller *et al* [132] have used +ve ion self chemical ionization Fourier transform ion cyclotron resonance (self-CI FT-ICR) to show differences between O6-methyl guanine, **1**, and 7-methylguanine, **2**. A $[2M+H]^+$ peak was seen for **1**, but not for **2**. On the other hand, a $[M+H]^{2+}$ peak was observed for **2**, but not for **1**. In all cases, abundant molecular ions were produced, with very little fragmentation.

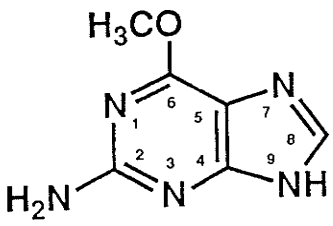

1

$[2M+H]^+$ (ex)

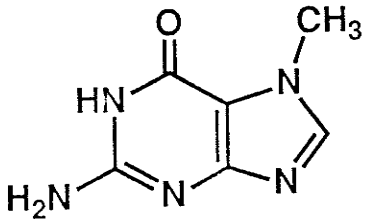

2

$[M+H]^{2+}$ (ex)

ex = exclusive

Negative ion CI mass spectra of four methyladenines were recorded by Hocart *et al* [70], but produced only $[M-H]^-$ ions (base peak) and $[M+13]^-$ ions of uncertain origin. However, when $[M-H]^-$ ions were subjected to collisionally activated dissociation with mass analyzed ion kinetic energy (CAD/MIKE) analysis of the products, all isomers could be distinguished on the basis of their $[M-H-(CH_3 \text{ or } NH_2)]^- / [M-H-(41 \text{or } 42)]^-$ ratios. The ratio increases according to mN6A < m3A < m1A < m2A. Contrary to the other three isomers, m2A contains a methyl group linked to a carbon atom instead of a nitrogen and is also the only one to contain a free NH_2 group. Its CAD/MIKE spectrum of $[M-H]^-$ ions is the only one to show a $[M-H-16]^-$ peak instead of a

$[M-H-15]^-$ peak.

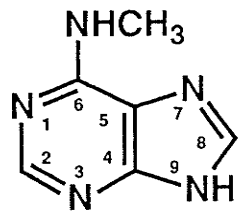

mN6A

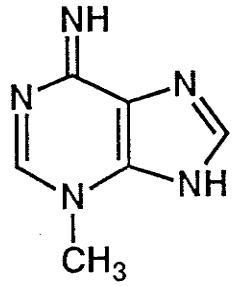

m3A

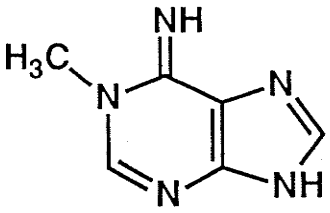

m1A

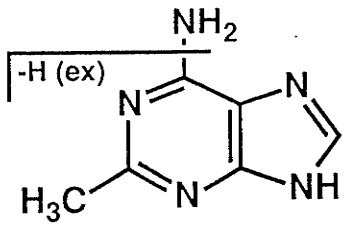

m2A

The two isomeric 2- and 4-selenouracils **3** and **4** were compared by Liehr *et al* [90], using +ve ion EI mass spectrometry. The corresponding thiated uracils **5** and **6** were included in that study. It was found, first of all, that molecular ion abundance was enhanced by replacement of selenium by sulfur. Positional effects differed, however. The positional order of molecular ion abundances was found to be 2>4 for selenouracils and 4>2 for thiouracils. Sequential losses of HCN and CO from $M^{+\cdot}$ of **3** led to ions at m/z 149 and m/z 121, respectively. This isomer, but not **4**, also produced an m/z 69 ion, $[HNC_2H_2CO]^+$, a typical fragment resulting from a retro-Diels-Alder reaction in which N-3, C-2 and attached groups are expelled from $M^{+\cdot}$. This process is also less apparent for **6** than for **5**. Direct expulsion of CO from $M^{+\cdot}$ was more favored from **6** than from **5**. The trimethylsilyl (TMS) derivatives of **3**, **4**, **7** and **8** were also examined. The position of selenium is easily derived by the presence of a prominent m/z 99 ion for **7** ($[C_2HOSi(CH_3)_2]^+$, derived from $[M-CH_3]^+$) which doesn't have a counterpart at m/z 163 for **8**.

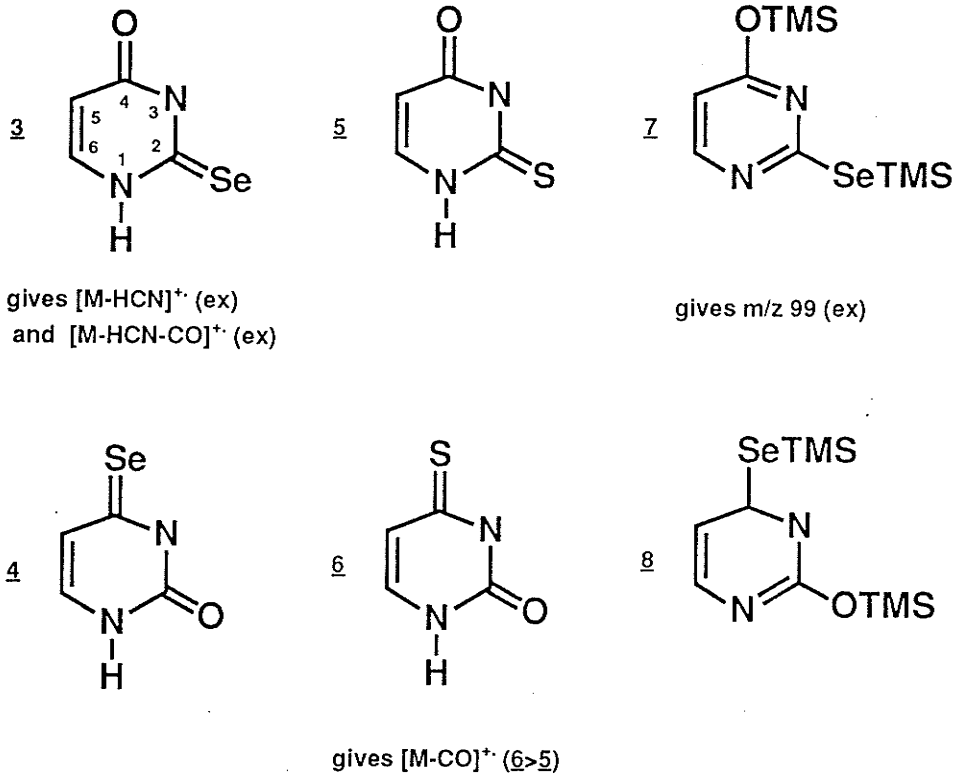

Hecht *et al* [133] also compared **5** and **6** by EIMS. Successive losses of HNCS and HCN from $M^{+\cdot}$ produced strong signals at m/z 69 and m/z 42 for **5**, which were almost absent in the EI spectrum of **6**. Conversely, ions at m/z 85 and m/z 58 corresponding to successive elimination of HNCO and HCN from $M^{+\cdot}$ were found in much greater abundance for the S4-isomer **6**.

The 2- and 4-thiouracil-$(TMS)_2$ derivatives were differentiated by McCloskey[62], using EIMS. An ion at m/z 99, $[C_4H_7SiO]^+$, in the TMS derivative of **5** was shifted to m/z 115 for **6**, corresponding to $[C_4H_7SiS]^+$, in accordance with the presence of sulfur in the 4- position.

The origin of ion **d** ($[BH+C_2H_3O]^+$, see below), which incorporates the nucleobase with C-1' and C-2' of the sugar unit, was clearly demonstrated by Jiang *et al*[94], who synthesized 2'-^{18}O (**9**) and 3'-^{18}O-adenosine (**10**) and compared their +ve EI mass spectra. With about 50% ^{18}-O incorporation, the mass spectra of **9** and **10** were very similar except for the presence of **d** ions. While the ratio $[B+44]^+/[B+46]^+$ was close to

1:1 for **9**, it turned out to be more than 15:1 for **10**, which is consistent with a **d** ion that includes the 2'-oxygen. The same results were observed for 2'-^{18}O- and 3'-^{18}O-(arabinofuranosyl)adenine.

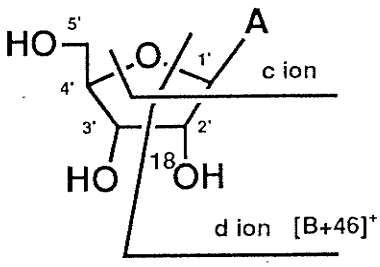

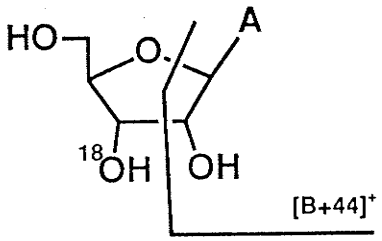

9 10

Wilson and McCloskey [67] have compared positive chemical ionization mass spectra (CIMS) of adenosines methylated at the 1- (**11**), N6 (**12**) and O2' (**13**) positions. With methane as a reagent gas, they found that the MH^+/BH_2^+ ratio of relative abundance (%RA) increased according to 1-methyl < N6-methyl < O2'-methyl (0.5:1:2.4, compared to 0.9 for adenosine), indicating that methylation of N1 causes the greatest increase in glycosyl bond lability. Compared to CIMS of adenosine, the relative abundance of $[B + 30]^+$ ions (**c** ions, see above) did not change with a CH_3 group on N1, but it was greatly increased with a methyl group on N6 and greatly reduced for the O2'-methyl isomer.

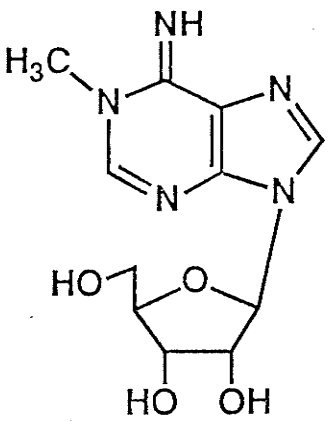

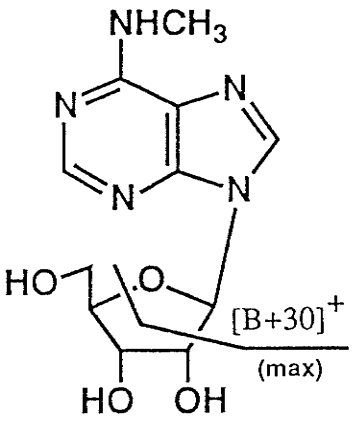

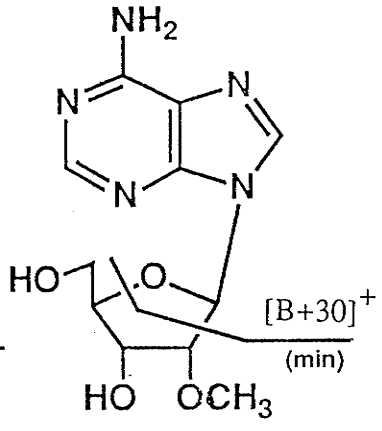

11 12 13

Replacement of methane by dimethylamine as CI reagent gas led to an increase in the MH^+/BH_2^+ ratio for all three isomers, with an almost complete suppression of BH_2^+ ions for **13**. This yielded support to their proposed mechanism of formation of BH_2^+ ions, that involved an O2'-hydrogen transfer to the base after the initial protonation of the parent molecule (scheme 1), with concomitant cleavage of the N-glycosyl bond. Substitution of the O2' hydrogen by a methyl group should induce a decrease in BH_2^+ ion relative abundance if this route is operative, which is indeed what is observed.

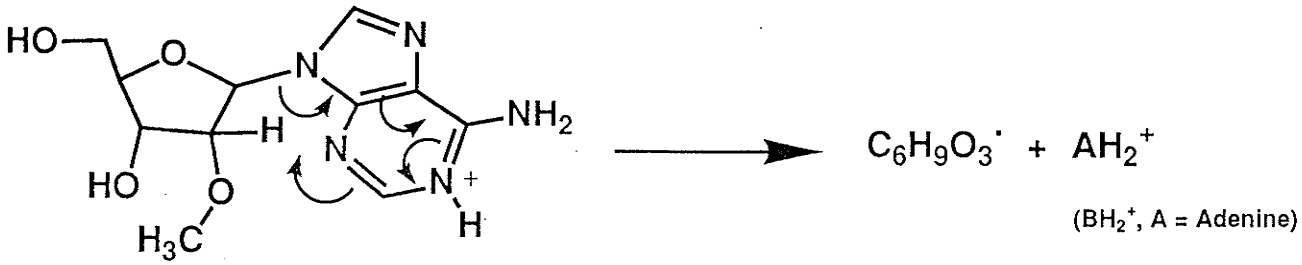

13

Scheme 1

Unger *et al* [85] have compared the iodide salt of 1-methyladenosine, **11**, with N6-methyl adenosine, **12**, by quadrupole secondary ion mass spectrometry (SIMS), and found in +ve ion spectra that the sensitivity for analysis of the former, which is a salt, was dramatically increased compared to the latter, which is a neutral compound. O2'-methyl adenosine **13** was also analyzed and distinguished from 1-methyl and N6-methyl isomers by the position of its base peak at m/z 136 (BH_2^+), instead of at m/z 150 for the other two compounds.

It appears that the CI conditions reported previously by Wilson [67] were much "softer" than the SIMS approach used by Unger *et al* [85], judging from the small %RA of MH^+ ions seen by SIMS. For example, no intact O2'-methyladenosine molecular ions

were detected by SIMS.

Negative ion electron ionization (EI) mass spectra of 1-, N6- and O3'-methyladenosine (**14**) obtained by Smith *et al* [134] showed very few differences between those compounds, except that **14** showed a much reduced abundance of m/z 71 ions, assigned as $[C_3H_3O_2]^-$, likely a result of ribose ion decomposition. In all instances, a very small %RA was observed for $[M-H]^-$ ions (1-2% of base peak, B^-).

Compounds **13** and **14** were differentiated by negative ion CI by Hocart *et al* [70]. Apart from the increase detection of B^- ions already mentioned above, **13** shows a greater abundance of $[B+56]^-$ ions and fewer $[B+42]^-$ ions than **14**, as depicted below. Selected ions from these spectra were subjected to collisionally activated dissociation with mass-analyzed ion kinetic energy (CAD/MIKE) analysis (tandem mass spectrometry). TMS derivatives of **13** and **14** were clearly distinguished by CAD/MIKE analysis of $[M-H]^-$ ions.

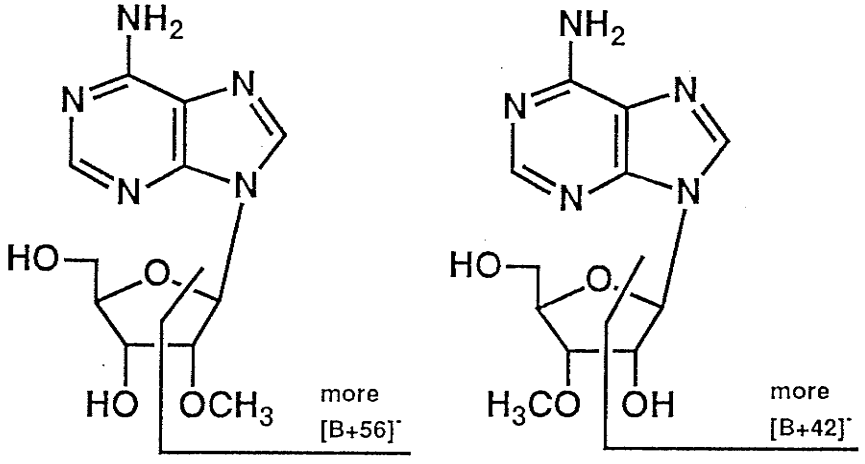

13 14

The involvement of H-2' in facilitating glycosyl bond cleavage was demonstrated by the greatly diminished abundance of $[S-H]^{+\cdot}$ when H-2' of isomer **15** is replaced by a methyl group (**16**). Positive EI mass spectra obtained by Pang *et al* [63] showed that the

$[S\text{-}H]^{+\cdot}$ %RA went from 10% to 0.6% for **15** and **16**, respectively (analyzed as TMS derivatives).

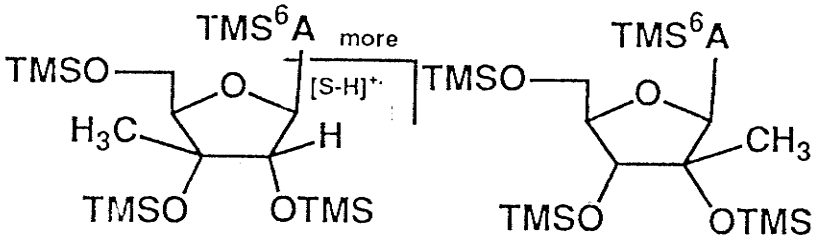

15 16

McCloskey [62] showed that the TMS derivative of 2'-O-methyladenosine (**13**) could be differentiated from that of 3'-O-methyladenosine (**14**) based on the fact that its +ve EI mass spectrum shows the loss of CH_3OH but not of trimethylsilanol from the molecular ion, while the latter shows both losses, an indication of selectivity for O-2' elimination.

Crow *et al* [73] have used fast atom bombardment (FAB)/CAD +ve ion mass spectra to demonstrate differences between O2'-methylguanosine (**17**), 1-methylguanosine (**18**) and N2-methylguanosine (**19**). The CAD spectrum of the $[M+H]^+$ ion of **17** shows a **c** ion at $[M+H-118]^+$ and a **d** ion at $[M+H-90]^+$, which confirm that methylation is at the 2'-oxygen, while the BH_2^+ fragment (the most prominent ion in both the full mass spectrum and the CAD spectrum) shows that substitution is not on the base portion of the molecule. Methylation on either N2 or N1 of guanine is confirmed by the 14 u shift in the mass of BH_2^+ ions . The difference between **18** and **19** is the presence in the latter of a m/z 136 peak corresponding to the loss of $NHCH_3$ from BH_2^+. No such signal is apparent for **18**.

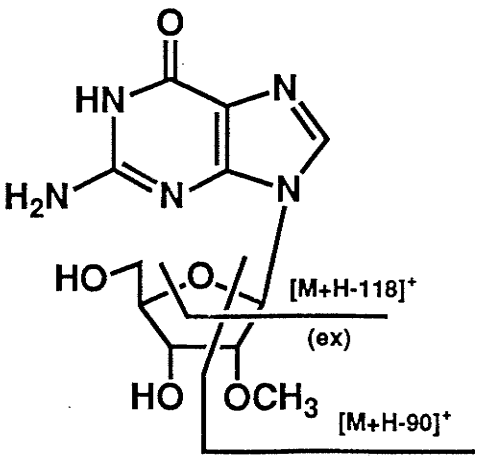

17

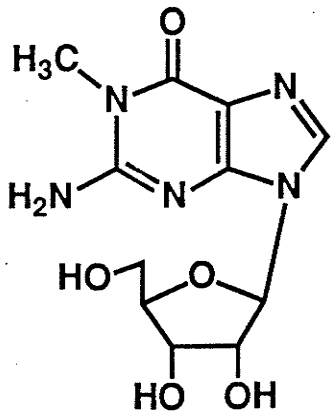

18

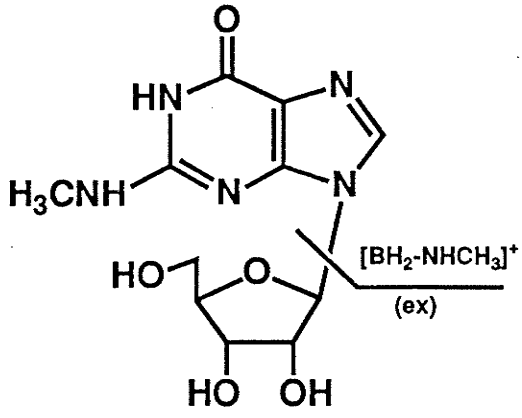

19

Negative ion laser desorption (LD)/FTMS was used by McCreary and Gross [115] to differentiate 1-methylguanosine (**18**) from O2'-methylguanosine (**17**). While the base peak was B^- for **18**, its %RA for **17**, for which it was shifted to lower mass by 14 u, was only 37%. Instead, the base peak in the spectrum of **17** was found at m/z 115. It could correspond to $[S\text{-}CH_3OH]^-$. Mass spectra of **18** and **17** differed also in the following: more than twice as much $[M\text{-}H]^-$ for **17** as for **18** (47% vs 20%); the presence of $[M\text{-}H\text{-}NHCO]^-$ and S^- peaks for **18** not seen for **17**.

Cory *et al* [135] studied +ve ion EI mass spectra of eleven monobenzylated nucleosides, including O3'-benzyladenosine (**20**), as well as its O5'-benzyl (**21**), N6-benzyl (**22**) and O2'-benzyladenosine (**23**) isomers. They found that the tropylium (m/z 91) ion was much less abundant for **22** , where the benzyl group is linked to a nitrogen atom. On the other hand, **22** was the compound that showed the greatest $M^{+\cdot}$ %RA. The benzylated adenine base is also readily distinguished from all other compounds by the position of its $[B+H]^+$ signal at m/z 225. Compound **21** was the only one not to show a $[M\text{-}30]^+$ signal (loss of CH_2O), giving a facile means to determine that O5'- is blocked. Its $[B+30]^+$ ions had a higher %RA with respect to the base peak (m/z 91 or $[B+2H]^+$). The **d** ions, which appear at $[B+134]^+$ for **23**, allowed facile identification of that isomer.

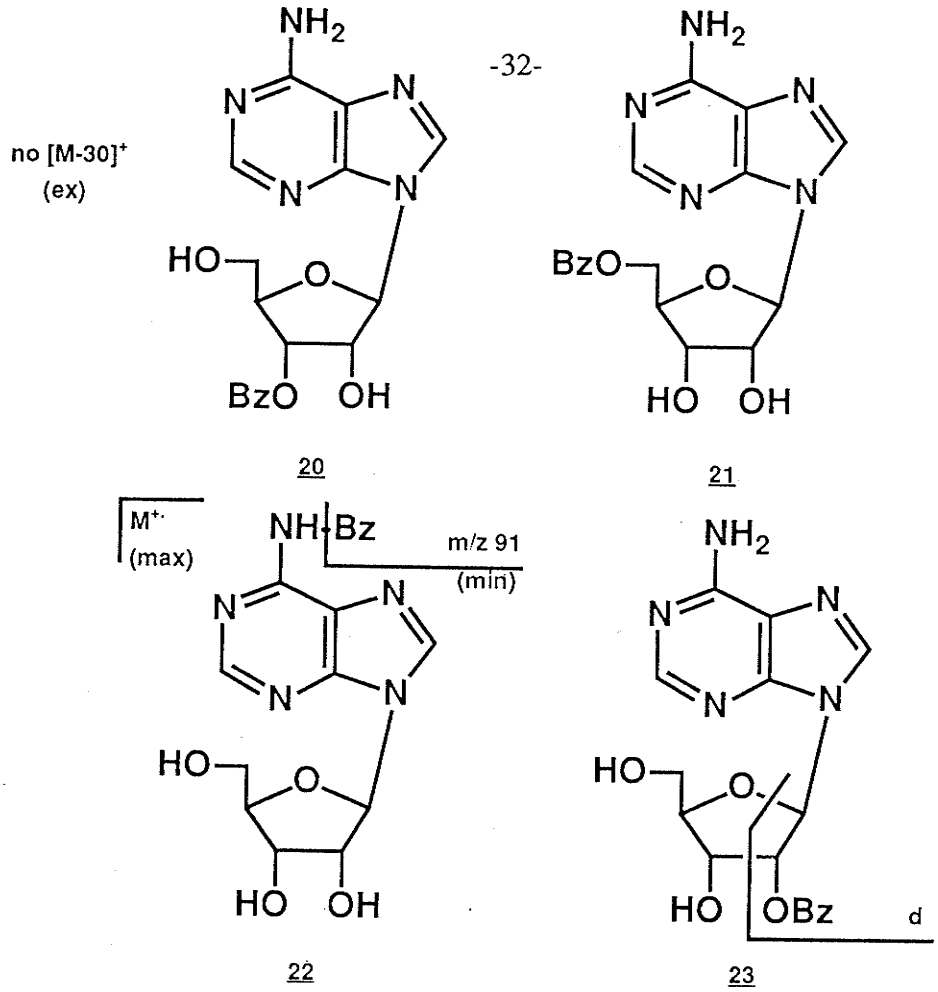

20 21 22 23

Three other pairs of O2'-benzyl and O3'-benzyl nucleosides were compared in the same study. While no real differences could be seen in the cases of O2'- (**24**) and O3'-benzylguanosine (**25**), the authors were able to find isomeric indicators between O2'- and O3'-benzyl uridine and inosine, **26**, **27** and **28**, **29**, respectively. First of all, O3'-isomers showed BH^+ ion %RA 2-3 times greater than those of O2'-isomers, while the latter compounds showed at least twice as much BH_2^+ in their +ve EI spectra. In addition, in the case of **26**, the %RA values for $[B+44]^+$ ions (**d** ions) were 17 times greater than they were for **27**. These ions are shifted to greater masses by 90 u for the O2'-benzylated compounds, which is another isomeric indicator.

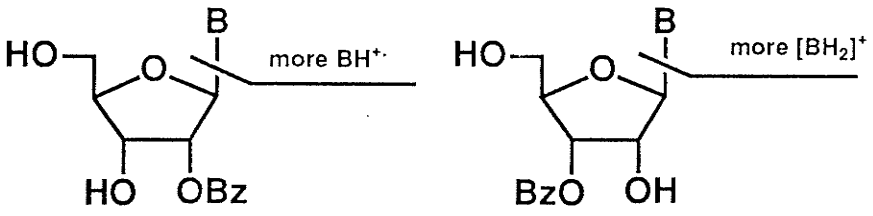

Base	*Benzyl* O2'	O3'
G	24	25
U	26	27
inosine	28	29

Positive ion FAB mass spectra of a series of 1- (**30**), N2- (**31**), O6- (**32**), 7- (**33**), and 8-(p-Y-benzyl)guanosines (**34**) (where Y included CH_3O-, H- and O_2N-) were examined by Tondeur *et al* [72] in order to identify spectral characteristics that might distinguish these positional isomers. For p-NO_2-benzylguanosines, the O6-derivatized compound showed by far the greatest relative amount of $[S+2H]^+$ ions and the smallest amount of BH_2^+ ions. The %RA of $[M+H]^+$ was greatest for N2- and C8-derivatized isomers, *i.e.* twice as great as for the others. The only difference between these two isomers is the much greater tendency for the C8-derivatized compound to lose its benzyl group. Compared to all other isomers, the latter also showed a much reduced GH^+ %RA. The N7- and N1-derivatized compounds also had very similar mass spectra. The +ve charge retention on the guanine base instead of the benzyl group was much greater for these two isomers than for any other compound, as attested by much higher $[MH-(pY-C_7H_7)]^+$ (see meaning of pY below) and GH^+ signals relative to $pY-C_7H_7^+$. The only notable difference between the spectra of N1- and N7-derivatives was the greater tendency of the latter to lose neutral $pY-C_7H_7$ from MH^+.

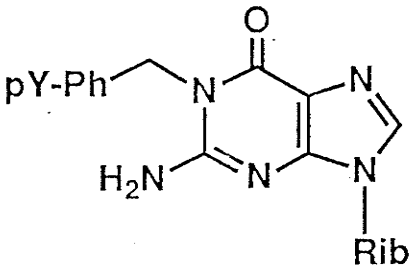

30

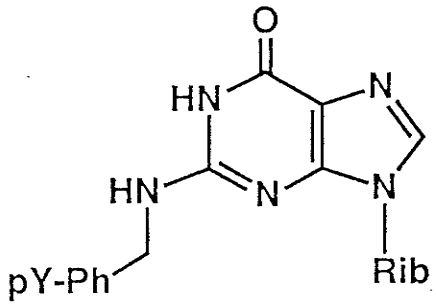

31

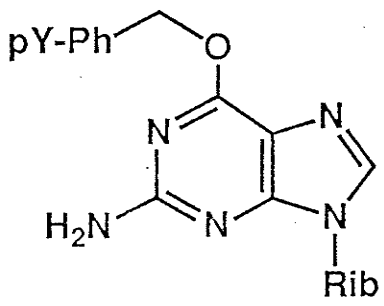

32

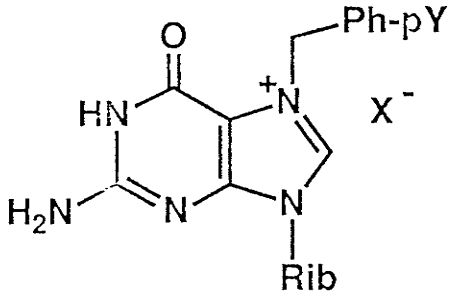

33

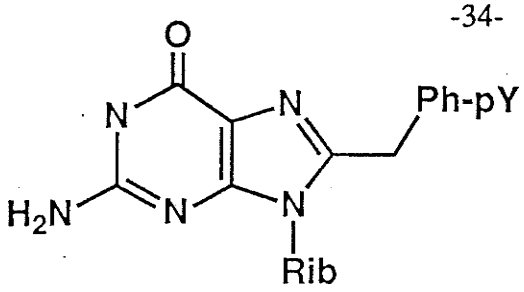

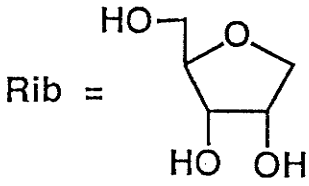

Y = H , H_3CO , NO_2

34

For p-OCH_3-benzylguanosines, C8 showed the greatest relative abundance of MH^+ and BH_2^+, an indication that its pBz-C bond is not broken as readily as it is for all other isomers. On the other hand, N2 and N7 showed the greatest tendency to produce pY-$C_7H_7^+$ ions as opposed to $[MH_2\text{-}(pY\text{-}C_7H_7)]^+$ or GH^+ ($[BH_2\text{-}(pY\text{-}C_7H_7)]^+$) ions. The main difference between N2 and N7 was the greater ratio of BH_2^+/ GH^+ signals for the former. N1 and O6 produced the greatest amount of $[MH_2\text{-}(pY\text{-}C_7H_7)]^+$ and GH^+ ions, though N1 had a greater tendency than O6 to produce BH_2^+ and $[BH_2\text{-}(pY\text{-}C_7H_7)]^+$ ions. For benzylguanosines, C8- showed the least amount of $C_7H_7^+$, and the largest amount of BH_2^+ ions. N1- produced the greatest abundance of $C_7H_7^+$ ions. The BH_2^+ / MH^+ and GH^+ / $[MH_2\text{-}C_7H_7]^+$ ratios were at least 3 times greater for N7 than for any other isomer. N2 was second lowest for detection of $C_7H_7^+$ and lowest by far in loss of C_7H_7 from either MH^+ or BH_2^+. Only C8 came close to N2 in that respect. In general, for p-CH_3O- , H- and NO_2-benzyl guanosines, increased electron-donating ability to the benzene ring resulted in increased formation of pY-$C_7H_7^+$ fragments, regardless of its origin on the guanine base. The tendency to lose the pY-C_7H_7 group as a neutral fragment also increased according to the trend CH_3O- < H- < O_2N- for all isomers.

The $M^{+\cdot}/[M\text{-}15]^+$ ratio was used by Pang *et al*[63] to differentiate TMS-derivatives of a series of three 2-substituted adenosines (**35**) and their respective 6-substituted position isomers (**36**, see below). In each instance, the $M^{+\cdot}/[M\text{-}15]^+$ ratio was at least 10 times larger when the TMS group is on the 2-position, an effect attributed either to increased siliconium stabilization (Westmore *et al* [136]) when the NHTMS group is not on the C-2-position, or increased $M^{+\cdot}$ stabilization when NHTMS is on the C-2 position.

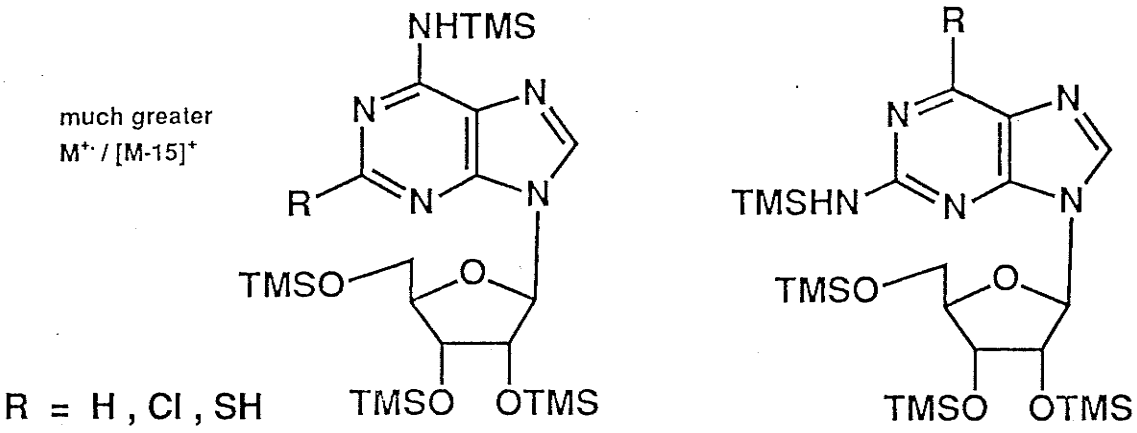

35 36

8-bromotubercidin (37) and 7-bromotubercidin (38) have been differentiated by Crow *et al* [73] using FAB/CAD spectra of $[M+H]^+$ ions. Although +ve and -ve ion FAB mass spectra of **37** and **38** are the same, the CAD spectrum of **38** showed a prominent $[M+H-HBr]^+$ peak not apparent for **37**. Interaction between an N6 -hydrogen and Br was thought to be the likely cause of HBr loss; these hydrogens could be accessible to Br on the 7-isomer, but not on the 8-isomer.

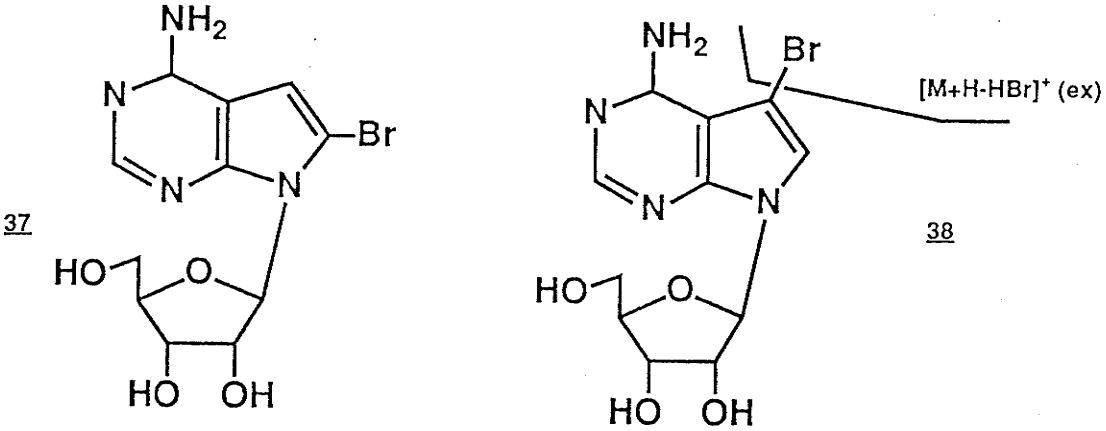

37 38

N4,O2'-dimethyl cytidine **39** and C5, O2'-dimethylcytidine **40** were differentiated by Edmons *et al* [137] using deuterium exchange from liquid chromatography (LC) thermospray mass spectrometry in D_2O. MD^+ ions from **40** contain 5 deuterium atoms (4 exchangeable hydrogens) and were detected at m/z 277 while MD^+ ions from **39**, containing three exchangeable hydrogens, were detected at m/z 276.

Negative ion LD/FTMS was used by McCreary and Gross[115] to distinguish 3-methyl (**41**) from O2'-methyluridine (**42**). Striking differences were reported. First of all, only three major ions were observed in the mass spectrum of **42**: a prominent $[M-H]^-$ peak (56%), a $[M-H-NHCO]^-$ peak (50%) and the B^- signal, the base peak. This B^- peak was also the most prominent one in the mass spectrum of **41**, where it was shifted to higher masses by 14 u. The $[M-H]^-$ ion for **41** was not stable enough under these conditions to be detected at all, and there was also a much smaller $[M-H-NHCO]^-$ peak for **41** compared to **42**. Finally, **d** ions ($[B+42]^-$, 10%) were observed for **41**, but not for **42**.

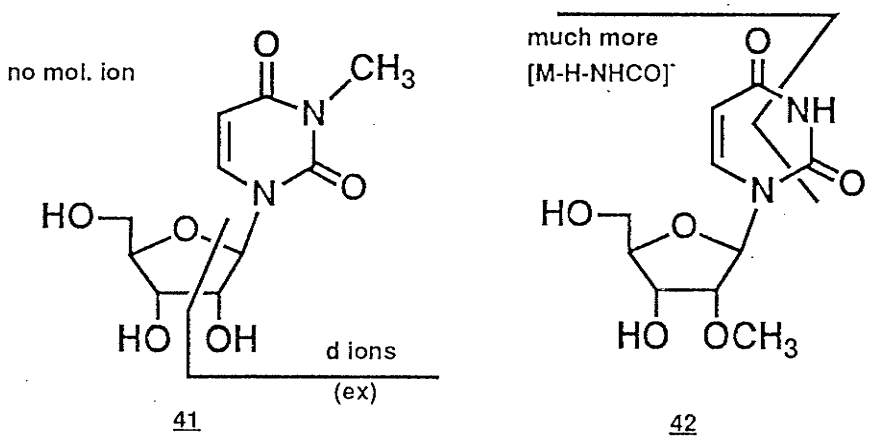

41 42

Comparisons between uridine (**43**) and pseudouridine (**44**) have been made by many groups. First, in a -ve ion EI study of **43** and **44**, Smith *et al* [134] have found that B^- ions produced the base peak for **43**, but were almost absent for **44**, while **d** ions produced the base peak for **44**, but were of very small %RA for **43**. Finally, while fragments from ribose decomposition were observed for **43** at m/z 71 and m/z 58, they were hardly found at all in the -ve ion EI spectrum of **44**.

Crow *et al* [73] produced FAB/CAD mass spectra of $[M-H]^-$ ions of **43** and **44** that were quite similar to those reported by Smith *et al* under EI conditions, with the same base peaks (B^- for **43**, $[B+42]^-$ for **44**). The $[B+28]^-$ ions were 9 times more intense for **44** than for **43**, while $[M-H-HNCO]^-$ ions were detected with a 76% RA for **43** but were

not found in the $[M-H]^-$ FAB/CAD mass spectrum of **44**.

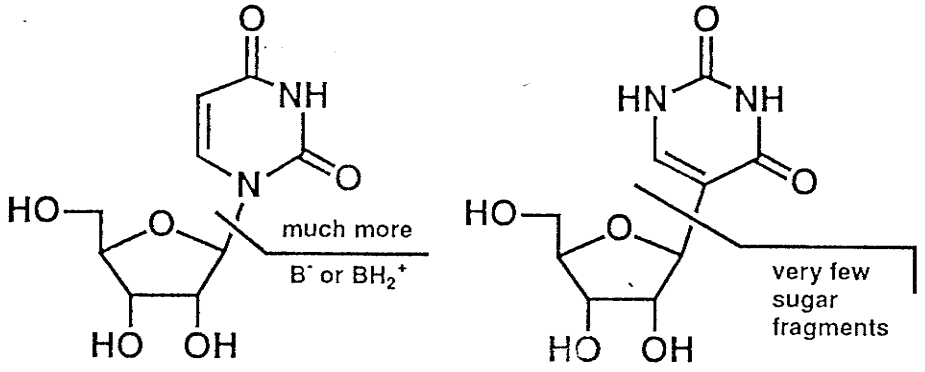

43 44

Compounds **43** and **44** were also compared by Slowikowski and Schram using FAB, CI and EI techniques in the +ve ion mode [23]. The greater strength of the C-C base-sugar bond of pseusouridine relative to the C-N bond of normal nucleosides led to increased relative intensity of $[M+H]^+$ ions for **44** compared to **43** with FAB and CI mass spectrometry. The base peak ion for **43** was BH_2^+ for all techniques while $[M+H]^+$, $[B+44]^+$ and $[B+30]^+$ (the two latter formed by sugar fragmentation with retention of the base-sugar bond) were the most prominent ions for **44** with FAB, CI and EI, respectively. Not surprisingly, as noted by Smith [134] and Crow [73], in the -ve ion mode, these two isomers could also be differentiated by the very small %RA of sugar fragments (not even detected by FAB and EI) for **44** compared to **43** , where S^+ varies in RA from 11% by FAB, to 57% by EI.

Sochacki *et al* [138] compared 2-thiouridine (**45**) and 4-thiouridine (**46**) by +ve ion EI mass spectrometry. The occurrence of a prominent $[B+41]^{+\cdot}$ ion in the mass spectrum of **45**, but not in that of **46**, led the authors to suggest that the sulfur atom at the 2-position facilitates the formation of $[B+41]^{+\cdot}$ ions.

Looking at the same compounds by EI in the -ve ion mode, Smith *et al* [134] found a $[B+43]^{-\cdot}$ ion at m/z 170 (9%) for **46** and no such ion for **45** (except a small $[B+42]^-$ ion

at m/z 169) (<1%). The only other significant difference reported between **45** and **46** was the much increased %RA of m/z 58 for **45** (assigned to NCS^-). Perhaps the clearest evidence to distinguish **45** from **46** is found in the FAB/CAD spectra of their respective $[M-H]^-$ ions, reported by Crow *et al* [73]. For **45**, prominent **d** ions were found (23%), but not for **46**, in contrast of what had been seen by Smith *et al* [134]. $[M-H-NHCO]^-$ ions were also seen only in the FAB/CAD spectra of **46**. Distinctive of **46**, in addition, was the absence of the familiar NCS^- ions at m/z 58 (present for **45**).

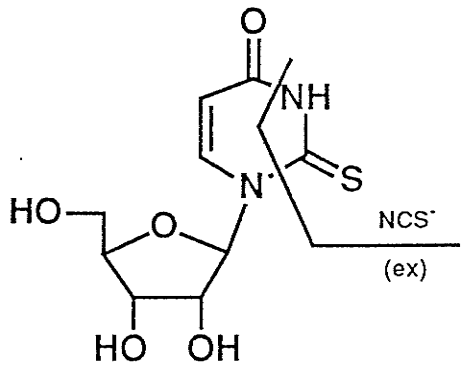

45

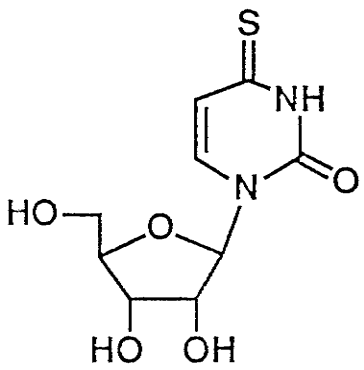

46

Sochacki [139] used the $[B+41]^{+\cdot}$ ion to differentiate a series of modified uridines (**47**) and their N3- isomers (**48**) by +ve ion EIMS. The four pairs of isomers analyzed are shown below. They found that the production of $[B+41]^{+\cdot}$ ions was always greater for N3-isomers than for their N1 counterparts, and could therefore be used for differentiation. They also found, on the other hand, that when the 2-oxygen was replaced by sulfur, the trend was completely reversed and that the $[B+41]^{+\cdot}$ ion was of significantly lower abundance for N3-isomers than for N1-isomers. Their rationalization for these results was a lack of double bond conjugation with the thiocarbonyl group, which appears to be important in the stabilization of the $[B+41]^{+\cdot}$ ion.

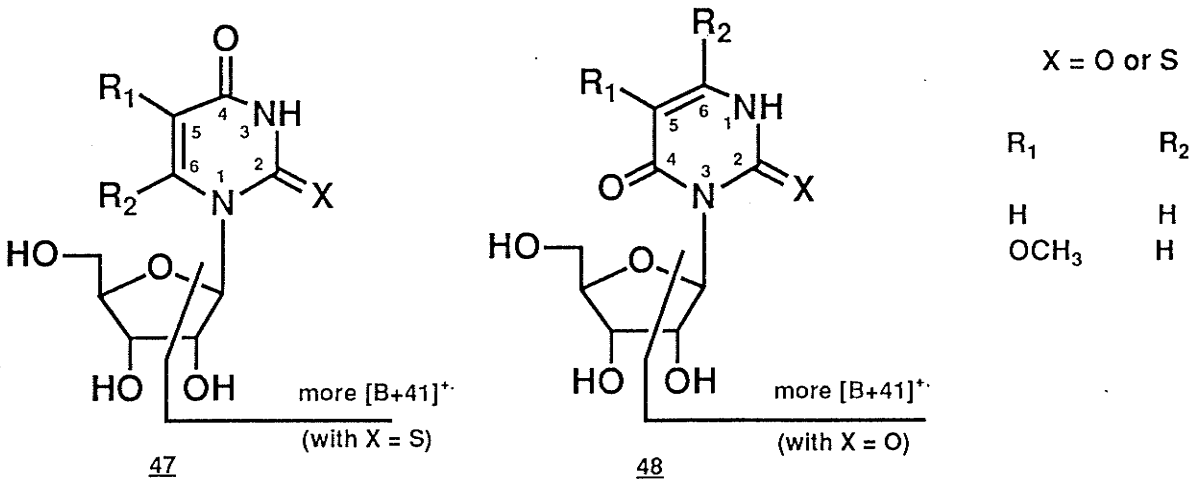

47 48

Schubert *et al* [140] have compared +ve ion EI mass spectra of the mesoionic 8-(β-ribofuranosyl)thiazolo[3,2a]-pyrimidine-5,7-dione (**49**) and a non-mesoionic analog (**50**) to determine if differences in fragmentation patterns attibutable to the mesoionic heterocyclic system were apparent. The spectra of both compounds reflected a pronounced "purine" character, *i.e.* strong $BH^{+\cdot}$ and weak S^+ ions, even though the N-glycosyl bond is made with a pyrimidine ring. Significant differences between **49** and **50** included peaks at m/z 140 ($[BH\text{-}CO]^+$), m/z 127 ($[BH\text{-}C_2HO]^+$) and m/z 100 ($[BH\text{-}C_3O_2]^+$), present only in the spectrum of **49** . In addition, contrary to mass spectra usually obtained from nucleosides (and from **50**), no fragment associated with cleavages across the sugar ring were detected in the mass spectrum of **49**.

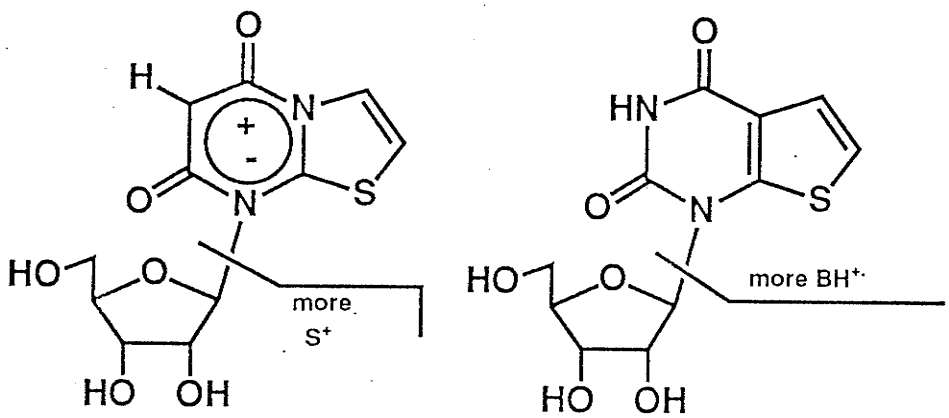

49 50

The CAD/MIKE spectra of the $[M-H]^-$ ions generated by CI (-ve mode) [70] were recorded to distinguish between the TMS derivatives of 2'-, 3'- and 5'-deoxyadenosine (**51**), (**52**), (**53**). Characteristic $[B+26]^-$ ions were found for **51**, with corresponding $[B+41+TMS]^-$ ions for **52** and **53**, while the same analysis applied to $[M-TMS]^-$ ions led to $[B+27-TMS]^-$ for **51** and to $[B+42]^-$ ions for **52** and **53**. Negative ion CI spectra with ammonia as reagent gas showed the greatest differences between **52** and **53**. On the one hand, B^- ions were seen in much greater relative abundance and $[B+H-TMS]^-$ ions were much less abundant for **52** than for **53** (and **51**); on the other hand, $[M-TMS-TMSOH]^-$ ions were more abundant for **52** (and **51**, for that matter), while $[M+H-2TMS]^-$ signals were detected in greater amounts for **53**.

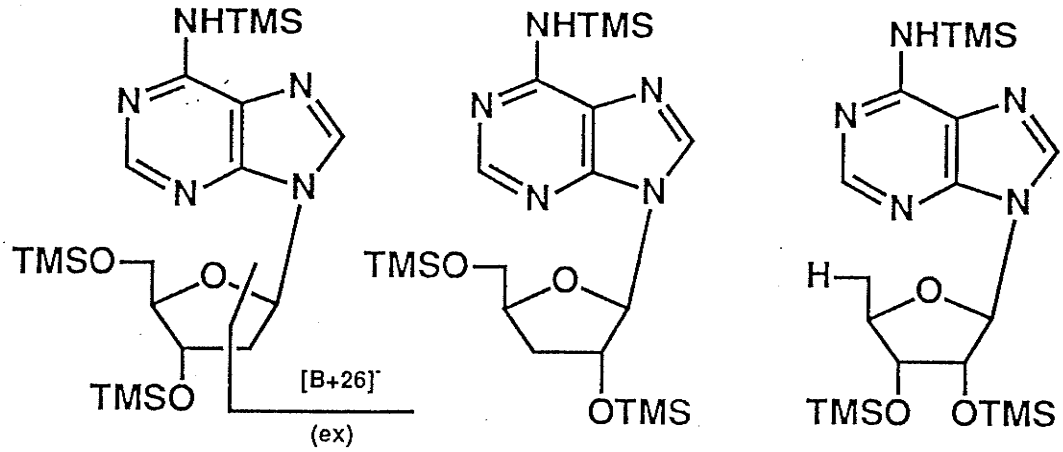

51 52 53

Pang *et al* [63] showed the influence of O2' in stabilization of the odd-electron $[S-H]^{+\cdot}$ ion since 2'-deoxyadenosine (**51**) led to a $[S-H]^{+\cdot}$ signal whose relative intensity was 15 times lower than that of 3'-deoxyadenosine (**52**) and 33 times lower than that of 5'-deoxyadenosine (**53**) (all as TMS derivatives).

Alder *et al* [92] studied the fragmentation of 2'- (**54**), 3'- (**55**) and 5'- (**56**) halogenated deoxyuridines (shown below) by +ve ion EIMS. They found, first of all,

that $[M\text{-}HX]^+$, $[M\text{-}HX\text{-}HCHO]^+$, $[S\text{-}H_2O]^+$ and $[M\text{-}HX\text{-}CH_3O_2]^+$ ions were much more prominent for 2'-halo than for 3'- and 5'-halo compounds. Conversely, 2'-halo isomers were the only ones that did not produce $[M\text{-}H_2O]^+$ ions and they had the lowest abundance of **c** ions. Compared to 3'-halogenated compounds, 5'-isomers showed signals much greater for $[M\text{-}H_2O]^+$, twice as great for S^+, and three times as great for **d** ions. The nature of the halogen did not appear to have a definite bearing on these trends. Globally, therefore, the trends observed were

$[M\text{-}H_2O]^+$	:5' only
$[M\text{-}HX]^+$	:2' only
$[S\text{-}H_2O]^+$	:3', 5' << 2'
$[M\text{-}HX\text{-}HCHO]^+$	:3', 5' << 2'
$[M\text{-}HX\text{-}CH_3O_2]^+$	:3',5, << 2'
$[B+30]^+$	:2' << 3' < 5'

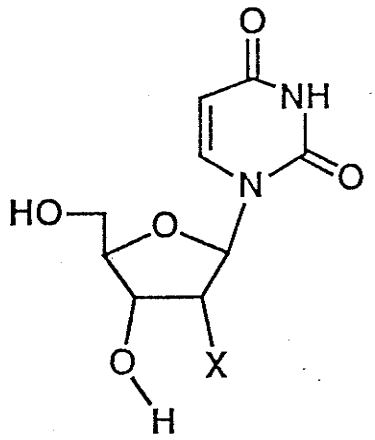

54

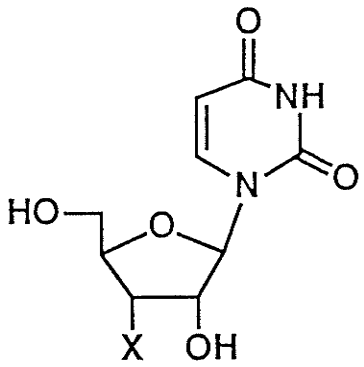

55

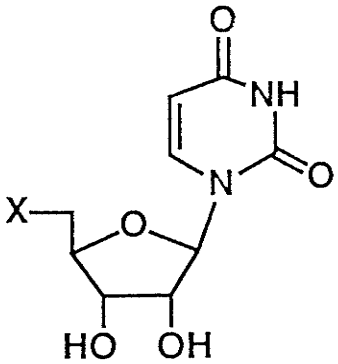

56

X = F , Cl , Br

Mikhailopulo *et al* [144] have used +ve ion EI to compare a series of halogenated pyrimidine and adenine nucleosides that included isomeric pairs such as 3'-chloro-3'-deoxyadenosine (**57**) and 2'-chloro-2'-deoxyadenosine (**58**), as well as

3'-chloro-3'-deoxyuridine (**59**) and 2'-chloro-2'-deoxyuridine (**60**). First of all, **57** showed a greater propensity to form $[M\text{-}Cl]^+$, and showed also a $[B+30]^+$ ion with 50% greater relative abundance than did **58**, while **58** showed almost three times as much **d** ion compared to **57**. For **58**, **d** ions were shifted 18/20 u to higher mass (m/z 196/198) compared to corresponding **57 d** ions (m/z 178). On the other hand, the loss of HCl from $M^{+\cdot}$ produced a very intense peak in the EI spectrum of **60**, not observed with **59**. The loss of HCl was also found from **d** ions. The cleavage of the N-glycosyl bond was a much favored decomposition pathway for **60** compared to **59**, as attested by much increased amounts of S^+, BH^+ and BH_2^+ for the **60** isomer.

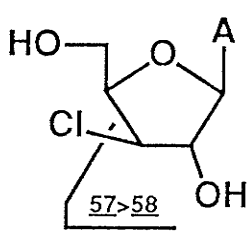

57

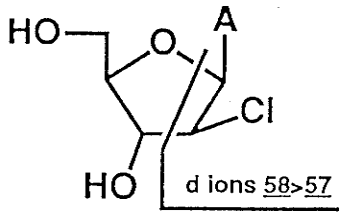

58

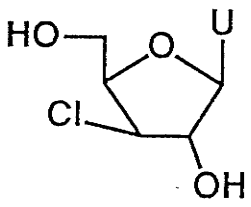

59

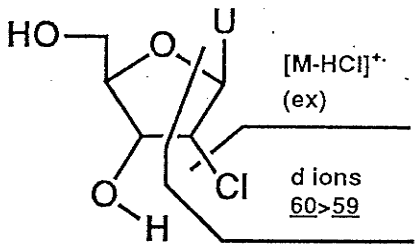

60

N3- and N4-(2-hydroxy-3-phenoxypropyl)deoxycytidine (3-RdC, (**61**), and 4-RdC, (**62**), were differentiated by Claereboudt *et al* [142] by FAB/CAD spectra of $[M+H]^+$ and $[M-H]^-$ ions. The daughter ion spectrum of $[M+H]^+$ of **61** showed a very intense $[BH_2\text{-}R]^+$ ion peak, which was almost absent in the equivalent spectrum of **62**. In the -ve ion mode, the CAD spectra of $[M-H]^-$ of **61** showed a distinctive $[M\text{-}H\text{-}RNCO]^-$ ion, while for **62** it was the NCO^- ion (m/z 42) and the $[\mathbf{d}\text{-}42]^-$ ion that were exclusive to that isomer.

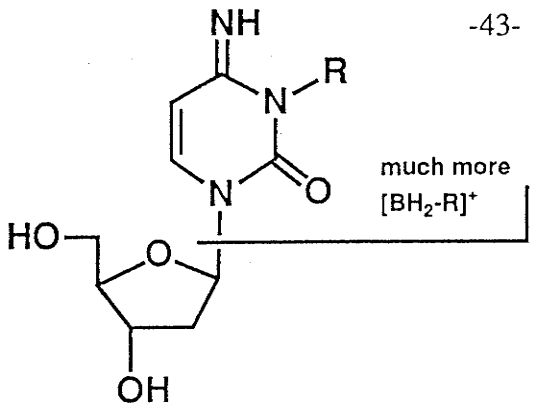

61

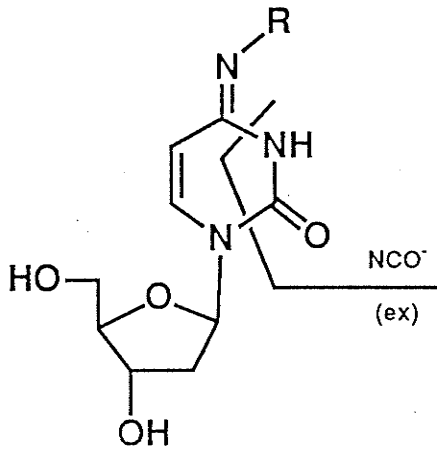

62

R = H_2C-CHOH-CH_2-OPh

Quilliam *et al* [25] studied +ve ion EI mass spectra of 2'-deoxynucleosides protected either at the 3'- (**63**) or 5'-position (**64**) with a silyl (t-butyldimethylsilyl) group. They found that $[M\text{-}R]^+$ ions (where R = t-Bu) were precursors for most prominent ions in the spectra and that decomposition pathways for those ions are dependent on isomeric form. For example, $[M\text{-}R\text{-}H_2O]^+$ and $[M\text{-}R\text{-}2H_2O]^+$ were present only in the mass spectra of 5'-O-silyl isomers, while $[M\text{-}R\text{-}H_2O\text{-}BH]^+$ ions were also more abundant for those compounds. Certain isomeric pairs (e.g. for B = U or T) produced mass spectra showing $[M\text{-}R\text{-}(B+C_2H_3)]^+$ ions that were much more prevalent from 3'-O-silyl isomers, a finding attributed to a lesser ability of the 5'-oxygen atom to stabilize the siloxonium ion produced along this fragmentation pathway. $[BH+(CH_3)_2SiOH]^+$ ions were also significant only for 3'-O-silyl compounds.

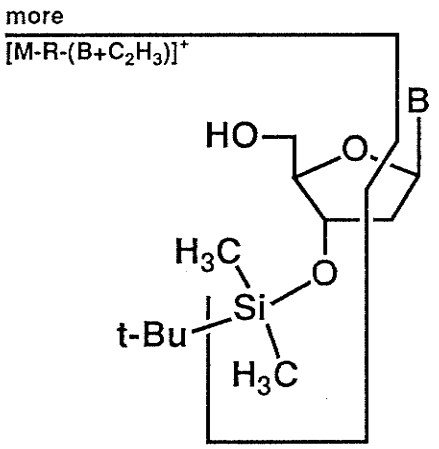

63

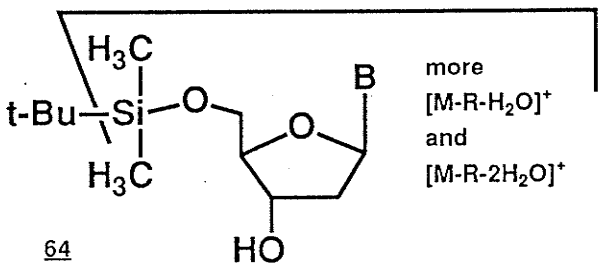

64

B = C, U, A, T, G

O2',3'-anhydroadenosine (**65**) and O3',5'-anhydroadenosine (**66**) were compared by Mikhailopulo *et al*[141] . The most noticeable difference between **65** and **66** is a 7 times greater $M^{+\cdot}$ relative abundance for the latter as well as a significant (18%) amount of **d** ion, which is completely absent in the +ve EI spectrum of **65**.

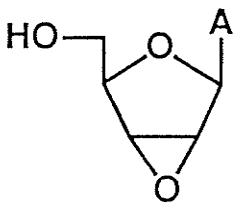

65

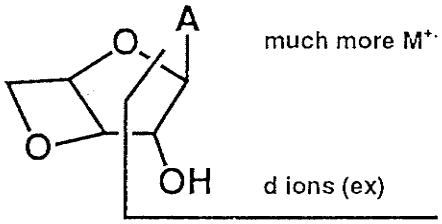

66

Puzo *et al* [58] compared O6,5'-anhydrouridine (**67**) and O2,2'-anhydrouridine (**68**) by +ve ion EI mass spectrometry. **67** showed a distinctive m/z 153 ion and **68**, a m/z 137 ion. A prominent fragment ion of mass 110 (70% RA) derived from the m/z 153 ion was also found in the EI spectrum of **67**. This ion, judged to be formed by retro Diels-Alder expulsion of HNCO, was absent for **68**, which doesn't contain the required cyclohexene-type structure for this ion to be formed.

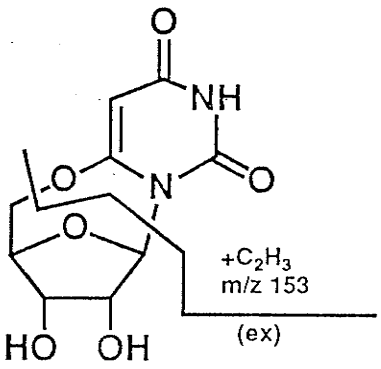

67

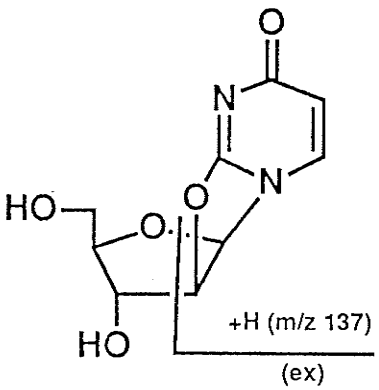

68

Westmore *et al* [58] compared 3',5'-di-O-acetyl-2,2'-anhydrouridine where the acetyl group had been deuterated either on the 5'-position (**69**) or on the 3'-position (**70**) by +ve ion EIMS. They found significant production of $[M\text{-}CH_3CO_2]^+$ (10%) for **69** and of $[M\text{-}CD_3CO_2]^+$ (17%) for **70**, demonstrating that the neutral fragment was lost

nearly exclusively from the 3'-position of the ribose ring. A second isomeric indicator was the presence of $[M\text{-}CD_2CHO]^+$ (16%) for **69** and $[M\text{-}CH_2CHO]^+$ (29%) for **70**, which showed that the loss of the 5'-acetyl group was much greater than that of the 3'-acetyl group.

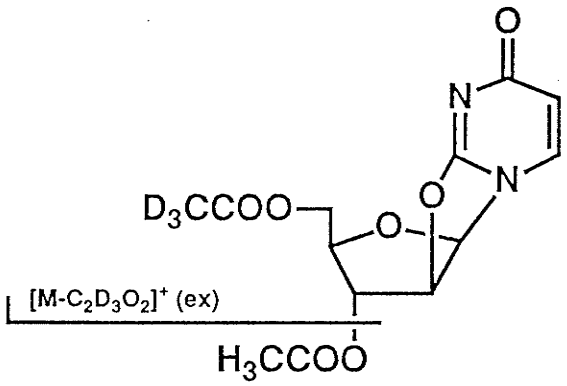

69

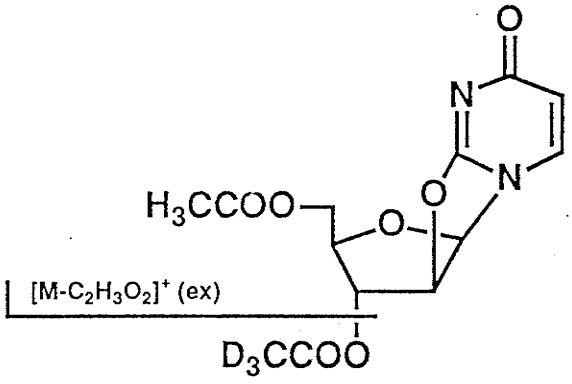

70

Ulrich *et al* [66] studied and compared the mass spectra of furanic (**73**) and pyranic (**72**) forms of thymidine, as well as those of their acetates by +ve ion EIMS. For non-acetylated compounds, S^+, $[BH+C_2H_3]^+$ and $[BH+C_2H_3\text{-}HNCO]^+$ ions were more abundant for **71** isomers, but these compounds showed a much lower abundance of $[M\text{-}2H_2O]^{+\cdot}$, $[S\text{-}H_2O]^+$, $[S\text{-}H_2O\text{-}H_2CO]^+$ ions compared to **72** compounds. On the other hand, detection of $[M\text{-}CH_2OH]^+$ (E), $[E\text{-}H_2O]^+$ and $[E\text{-}H_2O\text{-}HNCO]^+$ ions was reported exclusively, or almost exclusively, for furanic isomers. For acetylated thymidines, pyranic isomers showed a greater tendency to lose a molecule of acetic acid, AcOH, from $M^{+\cdot}$ or S^+, while the loss of two AcOH from these ions was greater for furanic compounds. These isomers also showed more abundant $[BH+C_2H_3]^+$ and $[BH+C_2H_3\text{-}HNCO]^+$ ions compared to pyranic (**72**) compounds.

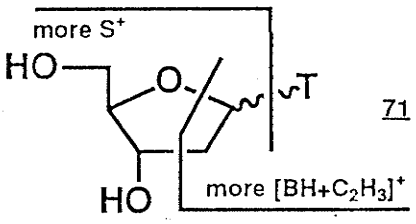

71

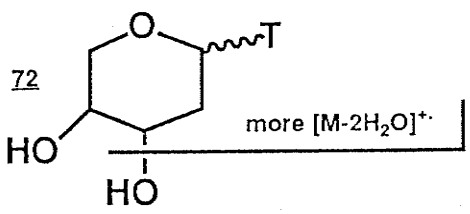

72

2.2.2. Nucleotides

Eicke *et al* [24] used secondary ion mass spectrometry (SIMS) to compare adenosine 5'-monophosphate (5'-AMP) (**73**) with a mixture of 2'- (**74**) and 3'-AMP (**75**). When the samples, deposited on silver foils, were bombarded by 3 keV argon ions, silver attachment frequently occurred, producing secondary ions that were easily recognizable in the mass spectra by the presence of ion doublets of approximately equal intensity ($X+^{107}Ag$: $X+^{109}Ag$ ~ 52:48), amongst which were found some isomeric indicators. It appears that the N-glycosyl bond is broken more easily for 5'-AMP than for 2'- or 3'-AMP as attested by the very dominant BH_2^+ ion (76% of total ion current compared to 52% for the other two isomers) observed in its mass spectrum, combined with a $[M+H]^+$ peak at half the intensity of that found with 2' and 3'-AMP. The only other isomeric indicator was the presence of a $[M+Ag-H_2O]^+$ ion found only for 2' and 3'-AMP.

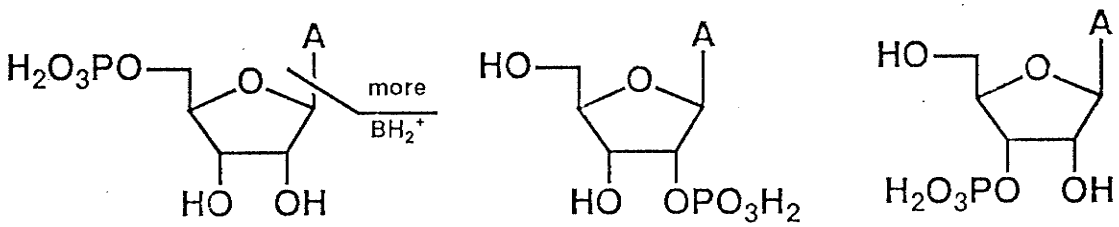

73 74 75

$[M+Ag-H_2O]^+$ (ex)

Lawson *et al* [22] studied +ve EI spectra of TMS derivatives of 5' (**73**), 2' (**74**) and 3'-AMP (75). They found that only 5'-AMP lost its phosphate moiety, leaving the charge on C-5 ($[M-OPO(OTMS)_2]^+$). Increased stabilization of the charge at 5' by the base was invoked as a possible explanation for this observation. Due to isomerization resulting from trimethylsilyl and phosphate migration after electron impact, the mass spectra of TMS esters of 2'- and 3'-AMP were essentially identical, but different from that of 5'-AMP. In addition, $[C_5H_4O + OTMS]^+$ (m/z 169) was much more abundant

for 5'-AMP. On the other hand, $[M-B]^+$ ions were much weaker for 5'-AMP.

FAB mass spectra of disodium salts of 3'- (**75**) and 5'-AMP (**73**) were compared by Eagles *et al* [26]. Although in the +ve ion mode the mass spectra were almost identical (except for a 50% increased RA of $[M+Na]^+$ for **75**), the -ve FAB spectra showed clearer signs for isomeric differentiation. While $[M-2Na+H]^-$ ions were most abundant (base peak) in the 5'-AMP FAB spectrum, it was the B^- signal that was detected in greatest yield with 3'-AMP, which also showed six times more abundant $[M-Na]^-$ ions than 5'-AMP relative to their respective base peaks.

Feistner [143] found a diagnostic ion to differentiate the four pairs of nucleoside phosphoric acid (TMS derivatives) isomers described below. All +ve ion EIMS mass spectra showed $[M-Base]^+$ ions at m/z 501 at least nine times more abundant for 3'-phosphate compounds (**76**) compared to that observed with 5'-phosphate isomers (**77**), a result likely associated with the increased acidity of the 2'-H when it is in proximity to the 3'-phosphoric acid moiety.

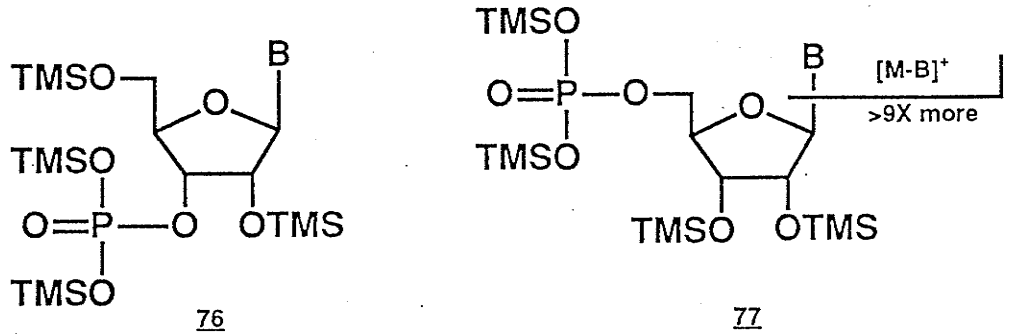

76 77

B = G , U (as TMS derivatives)

Positive ion EIMS was used by Wiebers [144] to differentiate thymidine 5'-phosphate (pT,**78**) from thymidine 3'-phosphate (Tp, **79**). The spectrum of the **78** contained a $[M-H_3PO_4-H_2O]^{+\cdot}$ (*i.e.* $[T+C_5H_5O]^{+\cdot}$) peak at m/z 206, absent for **79**, while the spectrum of the latter contained a $[M-T-C_2H_2]^{+\cdot}$ peak at m/z 171, absent for **78**.

Budzikiewicz [79] reported that the $[C_5H_4O + OTMS]^+$ ion also allowed differentiation between 3'(**80**)- and 5'-isomers (**81**) of TMS derivatives of GMP and UMP although their relative abundances were very similar in the case of CMP. The m/z

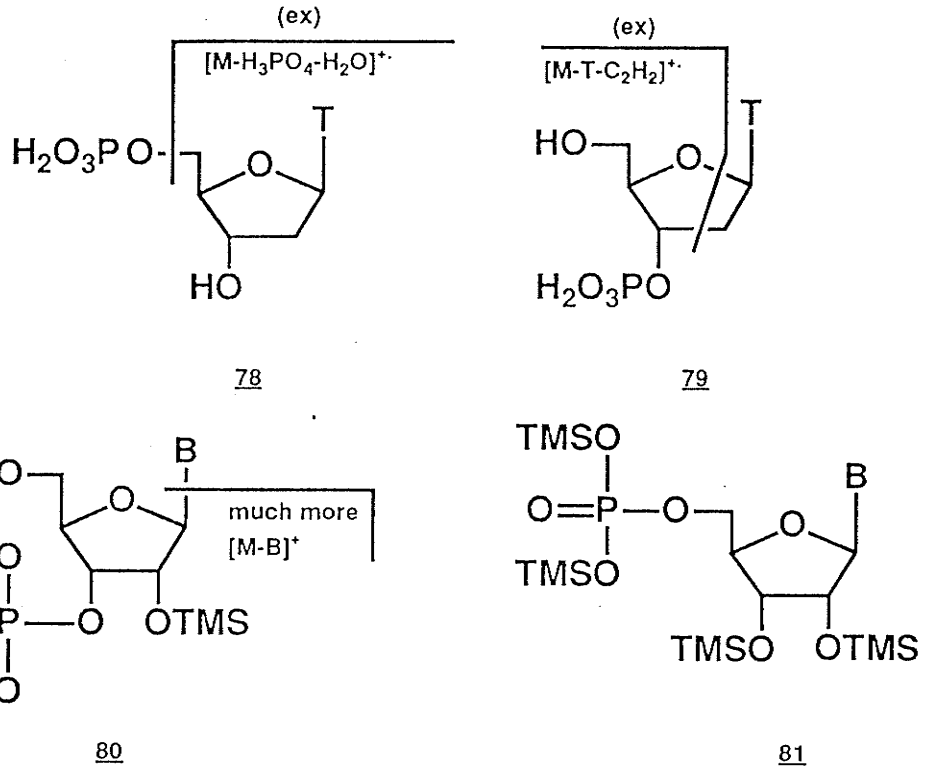

B = G , U (as TMS derivatives)

501 ($[M-B]^+$) ion was a much more reliable indicator for all four isomeric pairs. It was of much higher abundance for the 3'-isomers (**80**).

Cerny *et al* [68] compared FAB mass spectra and FAB/CAD and metastable ion decomposition spectra of $[M-H]^-$ ions for all standard 3'- (**82**) and 5'- (**83**) monophosphate ribo- and deoxyribo mononucleotides described below. First of all, upon collisional activation, all compounds showed a greater tendency to lose BH than to form B^- (two exceptions are 5'-dGMP and 5'-dAMP). This tendency was accentuated in metastable decomposition spectra but more importantly, it was more prominent with 3'-isomers than with 5'-isomers, whether with ribo- or deoxyribonucleotides (with the exception of 5'-GMP). Secondly, all pyrimidine nucleotides showed $[M-H-HNCO]^-$ ions (not found with purine nucleotides) that were much more prominent for 5'-phosphate compounds, providing another clue for isomeric differentiation.

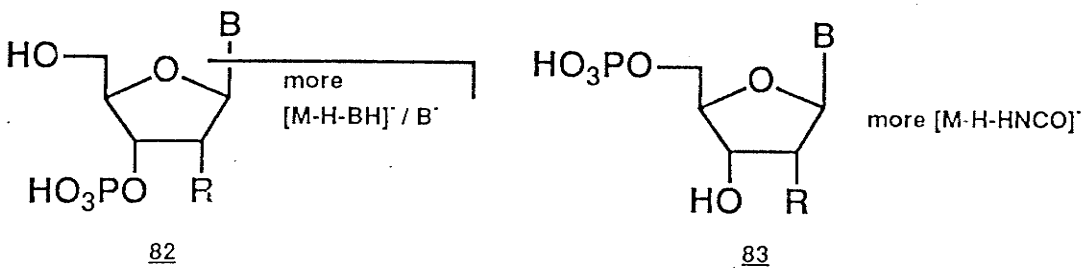

82 83

R = OH , B = A , C , G , U
R = H , B = A , C , G , T

Mallis *et al* [64] compared the FAB/CAD spectra of $[M+Na]^+$ ions of two uridine triphosphate positional isomers (**84**) and (**85**), both labelled with six ^{18}O-atoms. As expected, the two CAD spectra were almost identical except for a peak at m/z 345 for **84** that was shifted to m/z 347 for **85**, corresponding to the cleavage of the α–β bridging position, i.e. the neutral loss of $H_3P_2O_6^{\cdot}$, as shown below.

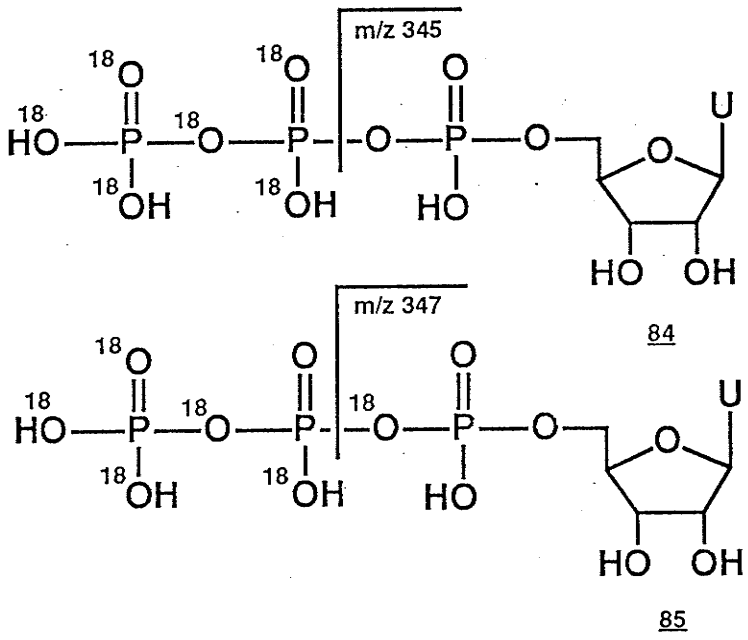

84

85

Grotjahn *et al* [145] used a similar approach to differentiate α–β ^{18}OATPαS (86) and α^{18}O-ATPαS (87). Linked scanning analysis techniques used in conjunction with FAB led to the finding that diphosphate ions lose $H_2{}^{18}O$ from **86** but not from **87**, whereas the triphosphate ion loses $H_2{}^{18}O$ from **87**, but not from **86**. Of course, the pyrophosphate ion from **86** also appeared at m/z 179 instead of at m/z 177 for **87**.

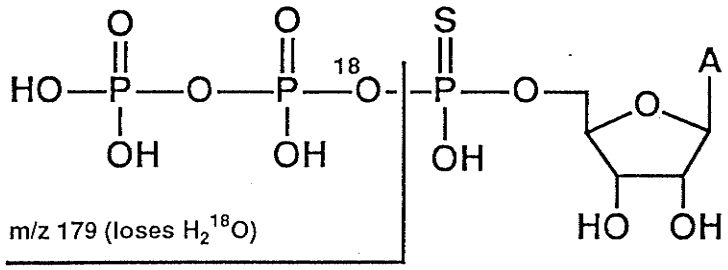

86

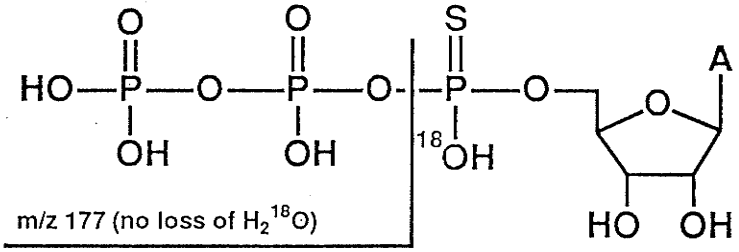

87

Non-appearance of key fragment ions was used by Marquez *et al* [146] in their -ve FAB study of three phosphonate analogs of thiazole-4-carboxamide adenine dinucleotide **88**, **89**, and **90**. These positional isomers were differentiated from one another by the fact that when an oxygen is replaced by a methylene group, cleavage of a P-CH_2 bond does not occur, thus eliminating fragment ions from the -ve FAB spectrum, and therefore attesting the nature of the isomer.

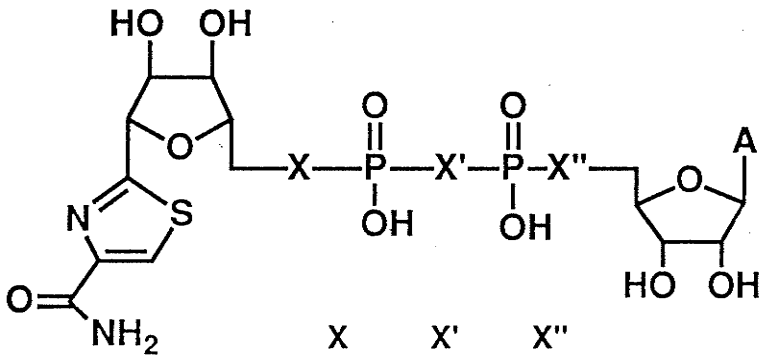

	X	X'	X''
88	CH_2	O	O
89	O	CH_2	O
90	O	O	CH_2

Viari *et al* [80] took +ve and -ve plasma desorption (PD) mass spectra of the di-deoxyribonucleoside monophosphate d(TpT), **91**, and compared them with those of its ultraviolet induced intramolecular isomeric photodimers d(T[p]T), (**92**). Two stereoisomeric forms of **92** were obtained by UV irradiation of **91**: a cis-syn and a trans-syn cyclobutyl d(T[p]T) dimer. Both stereoisomers gave essentially the same mass spectra, but molecular ions were more abundant for the photomodified **92** than for **91**. This is not surprising in view of the fact that for TH_2^+ ions to be produced by **92**, two C-C covalent bonds have to be broken. A phosphodiester bond must also be ruptured to allow for the formation of Y (or X) ions, in the case of **92**. The main differences between **91** and **92** were as follows: drastically reduced abundances for $[Y(\text{or } X)+H+Na]^+$ and $[Y(\text{or } X)+2Na]^+$ ions for **92**, as well as total absence of TH_2^+ ions.

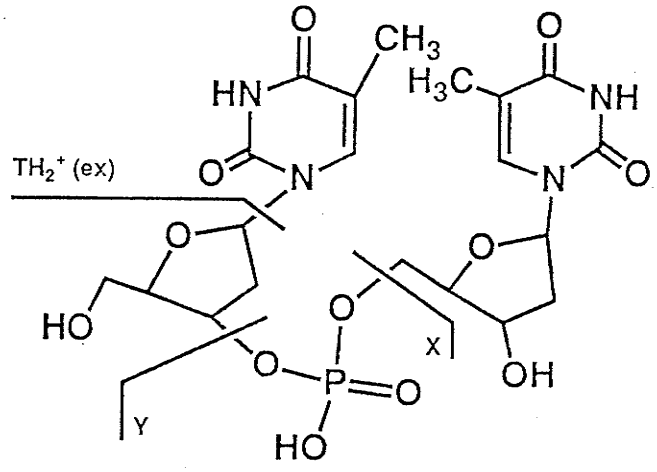

91

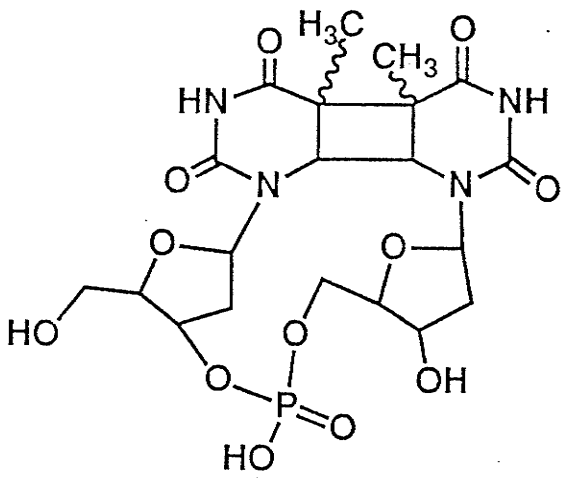

92 more $[M+H]^+$

Newton *et al* [95] compared MIKE spectra resulting from collision induced dissociation (CID) of $[M+H]^+$ ions stemming from butyryl derivatives of 3',5'- cyclic monophosphates of adenosine **93** and **94** (as their sodium salts). The 2'-O-butyryl-cAMP (**93**) was readily distinguished from its N6-isomer by the presence of a $[\text{butyrylribose-cyclicPO}_4+Na]^+$ ion at m/z 287 for **93**, that was absent for **94**.

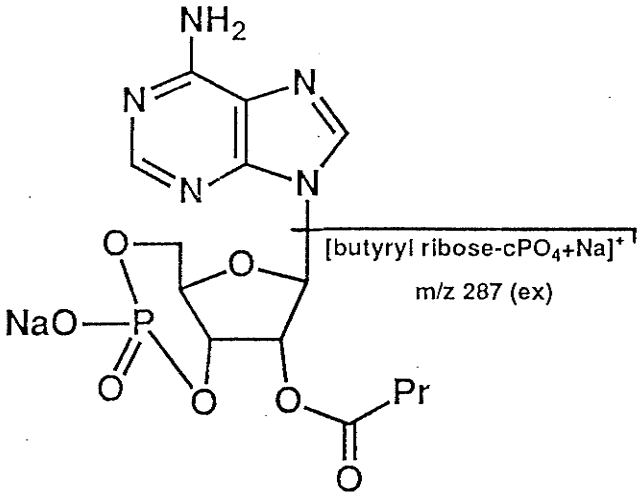

93

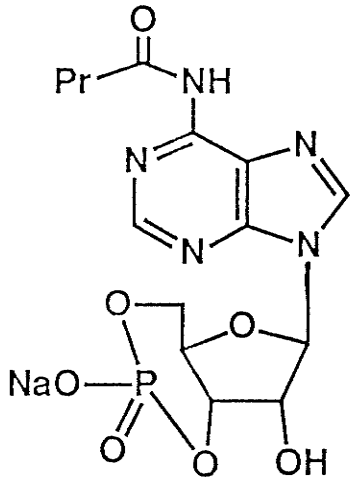

94

CID of $[M+H]^+$ ions resulting from FAB ionization was used by Kingston *et al* [75] to differentiate 3',5' cyclic-AMP (**95**) from its 2',3' isomeric analog (**96**, see below). MIKE spectra resulting from CID of isomeric $[M+H]^+$ ions of cAMP showed that $[B+44]^+$ ions were obtained only for the 3',5' structure (**95**) whereas the 2',3' structure (**96**) produced $[MH-H_3PO_4-CH_2O]^+$ ions through a pathway not available to **95**.

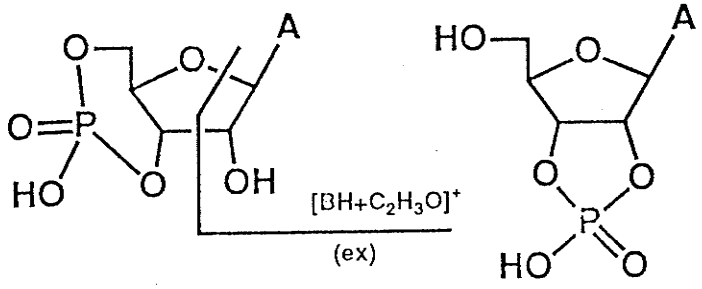

95

96

Sindona *et al* [76] compared 3',5'- (**97**) and 5',5'- (**98**) dithymidylic (TpT) acids, as their triethylammonium salts by FAB in the -ve ion mode. They found that **97** produced more B^- (m/z 125), more $[X \text{ (or } Y)\text{-}TH]^-$ (m/z 195, breakage of phosphate link followed by expulsion of the second base unit) and less X^-(or Y^-) (m/z 321) than **98**, compared to

the relative intensity of $[M-H]^-$. On the other hand, the -ve FAB mass spectrum of **98** contained peaks corresponding to $[B+H]^-$ and $[B+C_3H_6O_2]^-$ (m/z 199), as well as peaks at m/z 363, 245 and 237, all absent from the mass spectrum of **97**. Additional isomeric indicators were found when the same group[147] recorded MIKE/CID spectra of the $[M-H]^-$ ions generated by FAB. Under those conditions, only **98** produced a peak at m/z 502, corresponding to $[M-H-HNCO]^-$. A slow retro Diels-Alder (RDA) reaction was invoked to explain the mechanism of HNCO expulsion. For **97**, the loss of TH was by far the most abundant fragment produced by CID, presumably due to increased acidity of the 2'-H in the presence of a 3'-phosphate bond.

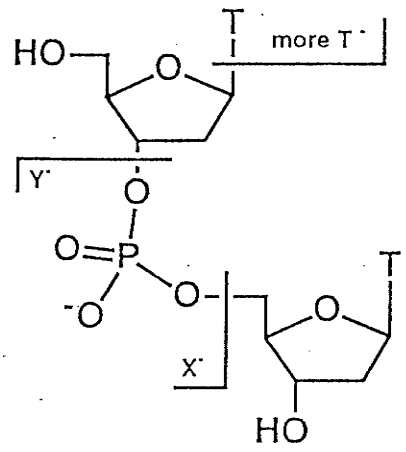

97

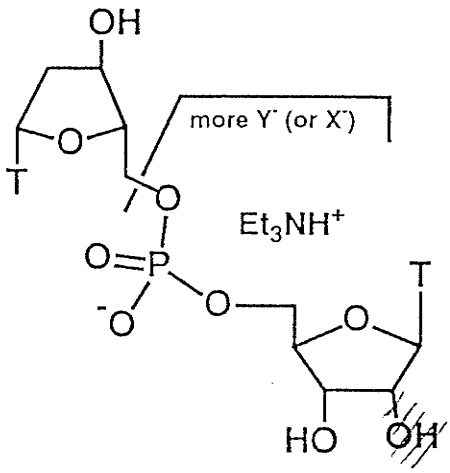

98

Positive ion EI was used by Pettit *et al*[78] to distinguish hexamethyl-5'-adenylic acid (**99**) from its 3'-(**100**) and 2'-(**101**) isomers. Compound **100** was the only one that did not show $[M-CH_3]^+$ or $[M-CH_3O]^+$ ions. Compound **99** contained both, and **101** contained only $[M-CH_3O]^+$ ions. The latter contained by far the most intense $[M-B]^+$ and $[M-B-2CH_3OH]^+$ peaks, as well as the most intense peak at m/z 142, assigned to $[M-B-(CH_3O)_2P(OH)_2]^{+\cdot}$. Compound **99** was the only one to show a distinctive $[M-B-CH_3OH]^+$ ion.

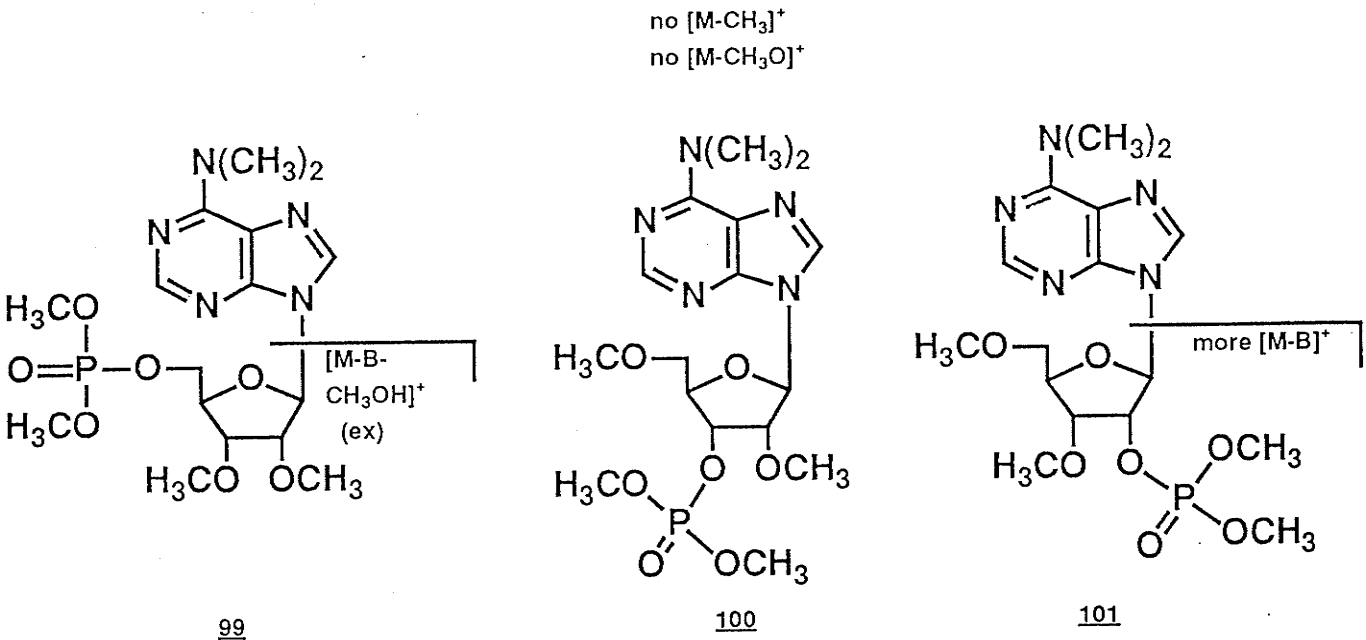

99 100 101

The +ve EI mass spectra of the TMS derivatives of thymidinyl-3' (**102**) and 5'-phosphordiamidates (**103**) were compared by Tamas *et al* [57]. The main isomeric indicator reported was the presence of a fragment ion at m/z 103 for **102** (27% of the base peak) assigned to $[CH_2OTMS]^+$ions, which was practically absent in the spectrum of the TMS derivative **103**.

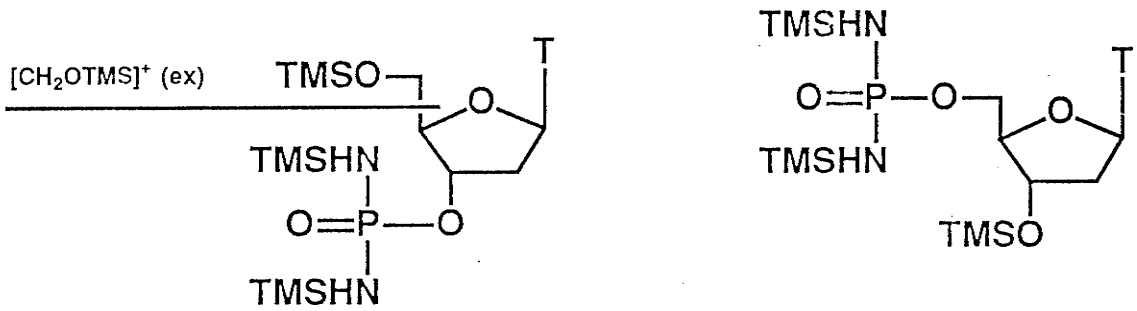

102 103

Negative ion CAD spectra of FAB generated $[M-H]^-$ ions were recorded by Crow *et al* [73] to differentiate adenylyl-(3',5')-cytidine (**104**) and adenylyl-(2',5')-cytidine (**105**). Two significant differences were found, as shown below. Compound **105** can yield a fragment at m/z 481, corresponding to $[(M-H) - C_3H_6O_3]^-$, absent in the CAD spectrum

of **104**, while **104** yielded instead a fragment at m/z 378, that involved the loss of A+$C_2H_3O_2$ (see below). This peak was not found in the CAD spectrum of **105**.

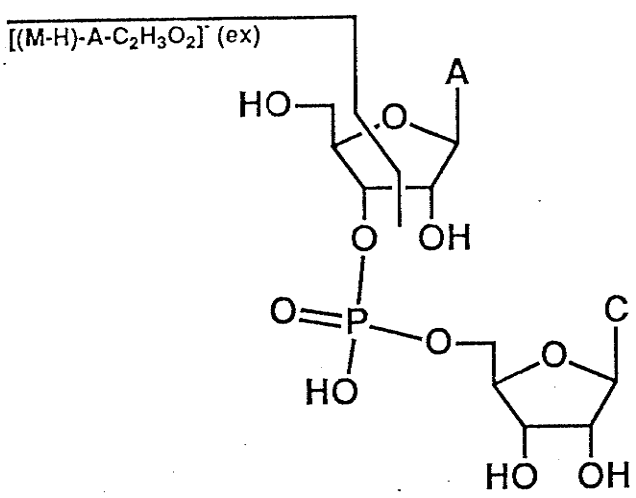

104

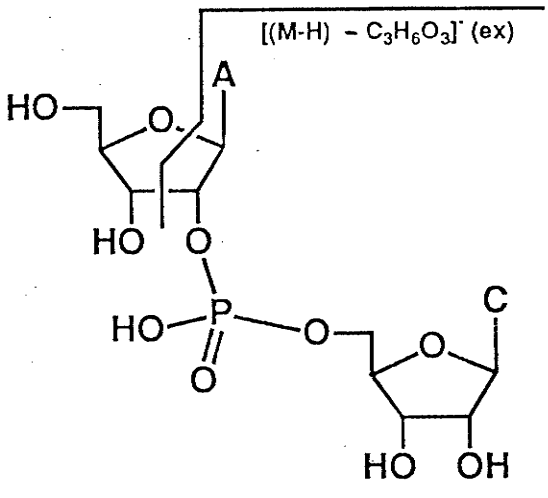

105

2.3 STEREOISOMERS

Kralj *et al*[147] compared a series of synthetic ribofuranosyl and arabinofuranosyl-methylene-thiazolidine-4-one nucleosides (see below) by FABMS in the +ve ion mode. No significant differences were reported between the mass spectra of stereoisomeric compounds, except between **106** and **107**, where **107** showed a $[M+H]^+$ peak (50% of base peak, BH_2^+) ten times more intense than **106** (5% of base peak, BH_2^+). On the other hand, CAD MIKE spectra were also obtained from $[M+H]^+$ and $[BH_2]^+$ ions generated by FABMS, producing data that were much more useful than direct FAB spectra to assess differences between stereoisomers. For instance, compounds **108**, **109** and **110** could be differentiated from one another by the following: of the twenty or so identified fragments lost from $[M+H]^+$ and $[BH_2]^+$, all were of greater relative abundance (vs $[M+H]^+$) for **108**, the main fragments being BH_2^+ from $[M+H]^+$ and $[BH_2 - CH_3OH]^+$, as well as $[BH_2 - HCOOCH_3]^+$ from BH_2^+. The CAD/MIKE spectra

of **109** and **110** were very similar, except that **109**, containing an arabino sugar, lost twice as much CH_3OH from BH_2^+ as did its ribo-diastereomer **110**.

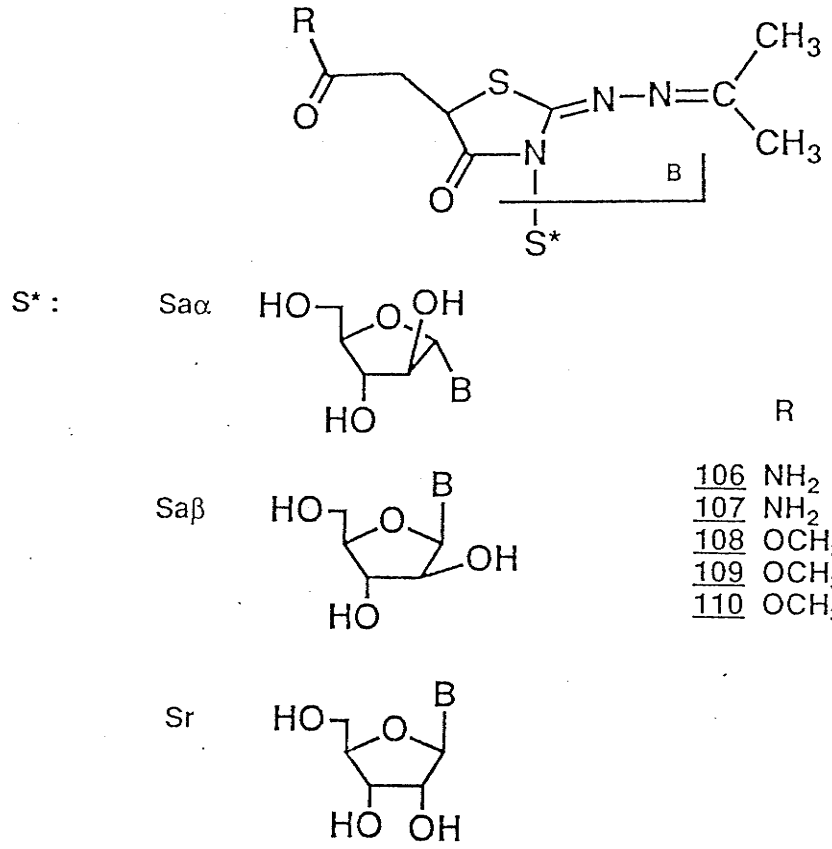

	R	S
106	NH_2	Sr
107	NH_2	Saα
108	OCH_3	Saα
109	OCH_3	Sr
110	OCH_3	Saβ

Ulrich *et al* [66] compared +ve ion EIMS of α (**111**) and β (**112**) anomeric forms of acetylated and non-acetylated thymidine. Furanic and pyranic anomers were included in the study. In all instances, molecular ions were found to be more stable for the β form. The favored decomposition pathway implied rupture ot the N-glycosyl bond with charge retention either on the base ($[BH]^{+\cdot}$ or $[BH_2]^+$ ions) or, to a larger extent, on the sugar (S^+, $[S\text{-}H_2O]^+$ or $[S\text{-}H_2CO]^+$ ions). The base peak was S^+ for furanic compounds and $[S\text{-}H_2O]^+$ from pyranic isomers. β forms (**112**) of all compounds showed greater $BH^{+\cdot}$ and BH_2^+ abundance than did α forms (**111**). The total %RA of fragment ions produced by N-glycosyl bond cleavage compared to fragments stemming from alternative decomposing routes was greater with β forms (i.e. more $BH^{+\cdot}$, BH_2^+, S^+etc.) . αT

(111)was the only compound to produce a peak at m/z 181 (possibly $[M\text{-}2H_2O\text{-}HNCO]^{+\cdot}$), and only the β forms showed an $[M\text{-}H_2O]^{+\cdot}$ peak at m/z 212. With acetylated compounds, β anomers produced more $[M\text{-}2AcOH]^{+\cdot}$, $[S\text{-}AcOH]^{+}$ and $[S\text{-}2AcOH]^{+}$ than did their α stereoisomers.

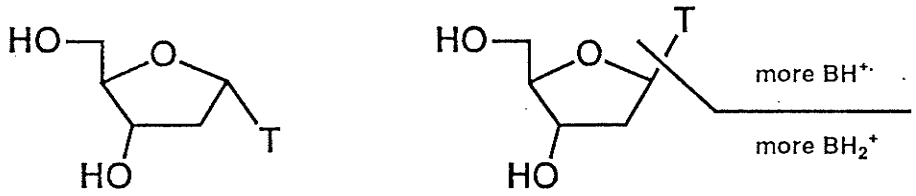

m/z 181 (ex)

m/z 212 ([M-H2O]+· ex)

111

112

Arlandini *et al* [148] compared three pairs of diastereomeric di- and trinucleotides (see below) by -ve FABMS. Even though most isomeric pairs gave very similar spectra, notable differences included: more $[(Bzo)_2A]^-$ at m/z 342 as well as more m/z 153 for **113** (vs **114**) and much more $[M\text{-}CH_3]^-$ for **114**. In the case of **115** vs **116**, the FAB spectrum of the former showed more $[M\text{-}H\text{-}2H_2O]^-$ (m/z 597), more $[Ade+41]^-$ (m/z 175) and a peak at m/z 421 not reported for **116**, while the mass spectrum of the latter contained more $[M+Na\text{-}2H]^-$ (m/z 655) and more X^- (or Y^-) ions at m/z 384 (loss of one nucleotide unit). Finally, differences between the isomeric trinucleotides **117** and **118** were as follows: more $[X_2\text{-}SPO_2Na]^-$ (m/z 633) and more $[X_2\text{-}SPO_2Na+H\text{-}Na]^-$ (m/z 611) as well as more $[M\text{-}2Na+H]^-$ (m/z 912) for **117**, and a peak at m/z 307 of greater %RA for **118**, as well as a peak at $[M\text{-}39]^-$ (m/z 962) for **118**, absent in the -ve mass spectrum of **117**.

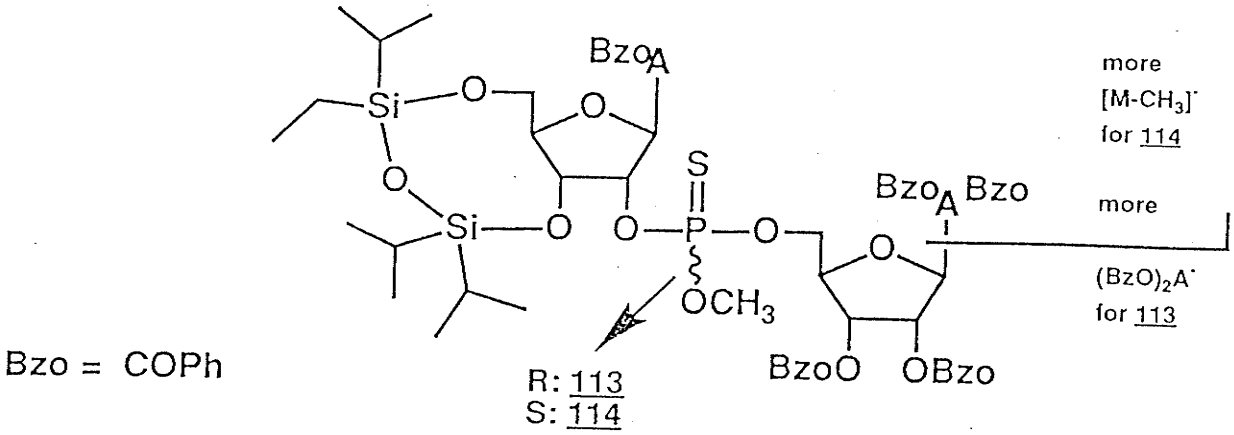
Bzo = COPh
more [M-CH3]- for 114
more (BzO)2A- for 113
R: 113
S: 114

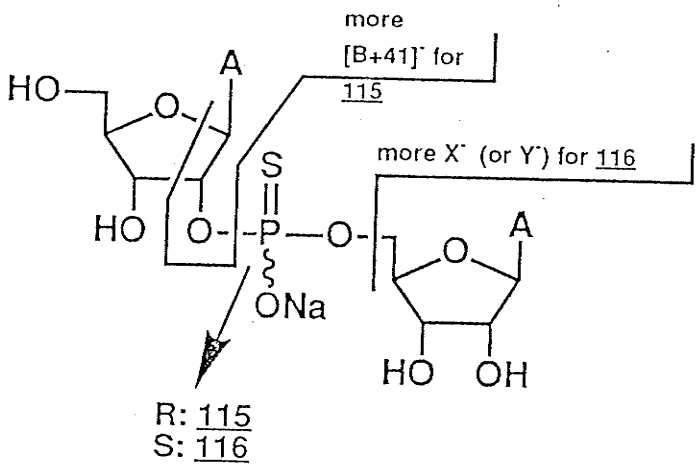
more [B+41]- for 115
more X- (or Y-) for 116
R: 115
S: 116

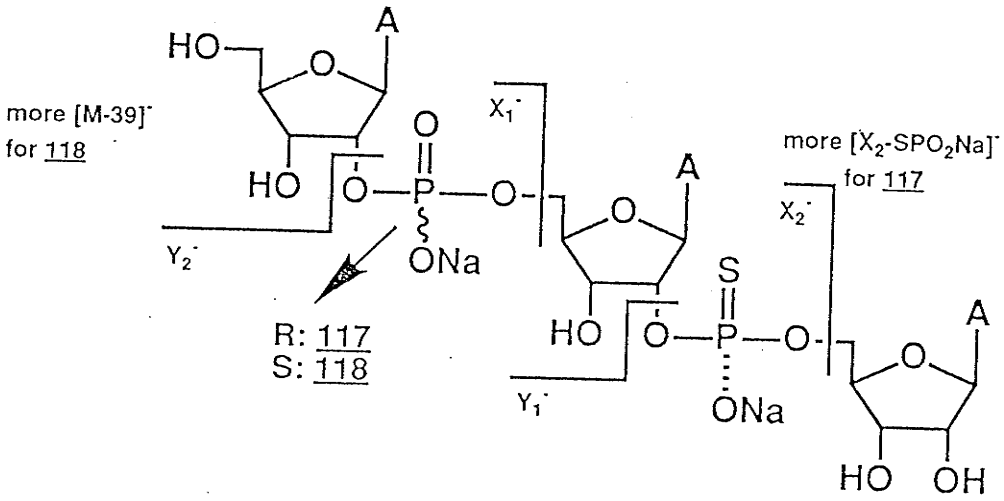
more [M-39]- for 118
more [X2-SPO2Na]- for 117
R: 117
S: 118

^{18}O2'- (**119**) and ^{18}O3'- (**120**) labelled adenosine, as well as ^{18}O2'-9-(β-D-arabinofuranosyl)adenine (^{18}O2'-ara-A (**121**)) and 3'^{18}O-ara-A (**122**), were synthesized and compared by Jiang *et al* [94], using +ve ion EIMS. Notable differences between ara-A and A diastereomers were as follows: a base peak at $[B+30]^+$ (m/z 178 (^{16}O) and m/z 180 (^{18}O)) for the former, while for riboadenosine (A) compounds, this peak accounted for 65-80 %RA of the base peak, BH^+ (m/z 135). The two ara-A compounds also showed a greater propensity (up to twice as much) to produce $[M-30]^{+\cdot}$ ions (m/z 237 or 239), compared to compounds **119** and **120**. In addition, the mass spectrum of **119** contained 50% more $[B+44]^+$ ions than did ^{18}O2'-ara-A (**121**). Those ions were of similar %RA for both ^{18}O3'- isomers. The trimethylsilyl derivatives of the same compounds were also analyzed; the most striking difference between the diastereomers was the presence of $[M-B-TMSOCH_2+H]^+$ ions at m/z 247 and m/z 249 that were 2-3 times less abundant for **121** and **122** compounds than for **119** and **120** isomers.

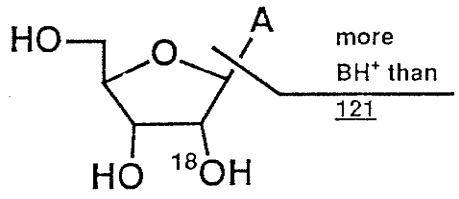

119

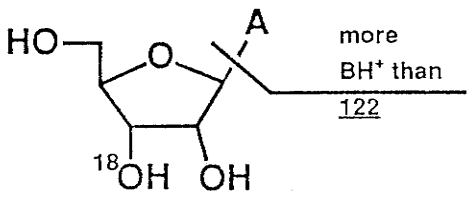

120

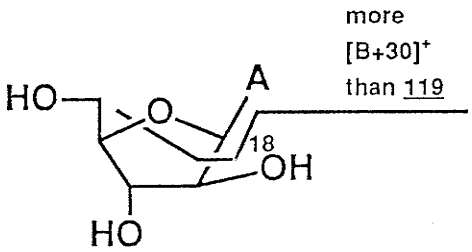

121

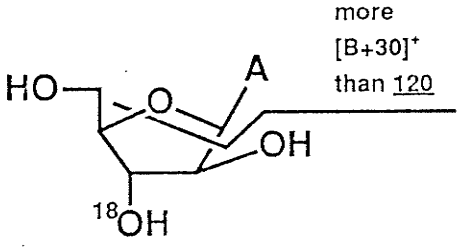

122

α and β anomers of cytidine (**123**, **124**) and pseudouridine (**125**, **126**) were differentiated by Wilson *et al* [67], using +ve ion CIMS in conjunction with various reagent gases. For instance, although the mass spectra of **123** and **124** contained the same base peak at m/z 112 (BH_2^+), with NH_3 as a reagent gas, the %RA of MH^+ ions was 50% greater for the α anomers (15% for **125** vs 9.5% for **124**). The $[B+44]^+$ ions were also 3 times more abundant for **123** (*vs* **124**). On the other hand, **125** and **126** could be differentiated by CIMS using CH_4 as a reagent gas. Under those conditions it appears, first of all, that the molecular ion is more stable for the α anomer (base peak for **125** *vs* 64 %RA for **126**). Secondly, BH_2^+ ions were nine times more abundant for **126** (28% *vs* 3 %RA with **125**). Finally, the fragment ions $[B+30]^+$ and $[B+44]^+$ were produced with greater ease for the β anomer (**126**) with 19% and 100 %RA, respectively, compared to 7% and 70% for **125**.

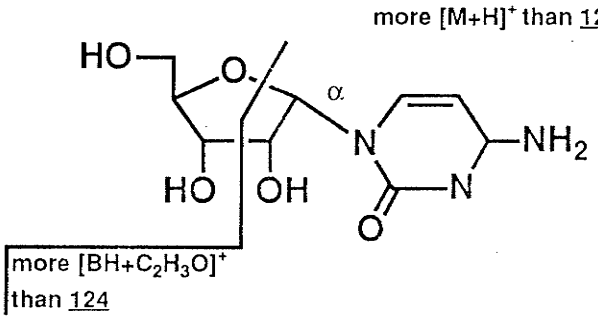

123

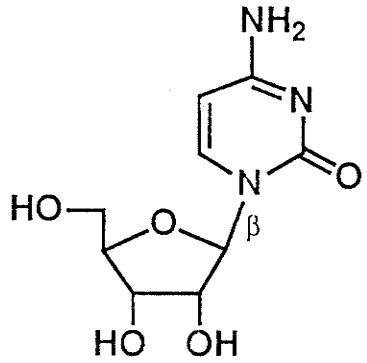

124

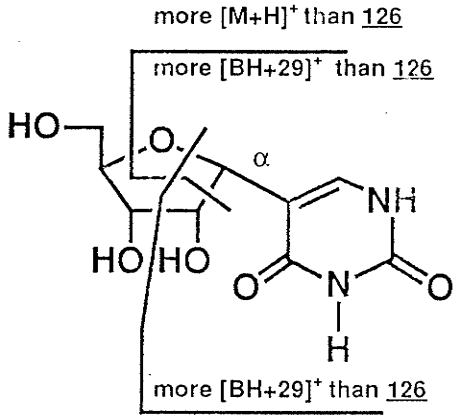

125

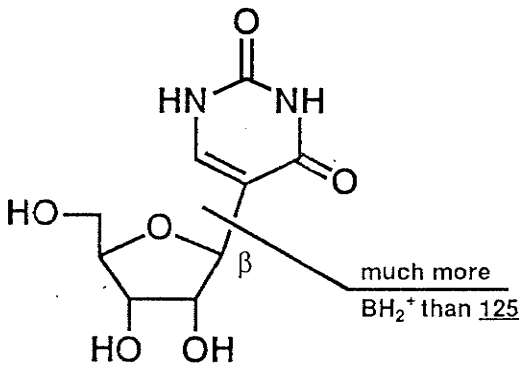

126

The $[S-H]^{+\cdot}$ ion abundance may be useful in assignment of anomeric configuration, as found by Pang *et al* [63] in their +ve ion EIMS study of a series or nucleosides (as TMS derivatives), including cytidine and uridine. The abundance of $[S-H]^{+\cdot}$ ions was found to be between five and seventeen times lower with the α anomer (**127**) than with the β anomer (**128**). The restricted steric access of H-2' to the base was the main reason invoked to explain the reduced abundance of $[S-H]^{+\cdot}$ ions with α anomers.

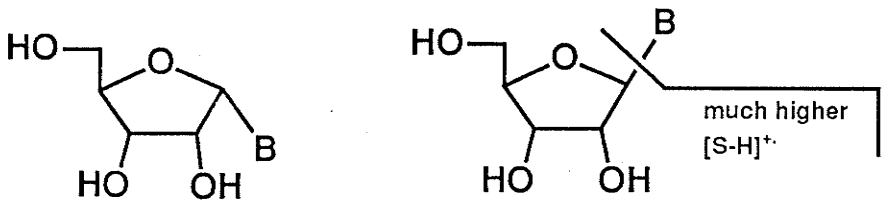

127 B = C,U 128

2.4 SEQUENCE ISOMERS

2.4.1 Dinucleotides

Liguori *et al*[76] used the MIKE spectra of FAB generated $[M-H]^-$ ions to differentiate d(TpU), **129,** from d(UpT), **130.** The preferred elimination of the base linked to the 5'-end deoxyribose unit provided a straightforward criterion to characterize the sampled molecules. Direct FAB spectra showed similar results, but the $[M-H-TH]^-$ (m/z 405) or $[M-H-UH]^-$ (m/z 419) ions produced were not abundant enough to provide the clear-cut evidence shown by the MIKES spectra. Increased acidity of the 2'-H vicinal to the phosphodiester bond was the explanation proposed for increased N-glycosyl bond cleavage observed for the 5'-terminal (top) base compared to the 3'-terminal (bottom) base with those sequence isomers.

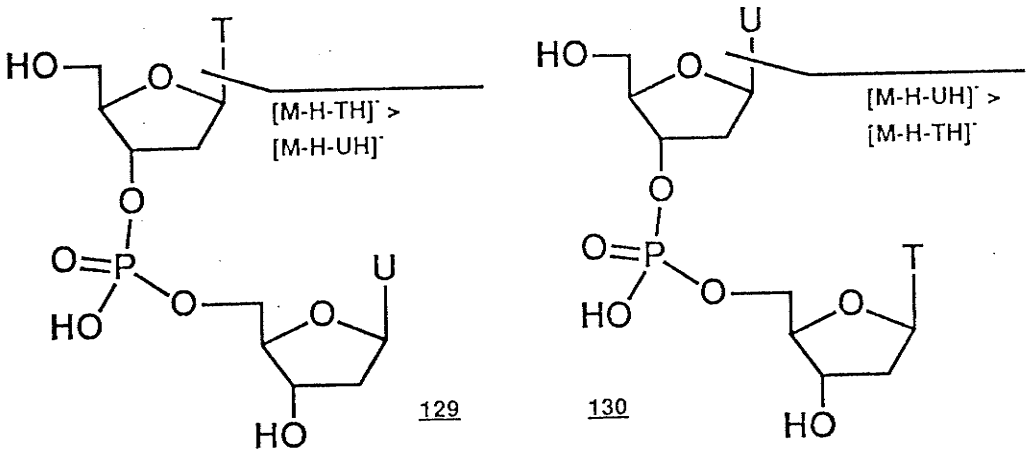

Hogg *et al* [81], in their -ve ion FAB analysis of d(ApC), **131**, and d(CpA), **132**, found a different diagnostic ion for sequence determination. The spectrum of **132** contained $[pA+C_3H_4O]^-$ (or $[M\text{-}Cyt\text{-}C_2H_4O]^-$) ions at m/z 402 (Cyt = cytidine), absent in the spectrum of **131**, while in the latter case, $[pCyt+C_3H_4O]^-$ (or $[M\text{-}A\text{-}C_2H_4O]^-$) ions were detected at m/z 378, which were not present in the spectrum of **131** (see below). Results reported did not indicate a preferred cleavage of the 3'C-3'O bond over the 5'C-5'O bond for those two compounds, under the conditions described.

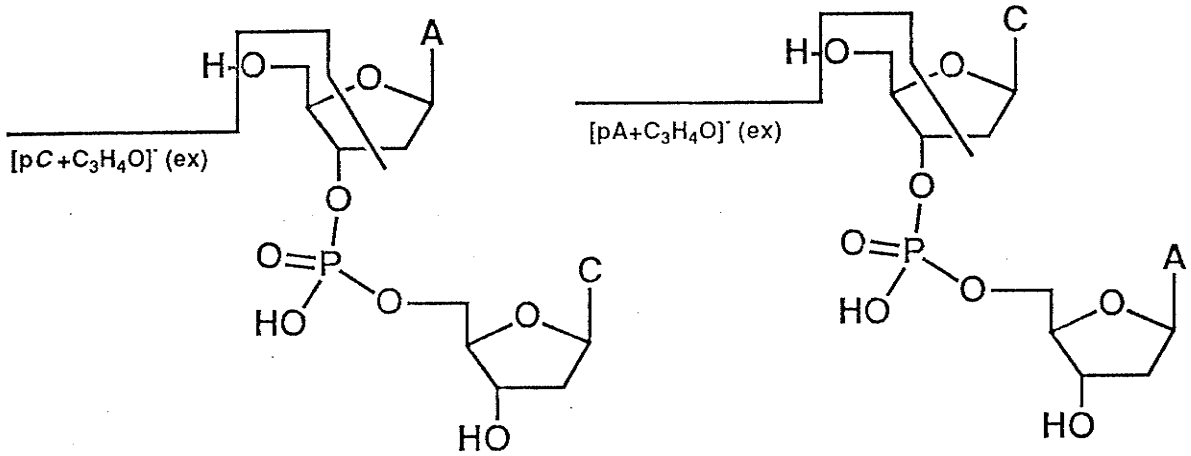

For dinucleotides, the enhanced %RA of $pNuc_2^-$ ions (Y^- ions) can sometimes (but not always) allow sequence determination. For example, Ulrich *et al* [60] compared six pairs of diisopropylammonium salts of protected deoxyribonucleotide 3'-phosphoric acids

(**133-144**), illustrated below, by -ve ion FABMS. For d(ApG) **135**, d(ApC) **133**, d(GpT) **143** and their respective sequence isomers d(GpA) **136**, d(CpA) **134** and d(TpG) **144**, they found that the Y^- ions were always more abundant than the X^- (Nuc_1p^-) ions (see below), enabling facile sequence determination of the isomers. However, although Y^- ions were also more abundant than X^- ions with d(ApT) **137**, d(CpG) **139** and d(CpT) **141**, the reverse was observed for their isomers d(TpA) **138**, d(GpC) **140** and d(TpC) **142**. However, the last three compounds contained greater abundances of $[M-H]^-$ ions compared to the previous three, thus providing a useful isomeric indicator for this series of molecules. However, more abundant Y^- sequence specific ions were found by Philips *et al* [91] who analyzed d(TpA) **138** and d(ApT) **137** (with an isopropyl group on the phosphate moiety) by -ve ion FABMS.

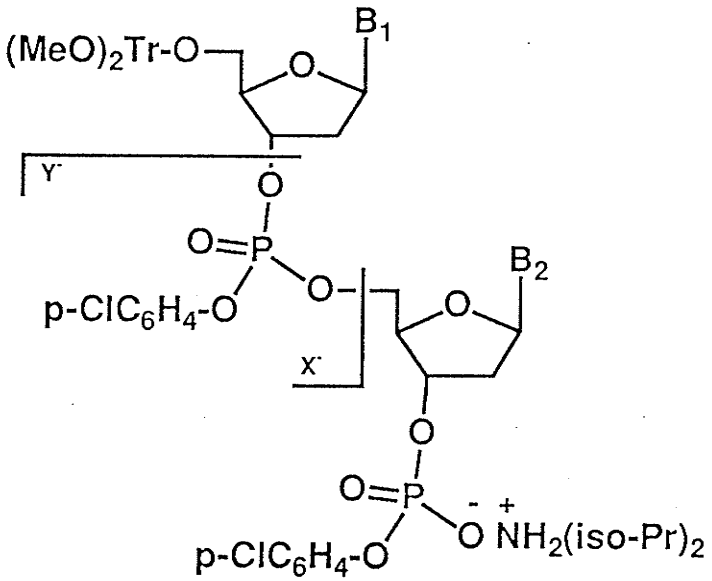

	B_1	B_2
133	A	C
134	C	A
135	A	G
136	G	A
137	A	T
138	T	A
139	C	G
140	G	C
141	C	T
142	T	C
143	G	T
144	T	G

where A, C and G are protected in the following way:

bzA = 6-N-benzoyladenine
Ctl = 4-N-o-methylbenzoylcytidine
Gdpg= 2-N-isobutyryl-6-N-N,diphenyl carbamoylguanine

Looking at six pairs of protected isomeric dinucleosidemonophosphates by -ve ion FABMS, Wolter *et al*[56] found that all twelve compounds (see below) yielded more abundant Y^- ions. They also found that B_1^- ions were always produced in greater abundance than B_2^- ions, except when B_1 was a thymine moiety (**150, 154, 156**). Finally, $[M-H]^-$ or $[M-EtCN]^-$ ions of compounds containing a guanine (G) base were always more stable with the G group on the 3'-end of the molecule (**147,151,156**), while those containing a thymine (T) base were always more stable when the T group was on the 5'-end of the compound.

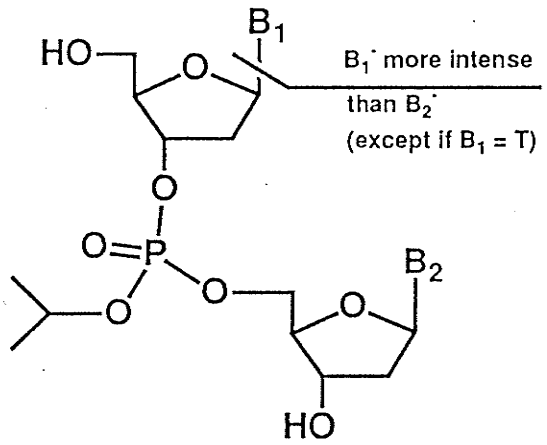

	B_1	B_2
145	A	C
146	C	A
147	A	G
148	G	A
149	A	T
150	T	A
151	C	G
152	G	C
153	C	T
154	T	C
155	G	T
156	T	G

where A, C and G are protected in the following way:

bzA = 6-N-benzoyladenine
Ctl = 4-N-o-methylbenzoylcytidine
Gdpg= 2-N-isobutyryl-6-N-N,diphenyl carbamoylguanine

Cerny *et al* [60] studied the same deoxyribonucleotides as Wolter *et al* [56], and also investigated the corresponding six pairs of ribodinucleotide isomers. All compounds were unprotected and were analyzed by -ve ion FAB mass spectrometry; metastable ion decomposition spectra and CAD spectra of $[M-H]^-$ ions were also recorded. The metastable and CAD spectra provided more information than the FAB mass spectra. The

$[M-H]^-$ ions of all dinucleotides decomposed to eliminate BH preferentially from the 3'- rather than the 5'-terminal of the molecule; isomers could be distinguished on that basis. The smaller abundance of the fragment ions formed by the loss of the 5'-BH group (B_1) was accounted for by a decreased effect of the phosphate moiety on the 5'-position. The formation of 3'-B^- (B_2) ions was also generally observed to be of greater abundance than that of 5'-B^- ions, with the exceptions: d(CpA), CpA, d(CpG), CpG and d(ApG). Upon collisional activation of $[M-H]^-$ ions, the formation of sequence ions was not as reliable an indicator as formation of the previously reported ions, since only nine of the twelve ribodinucleotides led to more Y^- ions than X^- ions (see below).

Wiebers [144] studied five pairs of deoxyribodinucleotide sequence isomers by +ve ion EIMS under pyrolytic conditions, as listed below. A diagnostic ion was found only for compounds containing a thymine base. Molecules with a T residue at the 5'-terminal (compounds **160**, **162**, **164**) showed a peak at m/z 206 in their mass spectra, corresponding to $[T+C_5H_5O]^{+\cdot}$ that was always more intense (vs the base peak, TH^+) than the equivalent peak when the T residue was at the 3'-terminal (compounds **159**, **161**, **163**). Other sequence isomers could not be distinguished. However, trifluoroacetylation of the molecules yielded ions diagnostic of the 3' and 5' terminals. Hence, $[B+C_5H_3O_3F_3]^+$ ions were observed for the base at the 5'-terminal of the nucleotide, while $[B+C_5H_4O_2F_3]^+$ ions were characteristic of the 3'-terminal of each compound. While the method was applied successfully to larger nucleotides, it did not enable identification of the sequence position of internal residues (*i.e.* d(TpCpGpA) vs d(TpGpCpA)). The greater abundance and higher m/z position of Y^- ions compared to X^- ions was also used by Hettich *et al* [71] to identify 3'-ends and isomeric form, in their matrix assisted LD-FTMS investigation of d(ApG), **157**, d(GpA), **158**, d(CpT), **161** and d(TpC), **162**.

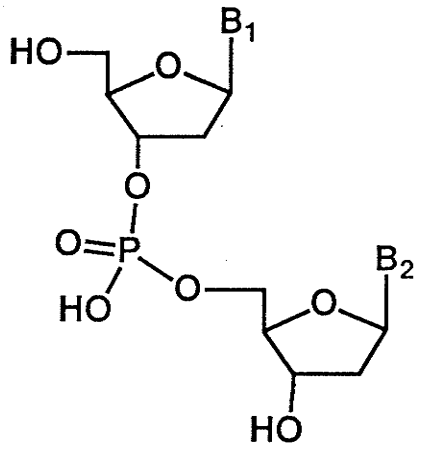

	B_1	B_2
131	A	C
132	C	A
157	A	G
158	G	A
159	A	T
160	T	A
161	C	T
162	T	C
163	G	T
164	T	G

Much "softer" ionizing conditions than those reported by Wiebers [144] were used by Eagles *et al* [26] in their +ve ion FABMS analysis of five pairs of sequence isomers (compounds **165-174**) listed below. The base peak in all instances was the $[M+H]^+$ ion. Under the conditions described, many compounds gave ions ranging from $[M-1]^+$ to $[M+4]^+$ in percentages greatly exceeding those expected from isotopic abundances. Interestingly, the %RA of $[M+3]^+$ and $[M+4]^+$ ions was greater for dinucleoside monophosphates that contained a purine base (A or G) only on the 3'-end (B2) of the molecule. It was greater therefore for CpA **166**, UpA **170** and CpG **173** than for their respective sequence isomers ApC **165**, ApU **169** or GpC **174.** This reduction process (addition of hydrogen atoms) was also more prevalent for GpA **168** than for ApG **167**, and a little greater for UpC **172** than for CpU **171**.

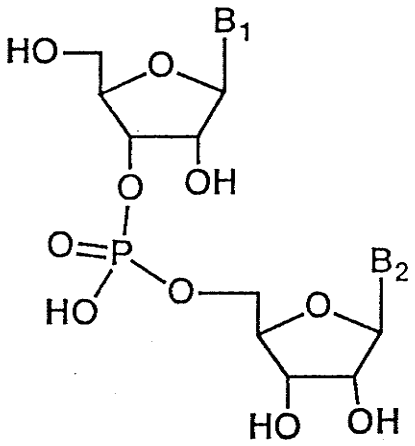

	B_1	B_2
165	A	C
166	C	A
167	A	G
168	G	A
169	A	U
170	U	A
171	C	U
172	U	C
173	C	G
174	G	C

Schulten *et al* [77] used FDMS to characterize the same dinucleoside phosphates analyzed by Eagles (except for CpG and GpC, which were replaced by UpG and GpU). Sequence specific fragments were found in +ve ion FD mass spectra of all five pairs of dinucleotides. It was noted that cleavage of the 5'O-5'C or 3'O-3'C bond, followed by the loss of water through cyclisation, led to the formation of cyclophosphate ions that were more abundant for the nucleoside in the 5'-end (B_1) position. Two explanations were proposed for those observations. First of all, after cleavage of the 5'-ester bond, cyclophosphate ions could be formed utilizing either the 2'-OH or the 5'-OH; only the 3'-OH group is available for ring closure after cleavage of the 3'-ester bond. Secondly, P-O cleavage and cyclisation could be facilitated by the participation of the vicinal 2'-OH of the nucleoside in position 1. This neighboring group participation is much less favored from the 3'-OH or 5'-OH.

FDMS was also used by Linscheid *et al* [149] who analyzed the collisionally activated dissociation of $[M-H]^-$ ions from isomeric pairs d(ApC) **131**, d(CpA) **132**, ApC **165** and CpA **166**. Protonation was produced by field desorption and linked scan spectra (B/E = constant) were generated for each compound. The ratio of signal intensity of $[adenine+H]^+$ and $[cytosine+H]^+$ was taken as an indicator of the sequence. In the spectrum of **165** (or **131**), the ratio I_{AH}/I_{CH} was close to 1 whereas in the spectra of **166** (and **132**), I_{AH}/I_{CH} was larger than 3. On all FD/CAD linked scan spectra, cleavage of a phosphodiester bond led either to XH^+ ions (cleavage of the 5'C-5'O bond) or YH^+ ions (cleavage ofthe 3'C-3'O bond). In all instances, the C-O bond broken usually belonged to cytidine, regardless of its position in the nucleotide. The position of adenosine could therefore always be ascertained based on the %RA of YH^+ vs XH^+, providing two additional diagnostic ions for sequence isomer differentiation for those particular compounds.

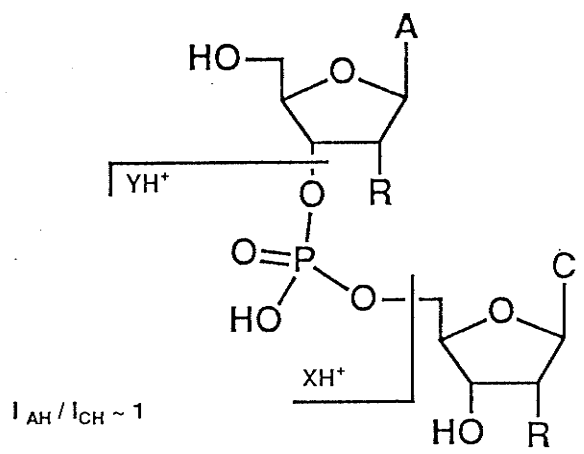

R = H : 131
R = OH : 165

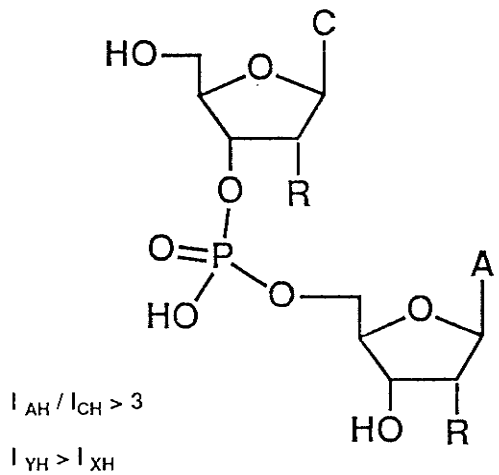

R = H : 132
R = OH : 166

2.4.2 Tri and oligonucleotides

Negative ion plasma desorption mass spectrometry (PDMS) was used by Viari *et al*[74] to compare d(GpGpA) **175**, d(GpApG) **176** and d(ApGpG) **177.** They found, first of all, that the %RA of $[M-H]^-$ ions increased according to **175<176<177**. They also found that the phosphodiester bonds around the central nucleoside (with formation of X_1^- or Y_1^- ions) were broken more easily than those from the terminal nucleosides (formation of X_2^- or Y_2^-ions). The Y_1^- ions were the base peak ion in each case (for **176**, X_1^- and Y_1^- have the same m/z value). Hence, **175** could be differentiated from its two sequence isomers since its base peak (Y_1^-) appeared at m/z 330 (and not at m/z 346 as for the other two other compounds). **177** could be differentiated from **176** on the basis of its peak at m/z 330 (X_1^-), which was not present in the spectrum of **176**, which only showed a peak at m/z 346, X_1^- and Y_1^-.

Two series of peaks were needed to ascertain the isomeric form of four oligonucleotide tetramers studied by Hettich *et al* [71], using matrix-assisted LD/FTMS. The compounds analyzed were d(CpCpGpG) (**178**), d(CpGpCpG) (**179**), d(GpCpGpC) (**180**) and d(GpGpCpC) (**181**). In general, the loss of terminal nucleoside (thus formation

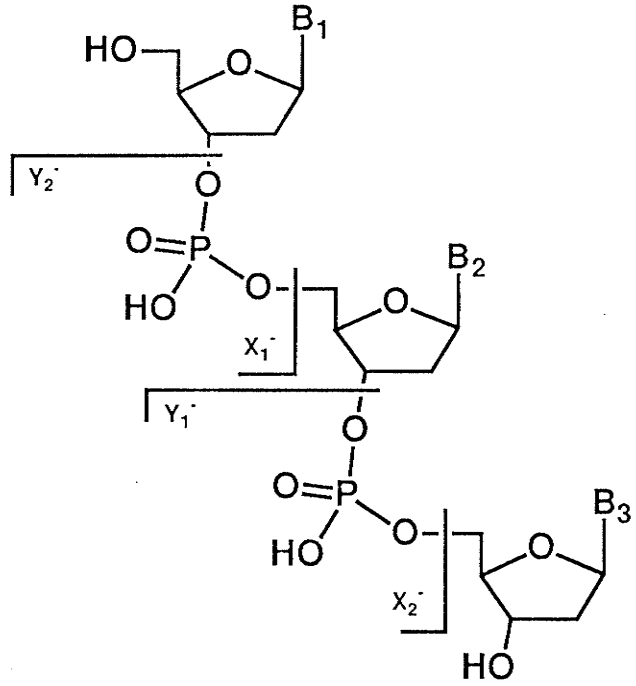

	B_1	B_2	B_3
175	G	G	A
176	G	A	G
177	A	G	G

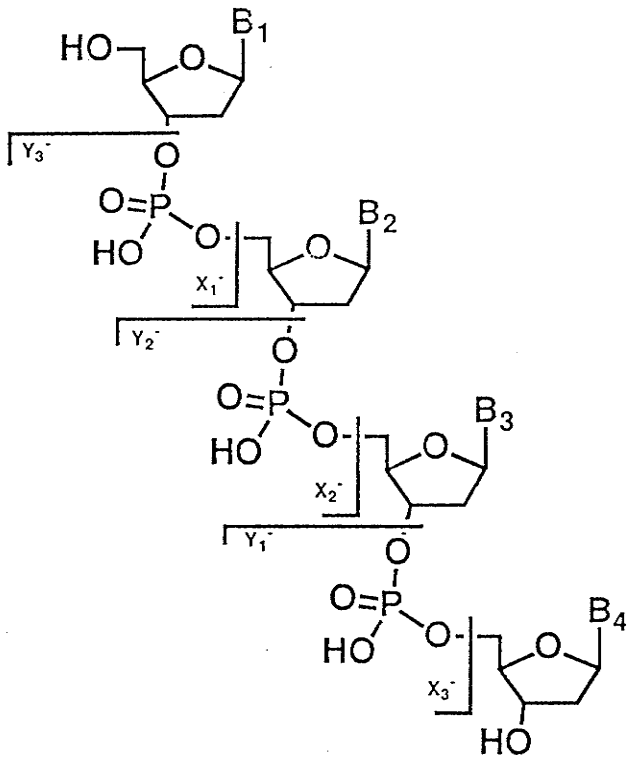

	B_1	B_2	B_3	B_4
178	C	C	G	G
179	C	G	C	G
180	G	C	G	C
181	G	G	C	C

of Y_3^- or X_3^- sequence ions, see above) was less favored than formation of X_1^-, Y_1^- and X_2^-, Y_2^-. Since all four isomers show peaks at m/z 924 and m/z 964 corresponding either to X_3^- or Y_3^-, as well as peaks at m/z 306 and m/z 356, indicating either X_1^- or Y_1^-, other sources had to be found to discriminate between those structures. Dimeric sequence ions X_2^- and Y_2^- enabled distinction between the **178**, **181** pair and the **179**, **180** pair of compounds, since in the latter case, Y_2^- and X_2^- should appear at the same m/z value, i.e. at m/z 635. Once this was recognized, the discriminating parameter became the presence of a small $[M-H-BH]^-$ fragment ion, only present if $B = B_4$, the 3'-end terminal base of the molecule. Hence, **178** and **179** showed a $[M-H-GH]^-$ peak, while **180** and **181** showed a $[M-H-CH]^-$ peak, providing all the information necessary to distinguish the four isomers.

Griffin *et al* [88] compared, by -ve ion FABMS, two isomeric deoxyribotetranucleotide analogs **182** and **183**, in which carbamate rather than phosphodiester linkages form the backbone. The two isomers were identified on the basis of two types of sequential cleavages, the **a** cleavage (see below) and the **b** cleavage.

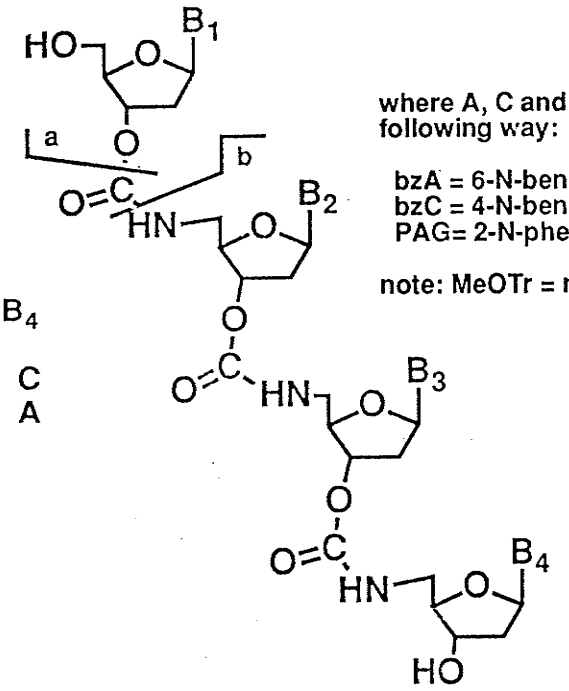

where A, C and G are protected in the following way:

bzA = 6-N-benzoyladenine
bzC = 4-N-benzoylcytosine
PAG= 2-N-phenylacetylguanine

note: MeOTr = methoxytrityl

	B_1	B_2	B_3	B_4
182	A	A	G	C
183	G	C	A	A

The fragmentation generated provided reliable structural information with respect to the base sequence. It is useful to note that the presence of a protecting group on the 5'-end of the molecule (or on the OH of the 3'-end) would be important if one wanted to differentiate symmetrical isomers such as BABA vs ABAB.

On the other hand, it was also found that when oligodeoxyribonucleotides are protected with a monomethoxytrityl group at the 5'-end, the fragmentation behaviour is different. The X^- sequence ions from the 5'-end are in general more abundant than the corresponding Y^- sequence ions. Grotjahn *et al* [48] investigated two pairs of unprotected isomeric oligodeoxyoctanucleotides by -ve ion FABMS. The two pairs were d(GpGpApApTpTpCpC) (**184**) and d(GpApApGpCpTpTpC) (**185**), as well as d(GpCpGpApTpCpGpC) (**186**) and d(GpCpApGpCpTpGpC) (**187**). Here again, the less abundant 3'-phosphate sequence ions (X^- ions) permitted determination of the sequence information in the correct direction, whereas the more abundant 5'-phosphate sequence ions (Y^- ions) determined the reverse sequence. All isomers could be differentiated on the basis of the different m/z values at which each sequence ion appeared.

The following chapters will focus on our contributions at the University of Manitoba to the central theme of this thesis: isomeric differentiation of nucleic acid components by time-of-flight secondary ion mass spectrometry.

CHAPTER 3

METASTABLE ION STUDIES WITH A SECONDARY ION TIME-OF FLIGHT MASS SPECTROMETER. ENHANCED DISTINCTION BETWEEN ISOMERS OF *O*-ALKYLATED THYMIDINES*.

3.1 INTRODUCTION

Secondary ion mass spectrometry (SIMS), incorporating a time-of-flight (TOF) mass analyzer, provides a technique which is useful for the characterization of non-volatile or thermally sensitive compounds. It combines high sensitivity with a very high mass range. Here, we describe its use to distinguish between isomeric compounds.

An interesting challenge was to distinguish between the positional isomers of O-alkylated nucleosides, which are of interest from their possible role in mutagenesis and carcinogenesis[151]. The mass spectra of 4-O-alkylthymidines (**188-190**) and 2-O-alkylthymidines (**191-192**) are quite similar. They may be compared with those reported for similar molecules by liquid SIMS[73], laser desorption[115], or thermospray [30] mass spectrometry, obtained with sector-field, Fourier transform, or quadrupole mass spectrometers, respectively. In each case, the positive ion mass spectra were dominated by $[M+H]^+$ and $[B+2H]^+$ ions. The isobutane chemical ionization mass spectrum of **188** showed $[B+2H]^+$ as the only significant ion[40]. Our spectra are sensitive to the method of preparation (e.g. whether electrosprayed or deposited from solution, and also the solvent and substrate used). In particular, the amount of adventitious Na^+ in the sample caused significant mass spectral variations. However, many of the secondary ions formed from these samples are metastable and the rates of decomposition of these ions appear to be insensitive to the method of sample preparation. In this paper, we show that the rates of decomposition of metastable ions can be used to distinguish between isomers

* F. Lafortune, W. Ens, F.E. Hruska, K.L. Sadana, K. G. Standing and J.B. Westmore, *Int. J. Mass Spectrom. Ion Processes*, **78**, 179 (1987).

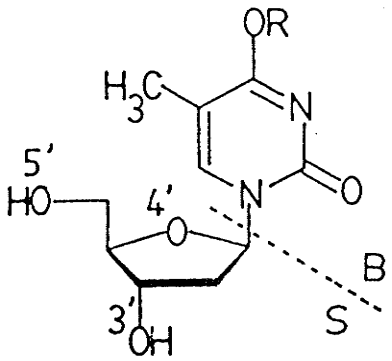

R = Me **188**
R = Et **189**
R = isoPr **190**

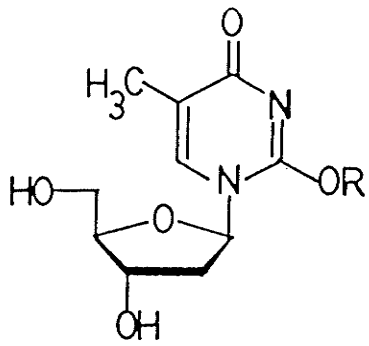

R = Me **191**
R = Et **192**

of these compounds. (This can be compared with a similar use of metastable ion *abundances* in sector-field mass spectrometers [152]). Liquid SIMS, combined with collisional activation of desorbed ions, has also been used to differentiate between isomers of benzylated guanosines[72]. The rates of decomposition are measured with the aid of a small 45^{o} ion mirror inserted into the ion flight path just before the detectors (see fig. 1.4, chapter 1). We have also analyzed some of the factors involved in this technique that influence the determination of the rates of decomposition of metastable ions.

3.2 EXPERIMENTAL

3.2.1 Sample preparation

The O-alkylthymidines were synthesized by Hruska *et al* [153,154], as described in Chapter 1. To prepare the 4-O-alkyl compounds, standard methods were used to convert thymidine to 3',5'-di-O-acetyl thymidine, which was then converted to the 4-(1,2,4-triazol-1-yl) derivative[155]. On treatment with the appropriate sodium alkoxide in the respective alcohol, the products **188-190** result. The product mixtures were neutralized with glacial acetic acid or IRC-50 resin and the nucleosides were isolated by thin layer chromatography. To prepare the 2-O-alkylthymidines, 3'-O-acetylthymidine was prepared by standard methods[156] and converted to O-2,5'-anhydrothymidine[157]. On gentle reflux with the appropriate alcoholic sodium alkoxide the products **191** or **192** result. Following neutralization of the reaction mixture, the nucleosides were purified by thin layer

chromatography. The O-alkyl thymidines were characterized by comparison of their UV and ^{1}H NMR spectra with published data [153,154,158].

A few μg of each sample were electrosprayed from a solution in methanol containing up to 10% water, with a solute concentration of *ca.* 1 mg ml^{-1}, to give a thin solid deposit on 12-50 mm^{2} of the metal surface of aluminized polyester film.

3.2.2 Mass spectrometry

Spectra of samples were obtained by using the Manitoba time-of-flight mass spectrometer[121,159] (see Figure 1.3). This instrument uses a thermionic cesium primary ion source[160] and a linear TOF analyzer maintained at an operating pressure of (0.5-5) x 10^{-7} Torr. Samples were bombarded by a pulsed beam of primary ions (3 ns pulses full width at half maximum, repeated at a frequency of 4kHz). For the positive ion studies reported here, the Cs^{+} ions strike the sample with an energy of 13 keV. The secondary ions are accelerated to 5 keV into a linear field-free region. When recording "normal" mass spectra, the ions travel along the spectrometer axis to a microchannel plate electron multiplier detector located at the far end of the flight tube 1.55 m from the acceleration grid. For the current experiments, a simple 45^{o} electrostatic mirror was installed just in front of this detector with its first grid 1.45 m from the target[124]. With sufficiently high potential on this mirror, charged particles are deflected through 90^{o} into a second detector while neutral species continue to pass straight through to the first detector. Both detector outputs are processed simultaneously by the data acquisition system[129].

3.3 RESULTS AND DISCUSSION

The principle of the experiment can be understood by examining a schematic diagram of the instrument shown in Fig. 1.3. Secondary ions produced by bombardment of the sample with energetic Cs^{+} ions are accelerated across a potential difference applied between the sample and a grid 2 mm from the sample surface. Secondary ions which are formed at the sample surface and do not fragment before they reach the grid will achieve

the maximum kinetic energy; these ions thus have lifetimes > ca. 10^{-7} s (see section 3.4). Some of these ions may decompose as they travel the length of the flight tube but the velocity of the fragments is unchanged except for the effect of the kinetic energy released during the decomposition. This contribution to the velocity (distributed over 4π steradians) is relatively small and results in a broadening of the measured flight time of the fragment ions and associated neutrals[161,162]. Although the velocities of parent and daughter ion species are approximately equal, their energies ($mv^2/2$) are, of course, different.

Two microchannel plate electron multiplier detectors are located at the far end of the flight tube. One of these, detector 1, is located behind a set of three grids oriented at 45^o to the ion flight path. With zero potential on these grids, both ions and neutrals pass through the grids and can be detected by detector 1. When a sufficiently high potential is placed on the central grid, the ions are deflected through 90^o into a second detector while neutral species pass through. Fragment ions generated in field-free flight have a lower kinetic energy and will reach detector 2 earlier than do their parent ions (see Appendix). Their mass can be determined from the time difference, though the short distances and time intervals in this small mirror limit the precision of the mass measurement (+/- 5%).

An example of the spectra of a pair of isomers is shown in Fig. 3.1. The spectra were obtained when the ion mirror was off (i.e. detector 1 was used) and therefore the peaks arise from both ion and neutral species. Parent ions (i.e. non-decomposing ions) contribute the sharp components of the peaks while products of metastable decomposition give rise to the broad features. The two spectra are quite similar. The most apparent difference concerns the intensity of a peak at m/z 177 (assigned as $[BH+Na]^+$, where B is the pyrimidine base). However, this peak is relatively sensitive to the amount of adventitious sodium ion in the sample and may not be a reliable indicator of isomeric form.

Closer inspection of Fig. 3. 2 reveals that the relative contribution of sharp and broad

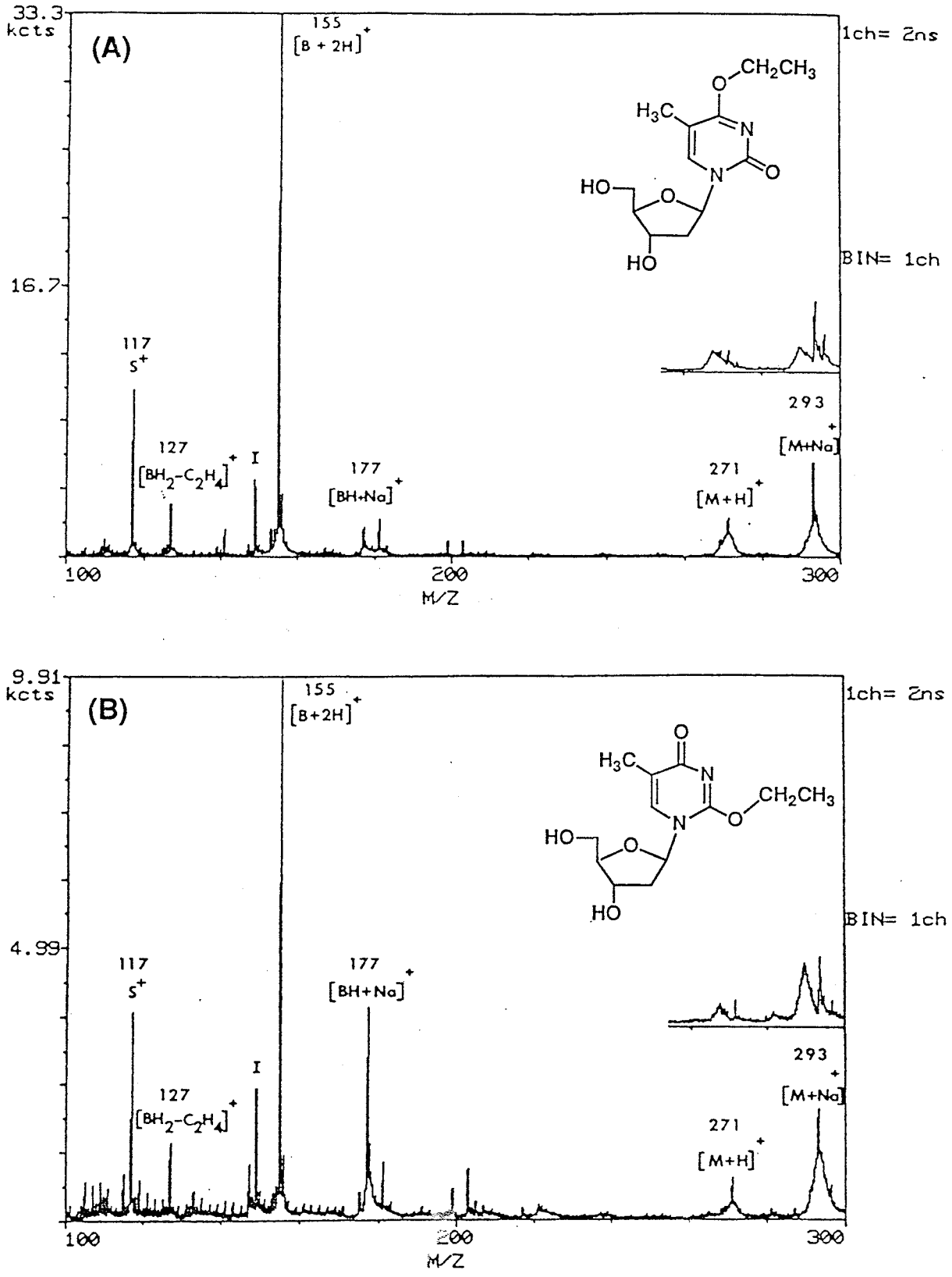

Fig. 3.1 "Normal" TOF mass spectra of (a) 4-O-ethylthymidine and (b) 2-O-ethylthymidine. (Insets show the high mass regions of the reflected ion spectra). In both molecules, the O-ethyl groups are shown in the *syn*-periplanar conformation. The N3-C2 and O2-C1 (ethyl) bonds are approximately co-planar with the N1 and C1 (ethyl) atoms on the same side of the central C2-O2 bond. In the *anti* conformation, the N3 and C1 (ethyl) atoms lie on opposite sides of the central bond.

components of corresponding peaks in the spectra sometimes differ. These differences can be exploited in the present apparatus by measuring the relative contributions of sharp and broad components of the peaks (i.e. non-decomposing ions and products) by methods to be described. From this, the rates of decomposition and the lifetimes of parent ions may be estimated.

With the mirror on, non-decomposing ions, as well as charged fragments, are recorded by detector 2. The most noticeable changes in the spectra occur in the $[M+H]^+$ and $[M+Na]^+$ regions. The insets in Fig. 3.1 show these regions of the spectra recorded by detector 2. As noted before, the broad parts of the peaks of Fig. 3.1 are now separated from the sharp components. Another example of the use of this technique is described elsewhere[120]. Ions which decompose after reflection by the mirror will be recorded as parent ions (with negligible peak broadening owing to the short distance to detector 2) but most of those which decompose within the mirror will be lost. An accurate measurement of the number of non-decomposing ions requires that the percentage of decompositions in the mirror be small. This means that the sampling time (i.e. the time spent in the mirror) should be small compared with the experiment time (i.e. the flight time of the parent ions). This is true in the present apparatus for which the maximum percentage of ions lost is ~ 1.4% (see section 3.4).

Events at detector 1 (and detector 2) are recorded in 2 ns wide time intervals (bins). However, to prevent recording of false events caused by ringing, we have imposed a 200 ns dead time after detection of an event in a data line. With the mirror off, the products of metastable decay will normally arrive at detector 1 with a time separation <200 ns (see Appendix), so that only one particle can be detected and recorded.

The results obtained are summarized in Table 3. 1. For each compound, the first column (headed RA%) gives the relative *areas* of each peak (i.e. sharp + broad components) as the percentage of the base peak (usually $[M+Na]^+$) with the mirror off.

Table 3.1

Mass spectra and ion fragmentations of *O*-alkylated thymidines

Parentheses denote values of doubtful accuracy.

Positive ion assignment	*O*2-Me		*m/z*	*O*4-Me		*O*2-Et		*m/z*	*O*4-Et		*O*4-isoPr		*m/z*
	RA%	Events (2/1)%		RA%	Events (2/1)%	RA%	Events (2/1)%		RA%	Events (2/1)%	RA%	Events (2/1)%	
[M + K]			295					309			1	(46)	323
[M + Na]	100	8	279	100	34	100	7	293	89	29	100	17	307
[M + H]	21	13	257	13	19	18	10	271	38	8	1	(46)	285
[M − 49]	1	(206)	207	8	62	3	42	221	1	(100)			235
[M − 67]	6	83	189	7	72	7	62	203	4	51	6	53	217
[B + 2Na]			185	14	84	4	63	199	2	(100)	10	75	213
$BHCH{=}CH_2$	8	87	167	10	74	4	76	181	6	85	1	(68)	195
[BH + Na]	55	45	163	22	44	56	42	177	30	10	24	17	191
[B + 2H]	63	111	141	95	87	48	90	155	100	102	25	40	169
[B + 2H − (R − H)]						10	65	127	14	73	23	99	127
S	25	61	117	34	49	28	45	117	31	72	13	54	117

Table 3.2

Rate constants and half-lives for decomposition of positive ions

The upper value of each pair is for a detector efficiency of 100%; the lower value for an efficiency of 50%.

Positive ion assignment	*O*2-Me		*O*4-Me		*O*2-Et		*O*4-Et		*O*4-isoPr	
	$k(s^{-1})$	$t_{1/2}(\mu s)$	$k(s^{-1})$	$t_{1/2}(\mu s)$	$k(s^{-1})$	$t_{1/2}(\mu s)$	$k(s^{-1})$	$t_{1/2}(\mu s)$	$k(s^{-1})$	$t_{1/2}(\mu s)$
[M + K]									(29 000	24)
									(22 000	32)
[M + Na]	102 000	6.8	44 000	15.9	105 000	6.6	49 000	14.2	68 000	10.1
	87 000	7.9	34 000	21	90 000	7.7	38 000	18.1	56 000	12.4
[M + H]	86 000	8.1	70 000	9.9	95 000	7.3	104 000	6.7	(31 000	22)
	72 000	9.7	57 000	12.2	80 000	8.7	89 000	7.8	23 000	30
[M − 49]			22 000	31	39 000	17.6	(0	∞)		
			16 100	43	30 000	23	(0	∞)		
[M − 67]	9200	76	16 100	43	23 000	31	32 000	22	29 000	24
	6300	110	11 300	61	16 200	43	23 000	30	21 000	33
[B + 2Na]			8700	80	22 000	31	(0	∞)	13 300	52
			5900	117	15 800	44	(0	∞)	9300	75
$BHCH{=}CH_2$	7300	95	15 700	44	13 800	50	8200	85	(18 700	37)
	5000	140	11 000	63	9600	72	5600	124	(13 200	52)
[BH + Na]	42 000	16.4	43 000	16.0	44 000	15.7	117 000	5.9	87 000	8.0
	32 000	22	33 000	21	33 000	21	99 000	7.0	71 000	9.8
[B + 2H]			7900	87	5700	121	(0	∞)	48 000	14.6
			5400	128	3900	179	(0	∞)	36 000	19.2
[B + 2H − (R − H)]					26 000	27	18 900	37	(600	1150)
					18 400	38	13 200	52	(400	1722)
S	31 000	22	45 000	15.6	50 000	13.9	21 000	34	38 000	18
	22 000	31	33 000	21	37 000	18.6	14 400	48	28 000	25

The second column (headed Events (2/1)%) gives the percentage of counts in detector 2 with the mirror on for *parent* ions (separated in time from fragment ions) to total counts for the same peak in detector 1 with the mirror off (i.e. parent ion plus daughter particles), the resulting value having been multiplied by the ratio of Na^+ counts in the two cases. The rationale for this procedure is as follows. It is necessary to normalize the events recorded at detectors 1 and 2 to those recorded in a similar way for an ion known not to decompose. The Na^+ ion, which is abundant in all spectra, is suitable for this purpose. Thus, all events in each detector are normalized to the same number of Na^+ events in each detector. This assumes that ion losses caused by ions missing the detector are similar for all ions. This follows from the argument that ion losses caused by a transverse velocity arising from kinetic energy release during metastable decomposition are minimal (see Appendix). Ideally, the values in the second column should not exceed 100% (expected for non-decomposing ions). Only in one case (a low abundance ion where areas are difficult to measure accurately) does the observed value greatly exceed 100%. Otherwise, no value exceeds 100% by more than the possible experimental error for the determination. This gives confidence that the results are of sufficient accuracy to draw meaningful conclusions. The first order rate constants and half-lives presented in Table 3.2 have been calculated from the data in Table 3.1.

Although the absolute values of the kinetic parameters remain uncertain, the situation is much more favorable when the relative values or these parameters for corresponding ions from isomeric molecules are compared, because virtually all the uncertain terms cancel. Some of the main findings will now be described.

The half-lives of the $[M+Na]^+$ ions from m4dT (**188**) and e4dT (**189**) are substantially longer than those of their O2- analogues. The major decomposition mode of the $[M+Na]^+$ ions involves scission of the glycosyl bond with the positive charge remaining on the base moiety. The enhanced stability of the $[M+Na]^+$ ions of the O4-alkyl

molecules suggests that the O2-keto oxygen is involved in chelation of Na^+, perhaps in a complex (structure **193**) which involves a syn orientation about the N-glycosyl bond and simultaneous binding to the sugar O4- and O5'- atoms.

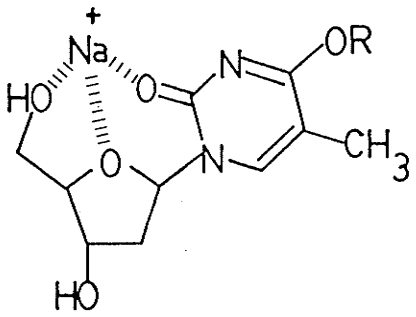

193

A similar complex would, for two reasons, seem less likely for the $[M+Na]^+$ ions of the O2 alkyl molecules. First, the O2-alkyl group would hinder the approach of the Na^+ ion. Second, O-alkylation converts O2 from a keto to a phenolic type of oxygen atom which bears a partial positive charge resulting from delocalization of its unshared pairs of electrons into the pyrimidine ring[163]. This oxygen would therefore be expected to bind cations less strongly. Support for electron delocalization is provided by the C4-O4 and C2-O2 bond lengths of O4 and O2 alkylpyrimidines, respectively (1.33Å); this value is greatly reduced from the normal C-O single bond length (1.43Å)[153,163,165]. Whether or not this rationalization of the differing half-lives is correct, it is apparent that the isomers can be distinguished by this measurement.

The $[M+H]^+$ ions are undoubtedly protonated on the base and probably have structures such as **194a,b** and **195a,b**. The half-lives of the $[M+H]^+$ ions from both isomers of O-methyl and O-ethylthymidines are slightly longer than those of the $[M+Na]^+$ ions from m2dT and e2dT but significantly shorter than those of the $[M+Na]^+$ ions from m4dT and e4dT. Thus, no appreciable stabilization of the $[M+H]^+$ ions of the O4-alkylthymidines is apparent.

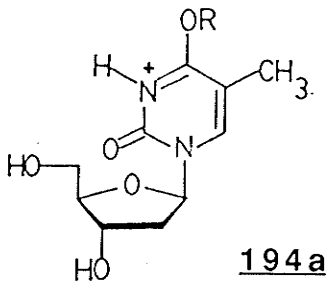

194a

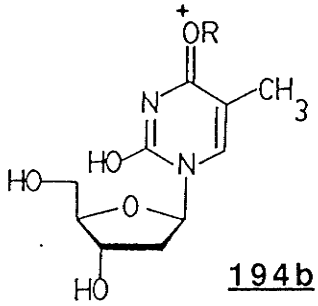

194b

+ other canonical forms

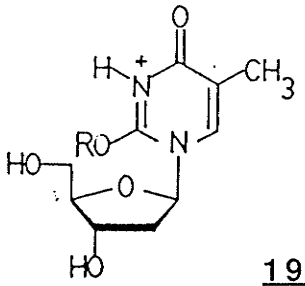

195a

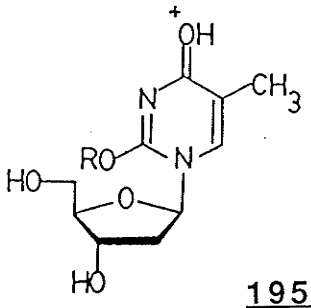

195b

+ other canonical forms

It is interesting to note that, in solution, alkylation of the O2 atom of deoxypyrimidine nucleosides greatly weakens the glycosyl bond [154,158]. However, this effect is not reflected in the half-lives of $[M+H]^+$ ions of compounds **191** and **192** vs **188** and **189**, respectively.

A further observation concerns the lifetime of the $[B+2H]^+$ ion. We have shown, by measuring the mass of the daughter ion produced, that an important decomposition pathway for e2dT, e4dT and i4dT involves loss of an alkene. This decomposition has been rationalized in Schemes 3.1 or 3.2 (illustrated for $[B+2H]^+$ from i4dT) by a mechanism *resembling* a McLafferty rearrangement. The rate of this decomposition is much greater for i4dT than for e4dT or e2dT. This enhanced rate can be easily rationalized on the basis of molecular models and available crystallographic data for m4dT, e4dT and i2dT [153,163,164] that demonstrate that the O2 and O4 alkyl groups prefer a *syn*-periplanar relationship to the N3 atom, (torsion angle N3-C4-O4-Cα and N3-C2-O2-Cα ~0^o, see Fig. 3.2 legend) rather than an *anti*-periplanar one which is destabilized by steric contacts with the bulky 5-methyl group. In the *syn*-periplanar

conformation of i4dT, one or the other or both of the β-methyl groups is *required* to be in close proximity to the N3 atom; this would facilitate the rearrangement of H on to N3 depicted in the schemes. On the other hand, the single methyl group of the O-ethyl substituent is not required to lie near to N3. Indeed, the favored conformation in the solid state is one in which the methyl projects away from N3, though in the gas (and solution) state, flexing about O-Cα will generate conformations in which the methyl is near to N3, thereby permitting H atom transfer.

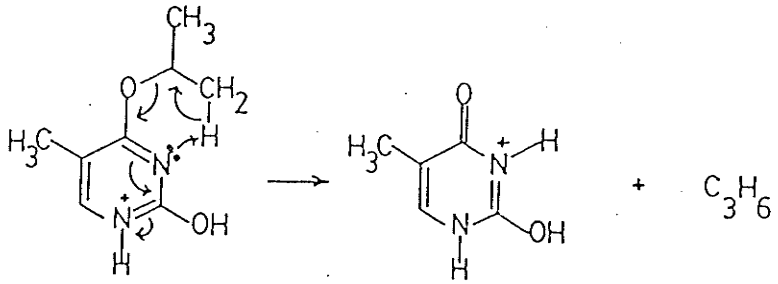

Scheme 3.1

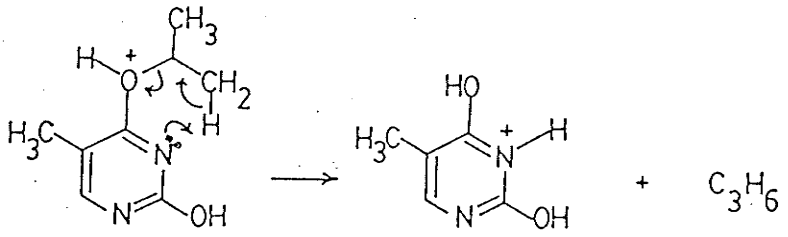

Scheme 3.2

We offer two final comments about assumptions that have been made. First, we have assumed that spontaneous decompositions of metastable ions occur, rather than collisionally induced factors such as decomposition or neutralization. Collisionally induced phenomena are only significant if the average distance between collisions of high-velocity ions and residual gas molecules is of the same order of magnitude as the flight path, or less. Note that, in the 45^{o} ion mirror, the ions retain their velocity component parallel to the mirror surface, so they do not come to rest. Their minimum

energy is half the incident energy (see section 3.4) so large variations in the collision cross-section are not expected. If we assume a rather high collision cross-section of 100Å^2 then, at 5×10^{-7} Torr, the average distance between collisions is ~60m. This assumption therefore appears justified.

The second comment concerns the assumption that the decompositions of the metastable ions can be treated as first-order rate processes. While this was not verified for the current experiments, there is evidence that some cases, at least, can be treated in this way. The decompositions of metastable ions produced from CsI and peptide samples have been studied by the incorporation of a movable detector assembly into our instrument [124,131]. In this way, the extent of decomposition was measured as a function of the distance the ions had travelled (i.e. of varying experiment time). The results, analyzed by standard methods, were consistent with a first-order rate law.

3.4 APPENDIX

3.4.1. Ion ballistics

After acceleration across a potential of V volts, a singly charged ion of mass m u has a velocity of magnitude $v_f = 1.39 \times 10^4 (V/m)^{1/2}$ m s^{-1}. In the acceleration region, the average velocity is $v_f/2$ for uniform acceleration. For an acceleration distance of 2 mm. between target and grid and an acceleration voltage V = 5 kV, the time spent is 4.07 $(m)^{1/2}$ ns, i.e. 40.7 ns for m = 100 u and 129 ns for m = 1000 u. Thus, ions with lifetimes > *ca.* 10^{-7}s will be fully accelerated.

For any ion, the time of field-free flight from the acceleration grid to the ion mirror is given by $t = D/v_f$, where D is the distance travelled. With V = 5kV, as before, and D = 1.45 m (the distance between the acceleration grid and the ion mirror), we have $t = 1.48 (m)^{1/2}$ µs.

The trajectories of ions in the mirror are shown in Fig. 3.3. If we define a set of axes as shown, with the electric field E along the y axis, the incident ion has a velocity

component $v_f/\sqrt{2}$ along the *x* axis (perpendicular to E) and a velocity component $-v_f/\sqrt{2}$ along the y axis. The *x* component is unchanged during reflection but the *y* component is

Fig. 3.2

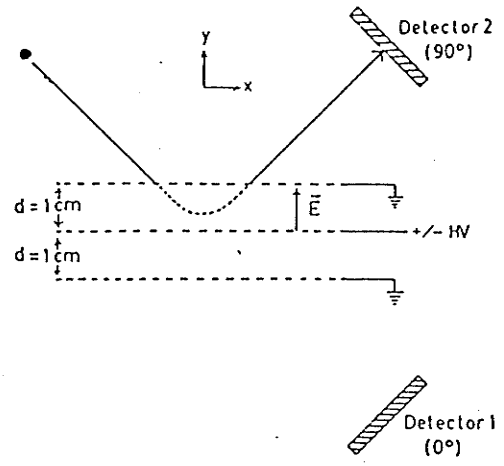

An ion trajectory in the electrostratic mirror; E is greater than the minimum value required to deflect the ion into detector 2

reversed, so the ion leaves the mirror with a velocity component $+v_f/\sqrt{2}$ along the *y* axis. The behavior of the y velocity component is, in fact, equivalent to that of an ion of velocity $-v_f/\sqrt{2}$ (energy $1/2\ mv_f^2/2$) incident along the *y* axis. Thus, a voltage of at least V/2 is necessary for reflection, the average *y* component of velocity has magnitude $v_f/2\sqrt{2}$, so the time for reflection is $4\sqrt{2}\ d/v_f$, where d is the separation between the first two grids of the mirror. Under these conditions, a daughter ion of mass *m'* will penetrate a distance of (m'/m)d so the time for reflection will be (m'/m) x the time for reflection of the parent.

The ratio of the *maximum* time that an ion spends in the mirror to its time in free flight is thus $(4d\sqrt{2}/D) = 0.039$ for d = 1.0 cm. The percentage of ions that decompose in the mirror, some of which may be lost, depends upon the half-life and is given by % decomposition = $100[\exp(-0.693\ t_f/t_{1/2}) - \exp(-0.693 \times 1.039\ t_f/t_{1/2})]$ where t_f is the time of field-free flight. When $t_f/t_{1/2} = 1.42$, this reaches a maximum of 1.41%.

A metastable ion may decompose at any point along its flight path. The kinetic

energy released by the decomposition is partitioned between the daughter products so that momentum is conserved. If T represents the kinetic energy released when an ion of mass m decomposes to daughter particles of masses m_1 and m_2, then

$$T = 1/2 m_1 u_1^2 + 1/2\, m_2 u_2^2$$

and $m_1 u_1 + m_2 u_2 = 0$

where u_1 and u_2 are the incremental velocities of the daughter particles. It readily follows that $u_1 = [T(2m_2/m_1 m)]^{1/2}$. If E represents the kinetic energy of the parent ion as a result of acceleration, then its velocity, v, is given by $v = (2E/m)^{1/2}$. The maximum effect of the velocity increment upon ion ballistics occurs when the decomposition occurs just after the acceleration grid. For this situation, two limiting conditions are discussed. First, for decompositions in which the velocity increment is parallel to the spectrometer axis, the percentage change in flight time is $+/- 100u_1/v = +/- 100\, [(m_2/m_1)(T/E)]^{1/2}$. For example, if $m_2/m_1 = 1$ (i.e. two daughter products of equal mass are produced) and the kinetic energy released is 200 meV (a rather high representative value*), then with E = 5 keV, the percentage change in flight time is +/- 0.63%. When one of the daughter products is lighter than the other, then the percentage change in flight time increases. Thus, if the lighter fragment has 10% of the mass of its parent, then $m_2/m_1 = 9$ and, for the same kinetic energy release as before, the percentage change in flight time is 1.9%.

In the second situation, the velocity increment is perpendicular to the spectrometer axis. The transverse velocity component from this source causes a percentage deviation from the spectrometer axis = $+/- 100\, [(m_2/m_1)(T/E)]^{1/2}$. For the maximum flight path of 1.55 m from the acceleration grid to detector 1 and noting that the diameters of our detectors are each 4 cm, both daughters of the metastable decomposition will strike the detector if the percentage deviation is < 1.3%. For the worst case situation, and with a high kinetic energy release of 200 meV, while a daughter with a mass <19% of the parent ion mass will miss the detector, the associated heavy daughter will strike it.

3.4.2 Kinetics of ion decomposition

We denote by n_o the number of fully accelerated parent ions produced by a given number of primary Cs^+ ions and the number of them that survive until reaching the ion mirror by n_t. We assume that the fully accelerated ions (i.e those with lifetimes $>10^{-7}$s, approximately), decompose according to a first-order rate law characterized by an average rate constant k. For these assumptions, $k = (1/t_f)\ln(n_o/n_t)$, where t_f is the ion flight time. The half-life is given by $t_{1/2} = 0.693/k$. Thus the ability to determine the kinetic parameters for ion decomposition depends upon the ability to measure n_o/n_t. Some factors influencing this measurement are now discussed.

We have shown that the percentage of ions lost by decomposition in the mirror is sufficiently small that only a small error (correctable, in principle) will be produced. Another requirement is that all the parent ions that would have been recorded in detector 1 with the mirror off be recorded in detector 2 with the mirror on. This requirement is assured by the procedure described in the text where all events are normalized to the number of Na^+ events in each detector. This procedure automatically compensates for the fact that reflected ions pass through a 90% transmission grid twice while, with the mirror off, ions and neutrals pass through three 90% transmission grids. The greatest uncertainty concerns the efficiency of the detectors. We have calculated[110] that accuracy of the kinetic measurements was greater when the percentage of events recorded in detector 2 relative to detector 1 was high and when the efficiency of both detectors was the same. A difference of up to a factor of 2 in the n_o/n_t ratio could be expected in the extreme situation where there was a very large difference in detector efficiency combined with low % of events recorded in detector 2 relative to detector 1.

CHAPTER 4

TIME-OF-FLIGHT SECONDARY ION MASS SPECTROMETRY OF ISOMERIC O-ALKYLTHYMIDINES*

4.1 INTRODUCTION

Alkylating agents such as the N-nitroso-N-alkylamides have been implicated in carcinogenesis and mutagenesis. Such molecules react readily with the nucleophilic nitrogen and oxygen atoms of the DNA bases, and with the oxygen atoms of the phosphate internucleotide linkages[166,167]. Early interest focussed on the alkylation of the N7-nitrogen of the guanine base, the site most susceptible to attack by these agents, but evidence is accumulating that the formation of O6-alkylated guanine and the O2- and O4-alkylated thymines are the more significant events. It is known, for example, that the mutagenic and carcinogenic potential correlates with the tendency of the alkylating agent to attack oxygen[168] and with the size of the alkyl group [169]. The significance of O-alkyl modifications is evidenced by the existence of repair enzymes for these lesions[170]. Furthermore, the site of alkylation can greatly affect the lability of glycosyl bonds, as observed with O-alkyl pyrimidine 2'-deoxynucleosides[169]. Kinetic and NMR studies have shown that alkylation of pyrimidines at O2, but not at O4, destabilizes the glycosyl bond[154,158,168].

To obtain information about the effects of alkylation on nucleic acid components in a solvent-free environment, we have initiated a program to study O2- and O4-alkylated thymidines, r^2dT and r^4dT, (Fig.4.1) by time-of-flight (TOF) secondary ion mass spectrometry (SIMS) on the Manitoba TOF instrument. We demonstrate here

* F. Lafortune, G.W. Buchko, F.E. Hruska, K.L. Sadana, K.G. Standing and J.B. Westmore, *Nucleosides and Nucleotides*, 11(7), 1305 (1992).

how TOF spectra, especially when metastable ion studies are included, are useful for characterizing these modified nucleosides, including the site of alkylation, and reveal clear trends regarding the effects of the size of alkyl groups on fragmentation patterns.

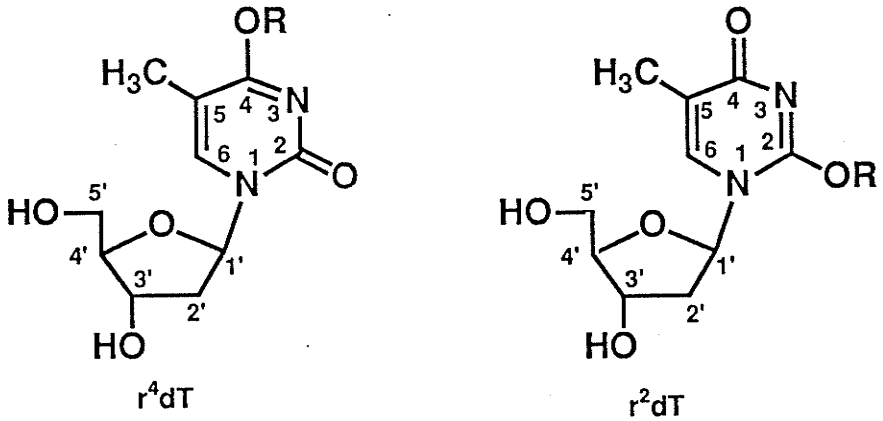

188, m^4dT
189, e^4dT
190, ip^4dT

191, m^2dT
192, e^2dT
193, ip^2dT

Figure 4.1. O2- and O4-alkylthymidines

In chapter 3, we described how evaluation of first-order rate constants and half-lives for decomposition of $[M+Na]^+$ ions could be used to differentiate O2 and O4 isomers of each pair of positional isomers and we discussed some factors influencing the accuracy of these measurements. In the present work (for which preliminary results have been communicated[171]) both positive and negative ion spectra are described for the methylated and ethylated pairs as well as for their isopropylated analogs (ip^2dT and ip^4dT). Genetic relationships between several secondary ions are established by using a metastable mapping procedure[172] analogous to the linked-scanning technique commonly used with sector instruments. Our results could be useful for the identification of oligonucleotides containing these modified constituents.

4.2.EXPERIMENTAL

4.2.1 Sample preparation:

The O2- and O4-alkylated nucleosides were prepared and purified chromatographically as described by Birnbaum *et al* [153]. For mass spectrometric analysis, they were dissolved in methanol containing less than 10% water, at a concentration of *ca* 1 mg/mL. A few μL of each solution were then deposited on anodized aluminum foil that had been boiled in water to produce a AlO(OH)(boehmite) surface[173,174].

4.2.2 Mass spectrometry:

The Manitoba II TOF secondary ion mass spectrometer[126] is shown schematically in Fig. 4.2. Sample targets were bombarded by a pulsed beam of primary Cs^+ ions (~2 ns pulses, repeated at a frequency of 2 kHz). The Cs^+ ions struck the target with an energy of 13 keV and 23 keV for the positive and negative ion studies, respectively. Of the secondary ions produced and ejected, those having a lifetime longer than *ca* 10^{-7}s were accelerated through a grounded grid by applying a voltage of +/- 5 kV to the target, and allowed to drift along the flight tube towards a "0^o detector", in front of which is an ion mirror. When the ion mirror is off, "direct" mass spectra are obtained. When an electric field is applied within the ion mirror, ions are reflected back along the flight tube toward a second "180^o detector" located near the sample target. In this way, "reflected-ion" mass spectra are produced in which stable parent ions are separated from daughter ions. Neutral daughters are recorded in the 0^o detector[120,172].

The detectors were multichannel plate electron multipliers, whose output was processed by a data system based on a LeCroy model 4208 time-to-digital converter (TDC) and a DEC LSI 11/23 computer[129]. After calibration, the time scale was converted to m/z values, and ion yields were displayed as ion counts in time bins a few ns wide.

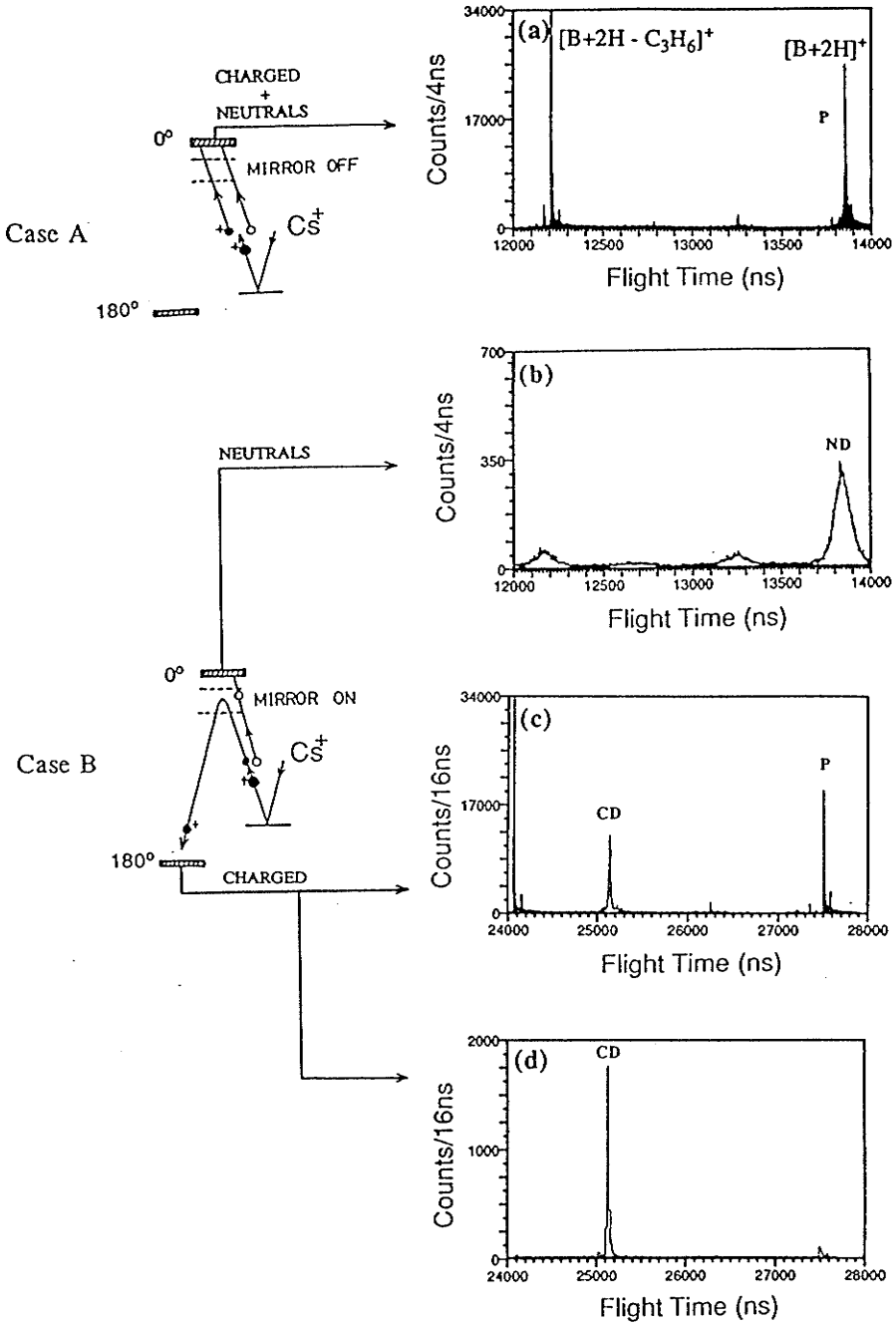

FIGURE 4.2 Analysis of ion decompositions in field-free flight. (a) Part of direct positive spectrum of ip^{4}dT recorded with the ion mirror "off". (b-d) Spectra recorded with mirror "on": (b) neutral daughters (ND) of $[B + 2H]^+$; (c) reflected parent (P) and charged daughter (CD) ions; (d) reflected CDs correlated with NDs.

4.3 RESULTS AND DISCUSSION.

4.3.1 Generation of Mass Spectra.

Genetic relationships between secondary ions can be established by separating parent ions from neutral and charged daughters as described (Fig. 4.2 (a-d)) for the positive ion spectra of ip^4dT (**190**). With the electrostatic mirror off [case A, fig. 4.2(a)] neutral and charged daughters of a given fragmenting parent ion are detected by the 0^o detector behind the mirror as a broadened peak centred at the same flight as a similar non-fragmenting ion, *e.g.* the "$[B+2H]^+$ peak" contains both the undissociated $[B+2H]^+$parent ions and the daughter species produced by parent ion decompositions in the first leg of the flight path. (B is the base moiety of the nucleoside). When the appropriate voltage is applied to the mirror, the three components of the peak are separated. Figure 2 (b) shows the neutral daughters (ND) formed in the field-free region between the acceleration grid and the mirror entrance. Because they are unaffected by the electric field of the mirror, the neutral daughters are detected in the 0^o detector at flight times corresponding to those of their parent ions. For example, ND is a neutral daughter of the $[B+2H]^+$ species, i.e. the neutral component of peak P in Fig. 2 (a). The reflected ion spectrum (Fig. 2 (c)) shows the improved resolution and well-separated peaks for charged daughter (CD) and unfragmented parent ions; the difference in flight time between daughter and parent ions is a function of their masses.

It is also possible to record in the 180^o detector the daughter ion that corresponds to arrival in the 0^o detector of its complementary neutral fragment resulting from the same parent ion decomposition. These events are stored in dedicated sections of computer memory and, in this way, it is possible to obtain a spectrum of fragment ions "correlated" with the decomposition of a selected parent ion. In other words, such a spectrum is a "daughter ion spectrum" resembling those obtained with the more

familiar types of tandem mass spectrometer. For example, Fig. 2 (d) shows the spectrum of ions recorded in the 180^{o} detector that are correlated with the neutral fragments from peak ND in the 0^{o} detector (Fig. 2 (b)), i.e. this is a daughter ion spectrum of ion P. In this example, the determined m/z values of P and CD are 169 and 127, assigned as $[B+2H]^{+}$ and $[B+2H-C_3H_6]^{+}$, respectively. This approach was used to establish genetic relationships between series of secondary ions.

In this chapter, emphasis is placed on the interpretation of the direct spectra of the rdT but reference is made to their metastable ion decompositions whenever they provide clues to mechanisms of ion formation.

4.3.2 General spectral characteristics

Table 4.1 lists positive and negative secondary ion abundances for dT and the rdT. For positive ions, results for the range m/z 90 up to that of $[M+Na]^{+}$ are expressed in % of total ion current (%TIC) because this quantity best reflects differences between spectra. For the negative mode, the prominent NCO^{-} ion (m/z 42) was added to the list.

In general, the spectral features, *i.e.* the ion types present, resemble those obtained for nucleosides by other "soft" ionization methods: liquid secondary ionization (LSI, also know as FAB[42, 68,73], laser desorption (LD)[115] and chemical ionization (CI)[67]. However, we do note differences in abundances of the ion types, which presumably reflect the presence of the O-alkyl group. We find sensitivity to be lower in the negative ion mode than in the positive ion mode, as indicated by a lower rate of data accumulation under similar detection conditions. This has also been noted in LSI mass spectra of nucleosides

The general features of the TOF spectra are illustrated in Fig. 4.3 by the positive and negative ion mass spectra of ip[4]dT. In each spectral mode many structurally diagnostic ions are observed. These arise from (a) ions characteristic of the intact molecule (i.e. $[M+H]^{+}$, $[M+Na]^{+}$, $[M-H]^{-}$, $[M+Cl]^{-}$), (b) from glycosyl bond

TABLE 4.1 Direct positive and negative ion mass spectra of O-alkylated thymidines (%TIC, see text).

	ION ASSIGNMENTS	dT	m/z	m^2dT	m/z	m^4dT	e^2dT	m/z	e^4dT	ip^2dT	m/z	ip^4dT
(+)	$[M+Na]^+$	30.5	265	20.2	279	19.0	3.2	293	12.3	8.0	307	0.6
	$[M+H]^+$	24.5	243	7.4	257	15.1	20.1	271	13.1	7.1	285	18.6
	$[BHCH{=}CH_2]^+$	---	154	3.2	168	3.5	2.7	182	2.9	0.7	196	1.1
	$[BH+Na]^+$	---	149	11.1	163	2.5	1.6	177	2.3	2.9	191	---
	$[B+2H]^+$	21.2	127	33.7	141	43.1	41.1	155	41.0	24.9	169	33.9
	153^+	1.6	153	9.4	153	0.4	2.6	153	1.0	2.5	153	2.2
	$[B+2H-(R-H)]^+$	---	---	0.8	127	0.6	6.4	127	8.2	29.7	127	25.7
	S^+	14.5	117	9.8	117	10.3	14.4	117	10.7	16.3	117	11.8
	110^+	2.0	110	0.7	110	0.9	2.3	110	4.4	2.1	110	2.4
	$[S-H_2O]^+$	2.0	99	3.6	99	4.7	5.6	99	4.1	5.6	99	3.6
	Σ B	24.8		55.7		47.5	54.0		56.9	62.1		64.2
	Σ S	16.5		13.4		15.0	20.0		14.8	21.9		15.4
(-)	$[M-H]^-$	8.7	241	0.7	255	0.5	---	269	---	0.6	283	2.1
	$[M-R]^-$	---	---	1.7	241	2.5	3.3	241	2.1	0.6	241	3.7
	179^-	---	179	0.7	179	0.8	0.6	179	1.3	1.4	179	0.5
	B^-	25.9	125	50.5	139	27.2	31.0	153	17.1	17.9	167	12.7
	$[BH-R]^-$	---	---	5.4	125	3.3	6.5	125	4.1	7.7	125	5.4
	109^-	---	109	2.3	109	1.4	1.7	109	0.9	1.8	109	0.9
	$[BH-R-18]^-$	---	107	1.3	107	3.1	0.7	107	3.4	1.2	107	1.0
	$[BH-R-CO]^-$	---	97	2.0	97	4.4	4.8	97	7.5	5.2	97	5.1
	NCO^-	29.6	42	35.3	42	55.1	51.4	42	60.6	63.7	42	68.6
	other	U	31.3		W	1.6		X	1.0			
		V	4.4					Y	1.9			

Note: U = $[M-H+42]^-$, V = $[M-H+14]^-$, W = $[M+Cl]^-$, X = $[M-R-NCO]^-$, Y = $[M-R-30]^-$

$\Sigma B = [BH+Na]^+ + [B+2H]^+ + 153^+ + [B+2H-(R-H)]^+ + 110^+$
$\Sigma S = S^+ + [S-H_2O]^+$

TABLE 4.2 Direct mass spectra of O-alkylthymidines: Highlights

Ions characteristic of the intact molecule:

+ve -$[M+Na]^+$ and $[M+H]^+$ usually present in significant yields.

-ve -$[M+Cl]^-$ and $[M-H]^-$ hardly detected at all.

Fragmentation pattern:

+ve -Deglycosylation followed by dealkylation of the base (with H transfer).

-ve -Deglycosylation mainly followed, but sometimes preceded, by dealkylation of the base.

Effect of alkyl group (presence and position):

+ve -%TIC of $[M+Na]^+ + [M+H]^+$ ions decreases according to: dT>mdT>edT>ipdT; it is greater for O4 isomers.

-%TIC of $[B+2H]^+ + [BH+Na]^+$ increases according to dT<ipdT<edT~mdT.

-%TIC of dealkylation of the base (m/z 127) increases when the size of R increases, and it is not affected by R position

-%TIC of sugar increases when the size of R increases for O2-isomers; this effect is not observed with O4-isomers.

-ve -%TIC of B^- decreases according to the trend: mdT>edT>ipdT;it is greater for O2-isomers than for 04-isomers, although this difference decreases when the size of R increases.

-%TIC of $[BH-R]^-$ is not affected by the size of R, although its relative abundance is slightly greater for O2-isomers.

-S^- is not detected.

-%TIC of NCO^- increases as R gets bigger; it is always slightly greater for O4-isomers, although this difference decreases as the size of R increases.

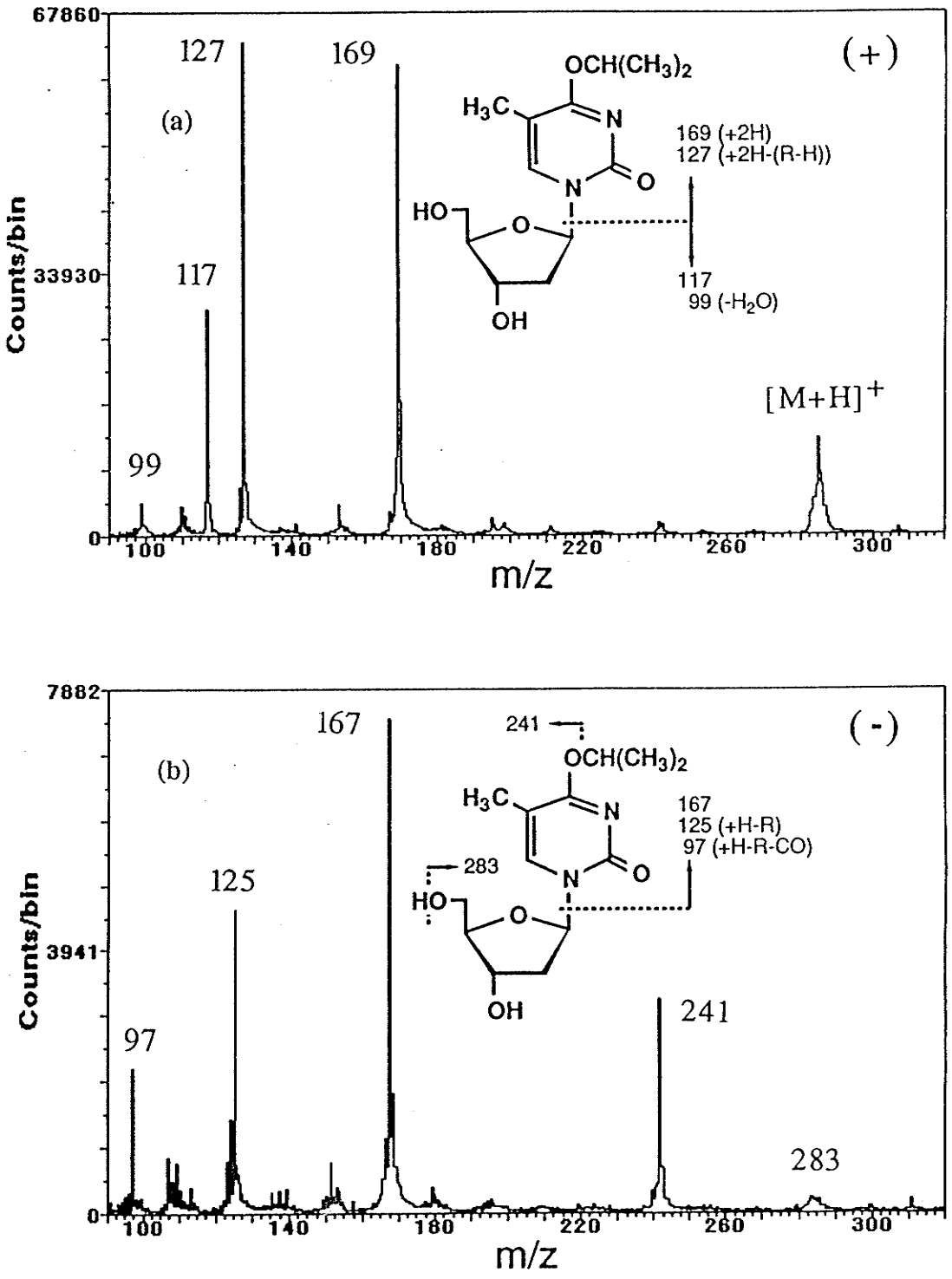

FIGURE 4.3 Direct spectra of ip^{4}dT: (a) positive ions, (b) negative ions.

cleavage, and (c) from dealkylation. Table 4.2 is a summary of the important trends in the data of Table 1, which we now discuss.

4.3.3 The positive mass ion spectra

Ions characteristic of the intact molecule. The ions $[M+H]^+$ and $[M+Na]^+$are both prominent (Table 1); in addition, some spectra show small signals for $[M-H+2Na]^+$ ions. While the relative amounts of $[M+H]^+$ and $[M+Na]^+$ vary from sample to sample (presumably due to variable amounts of adventitious Na^+), their combined %TIC show that alkylation at the O2 or O4 positions of dT increases the extent of fragmentation, i.e. the overall stability decreases according to the trend dT>mdT>edT>ipdT. Thus, these combined %TICs vary from 55% for dT compared to 15-34% for the rdT. The r^4dT are slightly more stable than the r^2dT.

Glycosyl bond cleavage. Using r^4dT as the example, Scheme 4.1 depicts four reactions involving glycosyl bond cleavage, three of them (a-c) leading to formation of a positive ion. It has been assumed that initial protonation is at N3, which is probably the most basic site[67,154]. Relative ion yields and decomposition rates of metastable ions of these compounds[110] indicate that reaction (a) occurs more readily for $[M+H]^+$ than for $[M+Na]^+$, a result explained by chelation of Na^+ by three oxygens, i.e. O2, O4' and O5'. However, the *decomposing* form of $[M+Na]^+$ may be that represented in reaction (a). The formation of $[B+2H]^+$ and $[BH+Na]^+$ by reaction (a) involves a well-documented hydrogen transfer from C-2' to O-2[42,67,73].

While formation of $[B+2H]^+$ and $[BH+Na]^+$ from the respective $[M+H]^+$ and $[M+Na]^+$ ions, reaction (a), is supported by detection of appropriate metastable ion decompositions, similar support for formation of S^+ ions from these precursors is lacking. Thus, S^+ ions must be formed prior to ion acceleration. For S^+ ions to be detected as a *sharp* peak they, or their precursors, must be emitted from the surface within *ca* 10^{-8}s and, to receive full acceleration , they must be formed at, or very near,

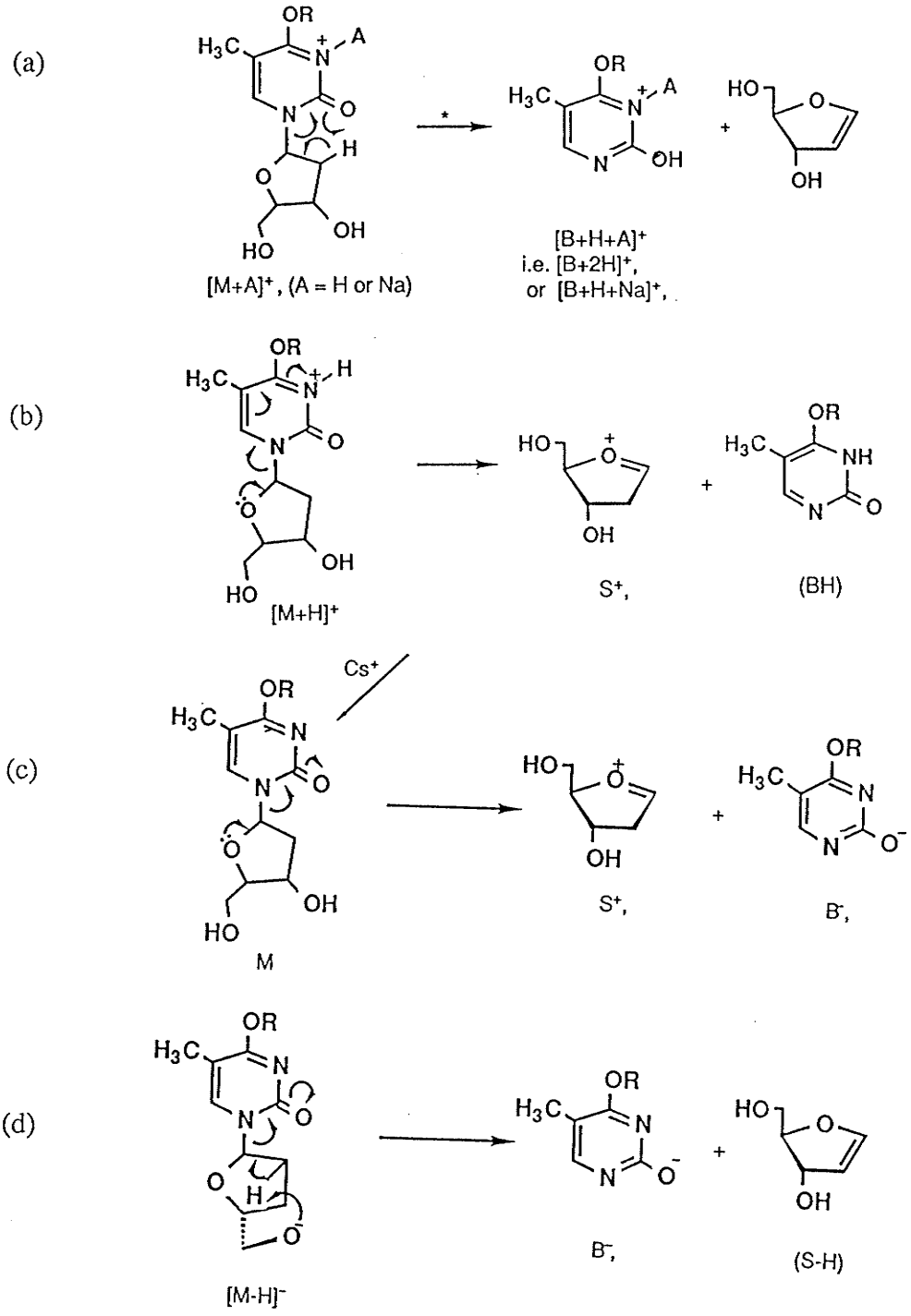

SCHEME 4.1

the surface (otherwise peak broadening would occur). Reactions (b) and (c) of Scheme 4.1 are proposed formation modes. Reaction (b) occurs only for a high energy population of $[M+H]^+$ ions (lower internal energy populations can decompose by alternative, slower, low-energy pathways, such as the rearrangement shown in reaction (a)). Formation of S^+ by a direct cleavage mechanism is consistent with the observations, but a rapid, high-energy rearrangement cannot be ruled out. The other proposed route, reaction (c), invokes ion pair production (i.e. formation of S^+ and B^- at, or near, the sample surface, following energization by primary Cs^+ ion impact. Such reactions are expected to be very rapid.

For discussion of fragment ions derived from glycosyl bond cleavage, it is useful to define ΣB as the sum of the %TICs of $[BH+Na]^+$, $[B+2H]^+$, $[B+2H-(R-H)]^+$, and 153^+; and ΣS as the sum of the %TICs of S^+ and $[S-H_2O]^+$. These numbers are included in Table 4.1. For all molecules, ΣB> ΣS, indicating that scission of the glycosyl bond favors positive charge retention by the base moiety rather than transfer of the charge to the sugar fragment. Furthermore, the data show that charge retention by the base is strikingly enhanced by O2 or O4 alkylation. Charge retention by the base was shown by Crow *et al* [73] to be a general feature of the LSI-collisional activation (CA) spectra of thirty nucleosides. In fact, in the case of *purine* nucleosides, in which the bases are particularly able to accommodate a positive charge, S^+ ions could not even be detected. In so far as isomer differences are concerned, we note that when the alkyl group is located on O4, its nature (m, e, or ip) does not seem to have much influence on the %TIC of S^+. On the other hand, for the O2-isomers, the %TIC increases slightly according to the trend mdT<edT<ipdT (Tables 4.1 and 4.2).

Both products of glycosyl bond cleavage undergo further decomposition. The S^+ ion decomposes in at least two possible ways; metastable ion decompositions show that

the ion of m/z 99 is formed by the loss of H_2O (reaction (a), Scheme 4.2), and the ion of m/z 73 by loss of C_2H_4O (reaction (b) Scheme 4.2). The $[B+2H]^+$ ion derived from the rdT undergoes alkene loss (see below). This fragmentation significantly lowers its abundance and prevents further analysis of the effect of alkyl group size on N-glycosyl bond scission.

(a)

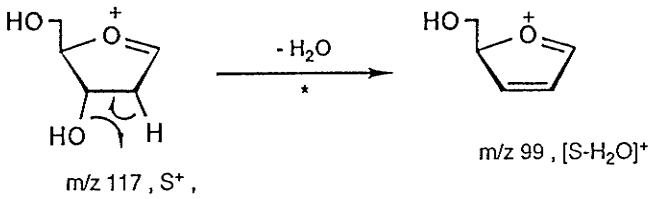

m/z 117 , S^+ ,

m/z 99 , $[S-H_2O]^+$

(b)

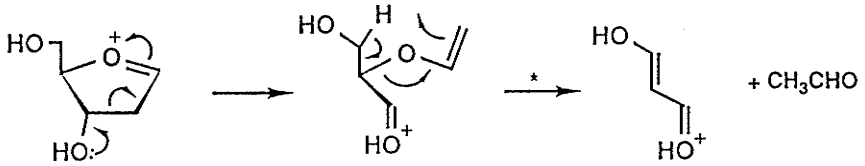

m/z 73

SCHEME 4.2

Dealkylation. Fragment ions resulting from dealkylation or dealkenation of $[M+H]^+$ and $[M+Na]^+$ are not detected. The observed dealkenation of $[B+2H]^+$ or $[BH+Na]^+$ fragments from e^4dT or ip^4dT likely proceeds through a cyclic six-membered rearrangement (illustrated for e^4dT in Scheme 4.3) involving transfer of hydrogen from the alkyl group to N3. (In the analogous rearrangement for the O2 derivatives hydrogen can be transferred, in either of the two monoprotonated tautomeric forms, to whichever of N1 or N3 is unprotonated). By this mechanism, for which metastable transitions give support, either ethene or propene is expelled from the base. The extent of dealkenation increases significantly in both of the O2 and

O4 series according to the trend mdT<edT<ipdT, and in the case of ip^2dT the resulting fragment at m/z 127 gives the most intense peak of the spectrum. A rationale for this trend was presented in chapter 3[110]. However, there is no consistent trend in the effects of the *position* of the alkyl group. Note that this rearrangement is not applicable to the mdT, and a mechanism involving a five-membered cyclic transition state would lead to the unlikely loss of $:CH_2$. It is probable that the $[B+2H-(R-H)]^+$ species, observed with small %TIC in the mdT spectra, results by some alternative route. In addition, a metastable ion decomposition was not observed for such a loss.

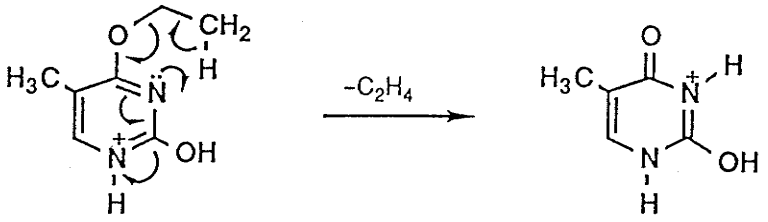

m/z 155
$[B+2H]^+$

m/z 127
$[B+2H-(R-H)]^+$

SCHEME 4.3

Alternative decomposition pathways for $[M+H]^+$. Table 4.1gives data for three minor ions observed in the positive ion mass spectra of rdT, namely $[BH+27]^+$ (listed as $[BHCH=CH_2]^+$) and two unalkylated fragments at m/z 153 and m/z 110, all of which could be genetically related in the manner illustrated for e^4dT in Scheme 4.4. Formation of $[BH+27]^+$ is widely known in electron ionization (EI)[62], CI[67] and LSI[42,73] mass spectra of unmodified nucleosides. Here, with rdT, it is formed in much smaller yields, because of the increased importance of other fragmentation pathways, such as glycosyl bond cleavage and alkene loss. Subsequent alkene loss from the $[BH+27]^+$ ion through a six-membered cyclic rearrangement[110] would produce **191**, at m/z 153, which could then lose HNCO by a retro-Diels-Alder (RDA) reaction to form the m/z 110 ion, **192** or **193**[62].

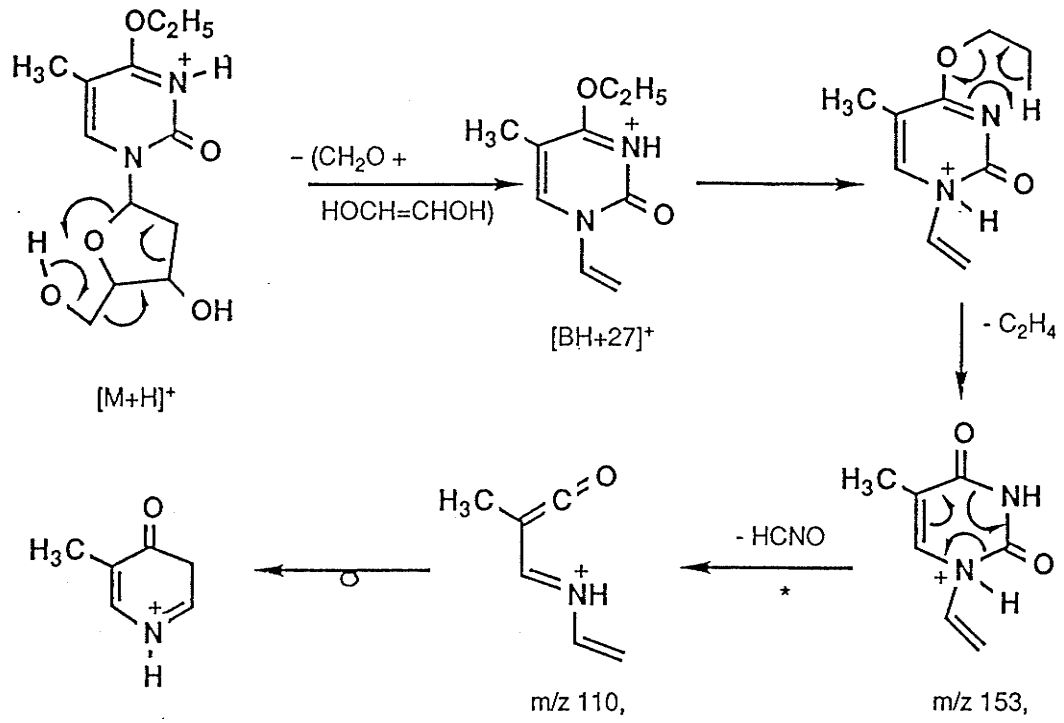

SCHEME 4.4

4.3.4 Negative ion spectra

Prominent ions. For the alkylated derivatives, B^- and NCO^- are the most abundant ions in the spectra. In addition, the largest peak in the spectrum of thymidine corresponds to $[M+41]^-$, which we assigned as an NCO^- adduct of $[M-H]^\cdot$ (see below). This adduct is not detected in the spectrum of any rdT.

Ions characteristic of the intact molecule. The $[M-H]^-$ ion of thymidine is prominent (%TIC~9%) whereas $[M-H]^-$ ions or rdT can barely be detected (%TIC<1%).

Glycosyl bond cleavage. One of the possible products of glycosyl bond cleavage, S^- is not observed in any spectrum. For the other product ion, B^-, the %TIC is always greater for r^2dT than for the corresponding r^4dT (Table 4.1), but as the size of the alkyl

group increases, its importance diminishes with a concomitant increase in %TIC of NCO^-. The observation that the %TIC for S^+ in positive ion spectra is usually greater for r^2dT isomers supports a mechanism that involves a common source for these two ions. A suitable mechanism is presented as reaction (c) of scheme 4.1. We note that, in the ion pair production, the formation of B^- would be facilitated by the resulting aromatization and extended charge delocalization possible for the pyrimidine ring. On the other hand, B^- ions can also be obtained from $[M-H]^-$ ions, as proposed in reaction (d) (Scheme 4.1), but this concerted mechanism could not be confirmed by metastable ion studies, because the %TIC of $[M-H]^-$ was too low for daughter ions to be detected. However, it represents a well-documented fragmentation pathway for other nucleosides[42,73].

Alkene loss. In the negative ion mode, alkene loss from $[M-H]^-$ (or, possibly, dealkylation of $M^{-\cdot}$) produces ions at m/z 241, $[M-R]^-$. Alkene loss from B^- produces ions at m/z 125 corresponding to $[BH-R]^-$. Mechanistic rationalizations (Scheme 4.5) leading to the latter ion involve either simultaneous H transfer and alkene loss from B^- to give **194** (illustrated for e^4dT, in reaction (a)) or hydrogen transfer *after* the loss of R to give **195** (reaction (b)).

(a)

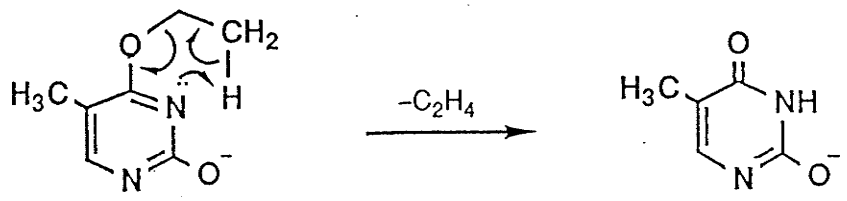

B^- m/z 125 $[B-(R-H)]^- \equiv [B+H-R]^-$,

SCHEME 4.5

(b)

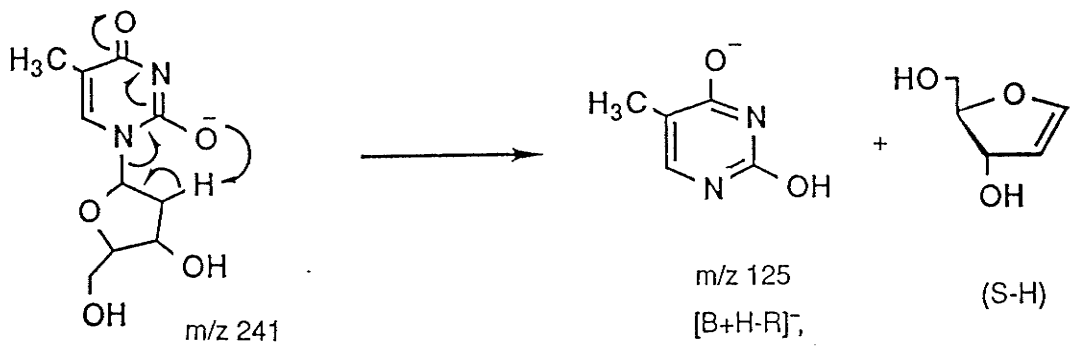

m/z 241 $[M-R]^-$, m/z 125 $[B+H-R]^-$, (S-H)

Easily rationalized on the basis of reaction (b) are (*i*) the presence of both $[M-R]^-$ and $[BH-R]^-$, and (*ii*) the observation that the %TIC of $[BH-R]^-$ for the mdT are almost the same as for the other rdT. On the other hand, reaction (a) better explains why the %TIC of $[BH-R]^-$ is greater for r^2dT than for r^4dT, because both N1 and N3 can serve as hydrogen acceptors during alkene loss from the O2 isomers. Transfer to N1 for e^2dT is shown in Scheme 4.6. An alternative mechanism (Scheme 4.7) for decomposition of $[M-R]^-$ provides a rationale for formation of the ion of m/z 179 (assigned as $[B-R+C_3H_3O]^+$), found in small yields in all rdT negative ion spectra.

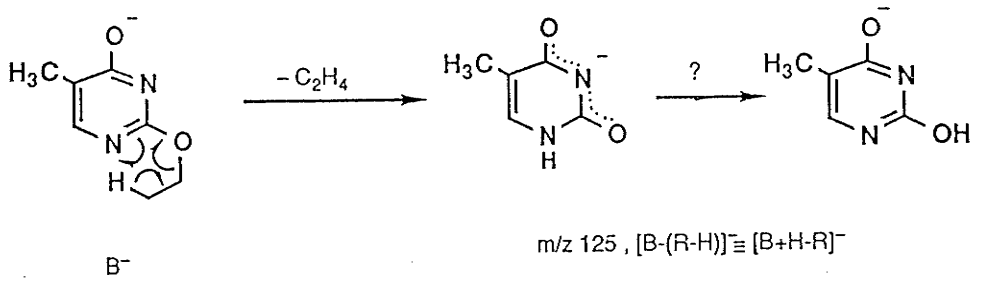

SCHEME 4.6

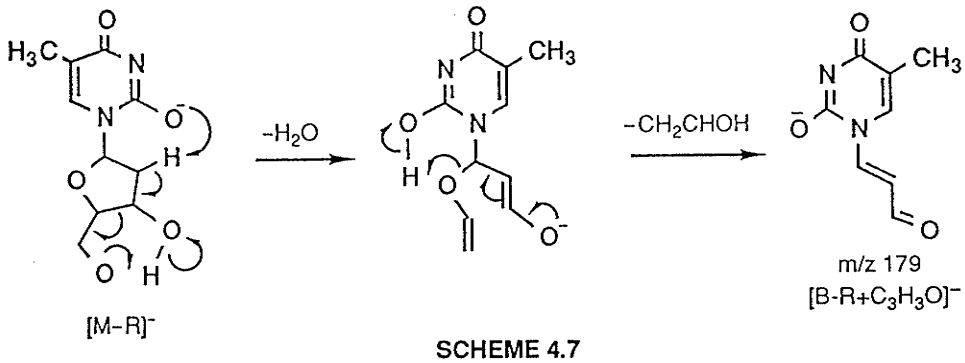

SCHEME 4.7

Formation of NCO^- ions. A striking feature of all negative ion spectra is the high relative abundance of m/z 42, assigned as NCO^-, which gives the base peak in all cases except those of dT and m^2dT. Crow *et al* [73] observed NCO^- and $[M-H-HNCO]^-$ in the negative ion CA spectrum of uridine, and McCloskey[62] observed $[M-HNCO]^+$ in the EI spectrum of thymine and uracil. In both studies strong evidence was found that the NCO fragment originated from N3-C2-O2 of the pyrimidine base, and RDA reactions were proposed for the losses of HNCO. However, in the absence of isotopic labelling, we cannot confirm the same mode of NCO^- formation for O2 and O4 alkylated molecules. That is, we cannot discount alternative sources (N1-C2-O2, N3-C4-O4) for the NCO^- ion.

Table 4.1 shows that the %TIC of NCO^- increases in both the r^2- and r^4dT series according to the trend dT< mdT < edT < ipdT. Furthermore, the %TIC is always greater for an O4 isomer relative to the O2 isomer but the difference between them decreases as the size of the alkyl group increases. A simple rationale for these observations can be given if the origin of the NCO^- ion is the N3-C2-N2 fragment in both the r^2dT and r^4dT series, as shown in reaction (a) of Scheme 4.8 for its formation from dealkylated r^2dT and r^4dT precursor ions. However, for the r^4dT, a dealkylated precursor ion is not essential for NCO^- formation. Thus, Scheme 4.8(b) depicts NCO^- formation by ion pair production in the substrate shortly after energization by the primary Cs^+ ions. On the other hand, for the r^2dT, conversion of the N3-C2-O2 fragment into NCO^- would require prior elimination of the O2 alkyl group and hence would be expected to proceed less readily. But, as the size of the alkyl group increases, its elimination becomes easier and thus the isomer difference should diminish.

(a)

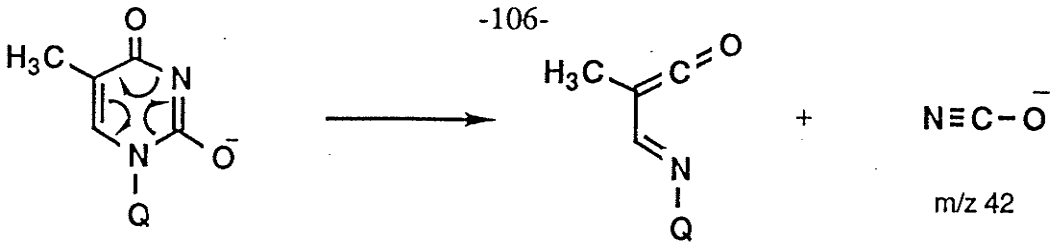

Q = sugar, $[M-R]^-$
Q = H, $[BH-R]^-$

SCHEME 4.8

(b)

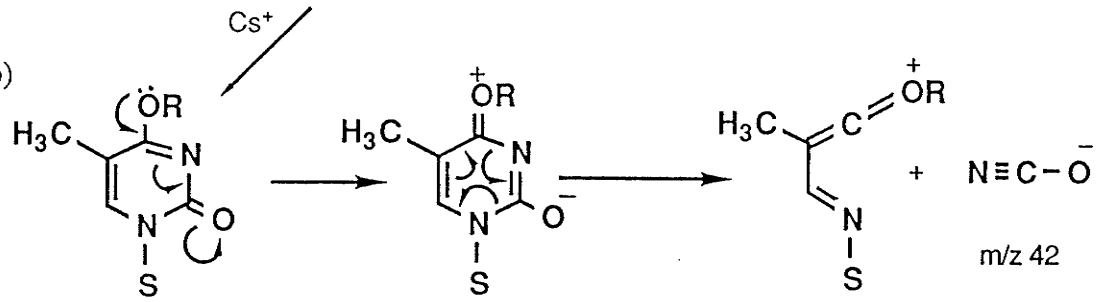

In the negative ion spectrum of thymidine (Fig. 4.2), two unusual peaks are observed at m/z 255 $[M+13]^-$, and at m/z 283, $[M+41]^-$, the latter, as noted above, being the most intense peak of the spectrum (Table 4.1). We assign these to $[M-H+14]^-$ and $[M-H+42]^-$, respectively. These ions are not detected in the rdT spectra, nor have they been reported in published LSI[42] or EI[134] mass spectra of thymidine. The formation of these ions can be explained by a reaction at the surface of the sample where, in addition to formation of ions, energetic particle bombardment also produces and desorbs larger quantities of energized neutral molecules and radicals. Possibly, in the present matrix-less samples, the readily formed NCO^- ions combine with $[M-H]^\cdot$ radicals by a Diels-Alder reaction (Scheme 4.9). The resulting $[M-H+42]^{-\cdot}$ radical anions could, by losing CO, yield the observed $[M-H+14]^{-\cdot}$ ions, and also act as another source of B^- ions. In view of these observations, it is intriguing that a $[B+42]^-$ ion species has been reported in the LSI mass spectrum[42] of this compound but was not observed here. (However, its assignment as $[B+C_2H_2O]^-$ is different from that expected from our proposed $[M-H+42]^-$ precursor). Decompositions of metastable $[M+41]^-$ were not detected in our reflected ion spectra and any reactions, if they do occur at all, must be very rapid ($<10^{-8}$ s). Isotopic labelling could shed some light on this matter.

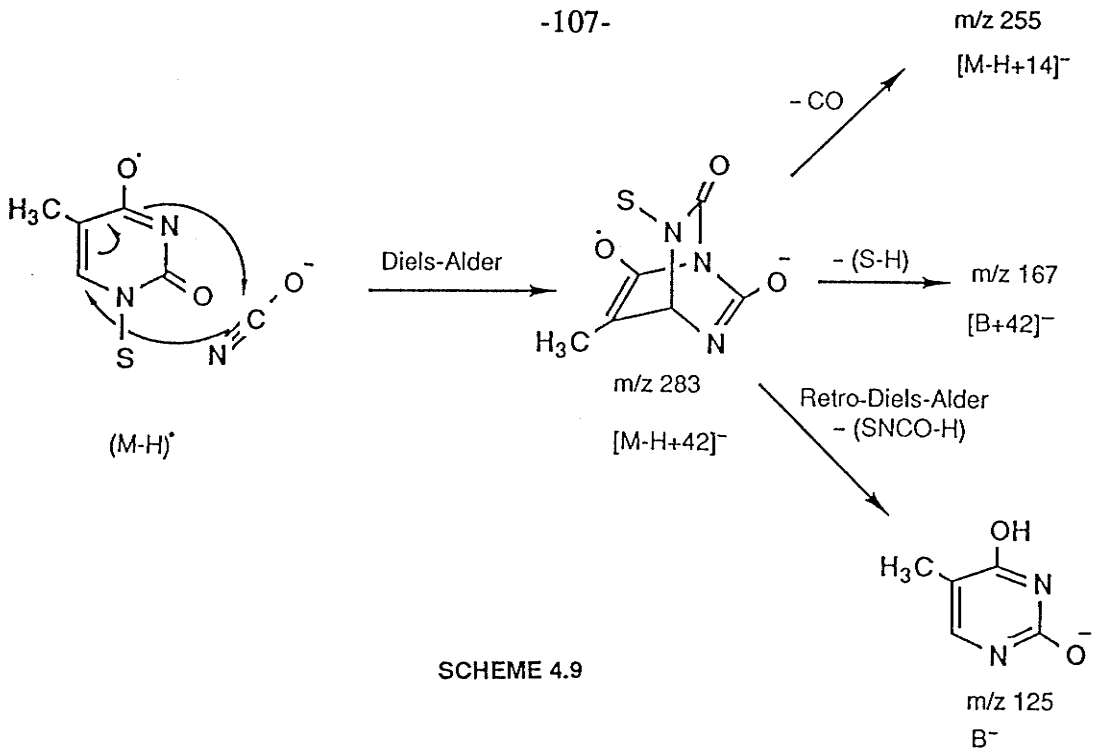

SCHEME 4.9

We note that we could not detect an $[M+41]^-$ ion in the LSI mass spectrum, recorded in a sector field mass spectrometer, of dT samples in a glycerol matrix in which NaOCN had been dissolved. It is possible, in this latter experiment, that the polar matrix inhibits the putative reaction, either by solvent effects or by physical separation of the supposed reactants.

4.3.5 Relative rates of dealkylation and glycosyl bond cleavage.

In the positive ion spectra of the rdT the absence of the dealkylation products of $[M+H]^+$ and $[M+Na]^+$ and the prominence of the glycosyl bond cleavage ionic products $[B+2H]^+$, $[BH+Na]^+$ and S^+, indicate that glycosyl bond cleavage proceeds more rapidly than dealkylation; subsequent dealkylation of $[B+2H]^+$ yields $[(B+2H)-(R-H)]^+$ (i.e. $[B+3H-R]^+$). On the other hand, all rdT negative ion spectra do show a small percentage of the dealkylation product $[M-R]^-$, and this percentage is not influenced by the size or the position of the alkyl group. Thus, dealkylation is competitive with glycosyl bond cleavage, meaning that the $[B-R]^-$ ion can be formed from a common precursor by, at least, two competing pathways. While the glycosyl bond cleavage product ion B^- is present, sugar-containing ions, as noted above, were not observed.

4.3.6 Summary and comparison of TOF/SIMS with LSI/CA in sector-fields instruments.

In our TOF-SIMS experiments matrix-free samples were bombarded by Cs^+ ions of several keV energy. In the positive ion mass spectra, molecular masses can be verified by the presence of prominent $[M+H]^+$ and $[M+Na]^+$ ions. Alkylation leads to a significant increase in fragmentation of these ions as the size of the alkyl group increases. The fragmentation is a consequence of enhanced glycosyl bond cleavage, as well as of dealkylation of the modified base. Cleavage of the glycosyl bond is more facile for both r^4dT and r^2dT (particularly for the latter) than for the unmodified nucleoside, and the extent of dealkylation increases as the size of the alkyl group increases (but is independant of its position). Glycosyl bond cleavage occurs more rapidly than dealkylation. In the negative ion spectra, molecular mass can be verified for dT by a prominent $[M-H]^-$ ion, which is not, or barely, detectable for the rdT. The prominent ions are B^- (of greater abundance for r^2dT than for r^4dT) and NCO^-. In addition, the latter ion appears to form an adduct with $(dT-H)^\cdot$ only, to give a prominent $[M+41]^-$ ion. Glycosyl bond cleavage and dealkylation of rdT occur at competitive rates.

In some respects, the capabilities of our reflecting TOF and sector-field mass spectrometers are similar, *e.g.* in the ability to study ion decompositions on the μs time scale. In our TOF instrument we can study only unimolecular ion decompositions, whereas collisionally-activated decompositions can be routinely studied with a sector-field instrument. Nevertheless, the greatest differences between the spectra recorded by the two techniques are likely to be more dependent upon the sample (*e.g.* matrix or matrix-free) than upon the type of mass spectrometer employed. These results demonstrate the utility of TOF-SIMS for analysis of compounds of biological importance.

CHAPTER 5
TIME-OF-FLIGHT SECONDARY ION MASS SPECTROMETRY OF PROTECTED OLIGODI- AND TRINUCLEOTIDES*

5.1 INTRODUCTION

In recent years, the chemical synthesis of DNA fragments has become increasingly important in molecular biosciences. Following major progress in synthesis technology, small DNA fragments can now be synthesized rapidly, in a matter of days. Before the advent of particle-assisted desorption mass spectrometry, sequence analysis of growing oligonucleotides involved deprotection, followed by the use of laborious methods of chemical degradation[6,7]. Since 1980, it has become possible to analyze chemically protected synthetic oligonucleotides directly by ^{252}Cf-PDMS[44,45,107], SIMS[53,54], and FABMS[50,56,81].

Apart from the MS reports of protected oligonucleotides synthesized by Professor K.K. Ogilvie et al[44,45,53,54], all other MS investigations of protected NACs found in the literature involved oligodeoxyribonucleotides or their analogs. In an ongoing effort to investigate the use of TOF-SIMS as an an analytical tool to characterize and differentiate isomeric NACs, we have analyzed two series of protected oligodi- and trinucleotides that contain either 3'-5' or unusual 2'-5' phosphodiester linkages (compounds **196-201**, shown in Figure 5.1). Also included is a series of trinucleotides (compounds **202-205**, Figure 5.1) that contain vicinal 2'-5' and 3'-5' phosphodiester bonds. These branched RNA fragments are key constituents of lariats (**206**, see below) which are believed to play an essential role in the splicing of messenger RNA precursors.

* published in part in the following:

175. F. Lafortune, W. Ens, K.G. Standing, J.B. Westmore, M.J. Damha and K.K. Ogilvie, *Adv. in Mass Spectrom*, Heyden & Son, London, **11**, 1402 (1989).

111. F. Lafortune, K.G. Standing, J.B. Westmore, M.J. Damha and K.K. Ogilvie, *Org. Mass Spectrom.* **23**, 228 (1988).

112. F. Lafortune, M.J. Damha, X. Tang, K.G. Standing, J.B. Westmore and K.K. Ogilvie, *Nucleosides and Nucleotides*, **9**, 445 (1990).

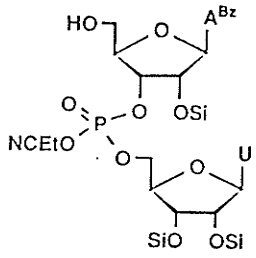

196

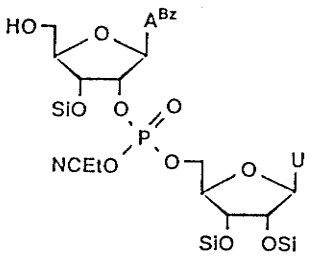

197

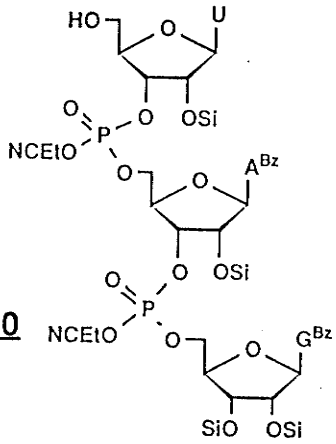

200

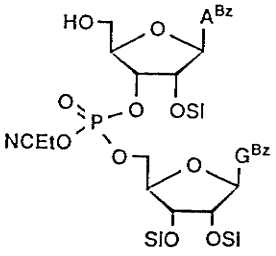

198

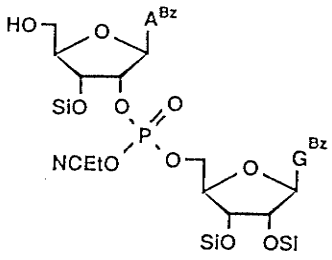

199

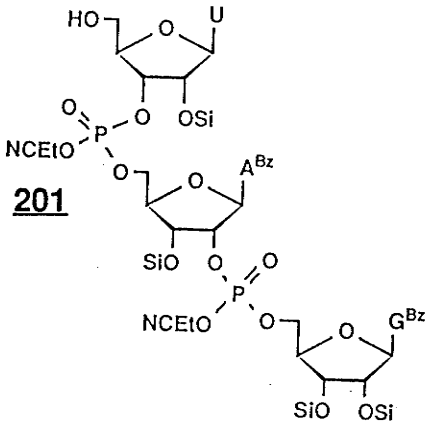

201

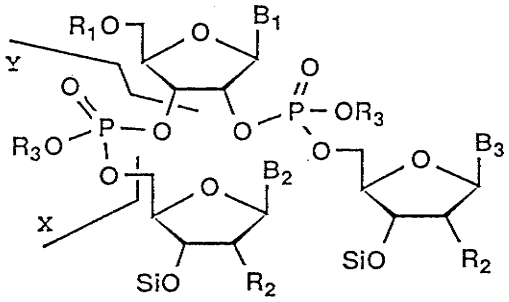

COMPOUND	R1	R2	R3	B1	B2	B3
202 $G^{U}U$	H	OSi	Me	$_{Bz}G^{NPE}$	U	U
203 $A^{C}C$	H	OSi	CE	A^{Bz}	C	C
204 $A^{T}T$	H	H	Me	A^{Bz}	T	T
205 $A^{U}U$	H	OSi	Me	A^{Bz}	U	U

Notes: Si = t-Bu$(CH_3)_2$Si-
Me = CH_3
CE = $NC\text{-}CH_2\text{-}CH_2$-
Bz = C_6H_5CO- (on N^2 of G and N^6 of A)
NPE = p-$NO_2C_6H_4CH_2CH_2$- (on O^6 of G)

Figure 5.1 Protected di- and triribonucleotides

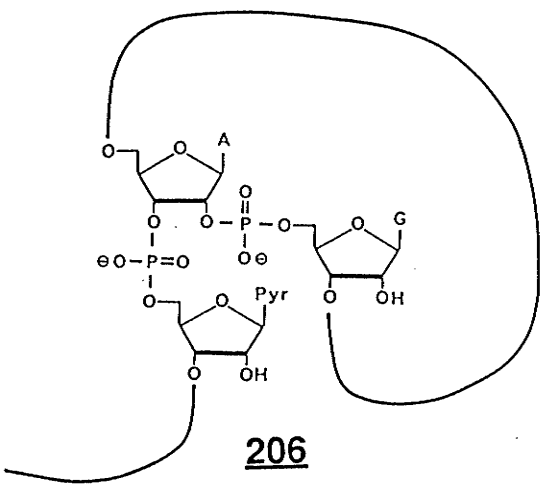

206

Negative ion mass spectra were obtained on the Manitoba TOF II instrument, which incorporates an ion mirror. We will demonstrate how this technique can help differentiating these very closely related biomolecules.

5.2 EXPERIMENTAL

5.2.1. Sample preparation.

All compounds were synthesized at McGill[176] by the phosphite method[177], using nucleoside phosphoramidite. The purified oligonucleotides were dissolved in methanol at a concentration of *ca* 1mg/ml. A few μL of each solution were then deposited on aluminum foil treated to give a boehmite, AlO(OH), surface[173,174].

5.2.2. Mass spectrometry:

Sample targets, introduced in the Manitoba TOF II secondary ion mass spectrometer[126], were bombarded by a pulsed beam of 23 keV Cs^+ primary ions. The secondary negative ions produced were accelerated to -5 keV, allowed to drift along the field-free region of the flight tube and they were then detected by microchannel plates. No electric field was applied within the ion mirror in the current study; therefore, only "direct" mass spectra were obtained.

5.3 RESULTS AND DISCUSSION

5.3.1.Dimers

Table 5.1 shows a list of the most prominent peaks obtained in TOF-SIMS spectra recorded in the negative mode for the two pairs of position isomers studied. Results are

expressed in % of total ionic current (%TIC) in the region m/z 100 up to the $[M-H]^-$ ions; this method better reflects differences between the isomeric pairs. Figure 5.2 illustrates some important fragments observed in the negative ion TOF-SI mass spectrum of A_pG. Figure 5.3 shows how the negative ion TOF mass spectrum of ApG and A^pG compare. Table 5.2 highlights and summarizes important trends obtained from the data found in Table 5.1.

In all instances, the %TIC of $[M-H]^-$ ions is very low, ranging from 1.2 to 3.0%. On the other hand, the loss of one or more protecting groups from M^- has led to three detectable signals in each spectrum. The loss of the cyanoethyl group (EtCN) from a phosphotriester moiety leads to $[M-EtCN]^-$ ions, which account for 5.6-6.7% of the %TIC. Losses of the benzoyl group (PhCO, or Bz), protecting the N-6 of adenine or the N-2 of guanine, or of the t-butyl dimethylsilyl group (Si), protecting 2' and/or 3' oxygens, yield $[M-EtCN+H-Bz]^-$ and $[M-EtCN+H-Si]^-$ ions, respectively. These ions contribute an additional 2 to 5% to %TIC. Formation of such ions, where an hydrogen seems to be replacing a protecting group, possibly from a neighboring molecule near the surface of the sample film, has been observed before, under FAB[50,56] and ^{252}Cf-Plasma Desorption[44] conditions, as well as by our group[53].

Sequence information has also been obtained for each dimer. In accordance with what has been observed with unprotected, normal 3'-5' oligodeoxyribonucleotides[60,68,81], 5'-phosphate sequence ions (Y^- ions, see Fig. 5.1) are not always more abundant than the corresponding 3'-phosphate sequence ions (X^- ions) for the 2'-5' dimers. This is true regardless of whether we compare Y^- and X^- ions of a given compound or whether we take into account the ions that have lost a protecting group, (i.e. %TIC (Y^- + $[Y-EtCN+H]^-$) vs %TIC (X^- + $[X-EtCN+H]^-$ + $[X-Bz+H]^-$)). What is more striking is that X series ions (X^-, $[X-EtCN+H]^-$ and $[X-Bz+H]^-$) in 3'-5' dimers are almost twice as abundant (in %TIC) as observed with 2'-5' isomers. Additionaly, the ratio (%TIC Y series) / (%TIC X series) is 80-90% greater for 2'-5' isomers. Comparing the relative

	3',5'ApU		2',5'ApU		3',5'ApG		2',5'ApG	
ASSIGNMENT	m/z	%TIC	m/z	%TIC	m/z	%TIC	m/z	%TIC
$[M-H]^-$	1072	1.2	1072	1.2	1215	3.0	1215	2.7
$[M-EtCN]^-$	1019	6.7	1019	5.6	1162	6.5	1162	6.4
$[M-EtCN+H-Bz]^-$	915	0.9	915	0.9	1058	2.2	1058	1.3
$[M-EtCN+H-Si]^-$	905	1.7	905	1.4	1048	2.8	1048	1.2
Y^-	605	10.4	605	6.5	748	6.5	748	5.3
$[Y-EtCN+H]^-$	552	9.0	552	10.4	695	3.0	695	2.8
X^-	617	6.6	617	2.7	617	11.9	617	6.8
$[X-EtCN+H]^-$	564	3.4	564	1.1	564	5.3	564	1.4
$[X-Bz]^-$	512	1.8	512	1.8	512	1.7	512	1.1
$[X-EtCN+H-HABz]^-$	325	1.3	325	3.8	325	2.5	325	6.0
$[GBz+C_2HOSi]^-$	---	---	---	---	410	2.2	410	2.0
$[U+C_2HOSi]^-$	267	3.4	267	4.5	---	---	---	---
GBz^-	---	---	---	---	254	17.1	254	18.4
ABz^-	238	35.3	238	42.7	238	32.3	238	40.8
OSi^-	131	4.4	131	5.2	131	3.9	131	4.0
U^-	111	14.0	111	11.8	111	---	---	---

Table 5.1 Negative Ion mass spectra and ion fragmentation of protected oligonucleotides

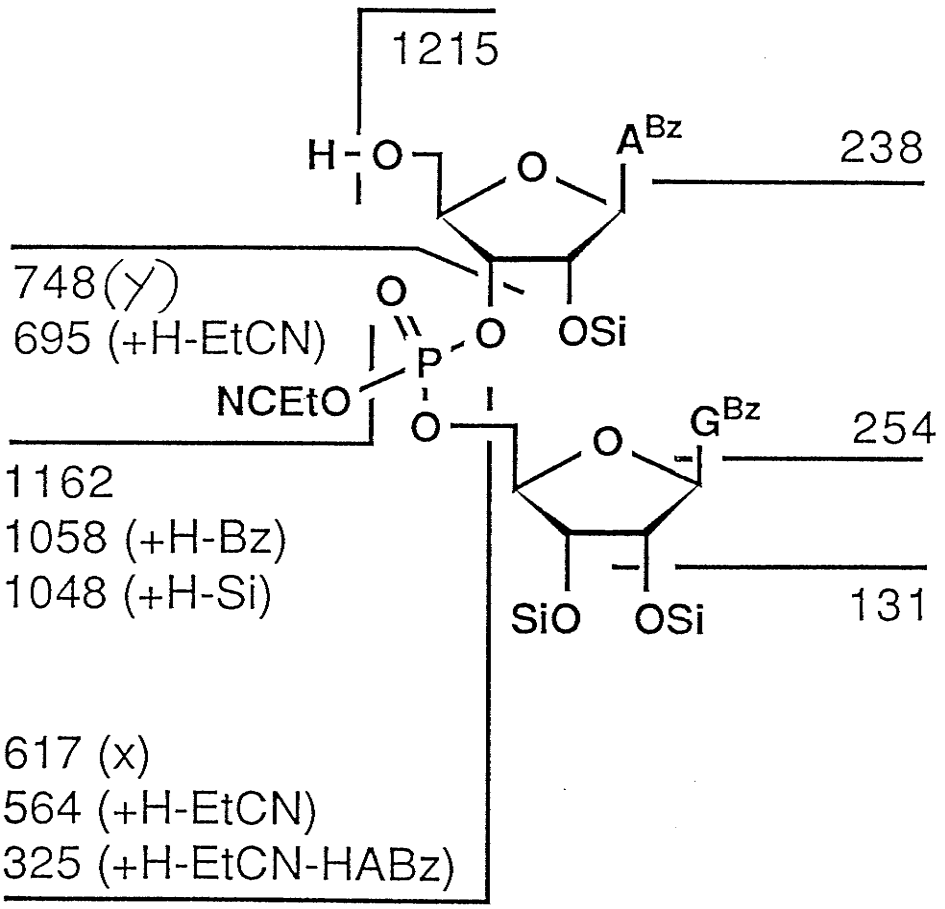

Figure 5.2 Some important fragments observed in the negative ion TOF-SI mass spectrum of ApG

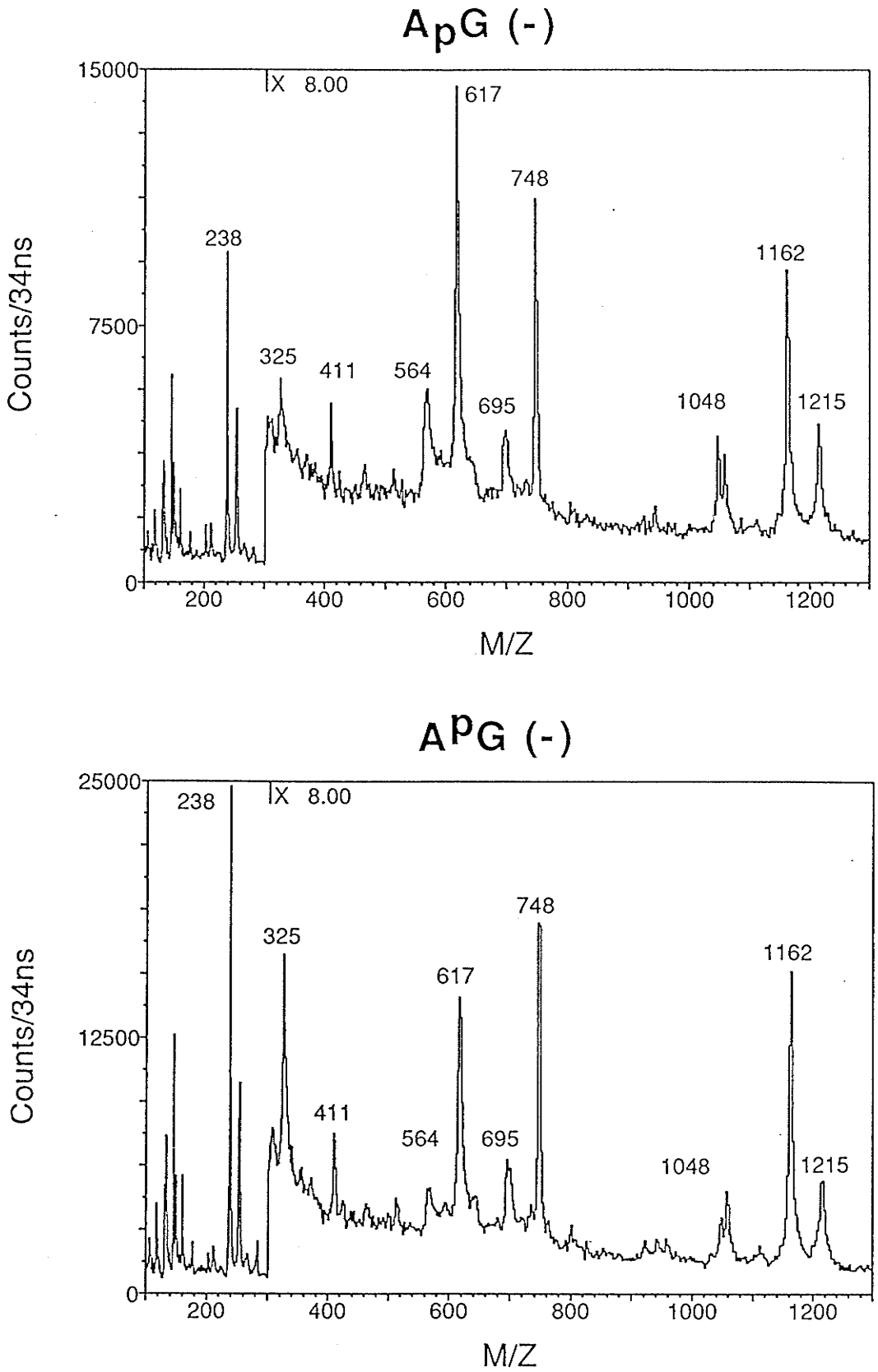

Figure 5.3 Negative ion TOF-SI mass spectra of ApG and A^{p}G

TABLE 5.2

OLIGODINUCLEOTIDES: HIGHLIGHTS OF NEGATIVE ION MASS SPECTRA

- %TIC of $[M-H]^-$ ions is very low (1-3%) in all cases.
- Ions produced by removal of one or more protecting groups from M^- account for 8-12% of TIC, which is 15-25% greater for 3'-5' dimers.
- The cyanoethyl group, EtCN, is the most labile amongst all protecting groups, producing $[M-EtCN]^-$ ions (5-7% TIC), as well as $[Y-EtCN+H]^-$ (3-10% TIC) and $[X-EtCN+H]^-$ (1-5% TIC). $[M-EtCN]^-$ ions can also lose a benzoyl (Bz) or a t-butyldimethylsilyl (Si) group.
- 5'-phosphate sequence ions (Y^- ions) and 3' or 2'-phosphate sequence ions (X^- ions) are produced in all instances. Y^- ions (with or without EtCN) are 1.6-3.0 times more abundant than X^- ions with ApU and A^pU, but for ApG and A^pG, they are 11-100% less intense than X^- ions.
- the ratio %TIC (Y^- +$[Y-EtCN+H]^-$) / %TIC (X^-+$[X-EtCN+H]^-$+$[X-Bz+H]^-$) is 70-80% greater for 2'-5' isomers than for 3'-5' isomers.
- The most prominent peak in all spectra corresponds to ABz^- ions, at m/z 238, which account for 32-43% of TIC. Formation of U^- and GBz^- is also highly favored (12-14% TIC for U^-, and 17-18% TIC for GBz^-).
- The %TIC top nucleobase / %TIC bottom nucleobase is 20-40% lower for 3'-5' isomers than for 2'-5' isomers.
- The %TIC of ABz^- ions is 20-30% higher for 2'-5' isomers than for 3'-5' isomers, which is attributed to the proximity of phosphotriester oxygens which can provide anchimeric assistance to departure of the ABz^- ion.

contribution of Y^- and X^- ions to %TIC hence provides an indication of isomeric form.

On the other hand, the base peak in all spectra is located at m/z 238, which corresponds to ABz^-. This ion is produced when the "top" glycosidic bond is cleaved, with charge retention on the more electrophilic nucleobase. It contributes 32-43% to the %TIC and is 20-30% more abundant for 2'-5' isomers than for 3'-5' isomers. Scheme 5.1 provides a rationale for these seemingly unrelated observations. In 2'-5' isomers, anchimeric assistance can be provided by a neighboring 2'-phosphate oxygen, facilitating the loss of ABz^- ions, thereby competing with X^- ion formation pathways. This would explain why 2'-5' dimers, when compared to 3'-5' isomers, show a much reduced %TIC due to X series ions, together with an increased %TIC due to ABz^- ions.

Neighbouring group or anchimeric assistance can also explain the fact that the "top" base, namely ABz^-, is detected in greater yield than the "bottom" base, either U^- or GBz^-, for both pairs of isomers. It also provides an explanation for the ratio (%TIC top base) / (%TIC bottom base), which is greater for 2'-5' isomers.

For both isomers, the glycosyl bond can be broken, with concomitant formation of a neutral HABz, through the well-documented hydrogen transfer from C-2' to O-2[42,67,73] using X^- (or more precisely, $[X\text{-}EtCN+H]^-$), as the parent ion. The formation of $[X\text{-}EtCN+H\text{-}HABz]^-$ ions at m/z 325 should be more favored with 2'-5' dimers, in view of the increased acidity of their 2'-hydrogens. The fact that for 2'-5' compounds, the %TIC of $[X\text{-}EtCN+H]^-$ ions (m/z 564) is more than three times lower than for 3'-5' isomers, while the %TIC of $[X\text{-}EtCN+H\text{-}HABz]^-$ ions (m/z 325) of the same compounds is at the same time 2-3 times higher than that of 3'-5'isomers gives further support to such a mechanism, illustrated in Scheme 5.2.

Apart from $[M-H]^-$ ions, sequence ions (X^- and Y^-) and nucleobase ions, from which one or more protecting groups can be expelled, there is another class of ions, analogous to **d** ions[33,73], frequently observed in FAB or CI mass spectra of unprotected oligonucleotides. These are the ions obtained at m/z 410 for ApG and A^pG , and at m/z 267 for ApU and A^pU. They likely correspond to $[(B-H)+C_2H_2OSi]^-$, **207**, as shown below.

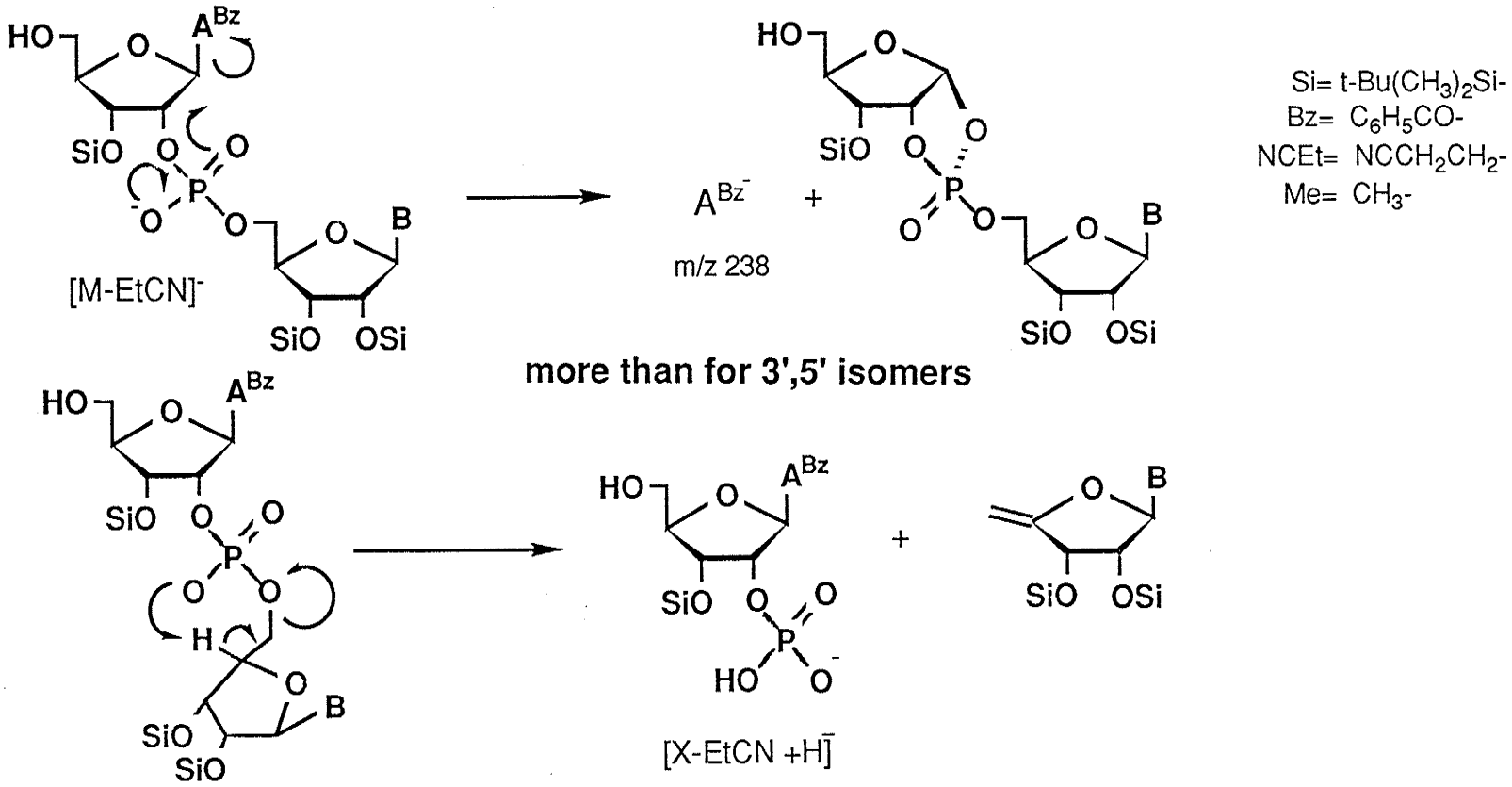
HO
A^Bz
SiO
O
P
B
[M-EtCN]^-
SiO
OSi
A^Bz^-
m/z 238
more than for 3',5' isomers
H
[X-EtCN +H]^-
less than for 3',5' isomers
Si= t-Bu(CH3)2Si-
Bz= C6H5CO-
NCEt= NCCH2CH2-
Me= CH3-

Scheme 5.1

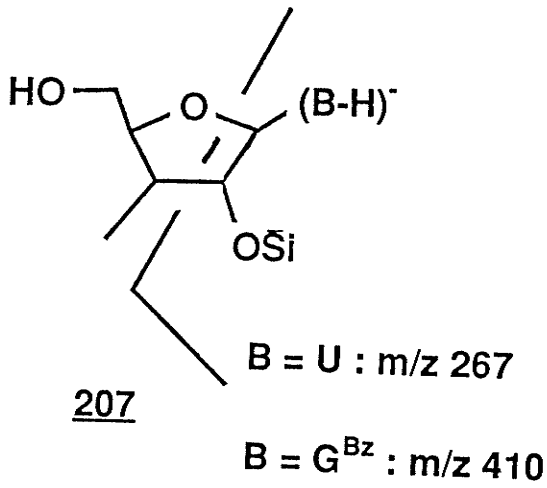

207

These peaks are detected only with the "bottom" nucleobase , i.e. no $[(ABz-H)+C_2H_2OSi]^-$ ion could be found in either ApU or ApG mass spectra.

5.3.2 Trimers

Table 5.3 shows the list of the most important peaks obtained in the negative ion TOF-SI mass spectra of UpApG and UpA^{p}G. Results are expressed in % of TIC, as was the case for the two pairs of dimers studied earlier. Figure 5.3 illustrates some important fragments observed in the negative ion TOF-SI mass spectrum of UpA^{p}G. The region of m/z 100 up to the $[M-H]^-$ ions is again covered. Table 5.4 highlights and summarizes some important trends from data given in Table 5.3.

The %TIC of $[M-H]^-$ ions is just as small for trimers as it was for dimers. It varies from 0.8% for UpApG to 1.1% for UpA^{p}G. Similarly, both compounds tend to lose one or more protecting groups to produce $[M-EtCN]^-$, $[M-EtCN+H-Bz]^-$, $[M-EtCN+H-Si]^-$ and $[M-Si]^-$ ions, for a combined %TIC contribution between 5 and 6% for both position isomers. Of these ions, UpA^{p}G shows 50% more $[M-EtCN+H-Si]^-$ and 50% less $[M-EtCN]^-$ ions than UpApG, an indication that the 2'-5'isomer loses a silyl group more readily than its 3'-5' counterpart.

The formation of B^- (U^-, ABz^- and GBz^-) ions produces the most intense peaks in both spectra; compared to UpApG, UpA^{p}G shows 40% less GBz^-, 10% more U^- and

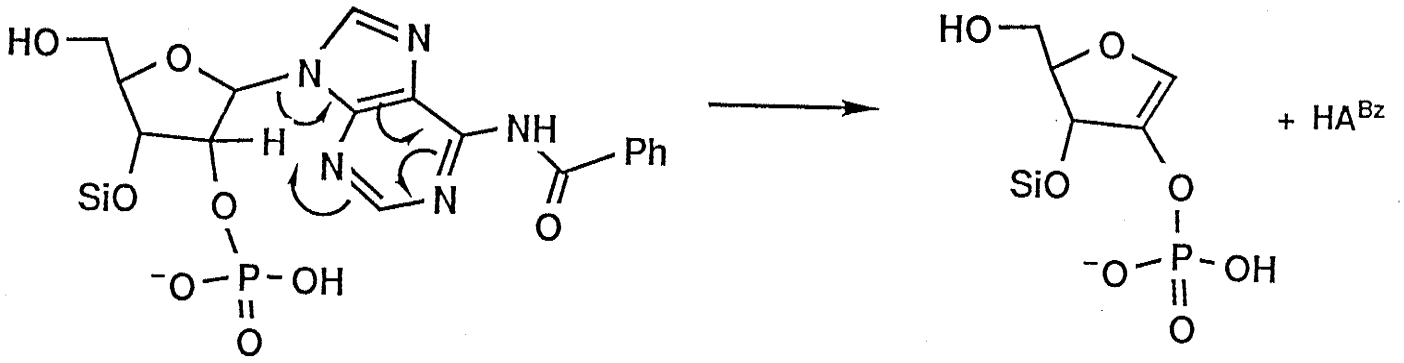

[X - EtCN + H]$^{-}$

m/z 564

much less intense for 2'-5' isomers

[X - EtCN + H - HA^{Bz}]

m/z 325

much more intense for 2'-5' isomers

Scheme 5.2

	UpApG		UpA^{p}G	
ASSIGNMENT	m/z	%TIC	m/z	%TIC
$[M-H]^-$	1689	0.8	1689	1.2
$[M-EtCN]^-$	1636	3.3	1636	1.6
$[M-Si]^-$	1575	0.5	1575	0.8
$[M-EtCN+H-Bz]^-$	1532	0.3	1532	0.3
$[M-EtCN+H-Si]^-$	1522	1.7	1522	2.5
Y2-	1349	1.5	1349	2.0
$[Y2-EtCN+H]^-$	1296	0.8	1296	1.7
$[Y2-Si+H]^-$	1235	0.7	1235	2.6
$X2^-$	1092	1.1	1092	1.4
$[X2-EtCN+H]^-$	1039	0.8	1039	0.8
$[X2-Si+H]^-$	978	---	978	1.3
$Y1^-$	747	4.1	747	6.2
$[Y1-EtCN+H]^-$	694	2.3	694	5.3
$[Y1-Si+H]^-$	633	1.2	633	0.8
$[Y1-Si\ OH]^-$	615	1.1	615	0.8
$X1^-$	490	1.4	490	5.5
$[X1-EtCN+H]^-$	437	1.0	437	4.9
$[X1-OEtCN+H]^-$	421	0.8	421	5.2
$[GBz+C_2HOSi]^-$	410	1.6	410	0.9
$[X1-EtCN+H-UH]^-$	325	5.1	325	3.8
GBz^-	254	17.2	254	12.4
ABz^-	238	28.5	238	14.5
OSi^-	131	5.7	131	2.2
U^-	111	17.4	111	19.5

Table 5.3 Negative Ion mass spectra and ion fragmentation protected oligotrinucleotides

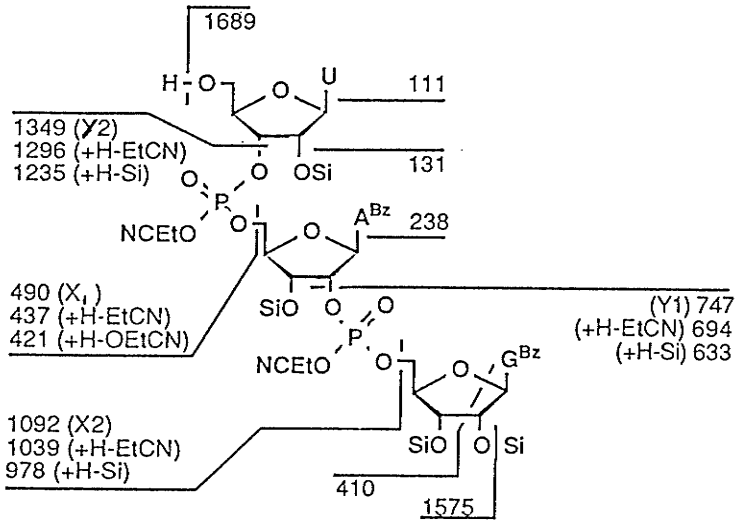

Figure 5.4 Some important fragments observed in the negative ion TOF-SI mass spectrum of UpA^{p}G

TABLE 5.4

OLIGOTRINUCLEOTIDES: HIGHLIGHTS OF NEGATIVE ION MASS SPECTRA

- %TIC of $[M-H]^-$ ions is very low (~1%) in both cases.
- The removal of one or more protecting group accounts for 5-6% of %TIC with both compounds.
- The cyanoethyl (EtCN) group is the most labile of all protecting groups. The %TIC of $[M-EtCN]^-$ is ~2-3%. This ion can also lose a benzoyl (Bz) or a silyl (Si) group, producing ions that globally contribute an additional 2-3% to the %TIC.
- 5'-phosphate sequence ions (Y^- ions) and 3' or 2'-phosphate sequence ions (X^- ions) produced by cleavage of O-glycosyl bonds at the 2', 3' or 5' positions account for a total of ~17% of %TIC for UpApG and for ~39% of %TIC for UpA^pG.
- Nucleobases B^- (U^-, ABz^- and GBz^-) constitute the most intense peaks obtained in the region covered. They globally account for ~63% of %TIC for UpApG and for ~46% of %TIC for UpA^pG. Their individual intensity decreases according to $ABz^- > U^- \sim GBz^-$ for UpApG, and according to $U^- > ABz^- > GBz^-$ for UpA^pG.
- For both compounds, the O-glycosyl bonds on the central nucleoside are broken more readily than the ones on the terminal nucleosides (i.e. X_1^- and Y_1^- ions are always more abundant than X_2^- and Y_2^- ions (included in those calculations are all signals derived directly from X^- and Y^- ions, in addition to the ones obtained by removal of one or two protecting group or another).
- The %TIC of X_1^- and Y_1^- sequence ions add up to ~29% for UpA^pG and to ~12% for UpApG.

almost 50% less ABz^- ions contributing to the %TIC. Globally, the trend in %TIC decreases according to A>U~G for UpApG and it decreases according to U>A>G for UpA^pG.

Many ions that provide sequence information are found in both spectra. The sequence ions X_1^-, Y_1^-, X_2^- and Y_2^- (see Figure 5.3), as well as signals corresponding to the loss of a protecting group from these ions, are responsible for *ca* 17% of %TIC for UpApG and *ca* 39% of %TIC for UpA^pG. Overall, it thus appears that the presence of a O2'-P-O5' phosphodiester linkage dramatically affects fragmentation patterns of molecular ions. In addition, in accordance with results by Viari *et al*[74], our findings show that the phosphodiester bonds around the central nucleoside (with formation of X_1^- and Y_1^- ions) are broken more easily than those from the terminal nucleosides (X_2^- or Y_2^-), regardless of isomeric form. However, in this case, it is the "normal" UpApG trimer that shows the greatest %TIC in ABz^- ions and the smallest %TIC in X_2^- ions, and not the variant 2'-5' isomer.

The trimer with the unusual 2'-5'phosphodiester bond thus appears much less inclined to produce ABz^- ions and much more inclined to withstand O-glycosyl bond cleavages around the central nucleoside (formation of X_1^- and Y_1^- ions). A combined %TIC of ~15% for ABz^- and ~31% for sequence ions with the modified trimer compound, compared to 29% for ABz^- and 12% for sequence ions from the normal trimer is indicative of this shift from N-glycosyl to increased O-glycosyl bond cleavage with UpA^pG. The origin of this shift remains uncertain.

It should be noted that the inverse relationship between the %TIC of the nucleobase (ABz^-) located on the ribose containing a O-2'-P bond and the %TIC of X^- ions, which was prevalent for dimers, still holds for trimers. However, in this case, it is the "normal" trimer UpApG that shows a greater %TIC in ABz^- and a smaller %TIC in X_2^- sequence ions, and not the variant 2'-5' isomer as expected. It could be that in the latter case, ABz^- production is repressed by the much increased formation of X_1^- and Y_1^-.

The situation is further complicated by the possibility that isomerization occurs under our mass spectrometry conditions upon desilylation, as shown in Scheme 5.3.

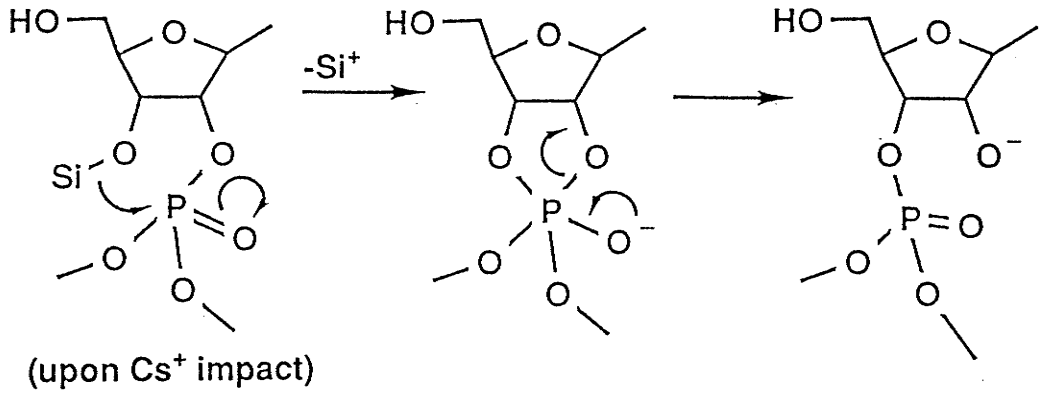

Scheme 5.3

Indeed, the loss of a silyl protecting group could hardly be detected in the negative ion TOF-SIMS of dimers; ions corresponding to $[M-Si]^-$, $[M-EtCN+H-Si]^-$, and to the expulsion of a silyl group from various sequence ions can be found in low yields in the mass spectra of the trimers. The %TIC for these ions adds up to ~4% for UpApG and to ~8% for UpA^pG. If the source of the silyl group loss comes from the O2' central ribose unit, isomerization of the "unusual" O2'-P ester bond would become possible.

5.3.3 Branched oligonucleotides

Table 5.5 shows a list of the main peaks observed in negative ion TOF-SI mass spectra of the four branched trimers described in Figure 5.1, to which ara-$A^{U}U$ (**208**, see below) was added. Figure 5.5 shows a comparison between the negative ion SI mass spectrum of $A^{U}U$ (**205**) and ara-$A^{U}U$ (**208**).

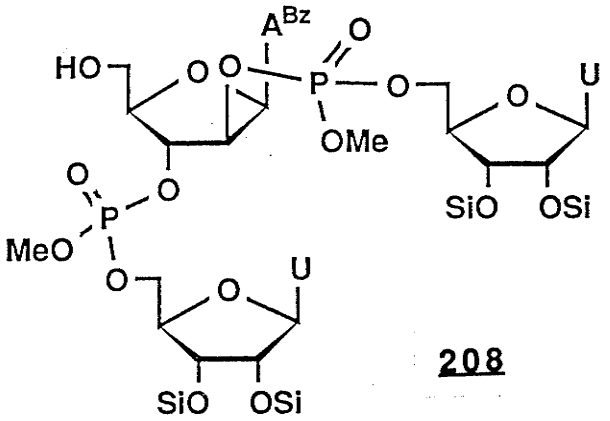

208

[M-H]⁻ ions and loss of protecting groups. The five branched trimers studied show prominent $[M-H]^-$ ion signals that range from ~6% of %TIC for ATT to ~16% of %TIC for $A^{U}U$. As seen in table 5.5, the %TICs of $[M-H]^-$ ions increase according to $A^{T}T$<ara-$A^{U}U$<$A^{C}C$<$G^{U}U$~$A^{U}U$. The loss of one or more protecting groups from nucleoside or phosphate oxygens is also readily observed, to give ions with 22% to 48% of the $[M-H]^-$ %TIC.

As shown in figure 5.1, each branched oligonucleotide is protected. The N6 position of all adenyl group were benzoylated, and so were the N4 position of cytosyl groups in $A^{C}C$ and the N2 position of guanine in $G^{U}U$. In addition, the OH on each phosphodiester group was replaced by OCH_3 on each compound (except for $A^{C}C$ where it was replaced by O-CH_2CH_2-CN). A p-nitrophenylethyl group was also introduced at the O6 position of guanine in $G^{U}U$. Finally, the free OH's on all 2' and 3' oxygens were replaced by a t-butyldimethylsilyl group, OSi. The presence of those protecting groups did complicate the mass spectral analysis, but at the same time, they provided helpful clues for identification of the main fragments.

ASSIGNMENT	$A^{T}T$ m/z	%TIC	$A^{U}U$ m/z	%TIC	a-$A^{U}U$ m/z	%TIC	$G^{U}U$ m/z	%TIC	$A^{C}C$ m/z	%TIC
$[M-H]^-$	1235	5.5	1468	15.9	1468	10.5	1633	15.1	1752	12.2
$[M-PG]^-$	1221	1.6	1454	2.3	1454	1.5	1619	1.5	1699	1.7
$[M-Si]^-$	1121	---	1354	2.8	1354		1519		1638	---
$[M-PG+H-Bz]^-$	1117	0.4	1350	2.5	1350	2.8	1515	1.8	1595	2.6
$[M-PG+H-Si]^-$	1107	0.6	1340		1340		1505		1585	0.4
$[M-NPE]^-$	---	---	---	---	---	---	1484		---	---
X^-	897	2.6	1014	1.9	1014	4.0	1179		1195	
$[X-PG+H]^-$	883	0.4	1000	0.2	1000	0.6	1165	1.2	1142	4.6
$[X-Bz+H]^-$	793	0.8	910	0.8	910	1.4	1075	---	1091	---
Y^-	449	5.8	565	16.3	565	20.5	565	8.5	707	14.0
$[Y-PG+H]^-$	435	1.3	551	1.7	551	0.9	551	1.8	654	12.9
$[Y-BH]^-$	323	2.7	453	1.1	453	0.7	453	---	492	---
$_{NPE}G^{Bz-}$	---	---	---	---	---	---	403	4.2	---	---
G^{Bz-}	---	---	---	---	---	---	254	26.6	---	---
A^{Bz-}	238	25.5	238	17.8	238	9.5	---	---	238	26.3
$[U-H+Bz]^-$	---	---	225	3.1	225	4.0	225	3.0	--	---
C^{Bz-}	---	---	---	---	---	---	---	---	214	10.8
OSi^-	131	2.1	131	2.5	131	2.5	131	3.8	131	2.1
T^-	125	4.6	---	---	---	---	---	---	---	---
U^-	111	13.6	111	17.1	111	25.1	111	15.2	---	---
NCO^-	42	21.3	42	9.8	42	11.7	42	14.0	42	12.4
OTHERS										
	1140	0.9	281	2.4	281	2.5	1229	3.5		
	816	3.3	211	1.7	211	1.6	211	3.3		
	368	4.7								
	281	2.3								

Table 5.5 Time-of-Flight Negative Secondary Ion mass spectra of branched oligonucleotides

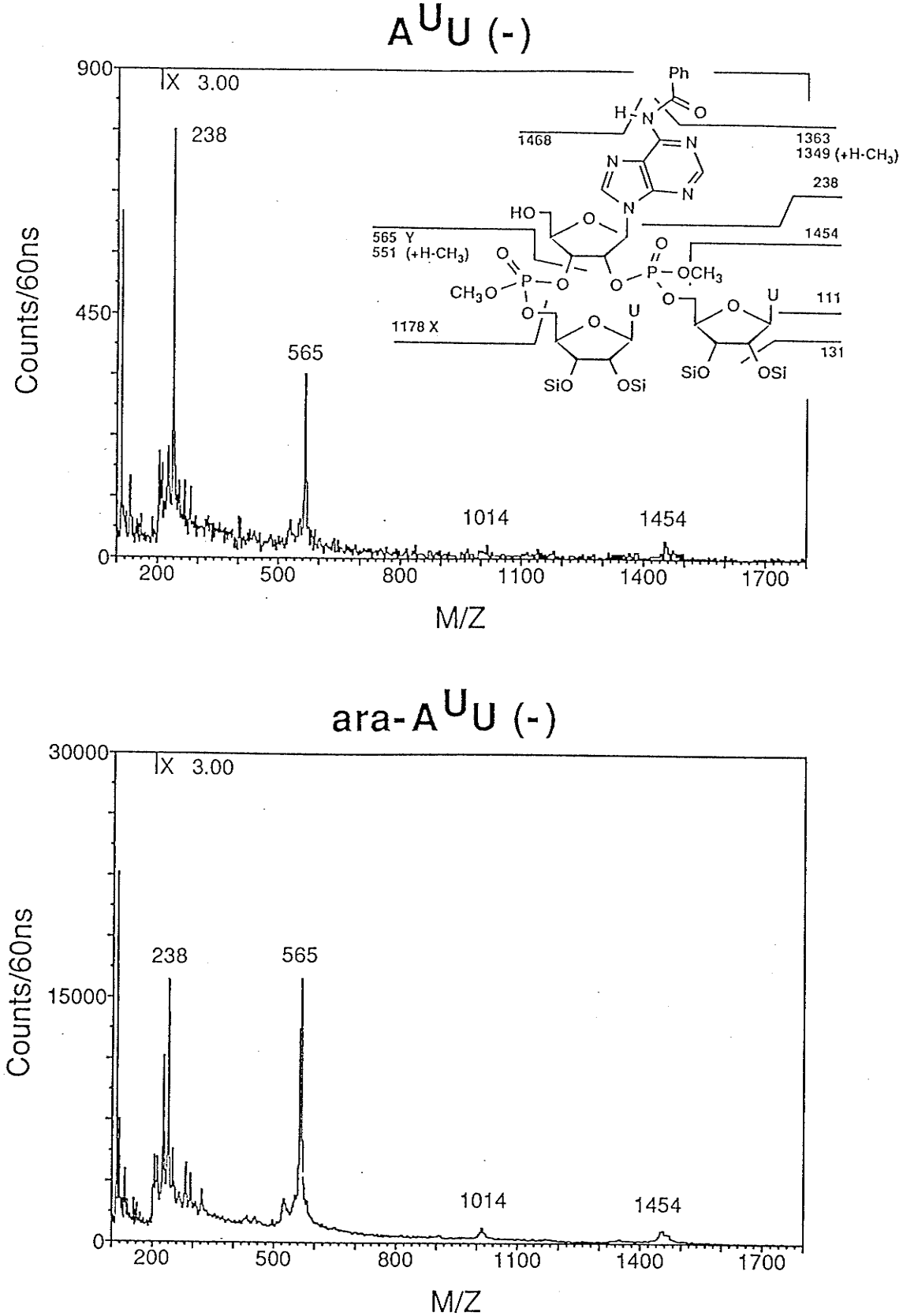

Figure 5.5 Negative ion TOF-SI mass spectra of $A^{U}U$ and ara-$A^{U}U$

N-glycosyl bond cleavage. As has been usually observed in negative ion mass spectra of linear oligonucleotides with regular 3'-5' phosphodiester linkages, the main fragmentations seen with branched nucleotides imply cleavage of glycosyl bonds with charge retention on the non-sugar moiety, either on the nucleobase (for cleavage of C1-N(1 or 9) bonds) or on a phosphate oxygen (for cleavage of C2'-O, C3'-O and C5'-O bonds). In the latter case, Y^- or X^- ions are produced (see Figure 5.1). It will be demonstrated here that those modes of fragmentation may be interelated.

Let us first compare the relative abundances of the nucleobase ions, both central and peripheral. In A^UU, for example, the central (branching) nucleoside is adenosine, to which two uridines have been added. For this compound, therefore, the adenyl group is called the central nucleobase, while the two uracyl groups are called peripheral nucleobases. The %TIC for the central base B_1^- varies from ~10% for ara-A^UU to ~27% for G^UU. It increases according to ara-A^UU<A^UU<A^TT~A^CC~G^UU. Moreover, in all instances, the abundance of base ions originating from the branching nucleotide is always greater than the total contribution of both peripheral bases, *i.e.* %TIC B_1^- > %TIC (B_2^- +B_3^-). This ratio increases according to A^UU<A^TT<G^UU<A^CC. For ara-A^UU, which contains an arabino sugar on the central nucleoside, that ratio is smaller than with any other compound; it is almost three times smaller than its ribo counterpart, A^UU. These results provide the best support for neighbouring group (anchimeric) assistance as a main source of ABz^- for ribonucleotides, where the central nucleobase and 2'-substituents are in a *trans* orientation, as seen in Figure 5.1. In other words, in A^UU, a phosphate oxygen can assist the fission of the N9-C1' bond, while this assistance cannot be provided when the phosphate and the nucleobase are in a *cis* orientation, which is the case with ara-A^UU. This argument therefore also provides an explanation for both the fact that ABz^- (ara-A^UU)< ABz^- (A^UU) and the fact that all ribotrimers show a greater %TIC for their central nucleobase than for their peripheral nucleobases, since anchimeric assistance is not available to the latter.

Another possible route to ABz^- ion production is through a concerted H-transfer[42,73] discussed earlier (see Scheme 5.5). In addition to not being able to use anchimeric assistance to produce ABz^- ions, ara-A^UU is also unable to use this rearrangement as a way to cleave its C1'-N9 bond. This likely has some bearing on explaining the low yield of ABz^- ions encountered with ara-A^UU.

The only branched trimer studied that does not contain an adenine as its central nucleoside is GUU. Its ratio of (%TIC G^-) / (%TIC U^-) (with or without its protecting groups) is about twice as high as the (%TIC A^-) / (%TIC U^-) ratio for A^UU. These results are consistent with those obtained by Cerny *et al* [68], which showed that, upon collisional activation, cleavage of the N-glycosyl bond of the dimer GpT produces a greater (%TIC G^-)/ (%TIC GH) ratio than the (%TIC A^-) / (%TIC AH) ratio of ApT. Note however that the %TIC of BzGNPE is ~4% whereas, upon losing the p-nitrophenyl O6- protecting group, $[BzGNPE - NPE+H]^-$ ions are formed at m/z 254, with a %TIC of ~27%. Hence, care must be exercised in comparing the ease of cleavage of the N-glycosyl bond, since the guanine base here contains a labile protecting group which could provide an additional driving force to promote excision of the base from the sugar moiety, possibly through a mechanism such as the one illustrated in Scheme 5.4.

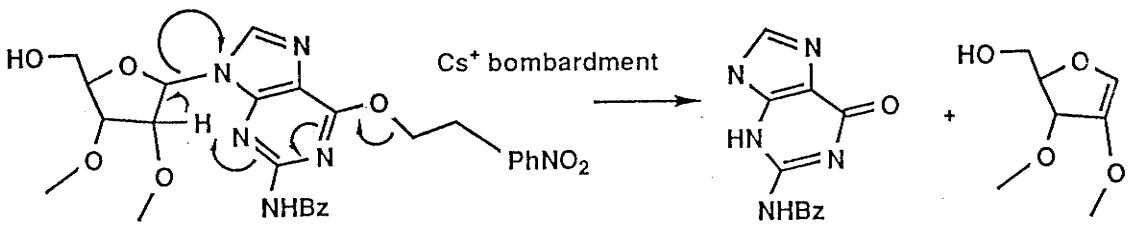

M

$[BzG^{NPE} - NPE + H]^-$

m/z 254

Scheme 5.4

Now, the (%TIC $B_{central}$) / (%TIC $B_{peripheral}$) ratios of A^UU, A^TT and A^CC are 1.0, 1.4 and 2.6, respectively. Since the central nucleobase is identical in all cases, these

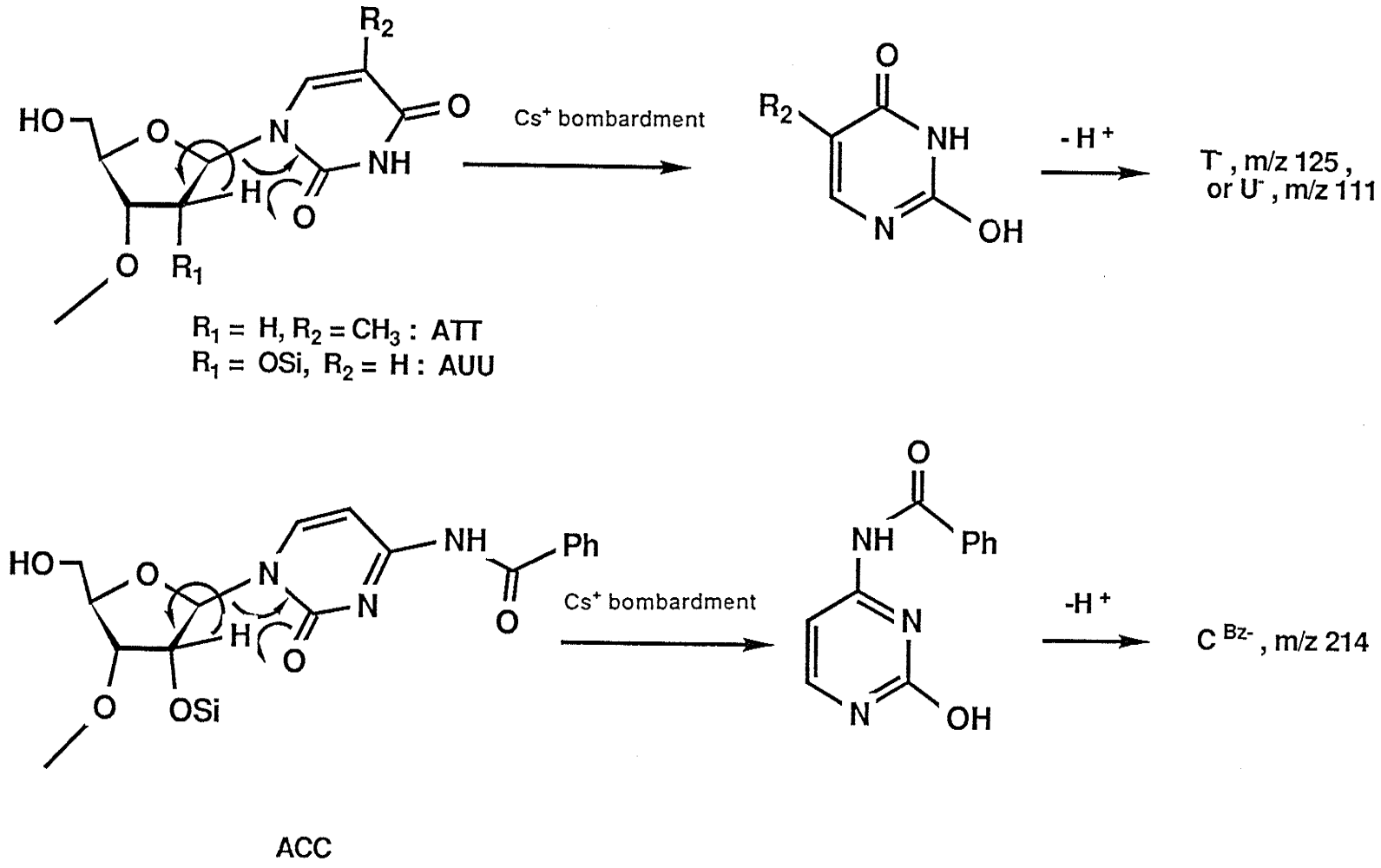
HO
O
N
NH
H
O
O
R1
R2
O
Cs+ bombardment
R2
O
NH
N
OH
-H+
T-, m/z 125,
or U-, m/z 111
R1 = H, R2 = CH3 : ATT
R1 = OSi, R2 = H : AUU
HO
O
N
NH
Ph
N
H
O
O
O
OSi
Cs+ bombardment
O
NH
Ph
N
N
OH
-H+
C Bz-, m/z 214
ACC

Scheme 5.5

ratios should give an indication of the relative tendency of U, T and C to accommodate a negative charge following cleavage of the N-glycosyl bond, accompanied by hydrogen transfer and then proton transfer to a neighboring molecule in the solid phase, after Cs^+ ion impact (Scheme 5.5). In other words, when $B_{central}$ is constant, (%TIC $B_{central}$) / (%TIC $B_{peripheral}$) ratios give us an indication of the relative acidity of the conjugate acid of the peripheral base. As suggested by Cerny[68] and others, it is unlikely that generation of B^- ions occurs via a simple cleavage of the glycosidic bond, since it would involve separation of positive and negative charges. For peripheral bases, therefore, in the absence of assistance from phosphate oxygens for the production of B^-, an increase in the ($B^-_{central}$) / ($B^-_{peripheral}$) %TIC ratio should correspond to a decrease in acidity of the peripheral BH. According to our results, then, the decreasing order of acidity for the compounds studied is UH>TH>CH, bearing in mind that the presence of the benzoyl group on N4 of cytosine could have an effect on this order. If anything, however, the replacement of the free amine by a benzamide group should increase the acidity of CH, so we would not expect this order to change with the deprotected cytosine. Let us not forget that, as illustrated in scheme 5.4, when we compare the acidity of CH, TH and UH, we likely are comparing the acidity of three phenols, where the proton most likely to be lost is on O2.

In the same manner, it would appear that GH is more acidic than AH, since the ($B^-_{central}$)/ ($B^-_{peripheral}$) %TIC ratio for G^UU is 1.75 compared to 1.0 for A^UU. For these two compounds, A^- or G^- ion production can be assisted by neighboring phosphate oxygens, in addition to the hydrogen transfer previously described. We would expect, however, that both compounds should be influenced in a similar manner by the proximity of these oxygens, and that the difference in %TIC for G^- and A^- is more an indication of how strongly GH and AH hold on to the H that has been transferred to those nucleobases from the sugar.

These results are in agreement with those of Cerny[68], who found that the relative

acidity order would be GH>AH,TH>CH, based on the % of ions formed by producing either B^- or losing BH from $[M-H]^-$ of a series of dimers upon collisional activation. Our results only allow for a comparison between GH and AH, and between UH, TH and CH, but they clearly follow the same trend identified by the aforementioned author.

For the cleavage of the N-glycosyl bond to be operative via a concerted, McLafferty type rearrangement, it has to involve the formation of a O2-H bond for U,T and C, and a N3-H bond for A and G (Scheme 5.4). It would be expected that the charge density on these atoms should have a bearing on their relative ability to abstract an hydrogen from the sugar. These charge densities have been calculated[178] for a number of nucleotides by applying Del Re's and Huckel's method to obtain partitioned σ and π charge contributions to the total charge. Some relevant results are shown in Table 5.6.

TABLE 5.6

Charge density distribution in selected nucleobase atoms
(adapted from ref. 178)

Atom	σ (e)	π (e)	Total (e)
O2 C	-0.06	-0.45	-0.51
O2 T and U	-0.06	-0.41	-0.47
N3 A	-0.28	-0.23	-0.51
N3 G	-0.28	-0.36	-0.64

Based on these calculations, the O2 on cytidine would appear to be a slightly better H-acceptor than the O2 on either thymidine or uridine, while the N3 on guanine is expected to be a better H-acceptor than the N3 on adenine. According to these charge density calculations, then, O2 of C is more basic than O2 of either U or T. We would hence anticipate from this a reduced tendency for CH to lose its phenolic proton, compared to UH and TH, which is congruent with our observations.

Such agreement between the magnitude of the calculated negative charge on N3 of G and A and the measured yield of G^- and A^- is not obtained with A^UU and G^UU. In other words, the N-glycosyl bond cleavage produces more G^- and less A^- (vs the abundance of their peripheral bases U) than would be expected from charge density calculations. Two explanations come to mind readily. First of all, the presence of a benzoyl protecting group on N2 of guanine should clearly weaken the N3-H bond, thereby increasing its acidity, because of the internal hydrogen bonding between the carbonyl oxygen of the benzoyl group and the N3-hydrogen (see Figure 5.6). Secondly, and maybe more importantly, we see very little G^- with its two protecting groups on (i.e. $NPEGBz^-$ ions). Instead, as indicated earlier, most of the guanine ions observed have lost their nitrophenylethyl group (i.e. producing $[NPEGBz+H-NPE]^-$ ions). In our study, G is therefore the only nucleobase that produces, to a large extent, ions resulting from the loss of a protecting group instead of a hydrogen. Rigorously, therefore, comparing A^-/U^- and G^-/U^- %TIC ratios gives us more a measure of the ability of A and G to become basic (producing A^- or G^- ions by losing an hydrogen or a protecting group) than a measure of the intrinsic Brønsted acidity of AH and GH.

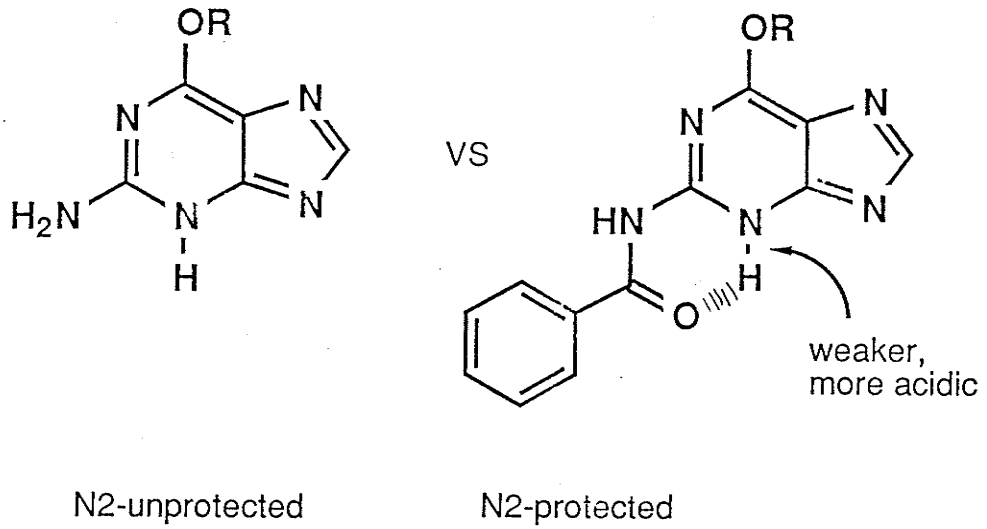

Figure 5.6

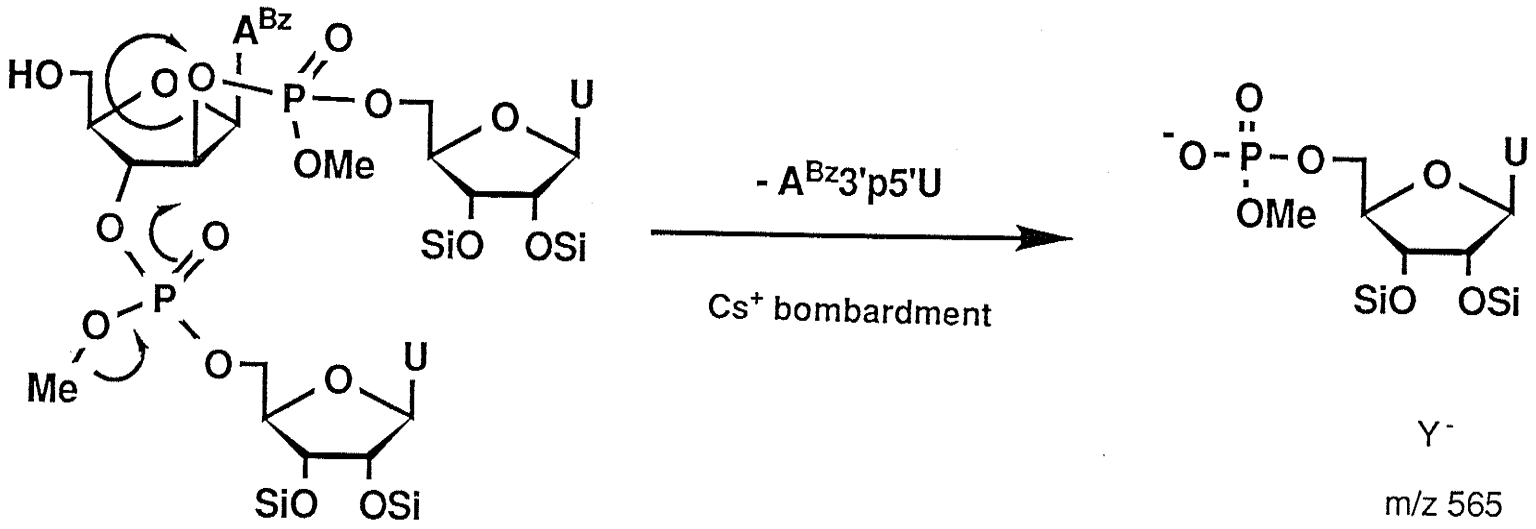

M or $[M-CH_3]^-$

Scheme 5.6

Sequence ions X^- and Y^-. As usual with oligonucleotides, 5'-phosphate sequence ions (Y^- ions, see Figure 5.1) and 3'- or 2'-phosphate sequence ions (X^- ions, see Figure 5.1) were obtained with every branched trimer studied. Y^- ions, with or without the loss of protecting groups, were found to be always more abundant than X^- ions (also with or without their protecting groups). For trimers, the (%TIC Y^-) / (%TIC X^-) abundance ratio (which includes ions produced by the loss of protecting groups) increases according to $A^{T}T$<ara-$A^{U}U$<$A^{C}C$<$A^{U}U$<$G^{U}U$ (contrary to what was reported in ref.76, where $A^{U}U$ was mistakingly placed at the bottom of that list). This ratio ranged from 2.6 for $A^{T}T$ to 8.6 for $G^{U}U$.

It hence appears that cleavage of sugar-phosphate bonds around the branching nucleotide is always more significant than those involving terminal nucleotides or, at least, that cleavage of a phosphate anion from a secondary C(2' or 3')-atom is preferred to that of a primary C5'-atom of a sugar, be it a ribose ($A^{U}U$,$A^{C}C$ $G^{U}U$), a deoxyribose ($A^{T}T$) or an arabinose (ara-$A^{U}U$). In view of the *trans* orientation between 2'- and 3' substituents with ara-$A^{U}U$, it is not surprising to notice an increase in the %TIC of Y^- ions with respect to that of its diastereoisomer $A^{U}U$, as shown in Scheme 5.6. Being able to distinguish stereoisomers provides yet another probative demonstration of the potential of the TOF-SIMS approach for characterization of nucleic acid components.

CHAPTER 6

SPECTROMETRIE DE MASSE FAB ET SIMS DE DI- ET DE TRI-DESOXYRIBONUCLEOTIDES O-ALKYLES*

ABSTRACT

O^4-alkyl di- and trinucleotides were analyzed by fast atom bombardment mass spectrometry (FABMS) as well as by time-of-flight secondary ion mass spectrometry (TOF-SIMS) in the negative ion mode. For dimers, a greater 5'-phosphate/3'-phosphate (pN_2^-/N_1p^-) relative intensity ratio was found in TOF-SIMS spectra while a greater loss of a nucleobase from those sequencing ions was observed in FAB spectra. Less fragmentation of $[M-H]^-$ ions was also noted under FAB conditions, for both dimers and trimers. Only TOF-SIMS spectra of trimers showed sodiated quasimolecular and sequence ions containing the central nucleoside. Many examples of the complementary nature of FAB-MS and TOF-SIMS applied to these modified nucleotides were also found.

6.1 INTRODUCTION

L'alkylation d'atomes d'oxygène sur les acides nucléiques et leurs précurseurs retient l'attention présentement en regard de son implication possible dans la mutagénèse et la carcinogénèse. On sait, par exemple, qu'il existe une corrélation entre le potentiel mutagénique et carcinogénique de certains agents alkylants et leur tendance d'attaquer l'oxygène[168], ainsi qu'avec la grosseur du groupe alkyle[169].

* published or submitted for publication as follows:

F. Lafortune, W. Buchannon, G.W. Buchko, F.E. Hruska, K.L. Sadana, K.G. Standing and J.B. Westmore, 37th ASMS Conf. on Mass Spectrom. and Allied Topics, Miami Beach, FL. p730, May 1989.

F. Lafortune, G.W. Buchko, F.E. Hruska, K.L. Sadana, K.G. Standing and J.B. Westmore, submitted to Analytica Chimica Acta (July 1992).

Lors d'une étude antérieure effectuée au moyen d'un spectromètre de masse à temps de vol (ionisation secondaire, SIMS*) sur des thymidines O-alkylées (voir chapitre 4), nous avons rapporté que l'alkylation des oxygènes-2 ou 4 de la thymine se traduit par une augmentation du degré de fragmentation du nucléoside, tant par brisure du lien glycosidique que par désalkylation de la base modifiée. Cette fois-ci, nous avons voulu évaluer quels effets aurait l'alkylation de petits nucléotides sur leurs modes de fragmentation[171].

Pour mener à bien cette étude, nous avons choisi d'utiliser concurremment les approches SIMS et FABMS* (bombardement par atomes rapides). Ainsi, nous avons voulu vérifier directement le degré de complémentarité de ces deux méthodes d'analyse, l'approche SIMS opérant dans un environnement non-solvaté, et l'approche FABMS opérant en suspension ou en solution dans une matrice liquide. On a en effet souvent observé un grand degré de similitude entre les spectres de masse obtenus par FABMS et ceux obtenus par SIMS dans des conditions comparables, mais on a aussi rapporté[179,180] que les premiers présentaient un degré de fragmentation moindre que les seconds.

Les composés analysés comprennent donc une série de di- et de trinucléotides alkylés en position-O4, soit deux paires de dinucléotides isomériques, les d(^{r4}TpT) et d(Tp^{r4}T), où r = Et ou i-Pr, en plus de trois trinucléotides, les d(Tp^{r4}TpT), avec r = Me, Et, et i-Pr (Figure 6.1). Nous décrivons ici quelles sont les principales similitudes et différences entre les spectres de masse enregistrés en mode négatif obtenus par FABMS et SIMS avec ces nucléosides modifiés.

* Les acronymes SIMS (Secondary Ion Mass Spectrometry) et FAB (Fast Atom Bombardment Mass Spectrometry), si répandus dans la littérature anglaise, seront dorénavant utilisés.

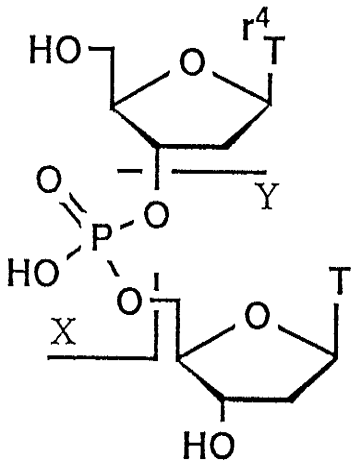

d(^{r4}TpT)

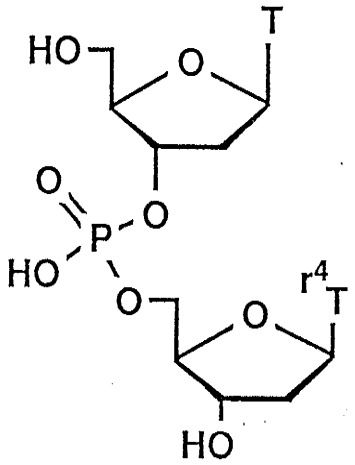

d(Tp^{r4}T)

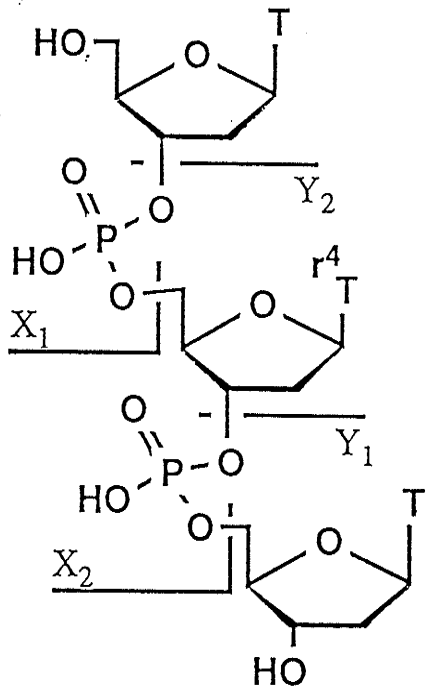

d(Tp^{r4}TpT)

r= Et, i-Propyl

r= Me, Et, i-Propyl

Figure 6.1: di- et trinucléotides O-alklylés

6.2 PARTIE EXPERIMENTALE

6.2.1. Préparation des échantillons:

Tous les composés ont été synthétisés dans notre département de chimie[181]. Pour fin d'analyse par FAB, les composés titrés furent dissous dans du glycérol selon une concentration d'environ 10 mg/mL. Quelques µL de chaque solution furent ensuite déposés sur l'extrémité d'une sonde à échantillon en acier inoxydable. Pour fin d'analyse par SIMS, les composés furent dissous dans un mélange de méthanol et d'eau (80:20) de façon à produire des solutions de concentration ~ 1mg/mL et quelques µL de chacune des solutions furent ensuite déposés sur une feuille d'aluminium traitée de manière à produire une surface de boehmite, AlO(OH)[173,174].

6.2.2 Spectrométrie de masse

Les spectres de masse obtenus par FAB en mode négatif furent enregistrés par un spectromètre de masse VG-7070E-HF à double foyer. Les échantillons furent bombardés par un canon de type Saddle-Field générant un faisceau d'atomes de xénon accélérés à 8 keV. Les ions anionisés furent accélérés jusqu'à 6 keV. Les spectres de masse obtenus par SIMS en mode négatif furent enregistrés par le spectromètre de masse à temps de vol Manitoba II, qui comprend un miroir électrostatique à ions[126]. Les cibles furent bombardées par un faisceau d'ions primaires de césium de 28 keV et les ions négatifs secondaires produits furent accélérés jusqu'à 10 keV.

6.3 RESULTATS ET DISCUSSION

6.3.1. Didésoxyribonucléoside-monophosphates:

Les spectres de masse FAB et SIMS en mode négatif du ^{e4}TpT et du Tp^{e4}T sont illustrés à la figure 6.2 et 6.3, respectivement. Le tableau 6.1 dresse une liste des principaux signaux obtenus lors de l'enregistrement en mode négatif des spectres de masse obtenus par FABMS et SIMS des

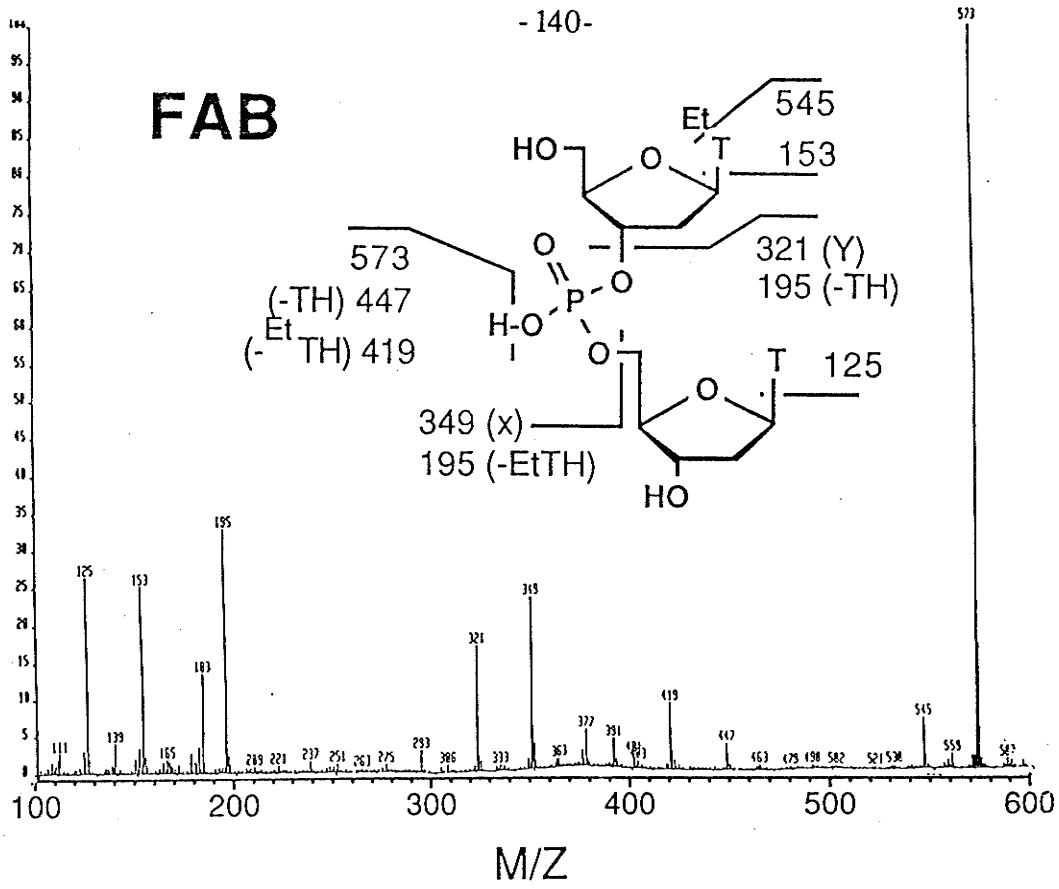

d(Et^{4}TpT)

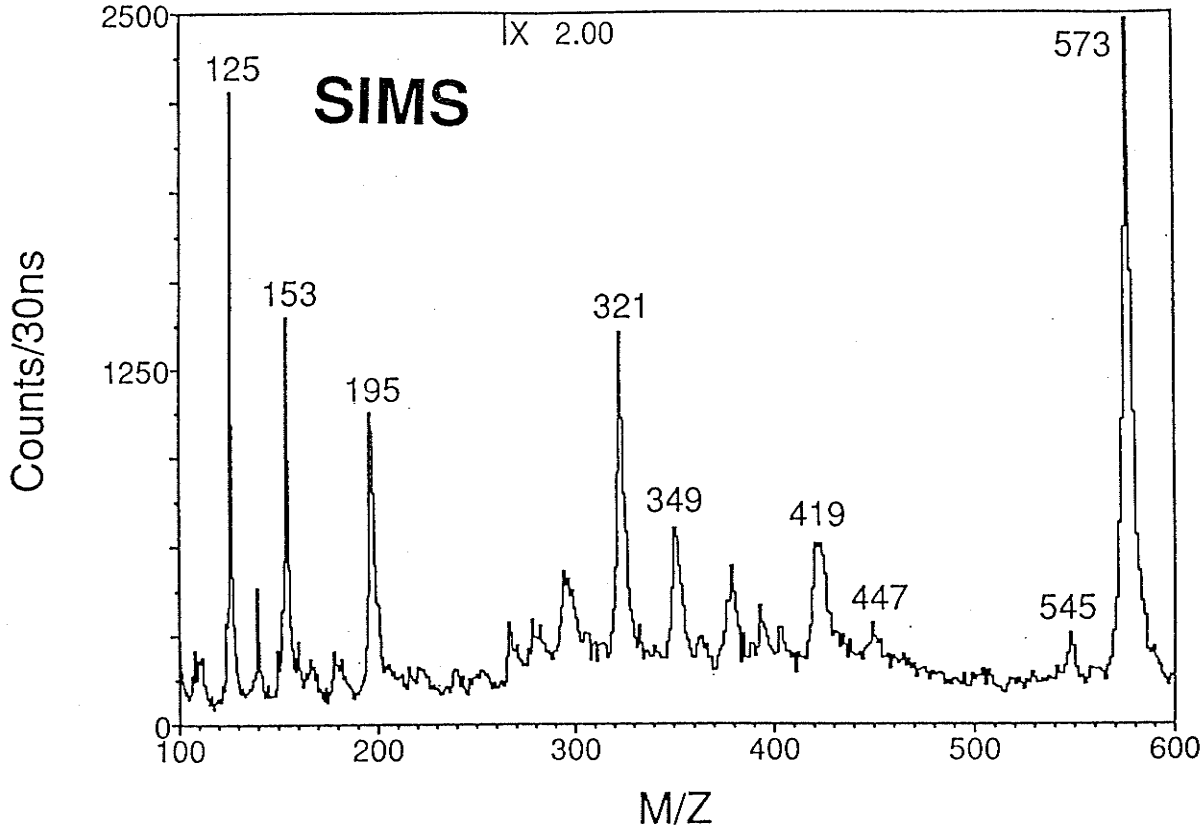

Figure 6.2 Spectres de masse FAB et SIMS en mode négatif du d(^{Et4}TpT)

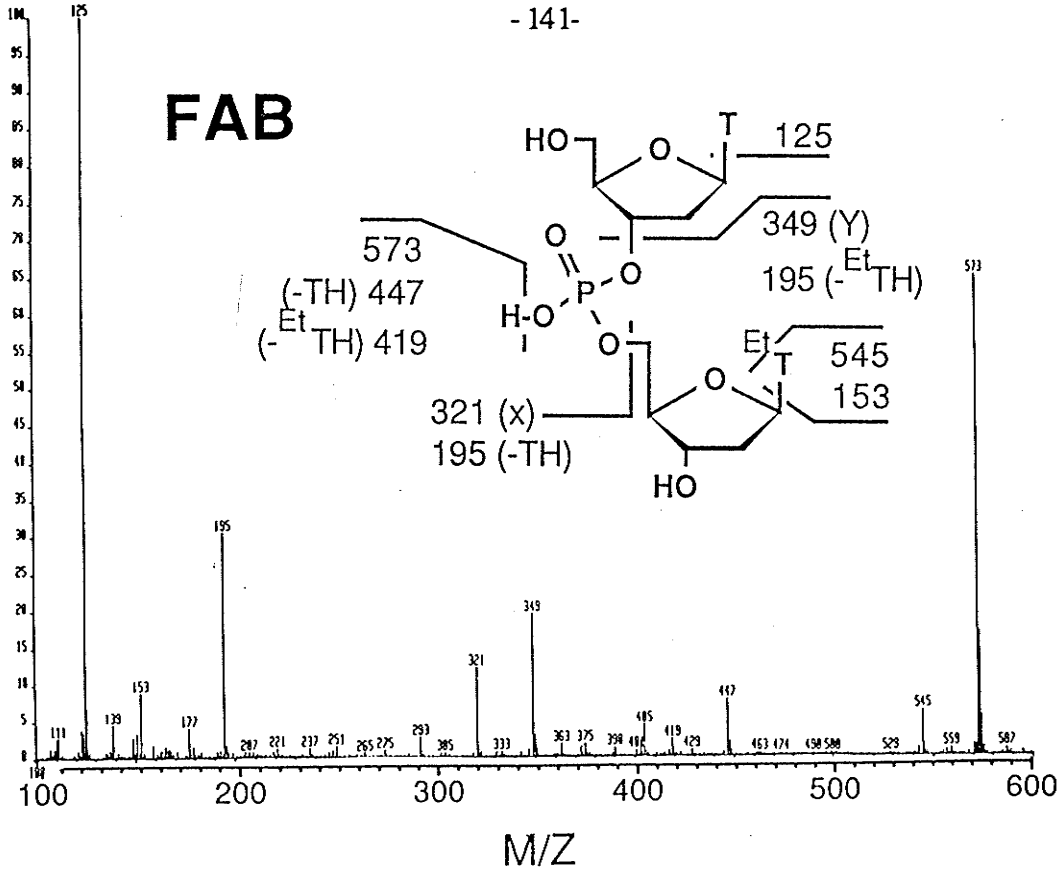

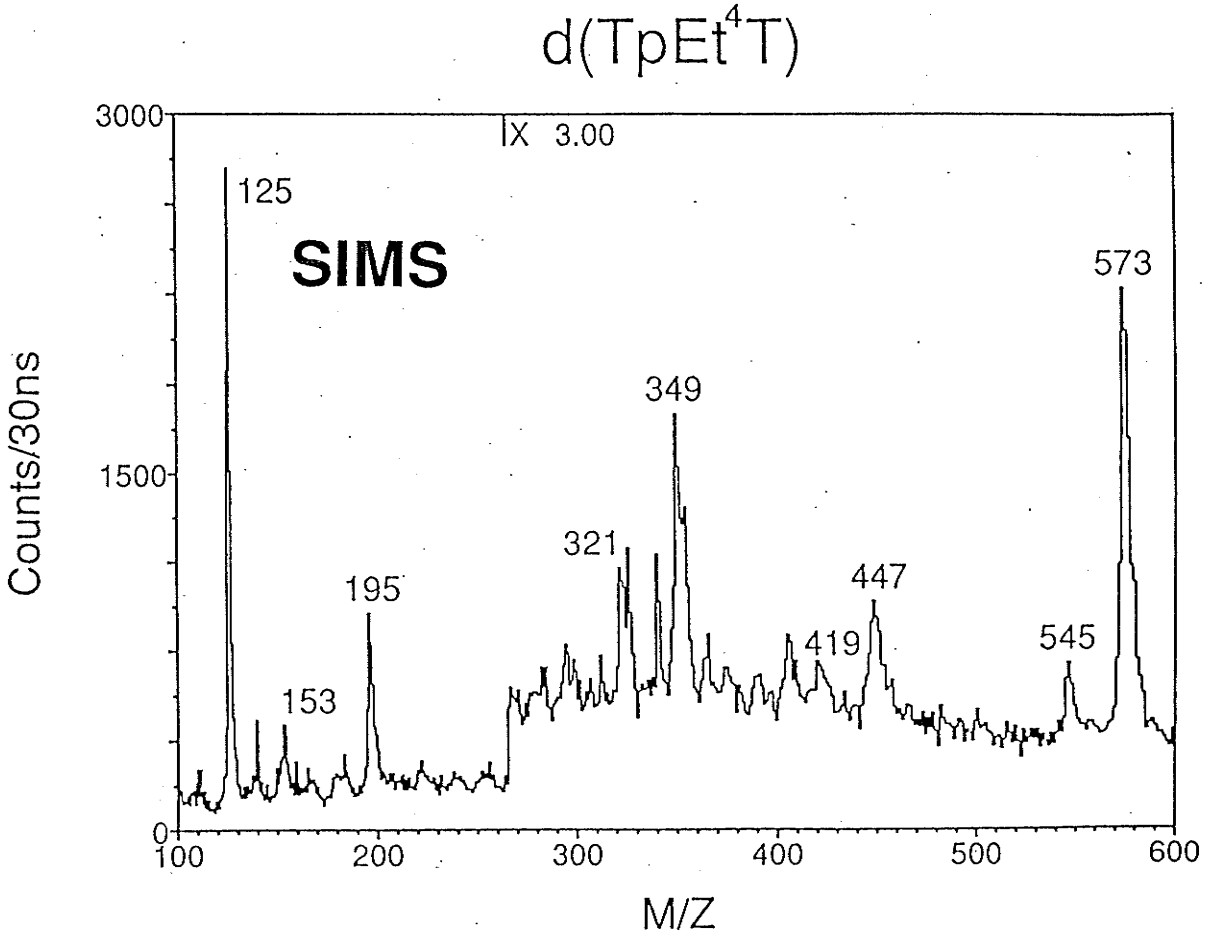

Figure 6.3 Spectres de masse FAB et SIMS en mode négatif du d(Tp^{Et4}T)

Tableau 6.1 Spectres de masse obtenus par FABMS et SIMS en mode négatif de didésoxyribonucléotides O-alkylés (en % de contribution au courant ionique total (%CIT) dans la région m/z 100 jusqu'aux ions $[M-H]^-$)

	d(TpT)			d(^{e4}TpT)			d(Tp^{e4}T)			d(^{ip4}TpT)			d(Tp^{ip4}T)		
ASSIGNATIONS	FAB	m/z	SIMS	FAB	m/z	SIMS	FAB	m/z	SIMS	FAB	m/z	SIMS	FAB	m/z	SIMS
$[M-H]^-$	48.1	545	5.0	40.6	573	20.4	25.4	573	15.2	31.5	587	12.5	38.5	587	10.1
$[M-r]^-$	-	-	-	2.6	545	1.3	2.4	545	1.9	1.7	545	2.3	6.5	545	2.0
$[M-H-^{3'}BH]^-$	2.4	419	2.1	3.4	419	6.1	2.8	447	6.7	5.0	419	7.8	1.9	461	7.3
$[M-H-^{5'}BH]^-$				1.4	447	0.4	0.8	419	-	1.3	461	1.8	2.7	419	4.7
X^-	14.9	321	7.5	9.3	349	5.9	4.8	321	4.2	7.1	363	4.7	7.3	321	6.1
Y^-				6.9	321	10.6	7.5	349	11.2	6.9	321	10.0	8.1	363	9.7
$[M-H-TH-^{r}TH]^-$	-	-	-	1.2	293	1.4	1.0	293	0.6	2.2	293	1.3	0.8	293	2.0
$[X-^{r}TH]^-+[Y-TH]^-$	5.3	195	21.4	13.4	195	17.9	12.1	195	18.1	17.5	195	21.0	7.9	195	16.4
$^{r}T^-$	NA	NA	NA	10.3	153	16.0	3.6	153	3.5	12.9	167	13.4	2.7	167	2.4
T^-	29.3	125	71.2	10.8	125	19.8	39.7	125	38.5	18.8	125	25.3	23.7	125	39.4

Note: $^{3'}BH$ = TH ou ^{r}TH
$^{5'}BH$ = TH ou ^{r}TH

didésoxyribonucléosides-monophosphates dans la région m/z 100 jusqu'aux ions $[M-H]^-$. Les résultats sont exprimés en % de contribution au courant ionique total (%CIT) dans la région désignée, puisque ces quantités reflètent mieux les différences entre les spectres.

Les spectres de masse obtenus par FABMS et SIMS des didésoxyribonucléoside-monophosphate O-alkylés montrent tous des abondances relatives importantes pour les signaux correspondant aux ions $[M-H]^-$, tel qu'attesté par un %CIT élevé. En fait, pour tous les spectres FAB sauf pour le $Tp^{e4}T$, les signaux correspondant aux ions $[M-H]^-$ présentent les %CIT les plus élevés. Il est à noter qu'en spectrométrie SIMS, à part le ^{e4}TpT, les ions $[M-H]^-$ ne conduisent jamais aux signaux les plus intenses des spectres, ce qui semble indiquer que dans les conditions expérimentales utilisées, l'approche FAB est une méthode d'ionisation plus douce que l'approche SIMS.

L'un des modes de fragmentation les plus privilégiés est la brisure du lien glycosidique avec rétention de la charge négative, soit sur la nucléobase (alkylée ou pas, schéma 6.1A et 6.1B), soit sur le reste de la molécule (schéma 6.1C et 6.1D). Les ions produits sont alors $^rT^-$ et T^- dans le premier cas, ainsi que $[M-H-TH]^-$ et $[M-H-rTH]^-$ dans le second cas. La contribution apportée au %CIT par ces quatre fragments varie de 42% à 73% pour les spectres SIMS, et de 26% à 47% pour les spectres FAB. Le schéma 6.1 illustre l'origine probable de ces types de fragments à partir de l'ion $[M-H]^-$, avec le $Tp^{i4}T$ choisi comme exemple. Si un hydrogène-2' est transféré sur un des oxygènes du groupement phosphate, la rétention de la charge négative peut se faire sur les nucléobases, ce qui conduit aux ions $^{i4}T^-$ (schéma 6.1A) ou T^- (schéma 6.1B). Si par ailleurs, un hydrogène-2' est transféré sur la nucléobase, selon un mécanisme s'apparentant au réarrangement cyclique à 6 membres de McLafferty[68,110], le lien glycosidique

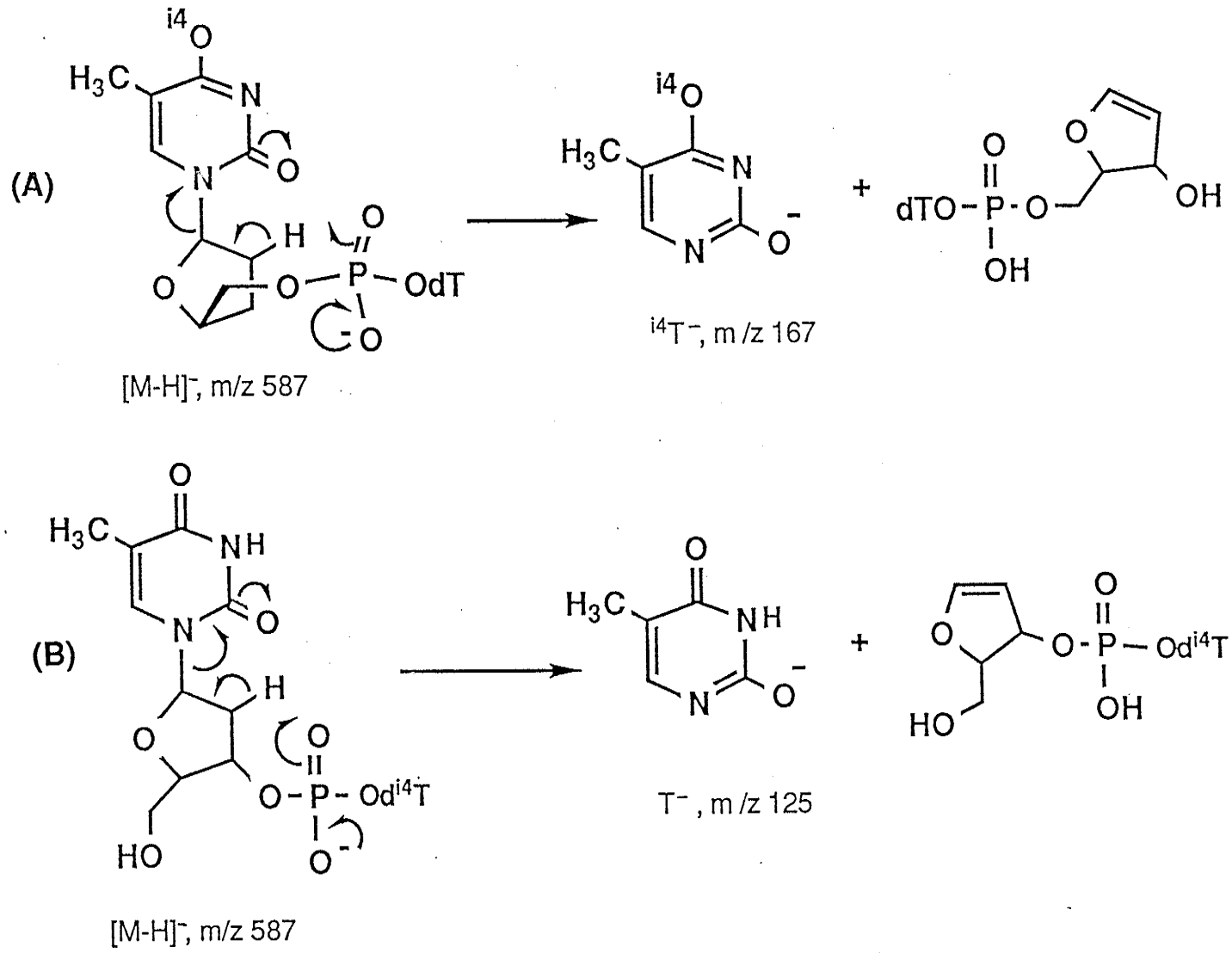
(A)
i4O
H3C
N
O
N
H
O
O
O
P
OdT
O
[M-H]-, m/z 587
i4T-, m /z 167
dTO
P
O
OH
OH
(B)
O
H3C
NH
O
N
H
O
O
O
P
Odi4T
HO
O-
[M-H]-, m/z 587
T- , m /z 125
HO
Odi4T
OH

Schéma 6.1

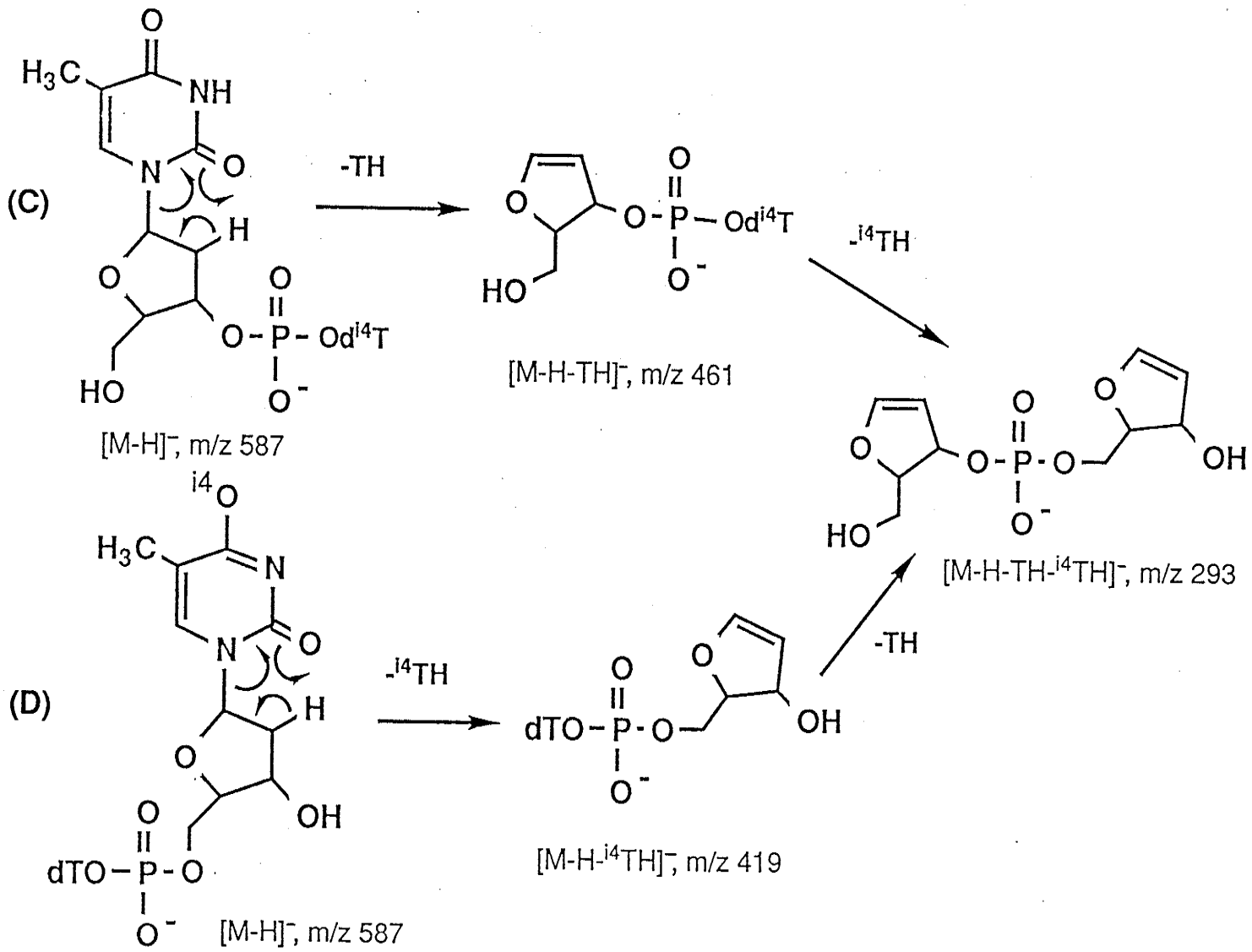
(C)
-TH
[M-H-TH]⁻, m/z 461
-i4TH
[M-H]⁻, m/z 587
[M-H-TH-i4TH]⁻, m/z 293
(D)
-i4TH
-TH
[M-H-i4TH]⁻, m/z 419
[M-H]⁻, m/z 587

Schéma 6.1

se brise avec rétention de la charge sur le reste de la molécule, ce qui produit les ions $[M-H-TH]^-$ (schéma 6.1C) ou $[M-H-^{i4}TH]^-$ (schéma 6.1D). Les deux liens glycosidiques des composés titrés peuvent aussi être brisés consécutivement, ce qui conduit dans tous les cas aux ions $[M-H-TH-^{r}TH]^-$ à m/z 293, qui contribue faiblement au %CIT (1-2%) (voyez à cet effet le tableau 6.1 et les schémas 6.1C et 6.1D).

Il est à signaler que les spectres de masse FAB et SIMS des deux paires d'isomères de position montrent un %CIT de $[M-H-BH]^-$ plus élevé lorsque la nucléobase est située sur le nucléoside à l'extrémité-3' de la molécule (une exception: le spectre FAB du $Tp^{i4}T$ où les %CIT de ces deux signaux sont à peu près égaux); ceci avait déjà été observé par Cerny *et al* [68] lors d'une étude de décompositions (métastables et activées par collisions) d'ions $[M-H]^-$ effectuées sur une série de désoxyribonucléotides. Ces auteurs ont suggéré que si le groupe phosphodiester est situé en position-3', les hydrogènes-2' deviennent plus acides et donc plus susceptibles d'être transférés sur l'oxygène de la nucléobase que si le groupe phosphodiester est situé en position-5' (voir les schémas 6.1C et 6.1D).

L'autre grande catégorie de fragments observés sur les spectres de dinucléotides est la présence des ions "séquentiels"[42] baptisés X^- et Y^- par Viari *et al*[74] (voir la figure 6.1). Tout comme pour les dinucléotides non-alkylés, et tel que noté par de nombreux investigateurs[42,47,51,68,74,81], les fragments Y^- (scission du lien O3'-C3') montrent un %CIT plus élevé que les fragments X^- (scission du lien O5'-C5') en mode d'analyse SIMS. Les schémas 6.2 et 6.3 permettent d'expliquer les observations suivantes: (a) le %CIT des ions X^- est plus faible que celui des ions Y^- et (b) le %CIT des ions $^{r}T^-$ est beaucoup plus élevé lorsque la nucléobase alkylée se retrouve sur le nucléoside à l'extrémité-5'

de la molécule (i.e. ^{r4}TpT) que lorsqu'elle se retouve sur son extrémité 3' (i.e. Tp^{r4}T).

Dans un premier temps, selon l'hypothèse de Cerny *et al* [68] (appuyée par analyse d'ions métastables), les ions X^- et Y^- pourraient être formés suivant un mécanisme concerté de type McLafferty, impliquant six atomes dans l'état de transition. Ainsi, la formation des ions X^- (schéma 6.2) impliquerait (i) un transfert de l'hydrogène-4' sur un oxygène du groupe phosphodiester, (ii) la formation d'un alcène exocyclique et (iii) la scission du lien C5'-O5'. En revanche, la formation des ions Y^- (schéma 6.3) impliquerait (i) un transfert d'hydrogène, soit H4', soit H2', (ii) deux possibilités de formation d'un alcène endocyclique, et (iii) la brisure du lien C3'-O3'. En d'autres mots, la formation de Y^- serait favorisée aux dépens de X^-, d'une part, à cause de la formation de produits neutres plus stables (alcènes endocycliques). De plus, une fois formés, les ions X^- et Y^- peuvent se décomposer par bris de la liaison glycosidique en formant des ions T^- (ou $^rT^-$) à m/z 125 (ou 124 + r) et des ions [X (ou Y)-TH (ou ^{r}TH)]$^-$ à m/z 195.

En prenant l'exemple du ^{e4}TpT illustré sur le schéma 6.2, les signaux spectraux obtenus à m/z 195 peuvent donc provenir de [X-^{e4}TH]$^-$ (schéma 6.2) ou de [Y-TH]$^-$ (schéma 6.3). Si l'on en juge par la tendance des ions [M-H]$^-$ à perdre la nucléobase provenant de l'extrémité-5' de la molécule, il semblerait donc que le signal à m/z 195 observé chez le ^{e4}TpT proviendrait davantage des ions [X-^{e4}TH]$^-$ que des ions [Y-TH]$^-$, selon l'argumentation développée plus haut.

Un élément de preuve additionnelle est obtenu si on jette un coup d'oeil à la stucture d'une nucléobase alkylée en position O4. On peut ainsi se rendre compte que le caractère électronégatif de l'oxygène-2 est augmenté par rapport à la base

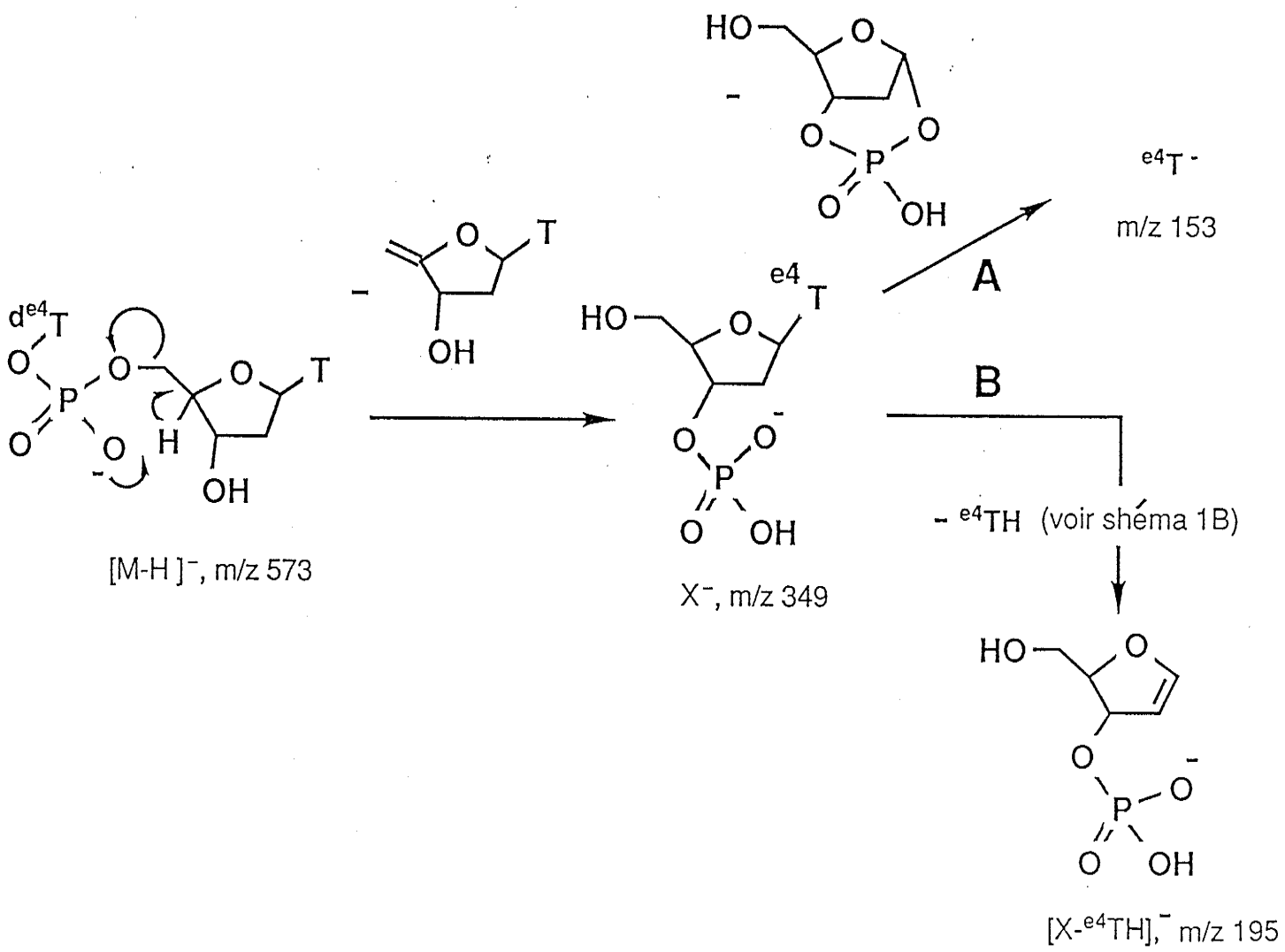
HO
O
O
P
O
OH
e4T -
m/z 153
A
B
- e4TH (voir shéma 1B)
[M-H]⁻, m/z 573
X⁻, m/z 349
[X-e4TH],⁻ m/z 195

Schéma 6.2

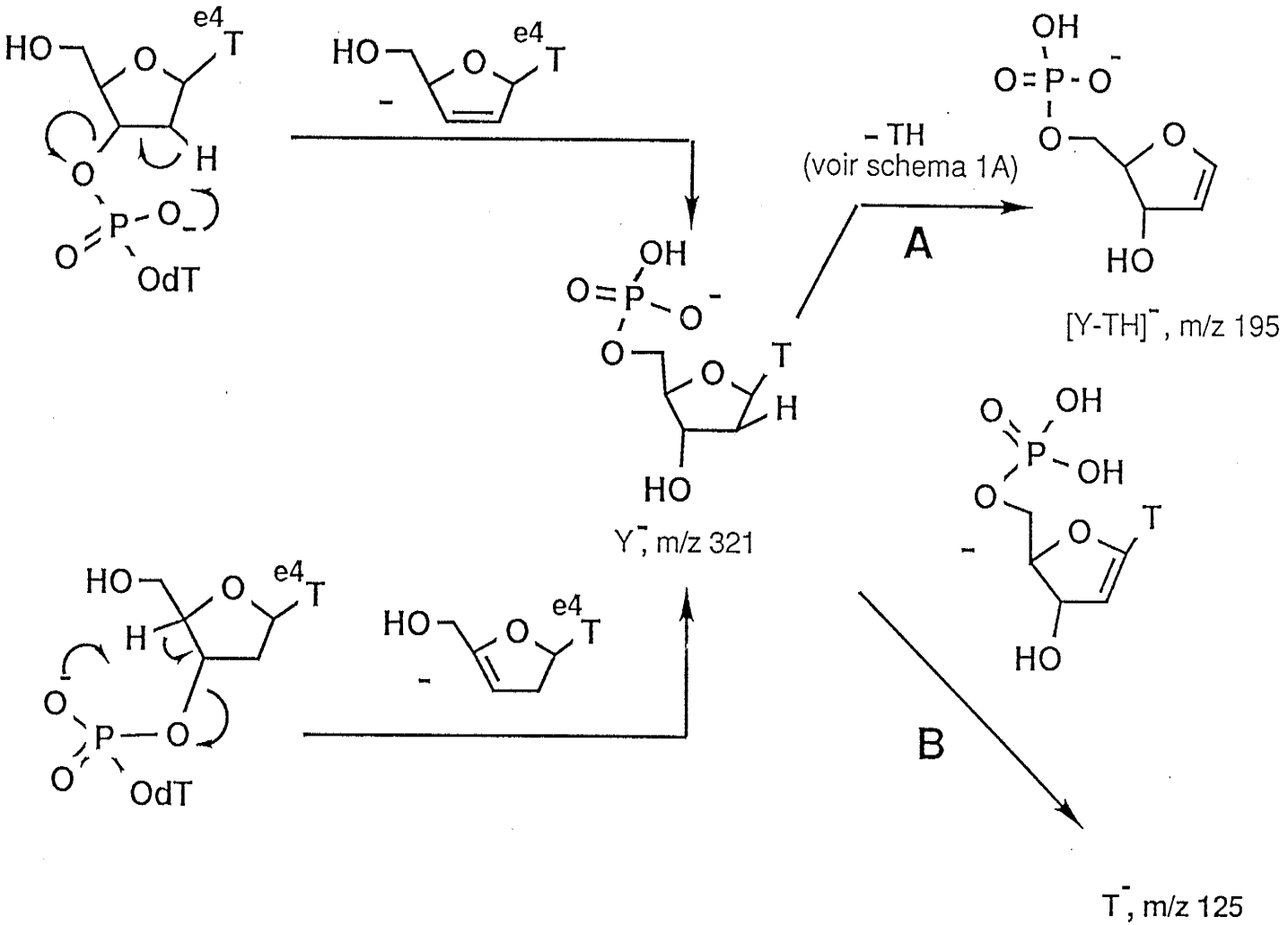
HO
e4
T
O
H
O
P
O
O
OdT
- TH
(voir schema 1A)
A
OH
O=P-O
HO
[Y-TH]⁻, m/z 195
Y⁻, m/z 321
B
T⁻, m/z 125

Schéma 6.3

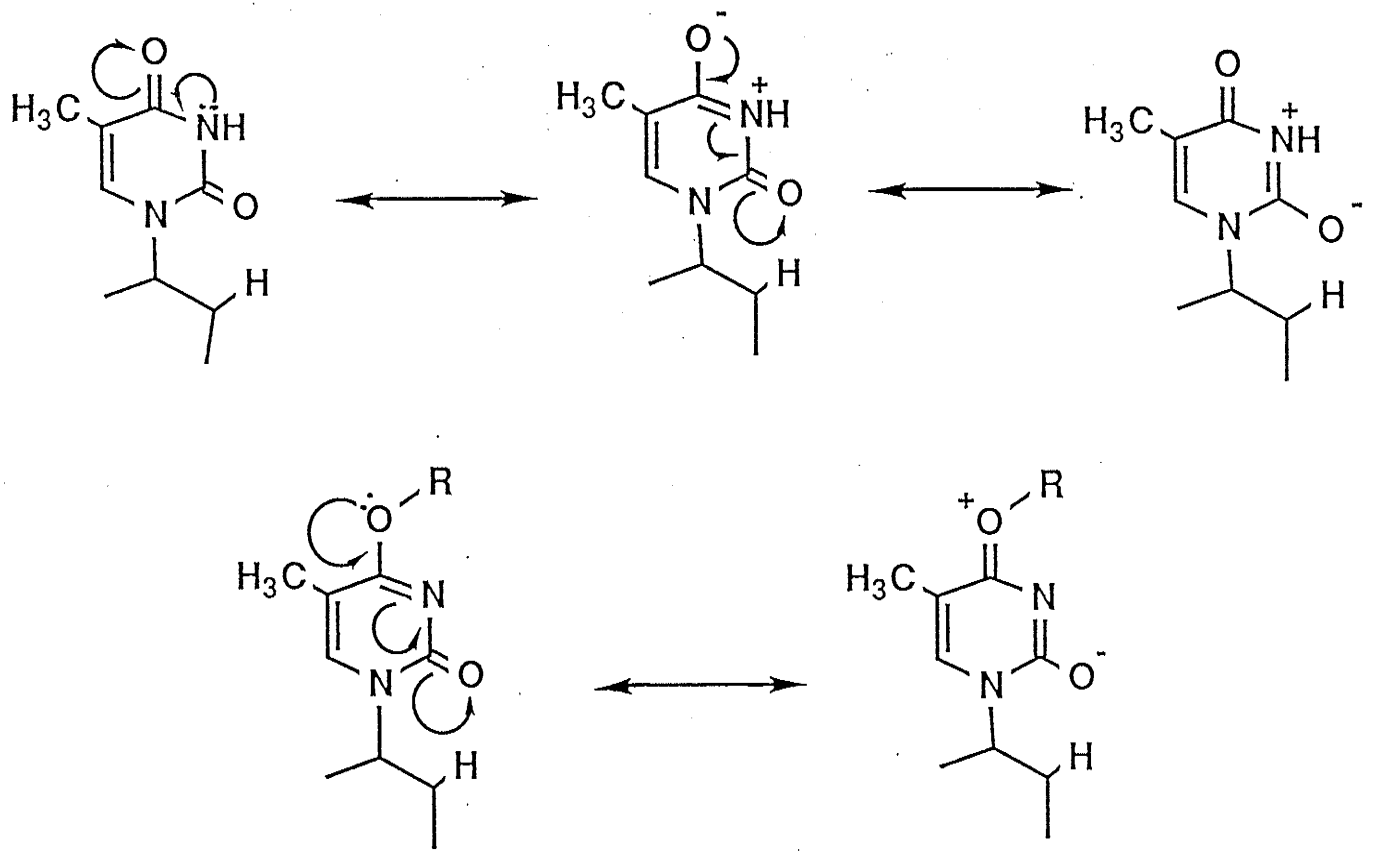

Figure 6.4: Augmentation du caractère nucléophile de l'oxygène-2 sur la nucléobase O-alkylée

non-alkylée, suite à la délocalisation des électrons non-liants de l'oxygène-4 alkylé (figure 6.4). Or la plupart des modes de fragmentation impliquent le transfert d'un hydrogène-2', soit sur l'ogygène-2 (formation de TH, schéma 6.1C) et de ^{r}TH (schéma 6.1D), en même temps que plusieurs autres ions, surtout ceux à m/z 195 (schémas 6.2 et 6.3), soit sur un oxygène du groupe phosphate (formation de Y^- (schéma 6.3), de T^- (schéma 6.1B) et de $^{r}T^-$ (schéma 6.1A). Il n'est donc pas surprenant de constater d'àprès le tableau 6.1 que le rapport (%CIT m/z 195) / (%CIT ($Y^- + T^- + {}^{r}T^-$)) est plus élevé quand la nucléobase alkylée se retrouve à l'extrémité-5' de la molécule. Dans ces conditions, en effet, l'affinité de l'oxygène-2 pour H2' est plus élevée, ce qui devrait se traduire par une augmentation du degré de formation de ^{r}TH et du signal à m/z 195 (schéma 6.2), surtout si la source de cet ion provient davantage de X^-. Qui plus est, le tableau 6.1 nous indique que le %CIT des ions $^{r}T^-$ par rapport aux ions T^- est beaucoup plus élevé pour les méthodes FAB et SIMS lorsque la nucléobase alkylée se retrouve à l'extrémité-5' de la molécule (^{r4}TpT). Nous croyons que ceci est dû au fait que la formation de $^{r}T^-$ ou T^- est davantage favorisée à partir des ions X^- (schéma 6.2A) où un oxygène d'un groupe phosphate peut faciliter le départ de la nucléobase par assistance anchimérique, selon un mécanisme S_N2 intramoléculaire déjà observé chez d'autres oligonucléotides[111] . Une telle approche vers le groupe partant $^{r}T^-$ ou T^- n'est pas possible pour les ions Y^-, car la position du groupe phosphate n'est pas propice à l'inversion de configuration requise pour rendre ce mécanisme opérationnel. Les ions Y^- peuvent toutefois assister la brisure du lien glycosidique et la formation de T^- par abstraction d'un hydrogène-2' (schéma 6.3, voie B), selon un mécanisme analogue à celui présenté sur le schéma 6.1B pour $[M-H]^-$; dans un tel cas, l'oxygène agit non pas comme nucléophile, mais comme base. Vue la

conformation syn-périplanaire associée à un tel mécanisme, on devrait s'attendre à ce que la réaction de formation de $^{r}T^{-}$ ou T^{-} à partir de X^{-} (schéma 6.2, voie A) soit beaucoup plus rapide que celle en provenance de Y^{-} (schéma 6.3, voie B).

En résumé, donc, on devrait s'attendre à ce que X^{-} se forme moins rapidement que Y^{-}; une fois formé, les groupes phosphates des ions X^{-} peuvent jouer le rôle de base ou de nucléophile, et les ions X^{-} voient donc misent à leur disposition des avenues de décompositions ultérieures plus efficaces que celles utilisables par les groupes phosphates des ions Y^{-}. Ceux-ci sont de moins bons nucléophiles et de moins bonnes bases que les groupes phosphates sur X^{-}, vu l'obligation q'ils ont d'attaquer les H2' selon une conformation *syn* plutôt qu'*anti*, comme c'est le cas pour les ions X^{-}. D'où un %TIC de X^{-} presque toujours plus faible que le % CIT de Y^{-}, selon l'approche SIMS.

Il est important de noter que les %CIT de X^{-} sont beaucoup plus rapprochés de ceux de Y^{-} par FAB, leur étant presqu'égaux pour le d(^{ip4}TpT) et même supérieur pour le d(^{e4}TpT). Ceci laisse entendre qu'en analyse par FAB, la source d'hydrogène donnant lieu à la formation des ions X^{-} et Y^{-} peut ne pas se limiter aux hydrogènes-4' et 2', puisqu'elle peut aussi provenir du glycérol.

Nous avons par ailleurs observé que la désalkylation peut précéder ou suivre la déglycosylation. Les ions $[M-r]^{-}$ constituent seulement 1 à 2% du CIT par SIMS, et 2 à 7% du CIT par FAB, tandis que les ions $(^{r}T^{-}-r)^{-}$ ou T^{-} varient de 11 à 40% du CIT. Le rapport (%CIT T^{-}) / (%CIT $^{r}T^{-}$) est beaucoup plus élevé quand la nucléobase **alkylée** est à l'extrémité-3' de la molécule (i.e. Tp^{r4}T); tel qu'illustré sur le schéma 6.5B, ceci pourrait être dû à la proximité d'un oxygène

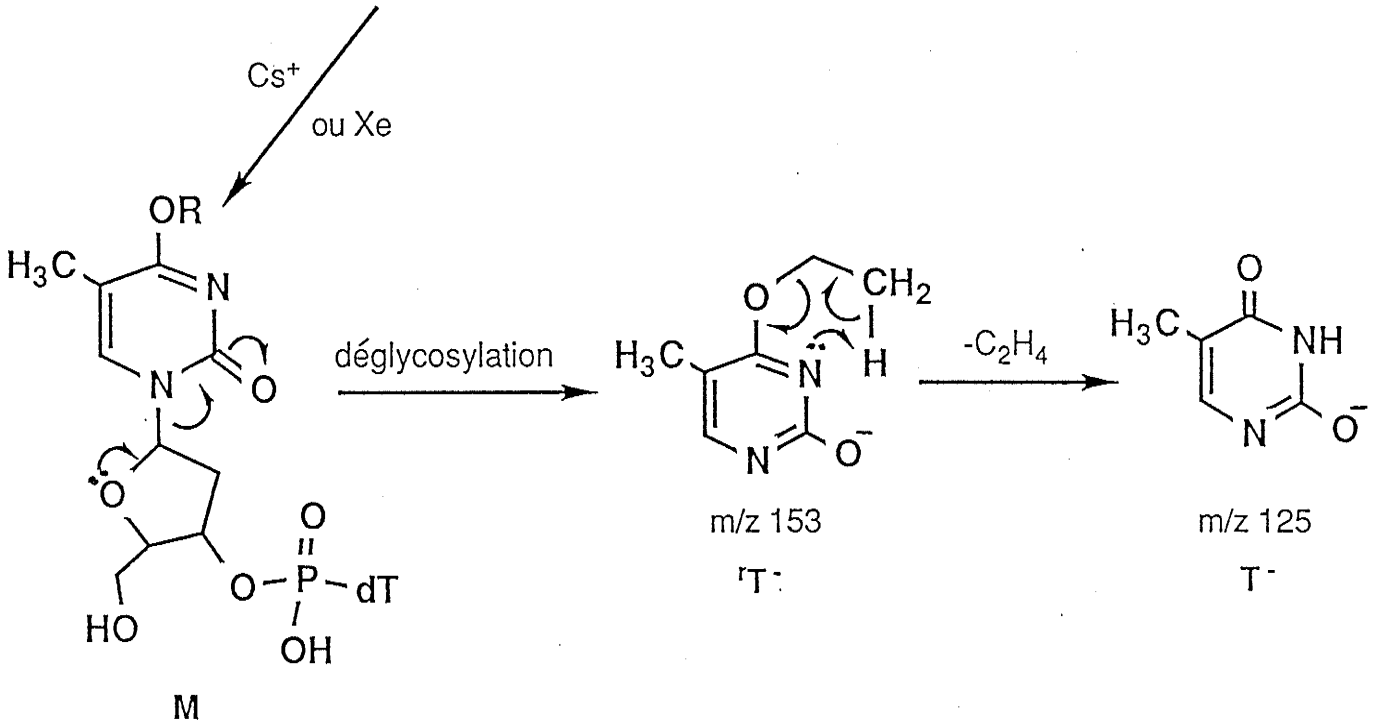
Cs+
ou Xe
OR
H3C
N
N
O
O
HO
O
O
P
dT
OH
M
déglycosylation
O
CH2
H3C
N
H
N
O-
m/z 153
rT-
-C2H4
O
H3C
NH
N
O-
m/z 125
T-

Schéma 6.4

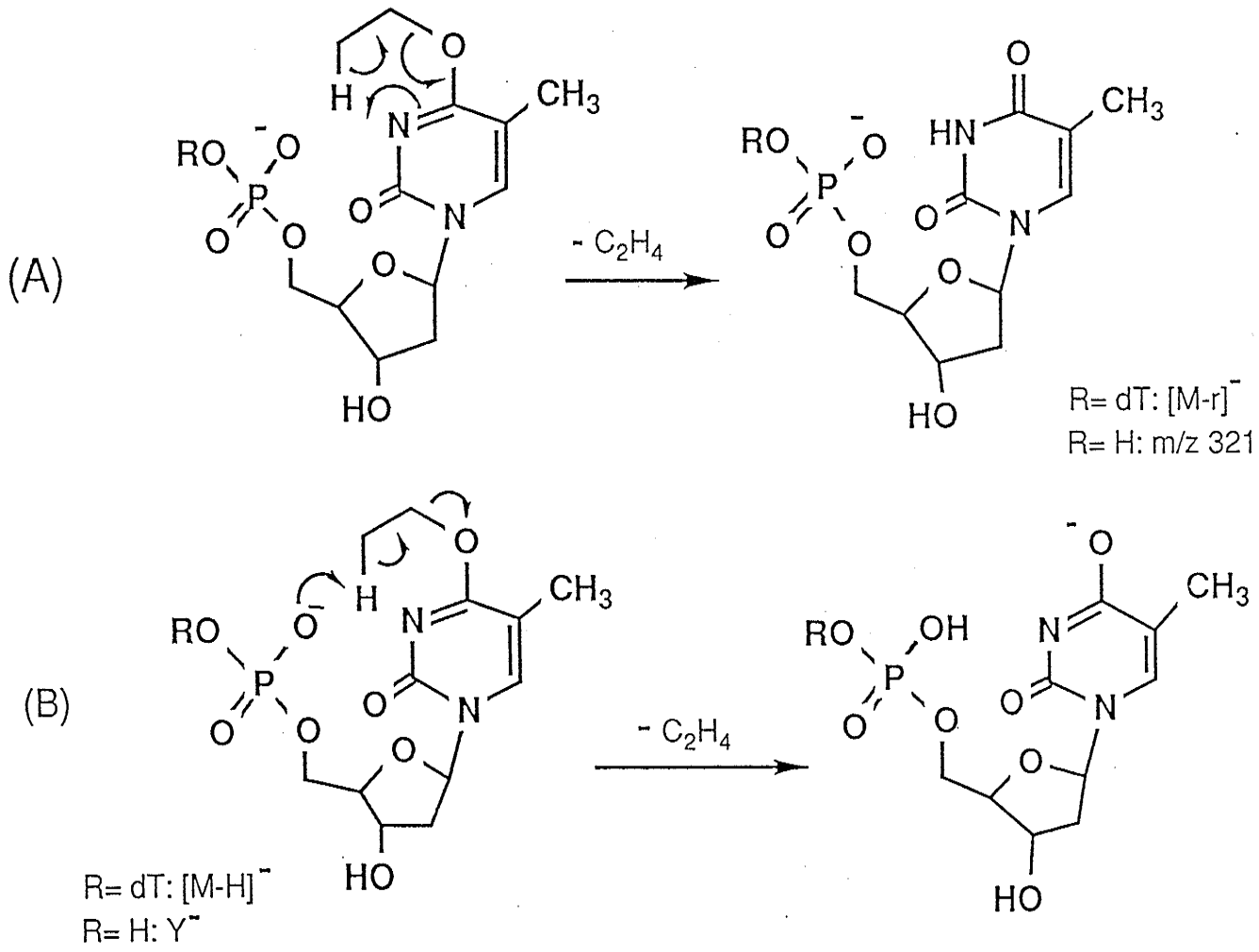

Schéma 6.5

du groupe phosphate qui peut faciliter la désalkylation de l'oxygène-4 selon le mécanisme illustré sur le schéma 6.4. Cette avenue mécanistique n'est pas accessible aux nucléotides dont la nucléobase alkylée est située à l'extrémité-5' de la molécule. Il est intéressant de noter que lors d'une étude antérieure par SIMS chez une série de nucléosides alkylés en position O2 et O4 (voir chapitre 4), le rapport (%CIT $^{r}T^{-}$) / (%CIT T^{-}) était toujours supérieur à l'unité, quoique diminuant selon $^{m}T^{-} > ^{e}T^{-} > ^{ip}T^{-}$. Une telle diminution de l'apport des $^{r}T^{-}$ au %CIT chez les nucléotides semble être un indice de l'implication d'un oxygène du groupe phosphate. Nous devons cependant noter que la désalkylation selon le réarrangement de McLafferty a été confirmée par étude de décompositions d'ions métastables chez les nucléosides ^{e}T et $^{ip}T^{110}$.

6.3.2. Tridésoxyribonucléoside-diphosphates

Le %CIT des ions $[M-H]^{-}$ et $[M-2H+Na]^{-}$ est à nouveau plus élevé en spectrométrie de masse FAB que par analyse SIMS, comme l'indique le tableau 6.2. Les spectres de masse SIMS et FAB en mode négatif du d($Tp^{Et4}TpT$) sont illustrés sur la figure 6.5. Le rapport %CIT FAB/SIMS de ces ions varie entre un minimum de 1.5 pour le $Tp^{e4}TpT$ et un maximum de 5.2 chez le $Tp^{m4}TpT$, des valeurs assez semblables à celles observées chez les dimères.

Par ailleurs, on se serait attendu à ce que le rapport (%CIT $^{r}T^{-}$) / (%CIT T^{-}) soit plus faible pour les trimères alkylés que pour les dimères alkylés, vu la présence d'une thymine supplémentaire chez les premiers. Certes, ce rapport est plus faible en comparaison avec celui observé chez les dimères ^{e4}TpT et ^{ip4}TpT; curieusement cependant, les dimères dont la nucléobase alkylée est "en bas" (à l'extrémité-3' de la molécule) montrent un rapport (%CIT $^{r}T^{-}$) / (%CIT

Tableau 6.2 Spectres de masse obtenus FABMS et SIMS en mode négatif de tridésoxyribonucléotides O-alkylés (en % de contribution au courant ionique total (%CIT) dans la région m/z 100 jusqu'aux ions $[M-H]^-$)

	d(TpTpT)			d(Tp^{m4}TpT)			d(Tp^{e4}TpT)			d(Tp^{ip4}TpT)		
ASSIGNATIONS	FAB	m/z	SIMS	FAB	m/z	SIMS	FAB	m/z	SIMS	FAB	m/z	SIMS
$[M-2H+Na]^-$	8.9	871	6.4	-	885	3.4	-	899	7.9	0.7	913	8.1
$[M-H]^-$	16.9	849	1.5	21.8	863	0.8	18.2	877	3.9	26.5	891	1.4
$[M-r]^-$	NA	NA	NA	2.3	849	0.6	1.7	849	0.6	2.9	849	0.8
$[X_2(Y_2)-H+Na]^-$	2.8	647	4.4	-	661	1.4	-	675	0.4	0.5	689	-
$X_2(Y_2)^-$	6.9	625	2.2	8.4	639	1.7	6.6	653	1.0	9.2	667	0.6
$[M-H-Y_1-H-TH]^-$	3.6	401	3.4	2.2	415	-	2.1	429	0.8	2.6	443	-
$[M-H-X_1-H-^rTH]^-$	NA	NA	NA	2.6	401	-	2.6	401	2.3	2.6	401	1.9
$X_1(Y_1)^-$	17.7	321	11.3	15.7	321	6.2	14.4	321	18.7	15.2	321	11.1
$[X_1(Y_1)-TH]^-$	11.9	195	21.6	13.7	195	15.3	16.5	195	21.2	12.4	195	16.2
$^rT^-$	NA	NA	NA	6.1	139	14.1	5.0	153	4.6	3.7	167	4.2
T^-	31.3	125	49.1	27.1	125	56.5	33.0	125	38.6	24.2	125	55.7

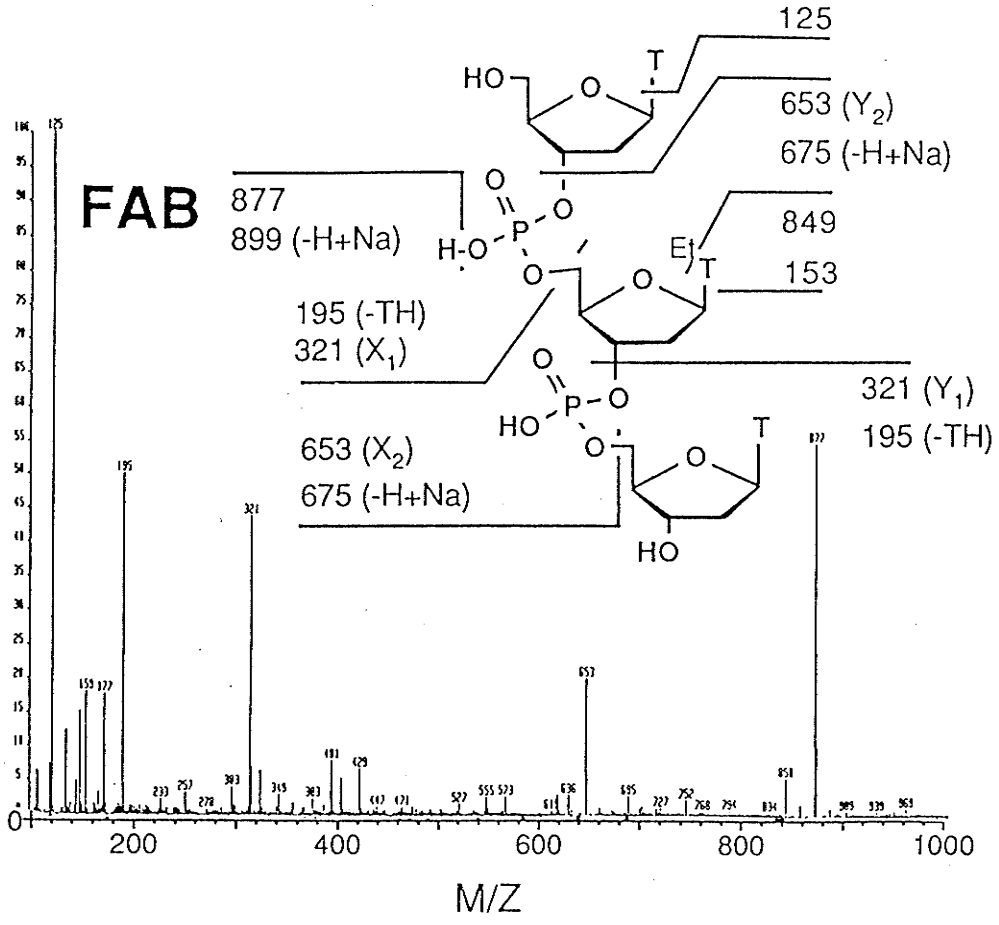

d(TpEt^{4}TpT)

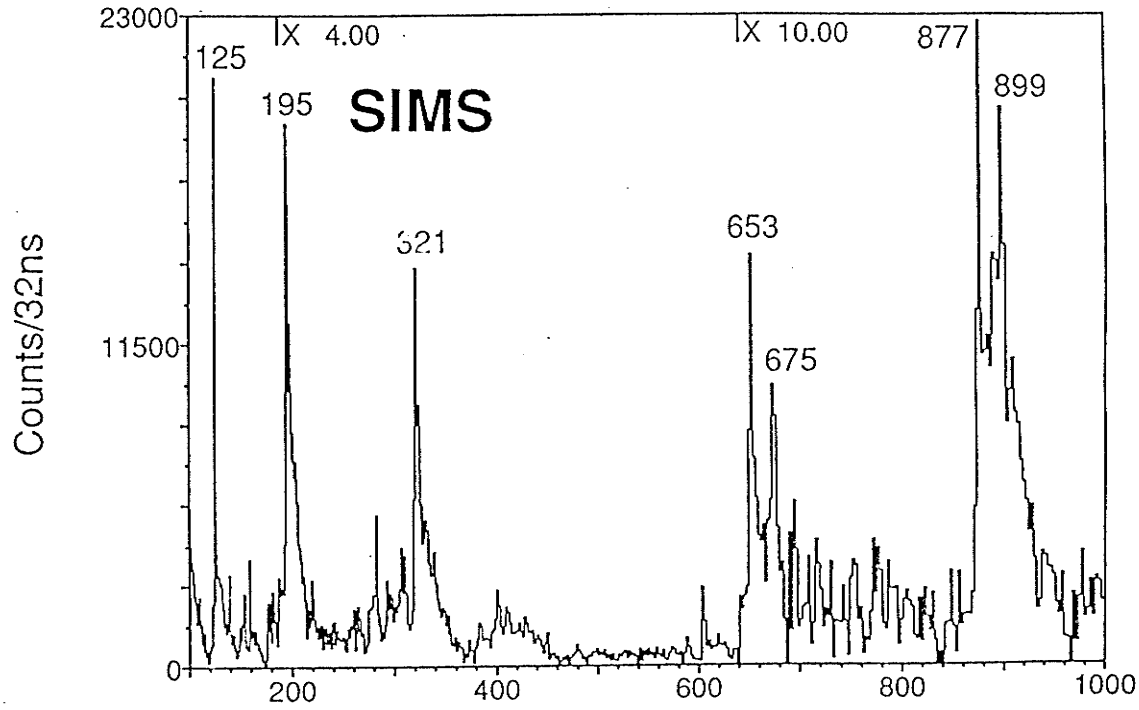

Figure 6.5 Spectres de masse FAB et SIMS en mode négatif du d(Tp^{Et4}TpT)

T^-) presque semblable à ce que l'on retrouve chez les trimères. C'est comme si pour ces derniers, l'une des thymines ne contribuerait que très peu au %CIT. En invoquant les arguments avancés dans la section précédente, on pourrait prévoir (i) que X_2^- contribue plus que Y_2^- à la formation de $^rT^-$, (ii) que X_1^- contribue plus que Y_1^- à la formation de T^-, et dans ce sens, que la source de T^- provient davantage du nucléoside à l'extrémité-5' de la molécule que de celui situé à son extrémité-3', (iii) que la contribution de Y_1^- au %CIT des ions à m/z 321 soit plus élevée que celle des ions X_1^- et (iv), que la perte de TH à partir des ions à m/z 321 provient davantage de X_1^- (perte du TH d'en haut) que de Y_1^- (perte du TH d'en bas). Malheureusement, puisque les ions X_1^- et X_2^- sont isobariques avec les ions Y_1^- et Y_2^-, respectivement, une étude des décompositions métastables ne nous permettrait pas de prouver directement les énoncés précédents. Nous disposons seulement de preuves indirectes pour les corroborer.

Le tableau 6.2 permet également de constater le faible niveau de désalkylation des ions $[M-H]^-$, à en juger par une contribution de moins de 3% au CIT des ions $[M-r]^-$ dans tous les cas, par FABMS et par SIMS. Un mécanisme analogue à celui invoqué pour les dimères sur le schéma 6.5 peut être imaginé, en n'excluant toutefois pas la possibilité de former $[M-r]^-$ directement à partir de M, sans réarrangement de type McLafferty. En effet, le $Tp^{m4}TpT$ montre un %CIT de $[M-r]^-$ semblable à ceux observés chez les composés éthylés et i-propylés; or, si la désalkylation du $Tp^{m4}TpT$ se faisait selon un mécanisme concerté avec l'assistance de l'azote-3 ou de l'oxygène d'un groupe phosphate (schéma 6.5), un carbène :CH2 hautement réactif serait produit, ce qui est improbable.

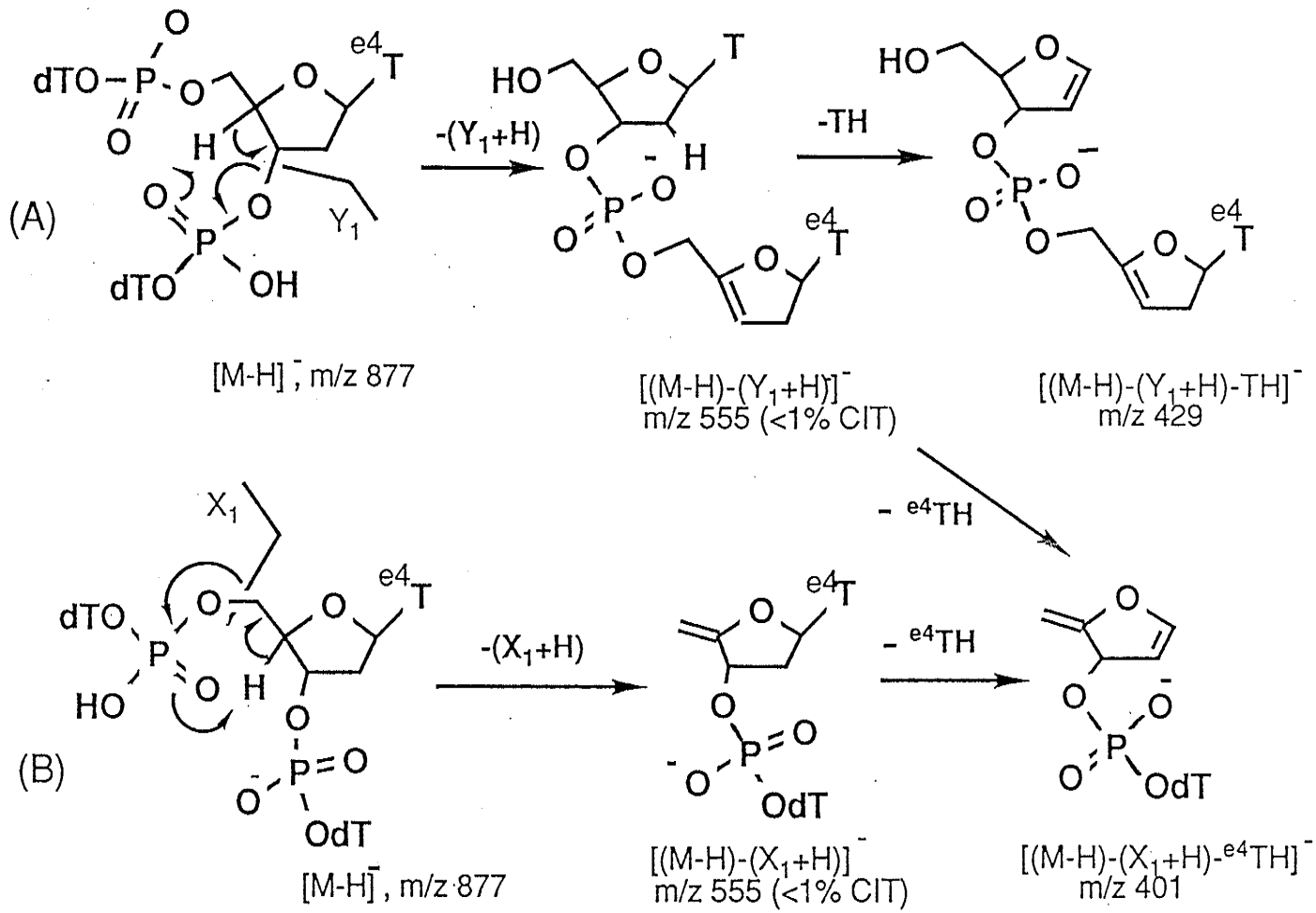
(A)
dTO
e4T
Y1
dTO
OH
-(Y1+H)
HO
-TH
[M-H]-, m/z 877
[(M-H)-(Y1+H)]-
m/z 555 (<1% CIT)
[(M-H)-(Y1+H)-TH]-
m/z 429
- e4TH
(B)
X1
dTO
HO
OdT
-(X1+H)
- e4TH
[M-H]-, m/z 877
[(M-H)-(X1+H)]-
m/z 555 (<1% CIT)
[(M-H)-(X1+H)-e4TH]-
m/z 401

Schéma 6.6

Le schéma 6.6 illustre à l'aide du $Tp^{e4}TpT$ l'origine possible des ions $[(M-H)-(Y_1 \text{ (ou } X_1)+H-TH)]^-$ et $[(M-H-(X_1 \text{ (ou } Y_1)+H-{}^rTH)]^-$, retrouvés à m/z 429 et 401, respectivement, pour ce composé. On s'attendrait donc ici à ce que l'ion à m/z 429 résulte davantage de la perte de (Y_1+H) et de la thymine du haut que de la perte de (X_1+H) et de la thymine du bas. Car pour des raisons énoncées précédemment, Y_1^- devrait se former plus facilement que X_1^-, et de plus, le TH du haut devrait pouvoir se former plus facilement que le TH du bas, en raison de l'acidité accrue des H2' quand ils sont situés au voisinage du groupe phosphate. Cette situation est décrite dans le schéma 6.6A.

Une différence notable entre les spectres FAB et SIMS est la présence chez ces derniers de signaux correspondant aux ions $[M-2H+Na]^-$ et aux ions séquentiels $[Y_2 \text{ (ou } X_2)-H+Na]^-$ d'abondance relative comparable ou supérieure aux signaux correspondant à $[M-H]^-$ et $[Y_2 \text{ (ou } X_2)]^-$. Il est intéressant de constater qu'aucun signal correspondant à $[Y_1-H+Na]^-$ ou $[X_1-H+Na]^-$ n'a pu être détecté. Il semblerait donc que le Na^+ soit localisé autour du nucléoside central qui est alkylé, peut-être selon la structure illustrée à la figure 6.6. Ces observations viennent corroborer les résultats d'une étude cinétique que nous faisions récemment[110], qui suggérait que le sodium avait une affinité particulière our les thymidines alkylées en position-O4.

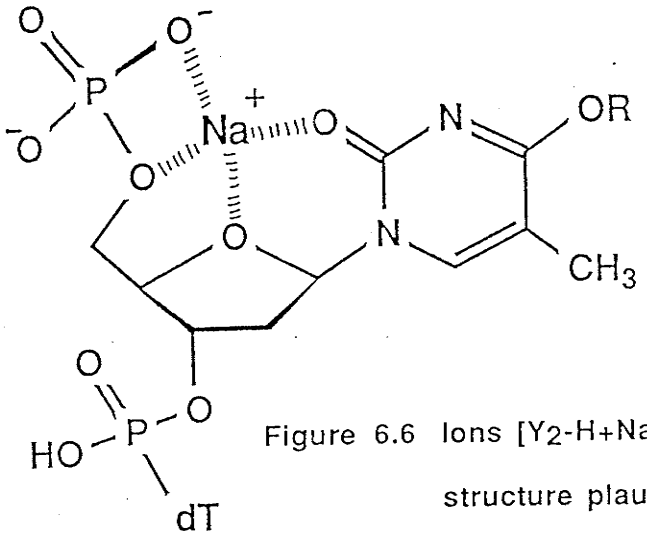

Figure 6.6 Ions $[Y_2-H+Na]^-$: structure plausible

Cette étude en mode négatif de di- et de trinucléotides O-alkylés a permis de mettre en relief la nature complémentaire des approches FABMS et SIMS. Chacune de ces techniques d'ionisation douce a non seulement permis de caractériser complètement les composés titrés, mais elles ont aussi toutes les deux permis de localiser le site d'alkylation et d'évaluer son influence sur les modes de fragmentation de ces nucléotides modifiés.

CONCLUDING REMARKS

The primary objective of this investigation was to evaluate how secondary ion time-of-flight mass spectrometry could be used to characterize and differentiate small, synthetic, isomeric nucleic acid components. Protected or unprotected, positional isomers or strereoisomers, all compounds have been differentiated, whether by differences in values of kinetic parameters, or in abundances of position or sequence specific fragments.

All compounds were analyzed with the Manitoba TOF I and TOF II mass spectrometers, more frequently in the negative ion mode. This had the advantage of producing less complex or easier to interpret spectra, compared to spectra recorded in the positive ion mode. This is particularly true for nucleotides and oligonucleotides. On the other hand, sensitivity and rate of data acquisition were significantly lower in the negative ion mode, under recording conditions, with the boehmite supports and instrumental configurations prevalent during the course of this research project. Since completion of this work, new sample preparation techniques such as the introduction of nitrocellulose substrates, together with considerable improvements in the MS/MS capability of the reflecting TOF II spectrometer, have resulted in better spectra quality and have increased even further the potential of our TOF-SIMS analytical arsenal to study compounds of biological interest, such O-alkylated and branched oligonucleotides. The recent use of more efficient ionization methods such as matrix-assisted laser desorption and event by event data logging now in use in Dr. Standing's laboratory appear to suggest obvious directions towards which future research endeavours could be directed in new mass spectrometric characterization s of nucleic acid constituents.

REFERENCES

1. C.A. Villee, E.P. Solomons, C.E. Martin, D.W. Martin, L.RA. Berg and P.W. Davis, "*Biology*", 2nd ed., Saunders College, Publ. chap. 15 (1989).

2. J. X. Stephens, M.L. Cavanaugh, M.I. Gradie, M.L. Mador and K.K. Kidd, *Science*, **250**, 237 (1990).

3. C.J. Howe and E.S. Ward, "*Nucleic Acid Sequencing: A Practical Approach*", IRL Press (1989).

4. J. Darnell, H. Lodish and D. Baltimore, "*Molecular Cell Biology*", Scientific American Books, W.H. Freeman, N.Y., chap. 6 (1986).

5. J. Stegemann, C. Schwager, H. Erfle, N. Hewitt, H. Voss, J. Zimmermann and W. Ansorge, *Nucleic Acid Res.*, **19**, no 3, 675 (1991).

6. A.M. Maxam and W. Gilbert, *Proc. Natl. Acad. Sci.*, **74**, 560 (1977).

7. F. Sanger, S. Nicklen and A.R. Coulson, *Proc. Natl. Acad. Sci.*, **74**, 5463 (1977).

8. G.W. Slater and G. Drouin, *Interface*, **12**, no 3, 115 (1991).

9. L.M. Smith, R.J. Kaiser, J. Z. Sanders and L.E. Hood, *Meth. in Enzym.*, **155**, 260 (1987).

10. W. Saenger, "*Principles of Nucleic Acid Structures*", Springer-Verlag, N.Y. Inc., chap. 3 (1984).

11. J.D. Watson and F.H.C. Crick, *Nature* (London), **171**, 737 (1953).

12. K. Wuthrich, "*NMR of Proteins and Nucleic Acids*", John Wiley & Sons, N.Y. (1986).

13. J.A. Gerlt and A.V. Youngblood, J. *Amer. Chem. Soc.*, **102**, 7433 (1980).

14. B.P. Cho and F.E. Evans, *Nucl. Acid Res.*, **19**, no5, 1041 (1991).

15. H. Iwahashi and Y. Kyogoku, *J. Amer. Chem. Soc.*, **99**, 7761 (1977).

16. G.W. Buchko, F.E. Hruska and K.L. Sadana, *Can. J. Chem.*, **67**, 109 (1989).

17. C. Griesinger, O.W. Sorensen and R.R. Ernst, *J. Amer. Chem. Soc.*, **109**, 7227 (1987).

18. G.J. Thomas, Jr., "*Structure and Conformation of Nucleic Acids and Proteins-Nucleic Acid Interactions*", M. Sundaralingam et al, Eds., University Park Press, Baltimore, (1975).

19. M. Tsuboi, "*Infrared and Raman Spectroscopy*", P.O.P. Ts'o, Ed., in *Basic Principles in Nucleic Acid Chemistry*, Academic Press, N.Y., vol.1. (1974).

20. D. Porschke, *Biopolymers*, **10**, 1989 (1971).

21. F.M. Pohl and T.M. Jovin, *J. Mol. Biol.*, **67**, 375 (1972).

22. A.M. Lawson, R.N. Stillwell, M.M. Tacker, K. Tsuboyama and J.A. McCloskey, *J. Amer. Chem. Soc.*, **93**, 1014 (1971).

23. D.L. Slowikowski and K.H. Schram, *Nucleosides and Nucleotides*, **4**, 347 (1985).

24. A. Eicke, W. Sichtermann and A. Benninghoven, *Org. Mass Spectrom.*, **15**, 289 (1980).

25. M.A. Quilliam, K.K. Ogilvie and J.B. Westmore, *Org. Mass Spectrom.* **16**, 129 (1981).

26. J. Eagles, C. Javanaud and R. Self, *Biomed. Mass Spectrom.*, **11**, 41 (1984).

27. T.R. Covey, R.F. Bonner, B.I. Shushan and J. Henion, *Rapid Commun. Mass Spectrom.* **2**, 249 (1989).

28. S. Kumar, P.C. Joshi, N.D. Sharma, S.N. Bose, R.J.H. Davies, N. Takeda and J.A. McCloskey, *Nucleic Acids Res.*, **19**, 2841 (1991).

29. H. Pang, D.L. Smith, P.F. Crain, K. Yamaizumi, S. Nishimura and J.A. McCloskey, *Eur. J. Biochem.* **127**, 459 (1982).

30. C.G. Edmonds, M.L. Vestal and J. A. McCloskey, *Nucleic. Acids Res.*, **13**, 8197 (1985).

31. J.A. McCloskey, in "*Mass Spectrometry in Biomedical Research*", Ed. S.J. Gaskell, John Wiley & Sons, Chichester, p. 75 (1986).

32. D.W. Phillipson, C.G. Edmonds, P.F. Crain, D.R. Davis and J.A. McCloskey, *J. Biol. Chem.*, **262**, 3462 (1987).

33. K.H. Schram, in "*Biomedical Applications of Mass Spectrometry*", Ed. C.H. Suelter, John Wiley and Sons, Chichester, p. 203 (1990).

34. M.L. Vestal, *Mass Spectrom. Reviews*, **3**, 447 (1983).

35. K. Isono, M. Uramoto, H. Osada, M. Ubukata, H. Kusakabe, T. Koyama, N. Miyata, S.K. Sithi and J.A. McCloskey, *Nucleic Acids Res.* **15**, 65 (1984).

36. M. Nishi, J.I. Inagaki, F. Nohara, K. Isono, H. Kusakabe, K. Kobayashi, T. Sakurai, S. Koshimura, S.K. Sithi and J.A. McCloskey, *J. Antibiot.*, **38**, 1440 (1985).

37. S. Della Negra, Y.N. Ginot, Y. Le Beyec, M. Spiro and P. Vigny, *Nucl. Instr. and Methods*, **198**, 159 (1982).

38. M. Dizdaroglu, *Anal. Chem.* **144**, 593 (1985).

39. K.B. Tomer, M.L. Gross and M.L. Deinzer, *Anal. Chem.*, **58**, 2527 (1986).

40. D.J. Ashworth, W. M. Baird, C. Chang, J.D. Ciupek, K.L. Busch and R.G. Cooks, *Biomed. Mass Spectrom.*, **12**, 309 (1985).

41. C. Finn, H.J. Schwandt and W. Sadee, *Biomed. Mass Spectrom.*, **6**, 194 (1979).

42. D.L. Slowikowski and K.H. Schram, *Nucleosides and Nucleotides*, **4**, 309 (1985).

43. M. Panico, G. Sindona and N. Uccella, *J. Amer. Chem. Soc.* **105**, 5607 (1983).

44. C.J. McNeal, K.K. Ogilvie, N.Y.Theriault and M.J. Nemer, *J. Amer. Chem. Soc.*, **104**, 972 (1982).

45. C.J. McNeal, S.A. Narang, R.D. Macfarlane, H.M. Hsiung and R. Brousseau, *Proc. Natl. Acad. Sci. USA*, **77**, 735 (1980).

46. C.J. McNeal and R.D. Macfarlane, *J. Amer. Chem. Soc.*, **103**, 1609 (1981).

47. L. Grotjahn, R. Frank and H. Blocker, *Nucleic Acids Res.*, **10**, 4671(1982).

48. L. Grotjahn, H. Blocker and R. Frank, *Biomed. Mass Spectrom.*, **12**, 514 (1985).

49. L. Grotjahn, R. Frank and H. Blocker, *Int. J. Mass Spectrom. Ion Phys.*, **46**, 439 (1983).

50. L. Grotjahn, R. Frank, G. Heisterberg-Moutsis and H. Blocker, *Tetrahedron Lett.*, **25**, 5373 (1984).

51. A. Viari, J.P. Ballini and P. Vigny, in "*Mass Spectrometry in the Analysis of Large Molecules*", Ed. C.J. McNeal, John Wiley & Sons, Chichester. p.199 (1986).

52. A. Viari, J.P. Ballini, P. Meleard, P. Vigny, P. Dousset, C. Blonski and D. Shire, *Biomed. Environ. Mass Spectrom.*, **16**, 225 (1988).

53. W. Ens, K.G. Standing, J.B. Westmore, K.K. Ogilvie and M.J. Nemer, *Anal. Chem.* **54**, 960 (1982).

54. R. Beavis, W. Ens, M.J. Nemer, K.K. Ogilvie, K.G. Standing and J.B. Westmore, *Int. J. Mass Spectrom. Ion Phys.*, **46**, 475 (1983).

55. H. Seliger, T.C. Bach, G. Siewert, W. Boidol, M. Topert, H.-R. Schulten and H.M. Schiebel, *Liebigs Ann. Chem.* **5**, 835 (1984).

56. A. Wolter, C. Mohringer, H. Koster and W.A. Konig, *Biomed. Environ. Mass Spectrom.*, **14**, 111 (1987).

57. J. Tamas and J. Tomasz, *Biomed. Mass Spectrom.*, **12**, 489 (1985).

58. J.B. Westmore, D.C.K. Lin, K.K. Ogilvie, H.Wayborn and J. Berestiansky, *Org. Mass Spectrom.*, **6**, 143 (1972).

59. G. Puzo, K.H. Schram, J.G. Liehr and J.A. McCloskey, *J. Org. Chem.*, **43**, 767 (1978).

60. J. Ulrich, A. Guy, D. Molko and R. Teoule, *Org. Mass Spectrom.*, **19**, 585 (1984).

61. P. Toren, D.F. Betsch, H.L. Weith and J.M. Coull, *Anal. Biochem.*, **152**, 291 (1986).

62. J.A. McCloskey, "Mass Spectrometry", in "*Basic Principles in Nucleic Acid Chemistry*", P.O.P. Ts'o, Ed., Academic Press, N.Y., vol. 1, p. 209 (1974).

63. H. Pang, K.H. Schram, D.L.Smith, S.P. Gupta, L.B. Townsend and J.A.McCloskey, *J. Org. Chem.*, **47**, 3923 (1982).

64. L.M. Mallis, F.M. Raushel and D.H. Russell, *Anal, Chem.*, **59**, 980 (1987).

65. R.L. Cerny, K.B. Tomer, M.L. Gross and L.Grotjahn, *Anal. Biochem.*, **165**, 175 (1987).

66. J. Ulrich, J. Cadet and R. Teoule, *Org. Mass Spectrom.*, **7**, 543 (1973).

67. M.S. Wilson and J.A. McCloskey, *J. Amer. Chem. Soc.*, **97**, 3436 (1975).

68. R.L. Cerny, M.L. Gross and L. Grotjahn, *Anal. Biochem.*, **156**, 424 (1986).

69. A. Liguori, G. Sindona and N. Uccella, *Biomed. Environ. Mass Spectrom.*, **17**, 451 (1988).

70. C.H. Hocart and U.P. Schlunegger, *Rapid Comm. Mass Spectrom.*, **3**, 36 (1989).

71. R. Hettich and M. Buchanan, *J. Amer. Soc. Mass Spectrom.*, **2**, 402 (1991).

72. Y. Tondeur, R.C. Moschel, A. Dipple and S.R. Koepke, *Anal. Biochem.*, **58**, 1316 (1986).

73. F.W. Crow, K.B. Tomer, M.L. Gross, J.A. McCloskey and D.E. Bergstrom, *Anal. Biochem.*, **139**, 243 (1984).

74. A. Viari, J.P. Ballini, P. Vigny, D. Shire and P.Dousset, *Biomed. Environ. Mass Spectrom.*, **14**, 83 (1987).

75. E.E. Kingston, J.H. Beynon, R.P. Newton and J.G. Liehr, *Biomed. Mass Spectrom.*, **12**, 525 (1985).

76. G. Sindona, N. Uccella and K. Weclawek, *J. Chem. Res. (S)*, 184 (1982).

77. H.-R. Schulten and H.M. Schiebel, *Nucleic Acids Res.*, **3**, 2027 (1976).

78. G.R. Pettit, J.J. Einck and P. Brown, *Biomed. Mass Spectrom.*, **5**, 153 (1978).

79. H. Budzikiewicz and G. Feistner, *Biomed. Mass Spectrom.*, **5**, 512 (1978).

80. A. Viari, J.P. Ballini, P. Vigny, L. Voituriez and J. Cadet, *Biomed. Environ. Mass Spectrom.*, **18**, 547 (1989).

81. A. Hogg, J.G. Kelland and J.C. Vederas and C.Tamm, *Helv. Chim. Acta*, **69**, 908 (1986).

82. G. Brewer and C.M. Grisham, *Biomed. Mass Spectrom.*, **11**, 400 (1984).

83. M. Green and J.M. Miller, *J. Chem. Soc. Chem. Comm.*, 1864 (1987).

84. M.J. Bertrand, V. Benham, R. St-Louis and M.J. Evans, *Can. J. Chem.*, **67**, 910 (1989).

85. S.E. Unger, A.E. Schoen, R.G. Cooks, D.J. Ashworth, J.D. Gomes and C.J. Chang, *J. Org. Chem.*, **46**, 4765 (1981).

86. I. Isern-Flecha, X.Y. Juang, R.G. Cooks, W. Pfleiderer, W.G. Chae and C.J. Chang, *Biomed. Environ. Mass Spectrom.*, **14**, 17 (1987).

87. C.R. Iden and R.A. Rieger, *Biomed. Environ. Mass Spectrom.*, **18**, 617 (1989).

88. D. Griffin, J. Laramee, M. Deinzer, E. Stirchak and D. Weller, *Biomed. Environ. Mass Spectrom.*, **17**, 105 (1988).

89. K.A. Jacobson, L.K. Pannell, K.L. Kirk, H.M. Fales and E.A. Sokoloski, *J. Chem. Soc. Perkin Trans. I*, 2143 (1986).

90. J.G. Liehr, C.L. Weise, P.F. Crain, G.H. Milne, D.S. Wise, L.B.Townsend and J.A. McCloskey, *Heterocyclic Chem.*, **16**, 1263 (1979).

91. L.R. Phillips, K.A. Gallo, G. Zon, W.J. Stec and B. Uznanski, *Org. Mass Spectrom.*, **20**, 781 (1985).

92. L. Alder, R. Donau, R.Stoesser and S. Cech, *Biomed. Environ. Mass Spectrom.*, **13**, 217 (1986).

93. P. Vigny and A. Viari, *Mass Spectrometry Applied to Natural Products: Nucleosides, Nucleotides and Nucleic Acids*, in "Mass Spectrometry", vol. 10, p. 253 (1988).

94. C. Jiang, R.J.Suhadolnik and D.C. Baker, *Nucleosides and Nucleotides*, **7**, 271 (1988).

95. R.P. Newton, T.J. Walton, S.A. Basaif, A.M. Jenkins, A.G. Brenton, D. Ghosh and F.M.Harris, *Org. Mass Spectrom.*, **24**, 679 (1989).

96. R.D. Smith, J.A. Loo, C.G. Edmonds, C.J. Barinaga and H.R. Udseth, *Anal. Chem.*, **62**, 882, (1990).

97. J.J. Thompson, *Philos. Mag. VI*, **24**, 209, 668 (1912).

98. K. Biemann and J.A. McCloskey, *J. Am. Chem. Soc.*, **84**, 2005 (1962).

99. R.J. Anderegg, in "*Biomedical Applications of Mass Spectrometry*", C.H. Suelter, Ed., John Wiley and Sons, Chichester, p.1 (1990).

100. R.J. Cotter and C. Fenselau, *Biomed. Mass Spectrom.*, **7**, 287 (1979).

101. E.L. Esmans, E.J. Freyne, J.H. Vanbroeckhoven and F.C. Alderweirelt,

Biomed. Mass Spectrom., **7**,377 (1980).

102. J. Van der Greef, *Trends in Anal. Chem.*, **5**, 241 (1986).

103. M. Barber, R.S. Bordoli, R.D. Sedgwick and A.N. Tyler, *J. Chem. Soc. (London) Chem. Commun.*, 325 (1981).

104. K.H. Schram, *Trends in Anal. Chem.*, **7**, 28 (1988).

105. M. Barber, R.S. Bordoli, G.J. Elliot, R.D. Sedgwick and A.N. Tyler, *Anal. Chem.*, **54**, 645A (1982).

106. D.F. Torgerson, R.P. Skowronski and R.D. Macfarlane, *Biochem. Biophys. Res. Commun.*, **60**, 616 (1974).

107. C.J. McNeal, Texas A & M University, Ph.D. thesis, 7 (1980).

108. A. Benninghoven and W. Sichtermann, *Org. Mass Spectrom.*, **12**, 595 (1977).

109. W. Ens, K.G. Standing, B.T. Chait and F.H. Field, *Anal. Chem.*, **53**, 1241(1981).

110. F. Lafortune, W. Ens, F.E. Hruska, K.L. Sadana, K.G. Standing and J.B. Westmore, *Int. J. of Mass Spectrom. and Ion Proc.*, **78**, 179 (1987).

111. F. Lafortune, K.G. Standing, J.B. Westmore, M.J. Damha and K.K. Ogilvie, *Org. Mass Spectrom.*, **23**, 228 (1988).

112. F. Lafortune, M.J. Damha, X. Tang, K.G. Standing, J.B. Westmore and K.K. Ogilvie, *Nucleosides and Nucleotides*, **9** (3), 445 (1990).

113. F. Hillenkamp, in "*Advances in Mass Spectrometry*", vol. 11A, P. Longevialle, Ed., Heyden & Sons Ltd., London, p. 354 (1989).

114. E.D. Hardin, T.P. Fan, C.R. Blakley and M.L. Vestal, *Anal. Chem.*, **56**, 2 (1984).

115. D.A. McCrery and M.L. Gross, *Anal. Chim. Acta*, **178**, 91 (1985).

116. M. Karas and F. Hillenkamp, in "*Advances in Mass Spectrometry*", vol. 11A, P. Longevialle, Ed., Heyden & Sons Ltd., London, p. 416 (1989).

117. B. Spengler, Y. Pan, R.J. Cotter and J.S. Kan, *Rapid Comm. Mass Spectrom.*, **4**, 99 (1990).

118. J.V. Iribarne and B.A. Thomson, *J. Chem. Phys.*, **64**, 2287 (1976).

119. A.P. Bruins, in "Advances in Mass Spectrometry" vol. 11A, Heyden & Son, London, p.23 (1989).

120. K. Standing, R. Beavis, G. Bolbach, W. Ens, F. Lafortune, D. Main, B. Schueler, X. Tang and J. B. Westmore, *Anal. Instr.*, **16**, 173 (1987).

121. B.T. Chait and K.G. Standing, *Int. J. Mass Spectrom. Ion Phys.*, **40**, 185 (1981).

122. K.G. Standing, R. Beavis, G. Bolbach, W. Ens, D.E. Main, and B. Schueler, in *Secondary Ion Mass Spectrometry, SIMS V*, A. Benninghoven (Ed.), Springer-Verlag, Berlin, 476 (1986).

123. A. Benninghoven, *in Ion Formation from Organic Solids*, Ed. A. Benninghoven, Springer Series in Chemical Physics Springer, Berlin, **25**, 64, (1983).

124 B. Schueler, R. Beavis, G. Bolbach, W. Ens, D.E. Main, and K.G. Standing, in *Secondary Ion Mass Spectrometry*, SIMS V, A. Benninghoven (Ed.), Springer-Verlag, Berlin, **476**, 57 (1986).

125. B. Schueler, R. Beavis, G. Boldach, W. Ens, D.E. Main, and K.G. Standing, in *Secondary Ion Mass Spectrometry*, SIMS V, A. Benninghoven (Ed.), Springer-Verlag, Berlin, **476**, 37 (1986).

126. X. Tang, R. Beavis, W. Ens, F. Lafortune, B. Schueler and K.G. Standing, *Int. J. Mass Spectrom. Ion Processes*, **85**, 43 (1988).

127. X.Tang, Ph.D. Thesis, University of Manitoba, 1991

128. B.A. Mamyrin, V.I. Kartaev, D.V. Schmikk and V.A. Zagulin, *Sov. Phys. JETP*, **37**, 45 (1973).

129. W. Ens, R. Beavis, G. Bolbach, D. Main, B. Schueler and K.G. Standing, *Nuclear Instruments and Methods in Physics Research* A245, 146 (1986).

130. W. Ens, Y. Mao, X. Tang and K.G. Standing, *Proceedings of the 37th ASMS Conference on Mass Spectrometry and Allied Topics*, Miami, (1989) p. 1059.

131. K.G. Standing, W. Ens, R. Beavis, G. Bolbach, D. Main, B. Schueler and J.B. Westmore, *Springer Proc. Phys.*, **9**, 37 (1986).

132. R.R. Weller, J.A. Mayernik and C.S. Giam, *Biomed and Environ. Mass Spectrom.*, **15**, 529 (1988).

133. S.M. Hecht, A.S. Gupta and N.J. Leonard, *Biochim. Biophys. Acta*, **182**, 444 (1969).

134. D.L. Smith, K.H. Schram and J.A. McCloskey, *Biomed. Mass Spectrom.*, **10**, 269 (1983).

135. H.T. Cory, K. Yamaizumi, D.L. Smith, D.R. Knowles, A.S. Broom and J.A. McCloskey, *J. Heterocyclic Chem.*, **16**, 585 (1979).

136. M.A. Quilliam, K.K. Ogilvie, K.L. Sadana and J.B. Westmore, *Org. Mass Spectrom.*, **15**, 207 (1980).

137. C.G. Edmonds, S.C. Pomerantz, F.F. Hsu and J.A. McCloskey, *Anal. Chem.*, **60**, 2314 (1988).

138. M. Sochacki, E. Sochacka and A. Malkiewicz, *Biomed. Mass Spectrom.*, **7**, 257 (1980).

139. M. Sochacki, *Nucleosides & Nucleotides*, **9**, 461(1990).

140. E.M. Schubert, K.H. Schram and R. A. Glennon *J. Heterocyclic. Chem.*, **22**, 889 (1985).

141. I.A. Mikhailopulo, E.M. Kalinichenko, G.V. Zaiseva and A.A. Akhrem, *Biomed. Mass Spectrom.*, **9**, 225 (1982).

142. J. Claereboudt, E.L. Esmans, E.G. Van den Eeckhout and M.Claeys, *Nucleosides & Nucleotides*, **9**, 333 (1990).

143. H. Feistner, Diplomarbeit, Univ. Koln, 1977.

144. J.L. Wiebers, *Anal. Biochem.*, **51**, 542 (1973).

145. L. Grotjahn, *32nd Ann. Conf. Mass Spectrom. Allied Topics*, San Antonio, TX, (1984) p.396.

146. V.E. Marquez, C.K.H. Tseng, G. Gebeyehu, D.A. Cooney, H.S.S. Ahluwalia, J. A. Kelley. M. Dalal, R.W. Fuller, Y.A. Wilson and D.G. Johns, *J. Med. Chem.*, **29**, 1726 (1986).

147. N. Neri, G. Sindona and N. Ucella, *Gazz. Chim. Italiana*, **113**, 197 (1983).

148. B. Kralj. V. Kramer, R. Suzic and J. Kobe, *Biomed. Mass Spectrom.*, **12**, 673 (1985).

149. E. Arlandini, B. Gioia, M.G. Brasca, S. Frestinoni, *Nucleosides & Nucleotides* **9**, 431 (1990).

150. M. Linscheid and A.L. Burlingame, *Org. Mass Spectom.*, 18, 245 (1983).

151. B. Singer, S.J. Spengler, H. Fraenkel-Corat and J.T. Kusmierek, *Proc. Natl. Acad. Sci. U.S.A.*, **83,** 28 (1986).

152. R.G. Cooks, J.H. Beynon, R.M. Caprioli and G.R. Lester, Metastable Iions, Elsevier, Amsterdam, 1973.

153. G.I. Birnbaum, K.L. Sadana, W.J.P. Blonski and F.E. Hruska, *J.Am. Chem. Soc.*, **108**, 1671 (1986).

154. B.B. Allore, A. Queen, W.J. Blonski and F.E. Hruska, *Can. J. Chem.*, **61**,2397 (1983).

155. K.J. Divakar and C.B. Reese, *J. Chem. Soc. Perkin Trans.*, **1**, 1171 (1982).

156. V. Amarnath and A.D. Broom, *Chem Rev.*, **77**, 183 (1977).

157. J.A. Secrist, *Carbohydr. Res.*, **42**, 379 (1975).

158. B. Singer, M. Kroger and M. Carrano, *Biochemistry* , **17**, 1246 (1978).

159. K.G.Standing, R. Beavis, W. Ens and B. Schueler, *Int. J. Mass Spectrom. Ion Phys.*, **53**, 125 (1983).

160. S.K. Allison and M. Kamegai, *Revue Sci. Instrum.*, **32**, 1090 (1961).

161. B.T. Chait and F.H. Field, *Int..J. Mass Spectrom. Ion Phys.*, **41**, 17 (1981).

162. B.T. Chait, *Int. J. Mass Spectrom. Ion Phys.*, **53**, 227 (1983).

163. D. Suck and W. Saenger, *Acta Crystallogr. B*, **29**, 1323 (1973).

164. R.G.Brennan, D. Pyzalska, W.J.P. Blonski, F.E. Hruska and M. Sundaralingam, *Biochemistry* , **25**, 1181 (1986).

165. G.I. Birnbaum, K.L . Sadana, T. Razi, T. Lee, R. Sebastien, G.W. Buchko and F.E. Hruska, *Can. J. Chem.* **66**, 1628 (1988).

166. B. Singer and J.T. Kusmierek, Ann. Rev. Biochem., **52**, 655 (1982).

167. L.A. Dodson, R.S. Foote, S. Mitra and W.E. Masker, *Proc. Nat. Acad. Sci. USA*, **79**, 7440 (1982).

168. R. Saffhill, G.P. Margison and P.J. O'Connor, *Biochim. Biophys. Acta*, **823**, 111 (1985).

169. B. Singer, *Cancer Research*, **46**, 4879 (1986).

170. T.V. McCarthy, P. Karran and T. Lindahl, *EMBO J.*, **3**, 545 (1984).

171. F. Lafortune, R. Beavis,, B. Schueler, X. Tang, K.G. Standing and J.B. Westmore, *Proc. 35th ASMS Conf. Mass Spectrom. Allied Topics*, Denver, Colorado, May 1987.

172. X. Tang, W. Ens, K.G. Standing and J. B. Westmore, *Anal. Chem.*, **60**, 1791 (1988).

173. R. Beavis, D.E. Main, X. Tang, F. Lafortune and K.G. Standing, *Proc. 35th ASMS Conf. Mass Spectrom. Allied Topics*, Denver, Colorado, May 1987.

174. R. Beavis, *Ph.D. Thesis*, University of Manitoba, 1987.

175. F. Lafortune, W. Ens, K.G. Standing, J.B. Westmore, M.J. Damha and K.K. Ogilvie, *Adv. in Mass Spectrom.* Heyden & Son, London, **11**, 1402 (1989).

176. M.J. Damha and K.K. Ogilvie, *J. Org. Chem.*, **53**, 3710 (1988).

177. K.K. Ogilvie, N.Y. Theriault, J.M. Seifert, R.T. Pon and M.J. Nemer, *Can. J. Chem.*, **58**, 2686, (1980).

178. V. Renugopalakrishnan, A.V. Lakshminarayanan and V. Sasisekharan, *Biopolymers*, **10**, 1159 (1971).

179. T.M. Tyan, R.J. Day and T. G. Cooks, *Anal. Chem.* **52**, 2054 (1985).

180. S.J. Pachuta and TJ.G. Cooks, *Chem. Rev.* **87**, 647 (1987).

181. G.W. Buchko, F.E. Hruska and K.L. Sadana, to be submitted.